COSMOGENIC NUCLIDES AS A SURFACE EXPOSURE DATING TOOL: IMPROVED ALTITUDE/LATITUDE SCALING FACTORS FOR PRODUCTION RATES

by

Darin Maurice Desilets

A Dissertation Submitted to the Faculty of the

DEPARTMENT OF HYDROLOGY AND WATER RESOURCES

In Partial Fulfillment of the Requirements
For the Degree of

DOCTORATE OF PHILOSOPHY
WITH A MAJOR HYDROLOGY

In the Graduate College

THE UNIVERSITY OF ARIZONA

2 0 0 5

THE UNIVERSITY OF ARIZONA
GRADUATE COLLEGE

As members of the Dissertation Committee, we certify that we have read the dissertation prepared by Darin Desilets entitled “Cosmogenic nuclides as a surface exposure dating tool: improved altitude/latitude scaling factors for production rates” and recommend that it be accepted as fulfilling the dissertation requirement for the Degree of Doctorate of Philosophy in Hydrology

Marek Zreda Date_____

Victor R. Baker Date_____

Timothy Jull Date_____

Brenda Ekwurzel Date_____

Paul Damon Date_____

Final approval and acceptance of this dissertation is contingent upon the candidate’s submission of the final copies of the dissertation to the Graduate College.

I hereby certify that I have read this dissertation prepared under my direction and recommend that it be accepted as fulfilling the dissertation requirement.

Marek Zreda Date_____

STATEMENT BY AUTHOR

SIGNED: _____

ACKN OWLEDGEMENTS

I owe a deep gratitude to my advisor, Marek Zreda, who first encouraged me to pursue research in the field of cosmogenic nuclides. I have greatly benefited from Marek's guidance and wisdom. His curiosity and infectious enthusiasm will always be an inspiration to me.

Several others have also provided valuable help and advice in completing this work. I am truly honored to have received encouragement and critical comments from Devendra Lal, whose devotion to the field of cosmogenic nuclides dates back to his own Ph.D. dissertation nearly fifty years earlier. Lal introduced me to Venkataraman Radhakrishnan, who was instrumental in arranging neutron flux surveys in India and was supremely gracious in hosting our trip to Bangalore. Rad along with the staff at Raman Research Institute provided invaluable assistance and expertise and made our experience in India an unforgettable.

I thank Frank Trusdell and David Sherrod of the Hawaiian Volcano Observatory for assisting in preliminary work on Haleakala and Hualalai volcanoes and for sharing with me their extensive knowledge of Hawaiian lava flows. Correspondences with David Elmore at Purdue University helped me better understand Accelerator Mass Spectrometry and provided material for one of the manuscripts. I thank my dissertation committee, Tim Jull, Brenda Ekwurzel, Paul Damon and Vic Baker, for taking time out of their busy schedules and for sharing with me their comments and advice.

Finally I thank my wife Sharon and the rest of my family for their support. In particular, my father, Maurice Desilets, provided very tangible and valuable assistance in the field with balloon test flights and in the laboratory with the design and construction of electronic equipment.

TABLE OF CONTENTS

TABLE OF CONTENTS - *Continued*

TABLE OF CONTENTS - *Continued*

TABLE OF CONTENTS - *Continued*

LIST OF FIGURES

APPENDIX A

APPENDIX B

LIST OF FIGURES - *Continued*

APPENDIX C

LIST OF FIGURES - *Continued*

APPENDIX D

LIST OF FIGURES - *Continued*

APPENDIX E

LIST OF FIGURES - *Continued*

APPENDIX F

LIST OF TABLES

APPENDIX B

APPENDIX C

LIST OF TABLES - *Continued*

APPENDIX D

APPENDIX E

APPENDIX F

ABSTRACT

Applications of *in situ* cosmogenic nuclides to problems in Quaternary geology require increasingly accurate and precise knowledge of nuclide production rates. Production rates depend on the terrestrial cosmic-ray intensity, which is a function of the elevation and geomagnetic coordinates of a sample site and the geomagnetic field intensity. The main goal of this dissertation is to improve the accuracy of cosmogenic dating by providing better constraints on the spatial variability of production rates.

In this dissertation I develop a new scaling model that incorporates the best available cosmic-ray data into a framework that better describes the effects of elevation and geomagnetic shielding on production rates. This model is based on extensive measurements of energetic nucleon fluxes from neutron monitor surveys and on more limited data from low-energy neutron surveys. A major finding of this work is that neutron monitors yield scaling factors different from unshielded proportional counters. To verify that the difference is real I conducted an airborne survey of low-energy neutron fluxes at Hawaii (19.7° N 155.5° W) to compare with a nearby benchmark neutron monitor survey. Our data confirm that the attenuation length is energy dependent and suggest that the scaling factor for energetic nucleons is 10% higher between sea level and 4000 m than for low-energy neutrons at this location. An altitude profile of cosmogenic ^{36}Cl production from lava flows on Mauna Kea, Hawaii, support the use of neutron flux measurements to scale production rates but these data do not have enough precision to confirm or reject the hypothesis of energy-dependent scaling factors.

1. INTRODUCTION

Cosmogenic nuclides are an important quantitative tool for determining the chronologic context of Quaternary landforms. Relict end moraines, rock glaciers, fluvial incisions, fluvial and alluvial terraces and fans are a few of the landforms that record local geomorphic responses to fluctuating climate. Precise records of global scale climate variability in the Quaternary are available from marine records of stable isotopes which serve as proxies for global sea level and sea surface temperature (e.g. Vincent and Berger (1981), Aharon and Chappel (1986)). Terrestrial responses to global climate change are complex, highly variable geographically, and poorly understood (Bradley, 1985). Determining numerical ages of relict terrestrial landforms remains a major priority for Quaternary geologists. The need to correlate cosmogenic landform ages with the high-resolution marine isotope record and with other terrestrial dating methods such as ^{14}C has created a demand for accurate and precise *in situ* cosmogenic nuclide ages. Over the past several years it has been widely recognized that a major limitation on the accuracy of *in situ* cosmogenic ages is a lack of knowledge of the spatio-temporal distribution of production rates.

The central aim of this work is to increase the accuracy of the *in situ* cosmogenic nuclide dating method by obtaining an improved understanding of how production rates vary in space and time. This work began with an extensive background study of more than 50 years of cosmic-ray survey data. The physical framework and most of the data needed to fully characterize the spatial variability of terrestrial cosmic-ray intensity

already existed in the current body of cosmic-ray literature, but it had been mostly unrecognized in the cosmogenic nuclide field. My work has resulted in a fundamental recasting of the scaling problem into a framework that is consistent with advances in cosmic ray physics over the past 50 years. After exhaustively reviewing the literature and developing a scaling model based on existing data, I determined that new neutron flux measurements were needed to extend the range of previous surveys and to resolve discrepancies between neutron flux surveys conducted with different instruments. This led to new neutron monitor measurements in Hawaii in 2000 and southern India in 2002, and to measurements of low-energy neutron fluxes in Hawaii in 2003. To test the validity of using neutron measurements to scale production rates, I measured an altitude profile of cosmogenic ^{36}Cl production in two Hawaiian lava flows. Through experiments such as these the work presented in this dissertation will hopefully improve the cosmogenic dating method and guide future work in this area.

1.1 Background

The early investigations of Lal (1958) provided the foundation for what was until recently the most widely-accepted scaling model (Lal, 1991) for cosmogenic nuclide production rates. The main purpose of that pioneering work was to calculate global production rates of radionuclides produced through cosmic-ray interactions with atmospheric nuclei. Over the past several years it has been recognized that those scaling factors may lack the necessary accuracy required by surface exposure dating applications of cosmogenic nuclides (Lifton, 2000; Dunai, 2000). Reasons that Lal's scaling may be inaccurate are that: (1) Cosmic-ray measurements from latitude surveys are ordered

according to geomagnetic latitude calculated from an axially-symmetric centered dipole model. Such a model does not accurately describe the geomagnetic field's ability to deflect primary cosmic rays; (2) Atmospheric depth (pressure) data from altitude surveys were converted to elevation using a standard atmosphere. The model therefore does not account for spatial variations in the atmospheric pressure structure; (3) The model assumes that the shape of the nucleon energy spectrum is independent of altitude at energies below 400 MeV. Measurements performed more recently suggest that the energy spectrum may soften significantly towards sea level, even at energies below 400 MeV; (4) Measurements taken since the 1950s, representing the vast majority of cosmic-ray data, are not included; (5) The effects of solar activity are not explicitly addressed.

Dunai (2000) proposed a major revision to Lal's (1958,1991) model. Although his work incorporates some data more recent than Lal (1958), Dunai's model is also based on a small subset of the cosmic-ray data from the 1950s. In addition, Dunai orders cosmic-ray data according to geomagnetic inclination, which, like geomagnetic latitude, has a non-unique relation with cosmic-ray intensity. He also neglects the effect of solar activity and implicitly assumes that the energy spectrum is independent of altitude. For these reasons, both the accuracy and reported uncertainty (e.g. ~2% in the sea-level latitude curve) of that scaling model are questionable.

An important difference between the scaling models of Lal (1958,1991) and Dunai (2000) is the dependence of nucleon fluxes on altitude. Dunai's scaling model consistently gives effective attenuation lengths that are about 5% lower than those calculated from Lal's model. The different attenuation lengths result in a ~10% difference between

the two models when production rates are scaled between 1033 g cm^{-2} and 600 g cm^{-2} (0-5000 m). The two authors also give sea-level neutron fluxes that are different by as much as 12%, even though their scaling models utilize the same sea-level neutron monitor survey as a baseline. Given such discrepancies, and considering the inherent problems with these models, there is an obvious need to investigate the scaling problem in more detail.

A vast amount of neutron flux data is available from extensive neutron monitor surveys conducted over the past 50 years. The work in this dissertation represents the first attempt to fully utilize that resource for cosmogenic dating. There is only one other published scaling model based primarily on neutron monitor data (Ziegler, 1996). That model used an extensive survey during the International Quiet Sun Year (1965-66) to predict the altitude and latitude dependence of soft fail rates in integrated circuits. Another scaling model for cosmogenic nuclide production based primarily on neutron monitor data has also been proposed by Lifton (2000), but the final results of that work have not yet been published.

1.2 Present Study

This dissertation consists of six original research papers that are published, currently in review or will soon be submitted. The sequence of these papers represents a chronological progression in the understanding and interpretation of cosmic-ray data, and therefore earlier papers may partially be outdated by later ones.

The first paper (Appendix A), titled *Comment on Scaling factors for production rates of in situ produced cosmogenic nuclides: a critical reevaluation*, was written in response to a scaling model proposed by Dunai (2000). The comment was originally written as a lengthy paper that used Dunai's work as the context for addressing several important and commonly held misconceptions regarding neutron flux data. Because of page restrictions imposed by the editor, the manuscript had to be greatly shortened so that the final version included only our specific criticisms of Dunai's paper. The remaining material was turned into a second paper, *On scaling cosmogenic nuclide production rates for altitude and latitude using cosmic-ray measurements* (Appendix B), which summarized our state of knowledge at the time. This laid the foundation for the third paper, *Spatial and temporal distribution of secondary cosmic-ray nucleon intensity and applications to in situ cosmogenic dating* (Appendix C), in which we give new scaling factors based on a parameterization of neutron monitor data. A major finding of that work is that neutron monitors, which are sensitive to high-energy neutron fluxes (E>50 MeV) yield different scaling factors than the low-energy fluxes (E<1 eV) measured with proportional counters. In the fourth and fifth papers (Appendices D and E) some of the hypotheses in Appendix C are tested experimentally. The paper *New cosmic-ray measurements at low latitude: extended scaling factors for cosmogenic nuclide production rates* extends the measurements to the highest geomagnetic cutoff rigidity on earth, and gives additional evidence that the neutron energy spectrum softens toward sea level. The paper titled *Elevation profile of ^{36}Cl production from Hawaiian lava flows* seeks to test the validity of

using cosmic-ray measurements to scale ^{36}Cl production. The final paper *Determination of ^{36}Cl in rocks by isotope dilution* is to date the most thorough investigation of the benefits and potential pitfalls of preparing ^{36}Cl samples by isotope dilution.

The title of the paper, along with journal name and status at the time of completing this dissertation are:

APPENDIX A: Desilets, D., Zreda, M., and Lifton, N.A., 2001, Comment on "Scaling factors for production rates of in situ produced cosmogenic nuclides: a critical reevaluation": Earth and Planetary Science Letters, v. 188, p. 283-287.

APPENDIX B: Desilets, D., and Zreda, M., 2001, On scaling cosmogenic nuclide production rates for altitude and latitude using cosmic-ray measurements: Earth and Planetary Science Letters, v. 193, p. 213-225.

APPENDIX C: Desilets, D., and Zreda, M., 2003, Spatial and temporal distribution of secondary cosmic-ray nucleon intensity and applications to in situ cosmogenic dating: Earth and Planetary Science Letters, v. 206, p. 21-42.

APPENDIX D: Desilets, D., Zreda, M., and Radhakrishnan, V., 2005, New cosmic-ray measurements at low latitude: extended scaling factors for cosmogenic nuclide production rates (in preparation).

APPENDIX E: Desilets, D., and Zreda, M., 2005, Elevation profile of ^{36}Cl production from Hawaiian lava flows (in preparation).

APPENDIX F: Desilets, D., and Zreda, M., 2005, Determination of ^{36}Cl by isotope dilution (in preparation).

1.3 STATEMENT OF CANDIDATES CONTRIBUTION TO PAPERS

The candidate was the major contributor to the research and writing of all six papers. The second author, Marek Zreda, contributed in the form of guidance, advice and editing and was the principal investigator for the projects in Hawaii and India.

1.4 REFERENCES

Ackert, R.P., Barclay, D.J., Borns, H.W., Calkin, P.E., Kurz, M.D., Fastook, J.L., and Steig, E.J., 1999, Measurements of past ice sheet elevations in interior West Antarctica: Science, v. 286, p. 276-280.

Aharon, P., 1984, Implications of the coral-reef record from New Guinea concerning the astronomical theory of ice ages, *in* Berger, A., Imbrie, J., Hays, J., Kukla, G. and Saltzman, B. (eds.), Milankovitch and Climate. Understanding the Response to Astronomical Forcing: Reidel, Dordrecht, 337-379.

Aleksanyan, T.M., Dorman, I.V., Dorman, L.I., Babayan, V.K., Belov, A.V., Blokh, Y.L., Kaminer, N.S., Korotkov, V.K., Libin, I.Y., Manshilina, A.A., Mashkov, Y.E., Mymrina, I.V., Rogovaya, S.I., Sitnov, A.M., Yudakhin, K.F., and Yanke, V., 1982, Geomagnetic effects in cosmic rays and spectrum of the increase before magnetic storms: Izvestiya Akademii Nauk SSSR, Seriya Fizicheskaya, v. 46, p. 1689-1691.

Allkofer, O.C., Andresen, R.D., Bagge, E., Dau, W.D., and Funk, H., 1969, Der Einfluss des Erdmagnetfeldes auf die kosmische Strahlung, 1, Untersuchungen der Nukleonenkomponente der kosmische Strahlung waehrend der atlantischen Expedetion IQSY 1965 auf dem Forschungsschif "Meteor,", "Meteor" Forschungsergebnisse, Reihe B, Heft 3, Gebrüder Borntraeger: Berlin.

Allkofer, O.C., Andresen, R.D., Clausen, K., and Dau, W.D., 1972, Sea-level muon spectrum at two different latitudes: Journal of Geophysical Research, v. 77, p. 4251-4253.

Almasi, P.F., 2001, Dating the paleobeaches of Pampa Mejillones, Northern Chile by cosmogenic chlorine-36 [M.S. thesis]: Tucson, University of Arizona.

Aruscavage, P.J., and Campbell, E.Y., 1983, An ion-selective electrode method for determination of chlorine in geological materials: Talanta, v. 30, p. 745-749.

Ashton, F., 1961, The range-energy relationship for high-energy μ-mesons: Proceedings of the Physical Society, v. 77, p. 587-592.

Bachelet, F., Balata, P., Dyring, E., and Iucci, N., 1964, On the multiplicity effect in a standard cosmic-ray neutron monitor: Il Nuovo Cimento, v. 31, p. 1126-1130.

Bachelet, F., Balata, P., Dyring, E., and Iucci, N., 1965, Attenuation coefficients of the cosmic-ray nucleonic component in the lower atmosphere: Il Nuovo Cimento, v. 35, p. 23-35.

Bachelet, F., Iucci, N., and Villoresi, G., 1972a, The cosmic-ray spectral modulation above 2 GV during the descending phase of solar cycle number 19. I. A comprehensive

treatment of the neutron monitor data from the worldwide station network and latitude surveys: Il Nuovo Cimento, v. 7 B, p. 17-32.

Bachelet, F., Iucci, N., Villoresi, G., and Zangrilli, N., 1972b, The cosmic-ray spectral modulation above 2 GV. IV. The Influence on the attenuation coefficient of the nucleonic component: Il Nuovo Cimento, v. 11 B, p. 1-12.

Barrows, T.T., Stone, J.O., Fifield, K., and Cresswell, R.G., 2002, The timing of the Last Glacial Maximum in Australia: Quaternary Science Reviews, v. 21, p. 159-173.

Benedetti, L., R. Finkel, G. King, R. Armijo, Papanastassiou, D., Ryerson, F.J., Flerit, F., Farber, D., and Stavrakakis, G., 2003, Motion on the Kaparelli fault (Greece) prior to the 1981 earthquake sequence determined from ^{36}Cl cosmogenic dating: Terra Nova, v. 15, p. 118.

Bhattacharyya, A., and Mitra, B., 1997, Changes in cosmic ray cut-off rigidities due to secular variations of the geomagnetic field: Annales Geophysicae-Atmospheres Hydrospheres and Space Sciences, v. 15, p. 734-739.

Bierman, P.R., and Clapp, E.M., 1996, Estimating geologic age from cosmogenic nuclides: an update: Science, v. 271, p. 1606.

Bilokon, H., Castagnoli, G.C., Castellina, A., Piazzoli, D., Mannocchi, G., Meroni, E., Picchi, P., and Vernetto, S., 1989, Flux of the vertical negative muons stopping at depths .35-1000 hg/cm^2: Journal of Geophysical Research, v. 94, p. 12145-12152.

Bradley, R.S., 1985, Quaternary Paleoclimatology: Allen and Unwin, London.

Brown, E.T., Brook, E.J., Raisbeck, G.M., Yiou, F., and Kurz, M.D., 1992, Effective attenuation lengths of cosmic-rays producing ^{10}Be and ^{26}Al in quartz - implications for exposure age dating: Geophysical Research Letters, v. 19, p. 369-372.

Brown, E.T., Trull, T.W., Jean-Baptiste, P., Raisbeck, G., Bourlès, D., Yiou, F., and Marty, B., 2000, Determination of cosmogenic production rates of ^{10}Be, ^{3}He and ^{3}H in water: Nuclear Instruments and Methods in Physics Research B, v. 172, p. 873-883.

Brown, R.H., Camerini, U., Fowler, P.H., Heitler, H., King, D.T., and Powell, C.F., 1949, Nuclear transmutations produced by cosmic-ray particles of great energy. Part I. Observations with photographic plates exposed at an altitude of 11,000 feet: Philosophical Magazine, v. 40, p. 862-881.

Brown, W.W., 1954, Cosmic-ray nuclear interactions in gases: Physical Review, v. 93, p. 528-534.

Carmichael, H., and Bercovitch, M., 1969a, II. Cosmic-ray latitude survey in Canada in December, 1965: Canadian Journal of Physics, v. 47, p. 2051-2055.

Carmichael, H., and Bercovitch, M., 1969b, V. Analysis of IQSY cosmic-ray survey measurements: Canadian Journal of Physics, v. 47, p. 2073-2093.

Carmichael, H., Bercovitch, M., Steljes, J.F., and Magidin, M., 1969a, I. Cosmic-ray latitude survey in North America in summer, 1965: Canadian Journal of Physics, v. 47, p. 2037-2050.

Carmichael, H., and Peterson, R.W., 1971, Dependence of the neutron monitor attenuation coefficient on atmospheric depth and on geomagnetic cutoff in 1966 and in 1970, Proceedings of the 12th International Cosmic Ray Conference, p. 887-892.

Carmichael, H., Shea, M.A., and Peterson, R.W., 1969b, III. Cosmic-ray latitude survey in Western USA and Hawaii in summer, 1966: Canadian Journal of Physics, v. 47, p. 2057-2065.

Carmichael, H., Shea, M.A., Smart, D.F., and McCall, J.R., 1969c, IV. Geographically smoothed geomagnetic cutoffs: Canadian Journal of Physics, v. 47, p. 2067-2072.

Clem, J.M., Bieber, J.W., Evenson, P., Hall, D., Humble, J.E., and Duldig, M., 1997, Contribution of obliquely incident particles to neutron monitor counting rate: Journal of Geophysical Research, v. 102, p. 26919-26926.

Conversi, M., 1950, Experiments on cosmic-ray mesons and protons at several altitudes and latitudes: Physical Review, v. 79, p. 749-767.

Conversi, M., and Rothwell, P., 1954, Angular distributions in cosmic ray stars at 3500 meters: Il Nuovo Cimento, v. 12, p. 191.

Cooke, D.J., Humble, J.E., Shea, M.A., Smart, D.F., Lund, N., Rasmussen, I.L., Byrnak, B., Goret, P., and Petrou, N., 1991, On cosmic-ray cut-off terminology: Il Nuovo Cimento, v. 14, p. 213-233.

Coxell, H., Pomerantz, M.A., and Agarwal, S.P., 1965, Survey of cosmic-ray intensity in the lower atmosphere: Journal of Geophysical Research, v. 71, p. 143-154.

Croft, S., and Bourva, L.C.A., 2003, The specific total and coincidence cosmic-ray-induced neutron production rates in materials: Nuclear Instruments and Methods in Physics Research A, v. 505, p. 536–539.

Dep, L., Elmore, D., Fabryka-Martin, J., Masarik, J., and Reedy, R.C., 1994, Production rate systematics of in-situ produced cosmogenic nuclides in terrestrial rocks: Monte Carlo approach of investigating $^{35}Cl(n,g)^{36}Cl$: Nuclear Instruments and Methods in Physics Research, v. B92, p. 321-325.

Desilets, D., and Zreda, M., 2001, On scaling cosmogenic nuclide production rates for altitude and latitude using cosmic-ray measurements: Earth and Planetary Science Letters, v. 193, p. 213-225.

Desilets, D., and Zreda, M., 2003, Spatial and temporal distribution of secondary cosmic-ray nucleon intensity and applications to in situ cosmogenic dating: Earth and Planetary Science Letters, v. 206, p. 21-42.

Desilets, D. and Zreda, M., Determination of ^{36}Cl by isotope dilution, Department of Hydrology and Water Resources Technical Report 05-01, University of Arizona, Tucson, AZ, 2005.

Desilets, D., Zreda, M., and Lifton, N.A., 2001, Comment on "Scaling factors for production rates of in situ produced cosmogenic nuclides: a critical reevaluation": Earth and Planetary Science Letters, v. 188, p. 283-287.

Desilets, D., Zreda, M., and Radhakrishnan, V., 2005, New cosmic-ray measurements at low latitude: extended scaling factors for cosmogenic nuclide production rates: Earth and Planetary Science Letters, (in preparation).

Desilets, D.M., 2001, The global distribution of secondary cosmic-ray intensity and applications to cosmogenic dating [M.S. thesis]: Tucson, Arizona, University of Arizona.

Dixit, K.R., 1955, The statistics of 29000 stars observed in nuclear emulsions in Kenya: Zeitschrift für Naturforschung, v. 10a, p. 339-341.

Dorman, L.I., 1974, Cosmic Rays Variations and Space Explorations: Amsterdam, North-Holland Publishing Co.

Dorman, L.I., Villoresi, G., Iucci, N., Parisi, M., Tyasto, M.I., Danilova, O.A., and Ptitsyna, N.G., 2000, Cosmic ray survey to Antarctica and coupling functions for neutron component near solar minimum (1996-1997) 3. Geomagnetic effects and coupling functions: Journal of Geophysical Research, v. 105, p. 21047-21056.

Dunai, T.J., 2000, Scaling factors for production rates of in situ produced cosmogenic nuclides: a critical reevaluation: Earth and Planetary Science Letters, v. 176, p. 157-169.

Dunai, T.J., 2001, Inluence of secular variation of the geomagnetic field on production rates of in situ produced cosmogenic nuclides: Earth and Planetary Science Letters, v. 193, p. 197-212.

Dunai, T.J., and Wijbrans, J.R., 2000, Long-term cosmogenic ^{3}He production rates (152 ka-1.35 Ma) from ^{40}Ar/^{39}Ar dated basalt flows at 29° N latitude: Earth and Planetary Science Letters, v. 176, p. 147-156.

Elmore, D., Ma, X., Miller, T., Mueller, K., Perry, M., Rickey, F., Sharma, P., Simms, P., Lipschutz, M., and Vogt, S., 1997, Status and plans for the PRIME Lab AMS facility: Nuclear Instruments and Methods in Physics Research B, v. 123, p. 69-72.

Elmore, D., and Phillips, F.M., 1987, Accelerator mass spectrometry for measurement of long-lived radioisotopes: Science, v. 236, p. 543-550.

Elsasser, W., Ney, E.P., and Winckler, J.R., 1956, Cosmic-ray intensity and geomagnetism: Nature, v. 178, p. 1226-1227.

Elsheimer, H.N., 1987, Application of an ion-selective electrode method to the determination of chloride in 41 international geochemical reference materials: Geostandards Newsletter, v. 11, p. 115-122.

Fabryka-Martin, J.T., 1988, Production of radionuclides in the earth and their hydrogeologic significance, with emphasis on chlorine-36 and iodine-129 [PhD dissertation thesis]: Tucson, University of Arizona.

Forman, M.A., 1968, The relation between latitude and solar-cycle variations in the neutron-monitor mass-absorption coefficient: Canadian Journal of Physics, v. 46, p. S1087-S1089.

Fraser-Smith, A.C., 1987, Centered and eccentric geomagnetic dipoles and their poles, 1600-1985: Reviews of Geophysics, v. 25, p. 1-16.

George, E.P., and Evans, J., 1951, Disintegrations produced by the nuclear capture of slow negative μ-mesons: Proceedings of the Physical Society of London, v. 64A, p. 193-198.

Gosse, J.C., and Phillips, F.M., 2001, Terrestrial cosmogenic nuclides: theory and application: Quaternary Science Reviews, v. 20, p. 1475-1560.

Graham, I.J., Barry, B.J., Ditchburn, R.G., and Whitehead, N.E., 2000, Validation of cosmogenic nuclide production rate scaling factors through direct measurement: Nuclear Instruments and Methods in Physics Research B, v. 172, p. 802-805.

Griffiths, W.K., Harman, C.V., Hatton, C.J., and Ryder, P., 1965, Studies of the barometric coefficients of IGY and NM-64 neutron monitors, Proceedings of the 9th International Cosmic Ray Conference, v. 32.

Griffiths, W.K., Harmon, C.V., Hatton, C.J., Marsden, P.L., and Ryder, P., 1968, The intensity variations of selected multiplicities in the Leeds NM64 neutron monitor: Canadian Journal of Physics, v. 46, p. S1044-S1047.

Guyodo, Y., and Valet, J.P., 1996, Relative variations in geomagnetic intensity from sedimentary records: the past 200,000 years: Earth and Planetary Science Letters, v. 143, p. 23-26.

Guyodo, Y., and Valet, J.P., 1999, Global changes in intensity of the Earth's magnetic field during the past 800 kyr: Nature, v. 399, p. 249-252.

Hatton, C.J., 1971, The neutron monitor, *in* Wilson, J.G., and Wouthuysen, S.A., eds., Progress in Elementary Particle and Cosmic Ray Physics, Volume 10: Amsterdam, North-Holland Publishing Co., p. 1-100.

Hatton, C.J., and Carmichael, H., 1964, Experimental investigation of the NM-64 neutron monitor: Canadian Journal of Physics, v. 42, p. 2443-2472.

Hess, W.N., Canfield, E.H., and Lingenfelter, R.E., 1961, Cosmic-ray neutron demography: Journal of Geophysical Research, v. 66, p. 665-677.

Hughes, E.B., and Marsden, P.L., 1966, Response of a standard IGY neutron monitor: Journal of Geophysical Research, v. 71, p. 1435-1444.

Iucci, N., Villoresi, G., Dorman, L.I., and Parisi, M., 2000, Cosmic ray survey to Antarctica and coupling functions for neutron component near solar minimum (1996-1997) 1. Determination of meteorological effects: Journal of Geophysical Research, v. 105, p. 21,035-21,045.

Jackson, G.S., Elmore, D., Caffee, M., Mueller, K.A., Bonte, B.D., Muzikar, P., and Alexander, B., 2004, Ion source modeling and design at PRIME Lab: Nuclear Instruments and Methods in Physics Research, v. B 223-224, p. 155-160.

Juvik, S.P., Juvik, J.O., and Paradise, T.R., 1998, Atlas of Hawaii: Honolulu, University of Hawaii Press.

Kent, D.W., Coxell, H., and Pomerantz, M.A., 1968, Latitude survey of the frequency of multiple events in an airborne neutron monitor: Canadian Journal of Physics, v. 46, p. S1082-S1086.

Kent, D.W., and Pomerantz, M.A., 1971, Cosmic ray intensity variations in the lower atmosphere: Journal of Geophysical Research, v. 76, p. 1652-1661.

Kharaka, Y.K., Gunter, W.D., Aggarwal, P.K., Perkins, E.H., and DeBraal, J.D., 1988, Solmineq.88: A computer program for geochemical modeling of water-rock interactions: Menlo Park, CA, U.S. Geological Survey.

Knoll, G.F., 2000, Radiation detection and measurement: New York, Wiley, 802 p.

Krane, K.S., 1988, Introductory Nuclear Physics: New York, John Wiley and Sons, 845 p.

Kurz, M., 1986, Cosmogenic helium in a terrestrial igneous rock: Nature, v. 320, p. 435-439.

Lal, D., 1958, Investigation of nuclear interactions produced by cosmic rays [Ph.D thesis]: Bombay, University of Bombay.

Lal, D., 1988, In situ-produced cosmogenic isotopes in terrestrial rocks: Annual Reviews of Earth and Planetary Sciences, v. 16, p. 355-388.

Lal, D., 1991, Cosmic ray labeling of erosion surfaces: *in situ* nuclide production rates and erosion models: Earth and Planetary Science Letters, v. 104, p. 424-439.

Lal, D., 2000, Cosmogenic nuclide production rate systematics in terrestrial materials: Present knowledge, needs and future actions for improvement: Nuclear Instruments and Methods in Physics Research B, v. 172, p. 772-781.

Lal, D., Arnold, J.R., and Masatake, H., 1964, Cosmic-ray production of ^{7}Be in oxygen and ^{32}P,^{33}P,^{35}S in Argon at mountain altitudes: Physical Review, v. 118, p. 1626.

Lal, D., and Peters, B., 1967, Cosmic ray produced radioactivity on earth, *in* Sitte, K., ed., Encyclopedia of Physics: Cosmic Rays II, Volume 46/2: Encyclopedia of Physics: Berlin, Springer-Verlag, p. 551-612.

Lambeck, K., Esat, T.M., and Potter, E.K., 2002, Links between climate and sea levels for the past three million years: Nature, v. 419, p. 199-206.

Licciardi, J.M., Kurz, M.D., Clark, P.U., and Brook, E.J., 1999, Calibration of cosmogenic ^{3}He production rates from Holocene lava flows in Oregon, USA, and effects of the Earth's magnetic field: Earth and Planetary Science Letters, v. 172, p. 261-271.

Lifton, N., 2000, A robust scaling model for in situ cosmogenic nuclide production rates, Geological Society of America, Annual Meeting: abstracts with programs: Reno, Nevada, p. A400.

Lifton, N., Pigati, J.S., Jull, A.J.T., and Quade, J., 2002, Testing cosmogenic nuclide production rate scaling models using in situ cosmogenic ^{14}C from surfaces at secular equilibrium: Preliminary results, Eos Transactions AGU, Fall Meeting Supplement.

Liu, B., Phillips, F.M., Fabryka-Martin, J.T., Fowler, M.M., and Biddle, R.S., 1994, Cosmogenic ^{36}Cl accumulation in unstable landforms, 1. Effects of the thermal neutron distribution: Water Resources Research, v. 30, p. 3115-3125.

Lockwood, J.A., 1958, Variations in the cosmic-ray nucleonic intensity: Physical Review, v. 112, p. 1750-1758.

Ludwig, K.R., Szabo, B.J., Moore, J.G., and Simmons, K.R., 1991, Crustal subsidence rate off Hawaii determined from $^{234}U/^{238}U$ ages of drowned coral reefs: Geology, v. 19, p. 171-174.

Mabuchi, H., Reisuke, G., Yukio, W., and Hiroshi, H., 1971, Phosphorous-32 induced by atmospheric cosmic rays in laboratory chemicals: Geochemical Journal, v. 4, p. 105-110.

Makino, T., and Kondo, I., 1965, Modulation of cosmic ray threshold rigidity due to geomagnetic cavity field, Proceedings of the 9th International cosmic-ray conference: v. 32, p. 564-567.

Manual of the ICAO Standard Atmosphere extended to 80 kilometres (262 500 feet), International Civil Aviation Organisation, Doc. 7488, 1993.

Masarik, J., Frank, M., Schäfer, J.M., and Rainer, W., 2001, Correction of in situ cosmogenic nuclide production rates for geomagnetic field intensity variations during the past 800,000 years: Geochimica et Cosmochimica Acta, v. 65, p. 2995-3003.

Masarik, J., and Reedy, R.C., 1995, Terrestrial cosmogenic-nuclide production systematics calculated from numerical simulations: Earth and Planetary Science Letters, v. 136, p. 381-396.

McElhinny, M.W., and Senanayake, W.E., 1982, Variations in the geomagnetic dipole I: the past 50,000 years: Journal of Geomagnetism and Geoelectricity, v. 34, p. 39-51.

Merker, M., Light, E.S., Verschell, H.J., Mendell, R.B., and Korff, S.A., 1973, Time dependent worldwide distribution of atmospheric neutrons and their products, 1. Fast neutron obervations: Journal of Geophysical Research, v. 78, p. 2727-2740.

Messel, H., 1954, The development of a nucleon cascade, *in* Wilson, J.G., ed., Progress in Elementary Particle and Cosmic Ray Physics, Volume 2: Amsterdam, North-Holland Publishing Co., p. 134-216.

Mischke, C.F.W., 1972, Intensiteisvaiasies van neutrone vanaf kosmiese strale [M.S. thesis]: Potchefstroom, South Africa, University of Potchefstroom.

Moraal, H., Potgieter, M.S., and Stoker, P.H., 1989, Neutron monitor latitude survey of cosmic ray intensity during the 1986/1987 solar minimum: Journal of Geophysical Research, v. 94, p. 1459-1464.

NOAA, National Climatic Data Center radiosonde database available on-line [http://raob.fsl.noaa.gov/].

Nobles, R.A., Alber, R.A., Hughes, E.B., Newkirk, L.L., and Walt, M., 1967, Neutron multiplicity monitor observations during 1965: Journal of Geophysical Research, v. 72, p. 3817-3827.

Ohno, M., and Hamano, Y., 1992, Geomagnetic poles over the past 10,000 years: Geophysical Research Letters, v. 19, p. 1715-1718.

Ohno, M., and Hamano, Y., 1993, Global analysis of the geomagnetic-field: time variation of the dipole moment and the geomagnetic pole in the Holocene: Journal of Geomagnetism and Geoelectricity, v. 45, p. 1455-1466.

Phillips, F.M., 2003, Cosmogenic ^{36}Cl ages of Quaternary basalt flows in the Mojave Desert, California, USA: Geomorphology, v. 53, p. 199-208.

Phillips, F.M., Stone, W.D., and Fabryka-Martin, J.T., 2001, An improved approach to calculating low-energy cosmic-ray neutron fluzes near the land/atmosphere interface: Chemical Geology, v. 175, p. 689-701.

Phillips, F.M., Zreda, M.G., Flinsch, M.R., Elmore, D., and Sharma, P., 1996, A reevaluation of cosmogenic ^{36}Cl production rates in terrestrial rocks: Geophysical Research Letters, v. 23, p. 949-952.

Potgeiter, M.S., Moraal, H., Raubenheimer, B.C., and Stoker, P.H., 1980a, Modulation of cosmic rays during solar minimum. Part 3. Comparison of the latitude distributions for the periods of solar minimum during 1954, 1965 and 1976: South African Journal of Physics, v. 3, p. 90-94.

Potgeiter, M.S., Raubenheimer, B.C., Stoker, P.H., and van der Walt, A.J., 1980b, Modulation of cosmic rays during solar minimum. Part 2. Cosmic ray latitude distribution at sea level during 1976: South African Journal of Physics, v. 3, p. 77-89.

Press, W.H., Flannery, B.P., Teukolsky, S.A., and Vetterling, W.T., 1980, Numerical Recipes: New York, University of Cambridge, 818 p.

Pyle, R., Evenson, P., Bieber, J.W., Clem, J.M., Humble, J.E., and Duldig, M.L., 1999, The use of ^{3}He tubes in a neutron monitor latitude survey, Proceedings of the 26th International Cosmic Ray Conference, Volume 7: Salt Lake City, p. 386-389.

Quenby, J.J., 1967, The time variations of the cosmic ray intensity, *in* Sitte, K., ed., Encyclopedia of Physics: Cosmic Rays II, Volume 46/2: Encyclopedia of Physics: Berlin, Springer-Verlag, p. 310-371.

Quenby, J.J., and Webber, W.R., 1959, Cosmic ray cut-off rigidities and the Earth's magnetic field: Philosophical Magazine, v. 4, p. 90-113.

Quenby, J.J., and Wenk, G.J., 1962, Cosmic ray cut-off rigidities and the Earth's magnetic field: Philosophical Magazine, v. 7, p. 1457-1471.

Raubenheimer, B.C., and Stoker, P.H., 1971, Attenuation coefficients of various cosmic ray components in the lower atmosphere, Proceedings of the 12th International Conference on Cosmic Rays, p. 893-896.

Raubenheimer, B.C., and Stoker, P.H., 1974, Various aspects of the attenuation coefficient of a neutron monitor: Journal of Geophysical Research, v. 79, p. 5069-5076.

Roederer, J.G., 1952, Über die Absorption der Nukleonenkomponente der kosmischen Strahlung in -21° geomagnetischer Breite: Zeitschrift für Naturforschung, v. 7a, p. 765-771.

Rose, D.C., Fenton, K.B., Katzman, J., and Simpson, J.A., 1956, Latitude effects of the cosmic ray nucleon and meson components at sea level from the Arctic to the Antarctic: Canadian Journal of Physics, v. 34, p. 968-984.

Rossi, B., 1948, Interpretation of cosmic-ray phenomena: Reviews of Modern Physics, v. 20, p. 537-583.

Rossi, B., Sands, M., and Sard, R.F., 1947, Measurements of slow meson intensity at several altitudes: Physical Review, v. 72, p. 120-125.

Rothwell, P., 1958, Cosmic rays in the Earth's magnetic field: Philosophical Magazine, v. 3, p. 961-970.

Sands, M., 1950, Low energy mesons in the atmosphere: Physical Review, v. 77, p. 180-193.

Sandström, A.E., 1958, Cosmic ray soft component measurements during a flight from Scandinavia across the North Pole and around Asia and Europe: Nuovo Cimento VIII, Serie X, Suppl., p. 263-276.

Schwartz, M., 1959, Penumbra and simple shadow cone of cosmic radiation: Il Nuovo Cimento, v. 11, Serie X, Suppl., p. 27-59.

Shanahan, T.M., and Zreda, M., 2000, Chronology of Quaternary glaciations in East Africa: Earth and Planetary Science Letters, v. 177, p. 23-42.

Sharma, P., Bourgeois, M., Elmore, D., Vogt, S., Phillips, F., and Zreda, M., 2000, Simultaneous determination of Cl and ^{36}Cl in geological samples using AMS, Eos Transactions AGU 81, Fall Meeting Supplement, p. Abstract U21A-22.

Shea, M.A., and Smart, D.F., 1983, A world grid of calculated cosmic ray vertical cutoff rigidities for 1980.0, Proceedings of the 18th International Cosmic Ray Conference, v. 10-3: Bangalore, India, p. 415-418.

Shea, M.A., Smart, D.F., and Gentile, L.C., 1987, Estimating cosmic ray vertical cutoff rigidities as a function of the McIlwain L-parameter for different epochs of the geomagnetic field: Physics of the Earth and Planetary Interiors, v. 48, p. 200-205.

Shea, M.A., Smart, D.F., and McCall, J.R., 1968, A five degree by fifteen degree world grid of trajectory-determined vertical cutoff rigidities: Canadian Journal of Physics, v. 46, p. S1098-S1101.

Shea, M.A., Smart, D.F., and McCracken, K.G., 1965, A study of vertical cutoff rigidities using sixth degree simulations of the geomagnetic field: Journal of Geophysical Research, v. 70, p. 4117-4130.

Simonson, J.M., and Palmer, D.A., 1993, Liquid-vapor partitioning of HCl(aq) to 350°C: Geochimica et Cosmochimica Acta, v. 57, p. 1-7.

Simpson, J.A., 1951, Neutrons produced in the atmosphere by the cosmic radiations: Physics Reviews, v. 83, p. 1175-1188.

Simpson, J.A., 2000, The cosmic ray nucleonic component: the invention and scientific uses of the neutron monitor: Space Science Reviews, v. 93, p. 11-32.

Simpson, J.A., and Fagot, W.C., 1953, Properties of the low energy nucleonic component at large atmospheric depths: Physical Review, v. 90, p. 1068-1072.

Soberman, R.K., 1956, High-altitude cosmic-ray intensity variations: Physical Review, v. 102, p. 1399-1409.

Stoker, P.H., van der Walt, A.J., and Potgeiter, M.S., 1980, Modulation of cosmic rays during solar minimum, 1, Cosmic ray intensity survey at sea-level dring 1976: Experimental details: South African Journal of Physics, v. 3, p. 73-76.

Stone, J.O., 2000, Air pressure and cosmogenic isotope production: Journal of Geophysical Resarch, v. 105, p. 23753-23759.

Stone, J.O., Allan, G.L., Fifield, L.K., and Cresswell, R.G., 1996, Cosmogenic chlorine-36 from calcium spallation: Geochimica et Cosmochimica Acta, v. 60, p. 679-692.

Stone, J.O.H., Evans, J.M., Fifield, L.K., Allan, G.L., and Cresswell, R.G., 1998, Cosmogenic chlorine-36 production in calcite by muons: Geochimica et Cosmochimica Acta, v. 62, p. 433-454.

Störmer, C., 1955, The Polar Aurora: London, Oxford University Press.

U.S. standard atmosphere, 1976: United States Committee on Extension to the Standard Atmosphere, Washington, D.C., U.S. Government Printing Office.

Vincent, E., and Berger, W.H., 1981, Planktonic foraminifera and there use in paleoceanography, *in* Emiliani, C., ed., The Sea, Vol. 7; The Oceanic Lithosphere: Wiley, New York, p. 1025-1119.

Villoresi, G., Dorman, L.I., Iucci, N., and Ptitsyna, N.G., 2000, Cosmic ray survey to Antarctica and coupling functions for neutron component near solar minimum (1996-1997) 1. Methodolgy and data quality assurance: Journal of Geophysical Research, v. 105, p. 21,025 - 21,034.

Wolfe, E.W., and Morris, J., 1996, Geologic Map of the Island of Hawaii: Washington, United States Geological Survey.

Wolfe, E.W., Wise, W.S., and Dalrymple, G.B., 1997, The Geology and Petrology of Mauna Kea Volcano, Hawaii - A Study of Postshield Volcanism: Washington, United States Geological Survey, 129 p.

X-5 Monte Carlo Team, 2003, MCNP - A General Monte Carlo N-Transport Code, Version 5, Los Alamos National Laboratory.

Yang, S., Odah, H., and Shaw, J., 2000, Variations in the geomagnetic dipole moment over the last 12 000 years: Geophysical Journal International, v. 140, p. 158-162.

Ziegler, J.F., 1996, Terrestrial cosmic ray intensities: IBM Journal of Research and Development, v. 40, p. 19-39.

Zreda, M.G., and Phillips, F.M., 1994, Surface exposure dating by cosmogenic chlorine-36 accumulation, *in* Beck, C., ed., Dating in Exposed and Surface Contexts, University of New Mexico Press, p. 161-183.

Zreda, M.G., Phillips, F.M., Elmore, D., Kubik, P.W., Sharma, P., and Dorn, R.I., 1991, Cosmogenic chlorine-36 production rates in terrestrial rocks: Earth and Planetary Science Letters, v. 105, p. 94-109.

APPENDIX A

COMMENT ON "SCALING FACTORS FOR PRODUCTION RATES OF IN SITU PRODUCED COSMOGENIC NUCLIDES: A CRITICAL REEVALUATION" BY TIBOR J. DUNAI

Darin Desilets[1], Marek Zreda[1], Nathaniel A. Lifton[2]

[1]Department of Hydrology and Water Resources, University of Arizona, Tucson AZ, 85721, USA

[2]Department of Geosciences, University of Arizona, Tucson, AZ, 85721, USA

[*Earth and Planetary Science Letters*, 188: 283-287 (2001)]

1. Introduction

In a recent paper, Dunai [1] discusses several problems with the altitude and latitude scaling of production rates given by Lal [2-4]. Dunai describes three major flaws in Lal's scaling: (1) cosmic-ray measurements are ordered according to geomagnetic latitude calculated from an axial dipole representation of the geomagnetic field; (2) the high-altitude (atmospheric depth 580-770 g cm^{-2}) attenuation length at 41° N geomagnetic latitude is assumed to be constant down to sea-level; and (3) the scaling expression is given in terms of elevation rather than atmospheric depth. In an attempt to improve on Lal's scaling model, Dunai derives a new model following a procedure similar to [3, 4], but incorporating some neutron monitor, nuclear emulsion and cloud chamber data unavailable to [3, 4]. In this comment we show that Dunai's scaling model is based on several false assumptions and neglects to consider the large body of cosmic-ray data collected since the 1950s. We also point out that geological factors affecting production of cosmogenic nuclides can be difficult to evaluate, and suggest that the ^{3}He data [5] used to confirm Dunai's [5] scaling may underestimate production rates.

2. Neutron monitor data

The neutron monitor data now available far exceed those available to Lal [4], but unfortunately Dunai limits his analysis to data collected in the 1950s. Since the 1950s, numerous latitude and altitude surveys of nucleon intensity have been conducted with neutron monitors [e.g., 6-13], of which Dunai appears unaware. These surveys adequately characterize the nucleon attenuation length (Λ) as a function of atmospheric depth and cutoff rigidity, and therefore the procedure described by Dunai of linking latitude curves is unnecessary (by using a constant Λ at one latitude to link latitude curves at different altitudes, a constant Λ at all latitudes can be calculated). By linking latitude curves, Dunai assumes that the attenuation length is constant between sea level and 4000 m. This is a poor assumption, since the neutron monitor attenuation length varies with altitude by about 8 g cm^{-2} between sea level and 4000 m at low latitudes [7].

3. Instrumental biases

The neutron monitor data cited in section 2 provides a fairly detailed picture of how the neutron monitor counting rate varies with latitude, altitude and solar activity. These data, however, should not be used without first correcting the neutron monitor counting rate for instrumental biases. For example, correcting the high-latitude, sea-level neutron monitor attenuation length (Λ_{NM}) for the effects of muons and constant background contributions decreases Λ_{NM} by about 10 g cm^{-2} [7]. The size of this correction should increase towards lower latitudes and decrease towards higher elevations.

A correction is also needed to account for the energy bias of the neutron monitorresponse. This correction is important because the nucleon attenuation length decreases with increasing median nucleon energy [14, 15]. The neutron monitor response is biased towards the high end of the nucleon energy spectrum because relatively high-energy nucleons (E>400 MeV) are counted by the neutron monitor more times than lower energy nucleons (E<400 MeV) [14, 15]. The size of this correction should increase with both decreasing latitude and increasing altitude.

The cloud chamber and emulsion data cited by Dunai ([16-18]) are also biased towards the higher end of the nucleon energy spectrum. The cloud chamber experiment by Brown [16], for example, undercounted 1 and 2 prong stars (low energy disintegrations) while Dixit [17] and Roederer [18] neglected these altogether. In the silver bromide emulsions used by [17] and [18], 1 and 2 star prongs correspond to energies of about 41 MeV and 90 MeV, respectively [16]. Again, the effect here is to underestimate the nucleon attenuation length. We corrected the data of [16] for this effect using the procedure outlined by Lal ([4], p. 67) and have obtained a value of 137±5 g cm^{-2} for the flux weighted attenuation length of nucleons with E>40 MeV. This compares to a value of 132±4 g cm^{-2} given by [16] (and cited by Dunai) for the uncorrected nucleon attenuation length between 700 and 1032 g cm^{-2}.

4. Inclination versus effective cutoff rigidity for ordering neutron monitor data

A unique feature of Dunai's work is his use of geomagnetic inclination for ordering neutron monitor data. Since the late 1960s, most neutron monitor measurements have been ordered in terms of effective vertical cutoff rigidity (P_C) [19-21]. The reliability of P_C has been confirmed by numerous sea-level latitude surveys that show a smooth andconsistent relationship between cutoff rigidity and nucleon intensity [11-13, 19].

In contrast, the relationship between inclination and the neutron intensity given by Dunai ([1], Fig. 3a) is rough and non-unique. Dunai observes a large discrepancy between neutron monitor data collected by Rose et al. [22] in the South Atlantic, Antarctic Sea and elsewhere ([1], p. 164). Although Dunai attributes the discrepancy to a highly anomalous field in this area ([1], p. 164), the inconsistencies between latitude survey data clearly indicate the inadequacy of using inclination for ordering neutron intensity data. In figure 1, we show that trajectory derived cutoffs effectively order the data of [22] and eliminate the anomalies seen in Dunai's figure 3. Contrary to Dunai's statement that the dipolar equation (Dunai's equation 1) is essentially the same as 'trajectory tracing'of cosmic ray particles ([1], p. 158), the two types of cutoffs differ considerably in both how they are derived and how they order neutron monitor data. The dipolar equation is an analytical solution to the equations of charged particle motion in a dipole field [23], whereas the trajectory tracing is a numerical method of calculating cutoffs in an empirically derived model of the real geomagnetic field. Dunai's equation 2

is nothing more than a modified version of the dipolar equation that still does not adequately account for the effects of the real geomagnetic field.

The main problem with ordering neutron monitor data according to geomagnetic inclination is that the effects of the eccentric dipole field are inadequately characterized. The method described by Dunai of linking latitude curves is valid only if the two curves cross the geomagnetic equator at nearly the same cutoff rigidity (by using Λ at one latitude to link latitude curves at different altitudes, Λ at all latitudes can be calculated). However, Dunai links the sea-level survey of Rose et al. [22], which crosses the geomagnetic equator at 14 GV, with the airborne survey of Sandström [24], which crosses at 17.4 GV, using a high-latitude attenuation length. This causes the low-latitude counting rate to appear to increase with a greater Λ_N than the true Λ_N.

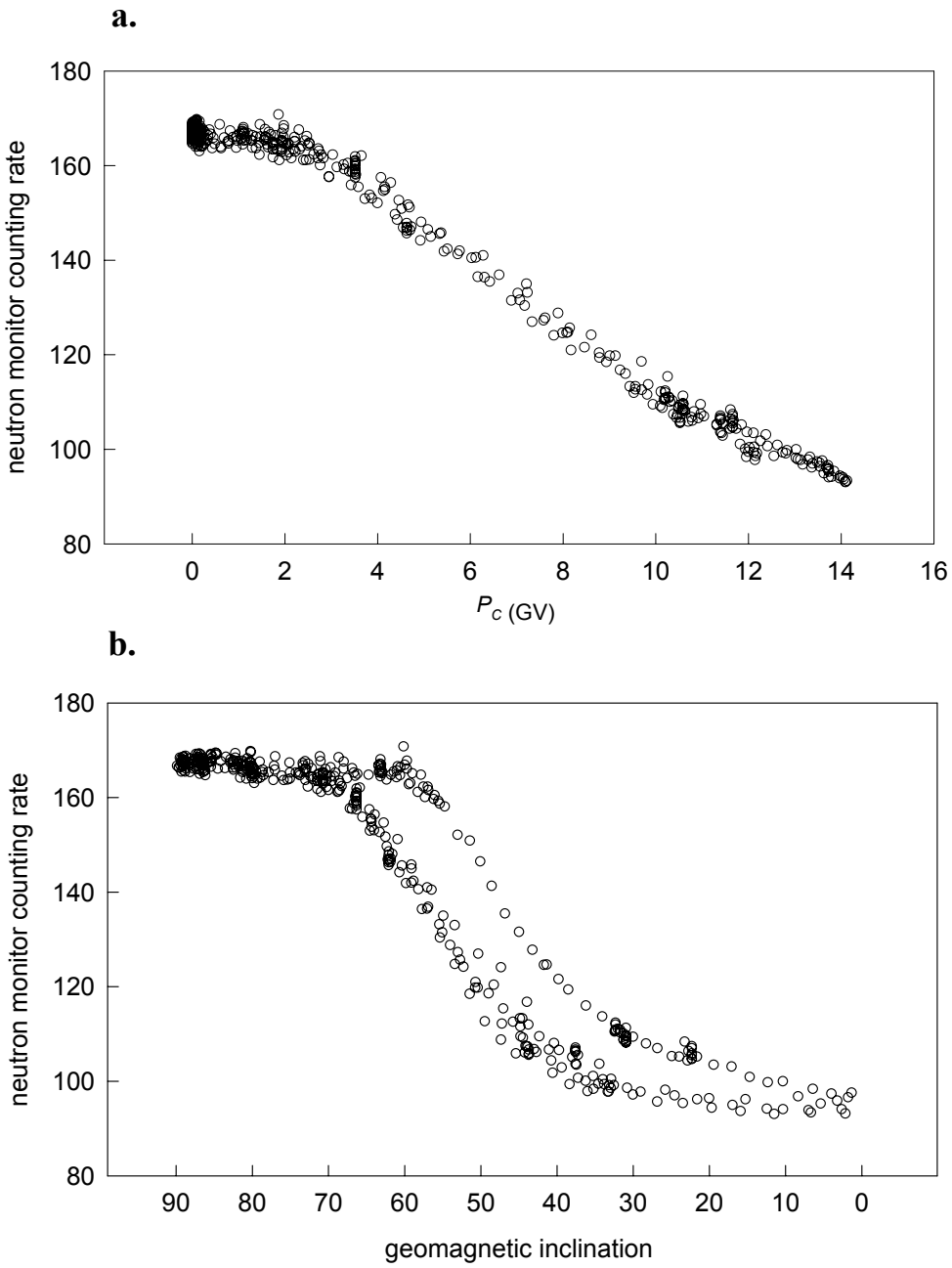

Figure 1. Sea-level neutron monitor data from Rose et al. [8] ordered according to ***a.*** effective vertical cutoff rigidity (P_C) and ***b.*** geomagnetic inclination.

5. Solar activity and the latitude effect

Dunai incorrectly assumes that the overall shape of the neutron flux versus latitude curves at large atmospheric depth (> 600 g cm^{-2}) is not affected by solar modulation of the primary flux ([1], p.163). He supports this claim by citing the results of Lockwood [25], who observed that fluctuations in the sea-level neutron monitor counting rates at Chicago, Ottawa and Durham, New Hampshire were of the same magnitude from 1954 to 1957 as those observed atop of Mt. Washington, New Hampshire (~820 g cm^{-2}). However, because all of these monitors were at low cutoffs (P_C~2 GV), it is impossible to ascertain the effect of solar activity on the shape of the neutron flux versus latitude curve from [25].

Several experiments since [25] have demonstrated that even at depths ranging from 680 to 1033 g cm^{-2} the shape of the latitude curve depends considerably on solar activity (Fig. 2) [26-29]. From solar minimum to solar maximum, the high-latitude sea-level nucleon flux decreases by about 8%, whereas at 680 g cm^{-2} the flux decreases by about 21%. At low-latitudes (~14 GV), solar modulations have a negligible effect on sea-levelneutron intensity [26], while at 680 g cm^{-2} the neutron flux varies by only about 5 % [30].

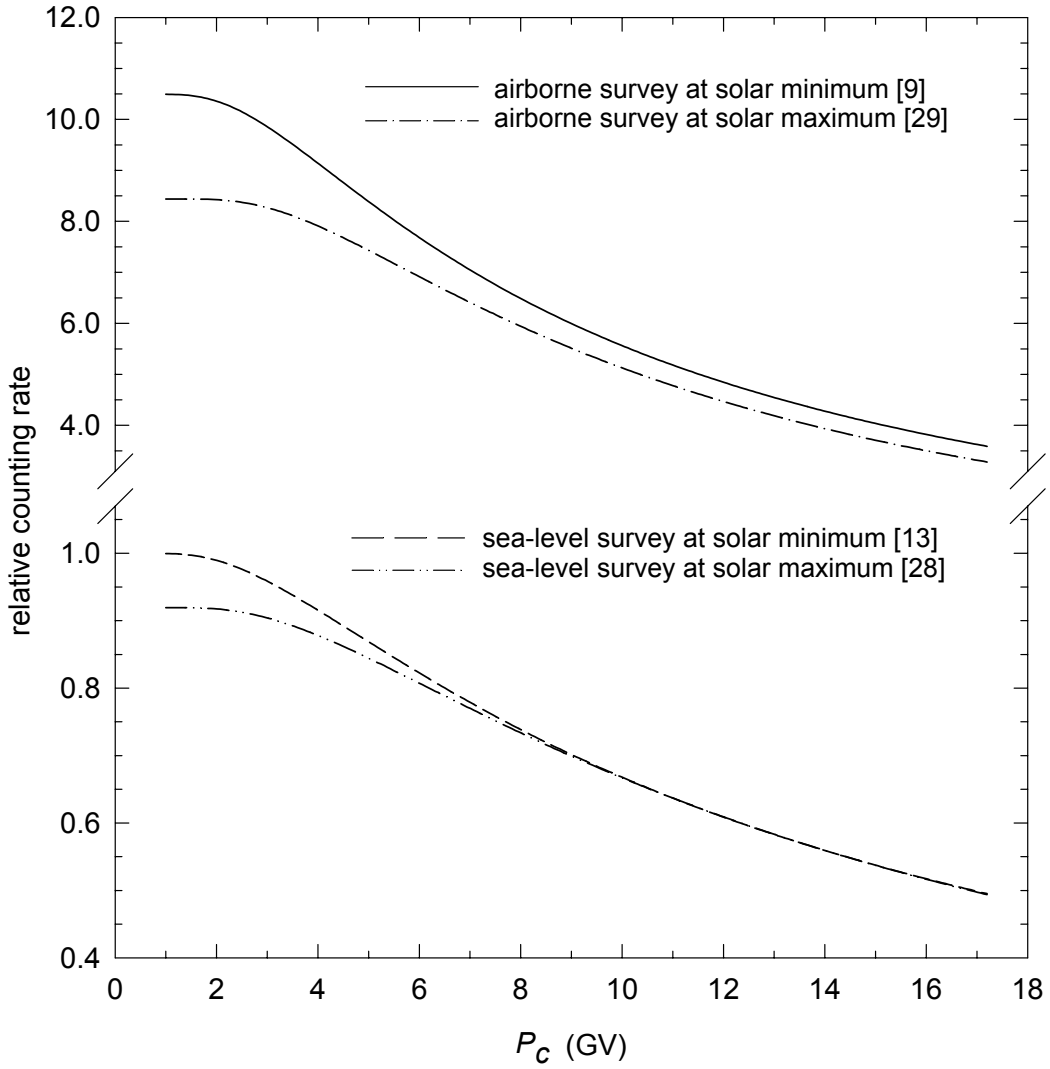

Figure 2. Latitude surveys of nucleon intensity conducted at solar maximum and solar minimum, normalized at 14 GV. Airborne and sea-level curves correspond to atmospheric depths of 680 g cm^{-2} and 1033 g cm^{-2}, respectively.

6. Measurements of cosmogenic ^{3}He

Geological samples can be used to test scaling models derived from neutron data [31], however, the uncertainty associated with geological samples is typically larger than the uncertainty in measurements of cosmic-ray intensity. This uncertainty is due to geological factors, such as erosion and ash cover, and analytical factors, such as errors in calculation of implanted ^{4}He. Here, we address three potential problems that may have affected the ^{3}He results of Dunai and Wijbrans [5] used to validate the scaling of [1]. First, the erosion depth of 2-4 mm reported in [5] is remarkably low for lava flows in the age range 150-280 ky. If the erosion rates reported in [5] are real, these lava flows could provide the best samples for calibration of other cosmogenic nuclides, such as ^{36}Cl.

Second, Dunai and Wijbrans [5] make no correction for sample thickness (in their case always about 5 cm). They assume that the neutron intensity is constant in the top 10 g cm^{-2} of rock, and, therefore, the production rate of ^{3}He is constant in the top 5 cm. But this constant neutron intensity result was derived using Monte Carlo simulations [32], with resolution insufficient for accurate determination of the shape of the neutron intensity function. The results of these computations have not been confirmed empirically and should be used with caution. Correcting the ^{3}He data of [5] for sample thickness using an exponential model would increase the production rates by approximately 3%.

Third, Dunai and Wijbrans [5] collected a small number of samples from each lava flow, and all samples from the same lava flow were within 10 m from each other. This sampling strategy makes the results vulnerable to effects of shielding by soil or ash,

which might have been present at some time. Problems associated with spatially varying ash cover and erosion may be minimized by collecting more samples from a wider area.

In addition to the above potential problems, Ackert's [33] and Dunai and Wijbran's [5] ^{3}He data are not directly comparable because of the following considerations. First, the ^{3}He data reported by Dunai [5] have been corrected for implanted ^{4}He; the data in Ackert [33] have not. If the correction for Ackert's samples is similar to the corrections in [5], the production rate of Ackert would decrease by approximately 10%. Second, Ackert [33] production rates are on clinopyroxene. Although ^{3}He production rates are not strongly composition dependent, variability of up to 8% is predicted by theory [2, 32]. Third, Ackert [33] corrected for sample thickness using the attenuation length of 160 g cm^{-2}; Dunai [5] did not make such corrections. Fourth, and most important, the production rate reported by Ackert [33] was preliminary. It has been revised due to new ^{40}Ar/^{39}Ar and K-Ar ages obtained from new samples, which were better suited to the technique (R. Ackert, personal communication, October 2000), and ^{3}He measurements in olivine. The new production rate is 25% higher than that reported by [33]. It cannot be reconciled with the production rate of Dunai [5] using the scaling formulation proposed by Dunai [1], and neither can the two production rates be reconciled using Lal's [2] scaling.

Acknowledgements

We thank Robert Ackert for providing useful information on ^{3}He production rates. We also thank Devendra Lal for his comments. This work was supported by National Science Foundation grants EAR-0001191 and EAR-9614366 and Packard Fellowship 95-1832.

References

1 T.J. Dunai, Scaling factors for production rates of in situ produced cosmogenic nuclides: a critical reevaluation, Earth and Planetary Science Letters 176, 157-169, 2000.

2 D. Lal, Cosmic ray labeling of erosion surfaces: *in situ* nuclide production rates and erosion models, Earth and Planetary Science Letters 104, 424-439, 1991.

3 D. Lal, P.K. Malhotra and B. Peters, On the production of radioisotopes in the atmosphere by cosmic radiation and their application to meteorology, Journal of Atmospheric and Terrestrial Physics 12, 306-328, 1958.

4 D. Lal, Investigation of nuclear interactions produced by cosmic rays, PhD thesis, 1958.

5 T.J. Dunai and J.R. Wijbrans, Long-term cosmogenic 3He production rates (152 ka-1.35 Ma) from ^{40}Ar/^{39}Ar dated basalt flows at 29° N latitude, Earth and Planetary Science Letters 176(1), 147-156, 2000.

6 F. Bachelet, P. Balata, E. Dyring and N. Iucci, Attenuation coefficients of the cosmic-ray nucleonic component in the lower atmosphere, Il Nuovo Cimento 35, 23-35, 1965.

7 H. Carmichael and M. Bercovitch, V. Analysis of IQSY cosmic-ray survey measurements, Canadian Journal of Physics 47, 2073-2093, 1967.

8 B.C. Raubenheimer and P.H. Stoker, Various aspects of the attenuation coefficient of a neutron monitor, Journal of Geophysical Research 79, 5069-5076, 1974.

9 H. Coxell, M.A. Pomerantz and S.P. Agarwal, Survey of cosmic-ray intensity in the lower atmosphere, Journal of Geophysical Research 70, 143-154, 1965.

10 H. Carmichael and M. Bercovitch, II. Cosmic-ray latitude survey in Canada in December, 1965, Canadian Journal of Physics 47, 2051-2055, 1967.

11 M.S. Potgeiter, H. Moraal, B.C. Raubenheimer and P.H. Stoker, Modulation of cosmic rays during solar minimum. Part 3. Comparison of the latitude distributions for the periods of solar minimum during 1954, 1965 and 1976, South African Journal of Physics 3, 90-94, 1980.

12 H. Moraal, M.S. Potgieter and P.H. Stoker, Neutron monitor latitude survey of cosmic ray intensity during the 1986/1987 solar minimum, Journal of Geophysical Research 94, 1459-1464, 1989.

13 G. Villoresi, N. Iucci, F. Re, F. Signoretti, N. Zangrilli, S. Cecchini, M. Parisi, C. Signorini, M.I. Tyasto, O.A. Danilova and N.G. Ptitsyna, Latitude survey of cosmic ray nucleonic component during 1996-1997 from Italy to Antarctica, in: 8th Annual GIFCO Conference 58, Bologna, 1997.

14 R.A. Nobles, R.A. Alber, E.B. Hughes, L.L. Newkirk and M. Walt, Neutron multiplicity monitor observations during 1965, Journal of Geophysical Research 72, 3817-3827, 1967.

15 W.K. Griffiths, C.V. Harmon, C.J. Hatton, P.L. Marsden and P. Ryder, The intensity variations of selected multiplicities in the Leeds NM64 neutron monitor, Canadian Journal of Physics 46, S1044-S1047, 1968.

16 W.W. Brown, Cosmic-ray nuclear interactions in gases, Physical Review 93, 528-534, 1954.

17 K.R. Dixit, The statistics of 29000 stars observed in nuclear emulsions in Kenya, Zeitschrift für Naturforschung 10a(339-341), 1955.

18 J.G. Roederer, Über die Absorption der Nukleonenkomponente der kosmischen Strahlung in -21° geomagnetischer Breite, Zeitschrift für Naturforschung 7a, 765-771, 1952.

19 M.A. Shea, D.F. Smart and J.R. McCall, A five degree by fifteen degree world grid of trajectory-determined vertical cutoff rigidities, Canadian Journal of Physics 46, S1098-S1101, 1968.

20 M.A. Shea and D.F. Smart, A world grid of calculated cosmic ray vertical cutoff rigidities for 1980.0, in: 18th International Cosmic Ray Conference, pp. 415-418, 1983.

21 M.A. Shea, D.F. Smart and L.C. Gentile, Estimating cosmic ray vertical cutoff rigidities as a function of the McIlwain L-parameter for different epochs of the geomagnetic field, Physics of the Earth and Planetary Interiors 48, 200-205, 1987.

22 D.C. Rose, K.B. Fenton, J. Katzman and J.A. Simpson, Latitude effects of the cosmic ray nucleon and meson components at sea level from the Arctic to the Antarctic, Canadian Journal of Physics 34, 968-984, 1956.

23 A. Bhattacharyya and B. Mitra, Changes in cosmic ray cut-off rigidities due to secular variations of the geomagnetic field, Annales Geophysicae-Atmospheres Hydrospheres and Space Sciences 15(6), 734-739, 1997.

24 A.E. Sandström, Cosmic ray soft component measurements during a flight from Scandinavia across the North Pole and around Asia and Europe, Nuovo Cimento VIII, Serie X, Suppl., 263-276, 1958

25 J.A. Lockwood, Variations in the cosmic-ray nucleonic intensity, Physical Review 112, 1750-1758, 1958.

26 M.A. Forman, The relation between latitude and solar-cycle variations in the neutron-monitor mass-absorption coefficient, Canadian Journal of Physics 46, S1087-S1089, 1968.

27 F. Bachelet, N. Iucci, G. Villoresi and N. Zangrilli, The cosmic-ray spectral modulation above 2 GV. IV. The Influence on the attenuation coefficient of the nucleonic component, Nuovo Cimento 11 B, 1-12, 1972.

28 T.M. Aleksanyan, I.V. Dorman, L.I. Dorman, V.K. Babayan, A.V. Belov, Y.L. Blokh, N.S. Kaminer, V.K. Korotkov, I.Y. Libin, A.A. Manshilina, Y.E. Mashkov, I.V. Mymrina, S.I. Rogovaya, A.M. Sitnov, K.F. Yudakhin and V. Yanke, Geomagnetic effects in cosmic rays and spectrum of the increase before magnetic storms, Izvestiya Akademii Nauk SSSR, Seriya Fizicheskaya 46, 1689-1691, 1982.

29 D.W. Kent and M.A. Pomerantz, Cosmic ray intensity variations in the lower atmosphere, Journal of Geophysical Research 76, 1652-1661, 1971.

30 D.W. Kent, H. Coxell and M.A. Pomerantz, Latitude survey of the frequency of multiple events in an airborne neutron monitor, Canadian Journal of Physics 46, S1082-S1086, 1968.

31 M.G. Zreda, F.M. Phillips, D. Elmore, P.W. Kubik, S. P. and R.I. Dorn, Cosmogenic chlorine-36 production rates in terrestrial rocks, Earth and Planetary Science Letters 105, 94-109, 1991.

32 J. Masarik and R.C. Reedy, Terrestrial cosmogenic-nuclide production systematics calculated from numerical simulations, Earth and Planetary Science Letters 136, 381-396, 1995.

33 R.P. Ackert, D.J. Barclay, H.W. Borns, P.E. Calkin, M.D. Kurz, J.L. Fastook and E.J. Steig, Measurements of past ice sheet elevations in interior West Antarctica, Science 286(5438), 276-280, 1999.

APPENDIX B

ON SCALING COSMOGENIC NUCLIDE PRODUCTION RATES FOR ALTITUDE AND LATITUDE USING COSMIC-RAY MEASUREMENTS

Darin Desilets and Marek Zreda

[*Earth and Planetary Science Letters*, 193: 213-225 (2001)

Abstract

The wide use of cosmogenic nuclides for dating terrestrial landforms has prompted a renewed interest in characterizing the spatial distribution of terrestrial cosmic rays. Cosmic-ray measurements from neutron monitors, nuclear emulsions and cloud chambers have played an important role in developing new models for scaling cosmic-ray neutron intensities and, indirectly, cosmogenic production rates. Unfortunately, current scaling models overlook or misinterpret many of these data. In this paper, we describe factors that must be considered when using neutron measurements to determine scaling formulations for production rates of cosmogenic nuclides.

Over the past 50 years, the overwhelming majority of nucleon flux measurements have been taken with neutron monitors. However, in order to use these data for scaling spallation reactions, the following factors must be considered: (1) sensitivity of instruments to muons and to background; (2) instrumental biases in energy sensitivity; (3) solar activity; and (4) the way of ordering cosmic-ray data in the geomagnetic field. Failure to account for these factors can result in discrepancies of as much as 7% in neutron attenuation lengths measured at the same location. This magnitude of deviation can result in an error on the order of 20% in cosmogenic production rates scaled from 4300 m to sea level. The shapes of latitude curves of nucleon flux also depend on these factors to a measurable extent, thereby causing additional uncertainties in cosmogenic production rates. The corrections proposed herein significantly improve our ability to transfer scaling formulations based on neutron measurements to scaling formulations

applicable to spallation reactions, and, therefore, constitute an important advance in cosmogenic dating methodology.

1. Introduction

Cosmogenic nuclides produced *in-situ* in terrestrial rocks have been applied to exposure dating since the mid 1980s, but until recently [1], there had been no critical review of the commonly used altitude and latitude scaling of cosmogenic production rates derived by Lal [2] and given in [3, 4]. Dunai [1] has proposed a major revision to [2-4] based on data from neutron monitors, nuclear emulsions and cloud chambers. However, as discussed by Desilets et al. [5], Dunai's scaling model has many similar shortcomings to Lal's model. These two models have the following weaknesses: (1) Cosmic-ray data are ordered according to parameters that inadequately describe the geomagnetic shielding effect. Latitude survey data are ordered according to geomagnetic inclination [1] and according to geomagnetic latitude [2]. However, the cosmic-ray intensity varies by as much as 15% along both constant geomagnetic latitude and inclination. (2) The effects of solar activity on latitude and altitude survey data are either completely neglected [1] or addressed unclearly [2]. (3) The energy dependence of the nucleon attenuation is either underestimated, because of limited data [2], or ignored [1]. (4) Both models are based on a small selection of cosmic-ray data, confined mostly to the 1950s.

In order for the cosmogenic nuclide dating method to be successfully applied at different locations, the altitude and latitude scaling of nucleon intensity must be accurately constrained. A more refined scaling model can be derived from the numerous

latitude and altitude surveys performed since the 1950s; however, these data must be used with caution. The purposes of this paper are to review some of the major cosmic-ray surveys conducted over the past 50 years and to discuss how these data can be used to derive an accurate scaling model. We also review some basic concepts and definitions in cosmic-ray physics in order to build the framework for these discussions.

2. Definitions

Primary cosmic rays are charged particles impinging on earth with relativistic energies. Cosmic rays arriving from outside the solar system are known as *galactic cosmic rays* (GCRs), whereas those arriving from the sun are known as *solar cosmic rays* (SCRs) [6]. Secular variations in solar activity cause the *low-energy* (E<1 GeV) GCR flux to vary by as much as an order of magnitude, whereas the *high-energy* GCR flux (E>10 GeV) is mostly insensitive to solar activity [7, p. 3].

Secondary cosmic-rays are produced through the interaction of primary cosmic rays with atmospheric and terrestrial nuclei. The secondary flux includes strongly interacting particles (e.g. neutrons, protons and pions), weakly interacting particles (e.g. muons), and electromagnetic radiation (e.g. gamma and beta radiation). Neutrons are responsible for the majority of nuclear transformations near the earth's surface [4].

Neutrons may be classified by energy according to the types of nuclear reactions in which they are involved. Although there is no standard convention for classifying neutrons, the following definitions are useful [8, 9, p. 445]:

High-energy neutrons are produced through direct reactions of primary and secondary cosmic-ray particles with terrestrial nuclei. In a direct reaction, the incident particle interacts separately with a small number of individual nucleons, usually at the surface of the nucleus. A high-energy neutron may in turn liberate additional high-energy particles in a chain-reaction process. These reactions may occur within the nucleus (intranuclear cascade) or between nuclei (internuclear cascade). The de Broglie wavelength of a particle is inversely related to particle momentum, and therefore at lower momenta, interactions with the entire nucleus become more probable. The energy of the incident particle is then distributed throughout the entire nucleus in what is known as a compound-nucleus reaction. Spallogenic production of nuclides may occur from both direct- and compound-nucleus reactions. We define high-energy neutrons to be those capable of producing spallation reactions, which corresponds to energies ranging from primary energies down to about 10 MeV.

Fast neutrons are produced primarily from the de-excitation of nuclei following compound-nucleus reactions. A common mode of de-excitation is through the emission of neutrons and protons according to a Maxwellian energy spectrum peaked at about 1 MeV [10]. This process is known as nuclear evaporation, by analogy to molecules evaporating from the surface of a heated liquid. Unlike neutrons produced in direct reactions, the energy spectrum and angular distribution of evaporation neutrons does not depend critically on the energy and direction of the initiating particle. In other words, the excited nucleus does not ‘remember’ these properties of the initiating particle. However, as the energy of the incident nucleon increases, the nucleus is more likely to be excited to

a higher ‘temperature’, and the average number of neutrons evaporated by the nucleus therefore increases. Evaporation reactions may also be induced by particles such as pions, muons and photons. Fast neutrons generally have insufficient energy to produce further evaporation reactions, and therefore do not initiate nuclear spallations. The energy range for fast neutrons is defined here to be approximately from 10 MeV to 100 keV.

Slow neutrons are produced from the slowing down (‘moderation’) of fast neutrons, through elastic and inelastic collisions with nuclei. We define slow neutrons to be those with energies on the order of 1 keV.

Thermal and *epithermal* neutrons are produced from the slowing down of fast neutrons to energies on the order of the vibrational motion of nearby molecules. An important characteristic of thermal and epithermal neutrons is their relatively high probability of being absorbed by nuclei. Thermal neutrons are defined to be in vibrational equilibrium with the molecules of the surrounding medium, which at temperature of 293.16 K corresponds to an average energy of 0.025 eV. Epithermal neutrons are defined here as those with energies between 100 eV and the cadmium cutoff energy for transparency to neutrons of 0.5 eV.

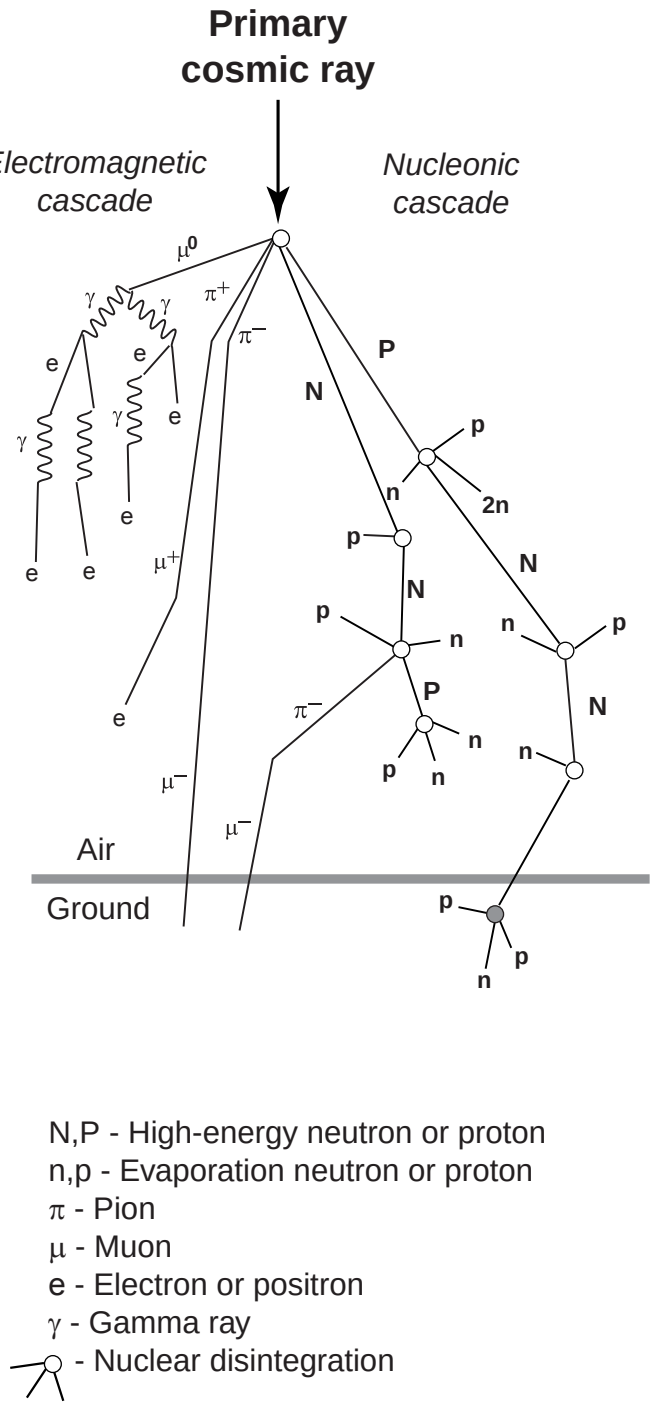

Figure 1. Propagation of the secondary cascade through the atmosphere (adapted from [11]).

3. The nucleon attenuation length

Primary cosmic rays collide with oxygen and nitrogen nuclei near the top of the atmosphere, initiating cascades of protons, neutrons and other secondary particles (Fig. 1). In the lower atmosphere (>200 g cm^{-2}), the nucleon flux diminishes as a function of mass-shielding depth approximately according to:

$$N_2 = N_1 \, exp\left(\frac{Z_1 - Z_2}{\Lambda_N}\right) \tag{1}$$

where N_1 and N_2 are the nucleon fluxes at depths Z_1 and Z_2 (g cm^{-2}), respectively, and Λ_N is the nucleon attenuation length (g cm^{-2}) (also referred to as the absorption mean free path, absorption length [12, p. 174] or e-folding length). A nucleonic cascade loses energy through nuclear collisions and electromagnetic interactions, and this energy loss depends on the total mass of air transited by the cascade. The earth's atmosphere is approximately 1033 g cm^{-2} thick and has a density that varies with altitude, latitude and time. A hypothetical relationship between mass-shielding depth and altitude corresponding to the year-round, mid-latitude pressure distribution is given by the U.S. standard atmosphere [13] (Fig. 2). Deviations from the U.S. standard atmosphere in areas of statistically high and low pressure, such as the Siberian High and the Aleutian Low, should be taken into account when scaling cosmogenic production rates [14].

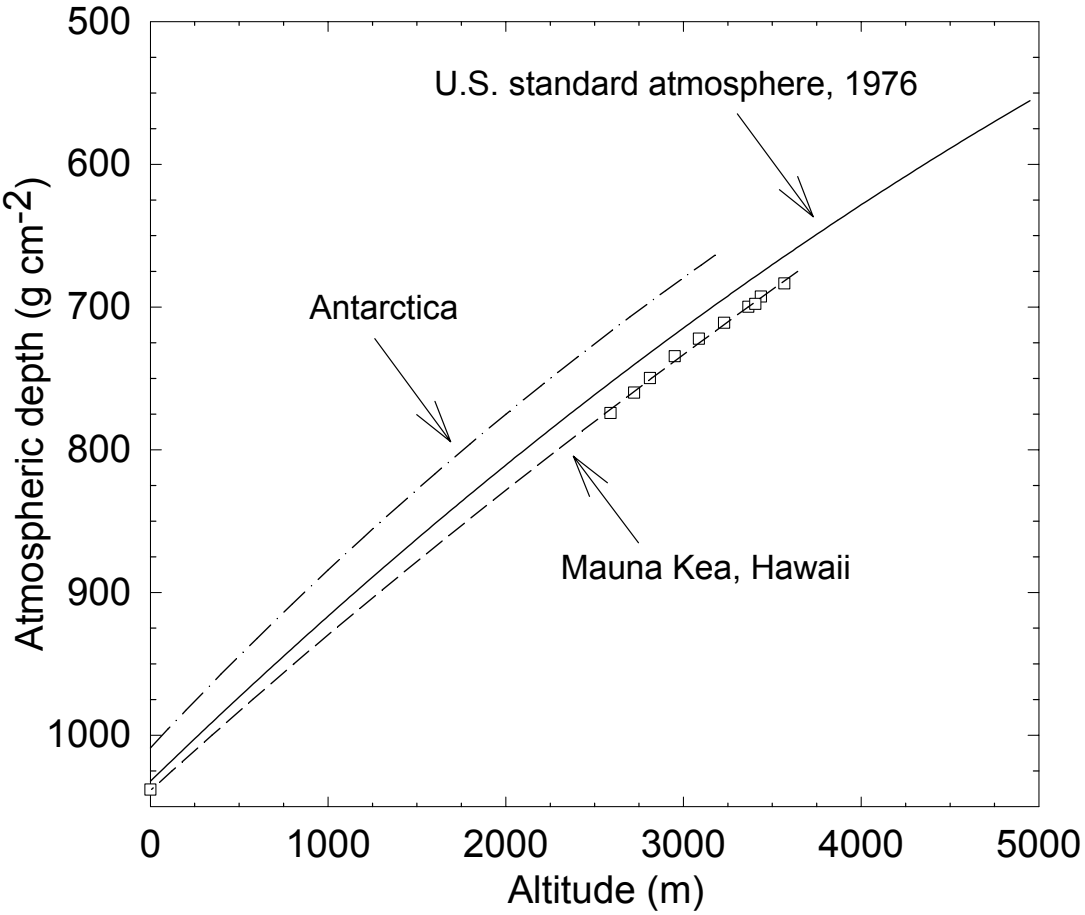

Figure 2. The relationship between atmospheric depth and altitude in the U.S. standard atmosphere [13]. For comparison, relationships found in Antarctica [14] and in Hawaii (our own data) are shown. The curve for Hawaii is based on Global Positioning System (GPS) and barometer measurements (given by open squares) taken on 7-12 April 2000. Barometric measurements are 10 minute averages and are therefore not necessarily representative of long term or even recent pressure conditions on Hawaii.

Equation 1 assumes a monodirectional, monoenergetic beam of stable particles that does not initiate chain reactions. The terrestrial cosmic-ray flux, however, follows an approximately power-law energy spectrum, propagates as a cascade, includes short-lived particles (e.g. pions and muons), and is distributed about the zenith roughly according to a cosine function [15]. Nonetheless, equation 1 provides a satisfactory description of cosmic-ray nucleon absorption over small atmospheric depths (~100 g cm^{-2}).

Previous workers [1, 4] used atmospheric measurements of nucleon intensity to derive the altitude dependence of spallation reactions. According to Dunai [1], Lal's [4] scaling model overestimates the value of the atmospheric attenuation length for cosmogenic nuclide production by nucleons (here termed $\Lambda_{prod,N}$) at both high and low latitudes. This claim is based on measurements from cloud chambers, nuclear emulsions and neutron monitors [1] that seem to indicate low-altitude attenuation lengths of 130 g cm^{-2} at high latitudes and 149 g cm^{-2} at low latitudes. Lal's scaling formula gives values of 135 g cm^{-2} and 157 g cm^{-2}, respectively, for these locations. Here, we discuss how instrumental biases affect measurements of the nucleon attenuation length and how these biases can at least partially reconcile discrepancies between measured attenuation lengths. We also introduce neutron monitor data from extensive altitude and latitude surveys of nucleon intensity.

3.1. Neutron monitor data

The most comprehensive and well-reported investigation of the global distribution of nucleon intensity is probably the neutron monitor survey conducted by Carmichael et al. [16-18] during the International Quiet Sun Year (1965-1966). These measurements are ideally suited for scaling neutron monitor counting rates because: (1) they cover a wide range of geomagnetic cutoffs (0.5-13.3 GV) and atmospheric depths (200-1033 g cm^{-2}); (2) they have been corrected for secular variations in the primary cosmic-ray intensity and temperature effects; and (3) they were taken with a land-based neutron monitor and an airborne monitor that had been cross-calibrated.

Several other surveys of neutron monitor attenuation lengths have also been published, but unfortunately the experimental procedures, corrections and raw data have not always been reported in adequate detail. The only survey of comparable scope to [16-18] covered a similar range of cutoffs, but was mostly limited to depths greater than 880 g cm^{-2} [19]. An earlier survey by Bachelet et al. [20] defined the general characteristics of the neutron monitor attenuation length (Λ_{NM}) as a function of atmospheric depth and cutoff rigidity, but was more limited in scope. Neutron monitor attenuation lengths have also been evaluated using data from the world-wide network of fixed neutron monitors [21]. Other surveys generally give relationships consistent with that found by [16-18].

The primary goal of [16-20, 22] was to determine the altitude and latitude dependence of Λ_{NM} so that counting rates of neutron monitors could be corrected for small temporal variations in barometric pressure. The survey by [16-18] shows that Λ_{NM}

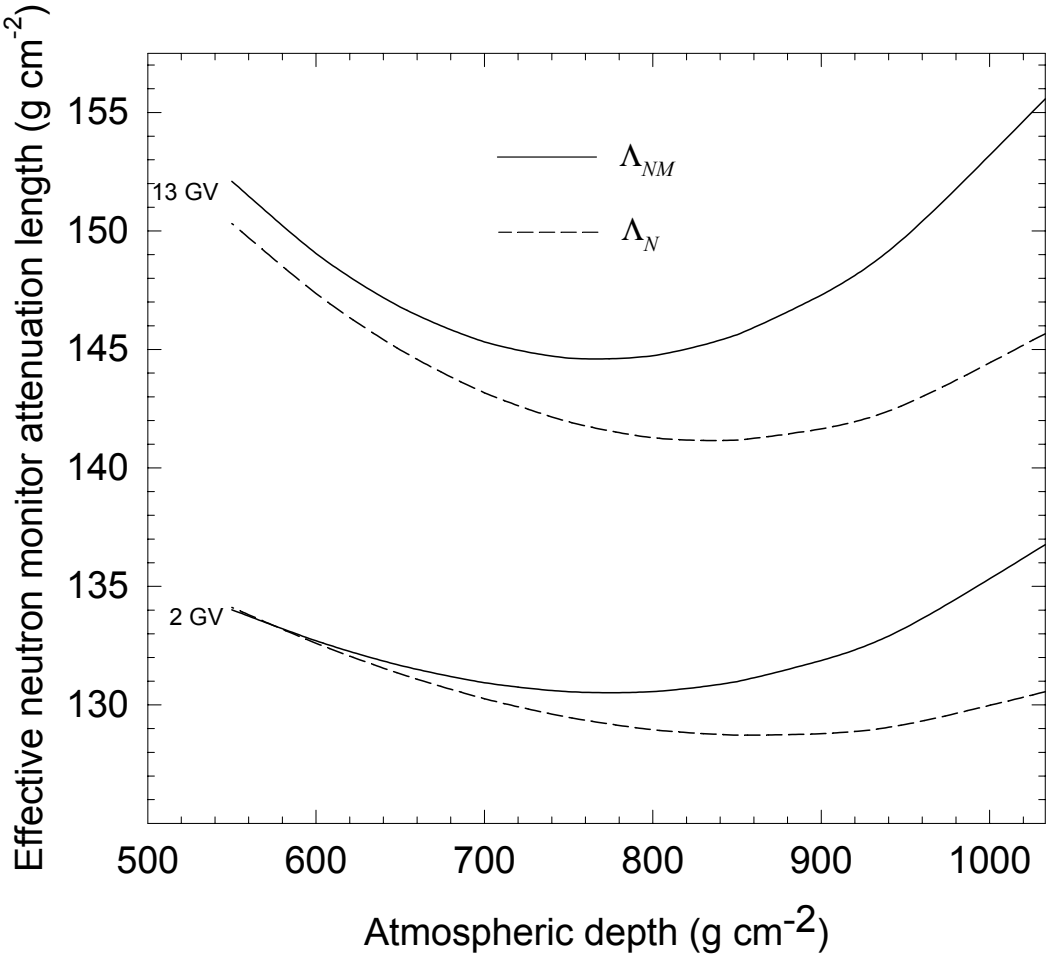

Figure 3. Effective attenuation lengths for an NM-64 neutron monitor based on measurements taken in April-June, 1965 [18]. The effective nucleon attenuation length was calculated by removing the contribution of muons and background to Λ_{NM} using Table 1 and equation 2. The effective attenuation length reduces the neutron monitor counting rate at some depth to the sea level counting rate.

reaches a minimum near 850 g cm^{-2} (Fig. 3), in agreement with [19] and [20]. Between the top of the atmosphere and 850 g cm^{-2}, Λ_{NM} decreases with increasing depth as the overall energy of the cascade dissipates [23]. However, beyond this depth Λ_{NM} increaseswith increasing depth, which is attributable to the combined effects of three phenomena [18]: (1) Muons interact with the lead portion of a neutron monitor to produce neutrons that contribute to the total counting rate. Because the muon flux is more highly penetrating than the nucleon flux, Λ_{NM} at greater atmospheric depths reflects the increased proportion of muons contributing to the counting rate. Muon sensitivity near sea level appears to be a feature of all neutron monitors based on the IGY/NM-64 design [24]. (2) Alpha contamination of the counter tubes produces a constant background amounting to about 1% of the high-latitude sea-level counting rate. (3) Cosmic-ray nucleons incident from oblique angles are selectively filtered with depth in the atmosphere. The omnidirectional nucleon flux therefore attenuates more rapidly with increasing atmospheric depth than does the vertical nucleon flux.

For neutron monitor counting rates to be used for scaling production rates, muon and background contributions must be removed. Fortunately, the relative contributions of muons and neutrons to the neutron monitor counting rate are fairly well known (Table 1).

Table 1. Contributions to the NM-64 neutron monitor counting rate [24] and attenuation lengths for fast and slow muons [15].

	2 GV		13 GV	
	Contribution (%)	Λ (g cm^{-2})	Contribution (%)	Λ (g cm^{-2})
Slow muons	3.6 ± 0.7	240	6.0	281
Fast muons	2.0 ± 0.4	560	3.3	640
Background	1.0	∞	1.8	∞

Attenuation lengths for fast muons and slow negative muons as a function of P_C are also fairly well known [15]. Assuming, after [18, 19] and based on [25], that slow and fast muon fluxes have similar latitude distributions, we calculated Λ_N from the neutron monitor data of [16, 17] and the values in Table 1 using the relationship:

$$\frac{1}{\Lambda_{NM}} = \frac{\sum_{i=1}^{n} \frac{\Lambda_i}{N_i}}{\sum_{i=1}^{n} N_i} = \frac{\frac{\Lambda_N}{N_N} + \frac{\Lambda_{\mu^-(s)}}{N_{\mu^-(s)}} + \frac{\Lambda_{\mu(f)}}{N_{\mu(f)}} + \frac{\Lambda_B}{N_B}}{N_N + N_{\mu^-(s)} + N_{\mu(f)} + N_B} \tag{2}$$

where N_i and Λ_i are the counting rate and attenuation length, respectively, for the i^{th} component. At sea level and high latitude, contributions from nucleons, slow negative muons, fast muons and constant background (N_N, $N_{\mu\text{-}(s)}$, $N_{\mu(f)}$, and N_B, respectively) account for more than 98% of the neutron monitor counting rate.

Attenuation lengths given by Dunai [1] (~130 g cm^{-2} at 2 GV) appear to agree reasonably well with Λ_N measured with a neutron monitor (Fig. 3). However, Λ_N is equivalent to $\Lambda_{prod,N}$ only if either the nucleon attenuation length is independent of energy (the shape of the nucleon energy spectrum is invariant with depth) or the energy sensitivity of the measuring apparatus is identical in form to the energy dependence of nuclide production. In the following three sections we show that, strictly speaking, neither assumption is valid.

3.2. Energy dependence of the nucleon attenuation length

Data from neutron multiplicity counters [26-28] demonstrate that Λ_N decreases with median nucleon energy. A multiplicity counter is a neutron monitor that records the number of counting events occurring within a gating time of about 700-1000 ms [27, 29]. Each high-energy nucleon interacting with the monitor produces about 1.44 counts, on average, at high latitude and sea level [29]. However, the number of counts resulting from each interaction depends on the energy of the incoming nucleon. This is because a neutron monitor records evaporation neutrons, and the average number of evaporation neutrons produced in a reaction increases with the increasing energy of the interacting nucleons. A neutron multiplicity counter, therefore, provides information on the energy spectrum of secondary cosmic-ray nucleons [29]. Figure 4 demonstrates that the attenuation length decreases with increasing median nucleon energy, at least in the range 120-700 MeV. This behavior is a consequence of the fact that the lower energy nucleons in a particle cascade are produced (both directly and indirectly) from nucleons of higher

energy, and since no cosmic-ray effect can decrease with increasing depth any faster than the primary radiation from which it originates [30, p. 558] the attenuation length must decrease or remain constant with increasing nucleon energy.

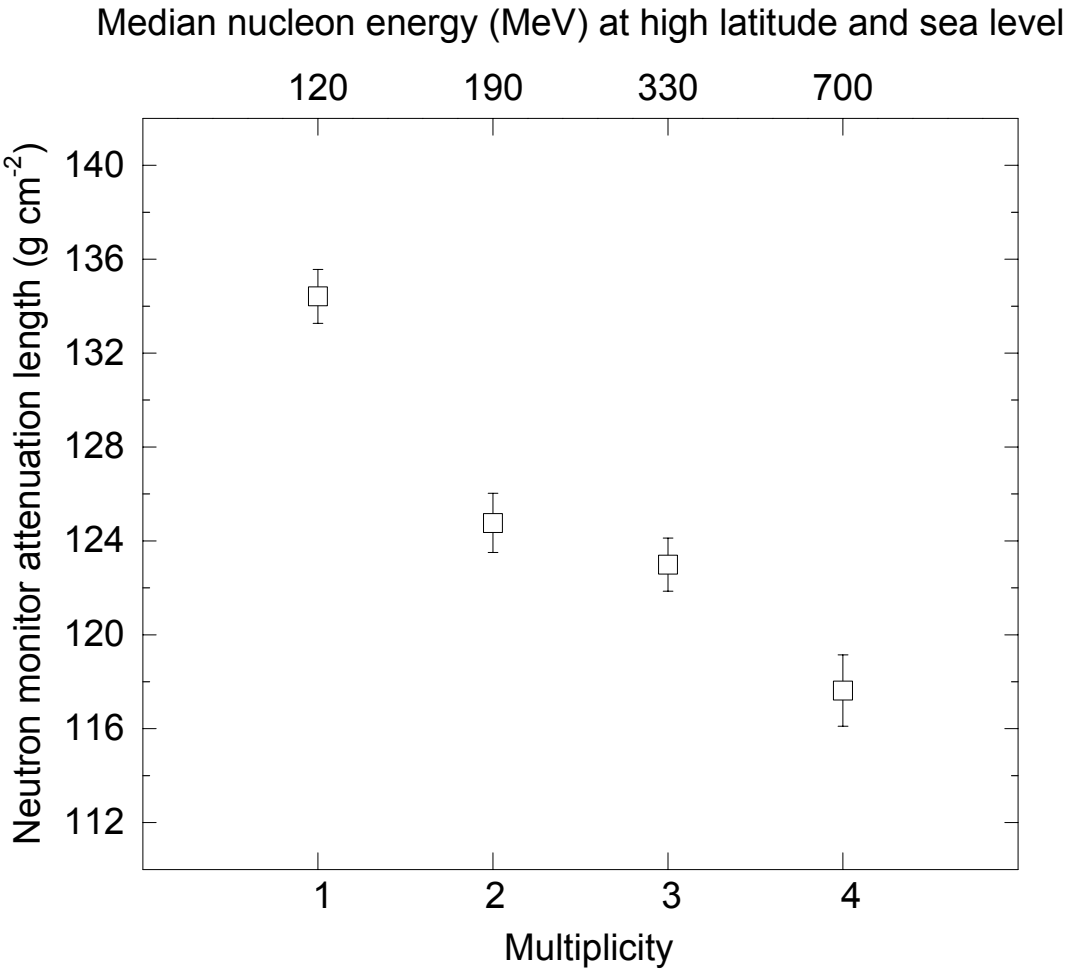

Figure 4. Neutron monitor attenuation length (corrected for muon and background contributions) as a function of neutron multiplicity. Measurements taken between 952 and 544 g cm^{-2} at 2 GV with an IGY type monitor [28]. Median nucleon energies are based on calculations for a high-latitude sea-level IGY neutron monitor [24].

In contrast to Dunai [1], Lal [2] explicitly recognized the energy dependence of Λ_N in deriving his scaling model. However, prior to [27], Λ_N was commonly assumed to be constant with energy up to about 400 MeV. This assumption was based on early experiments and simplified cascade models [2, 10, 12, 27], despite other experimentalevidence to the contrary [30, p. 564, 31, 32]. Under the assumption that the slow neutron flux is proportional to the high-energy nucleon flux for energies below 400 MeV, Lal [2] based a major portion of his scaling on airborne measurements of slow neutron fluxes [33]. Recognizing that for some reactions a significant portion of cosmogenic nuclide production occurs at energies above 400 MeV, and that at these higher energies the nucleon attenuation length decreases with energy, Lal [2] applied corrections that tended to decrease attenuation lengths derived from slow neutron measurements. Hence, Lal [2-4] gives scaling factors for both slow neutron fluxes and for the total nuclear disintegration rate in the atmosphere. Although the correction applied by Lal [2] is approximate and fails to account for the energy dependence of Λ_N below 400 MeV, Lal considered that the altitude dependence of a particular reaction may depend on the energy at which that reaction occurs. Future work should also consider this energy dependence.

3.3. Energy sensitivity of neutron monitors

Because high-energy nucleons produce more neutron monitor counts per interaction than low-energy nucleons, the neutron monitor response is biased towards the higher end of the nucleon energy spectrum. An additional effect is produced by 7.5 to 28 cm of

paraffin or polyethylene (known as the 'reflector') on the outside of the monitor which substantially modulates the flux of nucleons with E<50 MeV. Hughes and Marsden [29], for example, showed that an IGY neutron monitor records a negligible number of counts from nucleons with E<50 MeV. These considerations imply that for nuclide production at low thresholds (~20 MeV), such as $K(n,x)^{36}Cl$ and $Ca(n,x)^{36}Cl$ reactions [15], Λ_N measured from a neutron monitor may underestimate $\Lambda_{Prod,N}$, and, therefore, a correction may be needed in the direction opposite to that applied by [2] to slow neutron data. This correction should be most important for neutron monitors with thick reflectors, such as the IGY type, and less important for those with thin reflectors, such as the NM-64 type. On the other hand, for the reaction $O(n,x)^{10}Be$ produced by neutrons having a median energy (E_{med}) of ~140 MeV at high latitude and sea level, the neutron monitor response (E_{med} = 130-160 MeV) may accurately describe the altitude dependence of cosmogenic nuclide production [15].

3.4. Energy sensitivity of cloud chambers and emulsions

Cloud chambers and nuclear emulsions record the tracks of ionizing particles produced in nuclear disintegrations (or 'stars') initiated by cosmic rays. Each track is known as a prong, and the number of prongs (or 'star size') produced in a disintegration is proportional to the kinetic energy of the disintegration-producing particle. Although the precise relationship between incident nucleon energy and prong number is somewhat ambiguous, it is clear from theoretical considerations [34] that mean star size increases monotonically with increasing nucleon energy. Above sea level, most stars recorded in

emulsions are initiated by protons and neutrons, while the contribution from slow muons is negligible [35].

Due to the undercounting of one- and two-prong stars, nucleon attenuation lengths measured with cloud chambers and nuclear emulsions are typically biased towards high-energies. Undercounting occurs because tracks left by one- and two-prong stars are difficult to distinguish from tracks left by proton recoils and scattering events. Also, there is generally a low scanning efficiency for one and two prong stars [2]. For example, Brown [32] undercounted one- and two-prong stars occurring in a cloud chamber, while Dixit [36] and Roederer [31] neglected these altogether. In the silver bromide emulsions used by [36] and [31], one- and two-prong stars correspond to energies of about 41 MeV and 90 MeV, respectively [34]. As with neutron monitors, the effect of energy bias is to underestimate the total nucleon attenuation length. Correcting the data of [32] for this effect using the procedure outlined by Lal ([2], p. 67) yields a value of 137 ± 5 g cm^{-2} for the flux-weighted attenuation length of nucleons with E>40 MeV between 700 and 1032 g cm^{-2}. This compares to the value of 132 ± 4 g cm^{-2} originally given by [32] for the uncorrected nucleon attenuation length between these depths. Failure to make corrections such as this can account for apparent discrepancies between attenuation lengths.

4. The geomagnetic effect and cutoff rigidity

The geomagnetic field imposes a rigidity (momentum-to-charge ratio) cutoff on primary cosmic rays. The value of this cutoff tends to increase with decreasing latitude, resulting in lower cosmic-ray intensity towards the equator. However, only in a centered-dipole field is the cosmic-ray intensity a unique function of geomagnetic latitude. In a magnetic field with substantial non-dipole components, such as the present geomagnetic field, there is also a 'longitude effect' in cosmic-ray intensity. Data from so-called 'latitude surveys' must therefore be ordered in terms of a parameter that accounts for both latitude and longitude effects.

Prior to the mid 1950s most cosmic-ray measurements were ordered according to geomagnetic latitude (λ_m) calculated from a centered dipole representation of the geomagnetic field [8]. However, the first latitude surveys [8, 23] proved that non-dipole components have a substantial effect on the cosmic-ray intensity. Early investigators also attempted to characterize primary cosmic-ray access by using the lower vertical cutoff rigidity (P_L) based on a dipole representation of the geomagnetic field [37]:

$$P_L(\lambda_m) = \frac{30 M_0}{4 r^2} \cos^4 \lambda_m = 14.9\ \mathrm{GV} \left(\frac{M}{M_0} \right) \cos^4 \lambda_m \qquad (3)$$

where M_0 is a reference dipole moment (7.90622 x 10^{22} A m^2 for Epoch 1980.0 [37]), M is the dipole moment at some other time and r is the average radius of the earth

(6.371×10^6 m [37]). A coefficient of 14.9 GV, based on the magnetic survey of 1944 [7, p 10], is often given in equation 3.

Equation 3 gives the minimum momentum-to-charge ratio that a vertically incident primary cosmic-ray particle must possess in order to gain access to a certain geomagnetic latitude (λ_m) in a centered dipole field. Besides the limitation that equation 3 only applies to a centered dipole field, there is the additional shortcoming that it implicitly ignores the presence of the solid earth. Consequently, particles with rigidities above the lower cutoff may still fail to reach latitudes permitted by equation 3, since these particles may travel along complex trajectories which intersect the earth elsewhere [39]. Hence, there also exists an upper cutoff rigidity, P_U, above which all primary particles are accepted. The region between the lower and upper cutoff is termed the penumbra, and here acceptance or rejection of primary cosmic rays depends on individual particle trajectories. In the 1950s and early 1960s, several investigators [40-42] derived analytical and semi-empirical equations for cutoff rigidity in attempt to at least partially account for non-dipole and penumbral effects. Although these efforts led to successive improvements in ordering cosmic-ray data from latitude surveys, satisfactory cutoffs did not arise until computer-intensive calculations first became practical in the middle 1960s [43].

Since the late 1960s, most neutron monitor measurements have been ordered in terms of effective vertical cutoff rigidity (P_C) (Fig. 5) calculated by integrating cosmic-ray trajectories through a high-order mathematical model of the geomagnetic field [44-47]. This method involves tracing the paths of negatively-charged particles as they are

leaving specific locations above the earth in the vertical direction. Anti-protons that escape the geomagnetic field to infinity follow paths identical to those of cosmic-ray protons incident on the same location from infinity. In order to locate the lower, upper and effective cutoffs, a large number of trajectories corresponding to a range of particle energies must be numerically traced.

The primary flux is nearly omnidirectional and therefore a complete description of primary cosmic-ray access to the earth requires calculation of cutoff rigidities for all angles of incidence [48]. However, because vertically incident primaries produce most of the sea-level nucleon flux, it has proved adequate in practice to order cosmic-ray data according to cutoffs calculated only for the vertical direction. The reliability of P_C has been confirmed by numerous sea-level latitude surveys which show a smooth and consistent relationship between cutoff rigidity and nucleon intensity [45-47]. Failure to account for obliquely incident primary particles appears to have only a minor effect on ordering cosmic-ray data [47, 48].

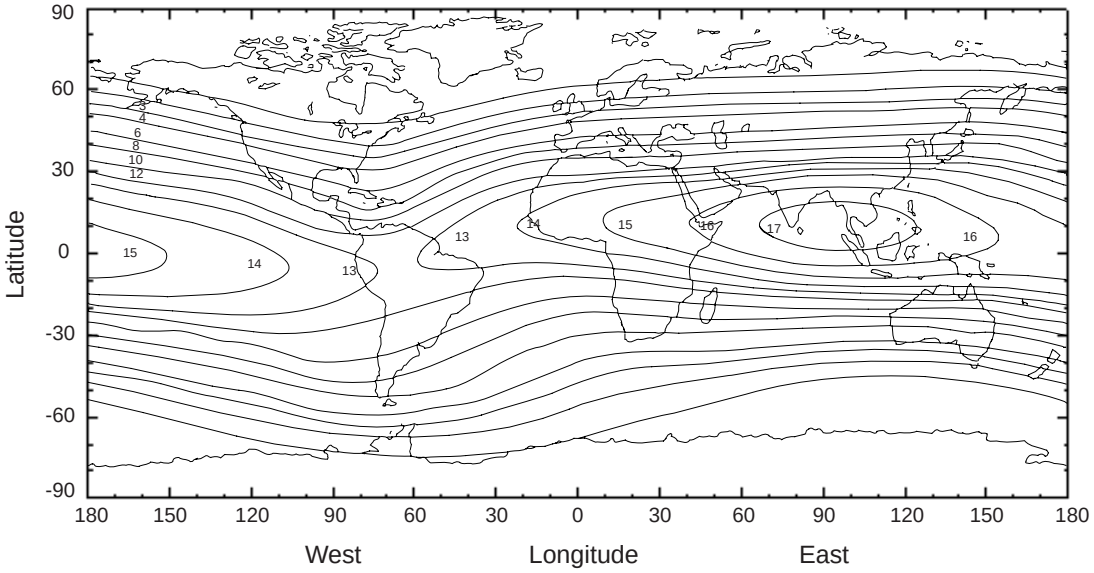

Figure 5. The world-wide distribution of P_C (GV) for Epoch 1955.0 [44].

The adoption of P_C for cosmic-ray surveys was a major advance in experimental cosmic-ray physics. However, the currently available scaling models order cosmic-ray data according to geomagnetic inclination [1] and geomagnetic latitude [2-4], both of which are ineffective at describing the prevailing geomagnetic field [5, 49]. Most importantly, the geomagnetic field contains a substantial quadrupole component, which makes the present-day geomagnetic field approximately equivalent to a dipole field shifted about 392 km from the center of the earth towards Southeast Asia [38]. This effect causes sea-level nucleon intensity along the cosmic-ray equator (the line of minimum cosmic-ray intensity around the earth) to decrease by about 15% from South America to Southeast Asia. Geomagnetic inclination and geomagnetic latitude cannot possibly account for this effect.

Direct measurements of the cosmic-ray intensity are collected in the present-day geomagnetic field and therefore should be ordered according to P_C. Unfortunately, P_C cannot be accurately calculated for the past 200-10,000 years because the geomagnetic field parameters are not known. However, if the long term (>10,000 - 20,000 years) behavior of the earth's magnetic field can be approximated by an axial dipole field, as is often assumed [1, 49] then geomagnetic latitude (λ_m) is equivalent to geographic latitude (λ) over the long term. P_L can then be calculated from equation 3, and P_C can be estimated from Figure 6. It should be noted that, strictly speaking, Figure 6 represents the penumbral correction corresponding only to a centered dipole model of the recent (past ~50 years) geomagnetic field. Deviations caused by non-dipole characteristics of the geomagnetic field (Fig. 5) and variations in dipole intensity are not accounted for.

5. Solar activity

Solar activity substantially reduces the flux of GCR particles at high latitudes, but has only a small effect on the flux at low latitudes. During periods of high solar activity, the sun emits a substantial flux of low-energy SCR protons, enhancing the overall flux of low-energy primary particles traveling through the interplanetary medium. However, associated with these low-energy SCR particles are traveling magnetic fields which screen the earth from low-energy GCR particles ([7, p. 3]). The net effect is a decrease in the cosmic-ray intensity reaching the earth while the sun is active.

Solar modulations cause the GCR flux reaching the earth to vary in time according to an 11-year cycle. Because low-energy primaries are always rejected by the geomagnetic field at low latitude (high P_C), the effects of solar modulation are significant only at high latitude (low P_C). Also, because secondary cascades initiated by low energy GCRs tend to be weakly penetrating, variations in secondary intensity due to solar effects become more subdued towards sea level.

Several experiments demonstrate that even at depths ranging from 680 to 1033 g cm^{-2} the shape of the neutron flux latitude curve depends considerably on solar activity (Fig. 7) [20, 50-52]. From solar minimum to solar maximum, the high-latitude sea-level nucleon flux decreases by about 8%, whereas at 680 g cm^{-2} the flux decreases by about 21%. At low latitudes (~14 GV), solar modulations have a negligible effect on sea-level neutron intensity [50], while at 680 g cm^{-2} the neutron flux varies by only about 5% [28].

The nucleon attenuation length also varies with solar activity (Fig. 8). This effect is related to changes in the primary energy spectrum caused by solar modulations. Periods of high solar activity are associated with a lower primary flux but a harder primary energy spectrum. Cascades initiated by more energetic primaries tend to have correspondingly longer attenuation lengths. During low solar activity, the overall nucleon attenuation length reflects the increased contribution of low-energy cascades which attenuate rapidly in the atmosphere.

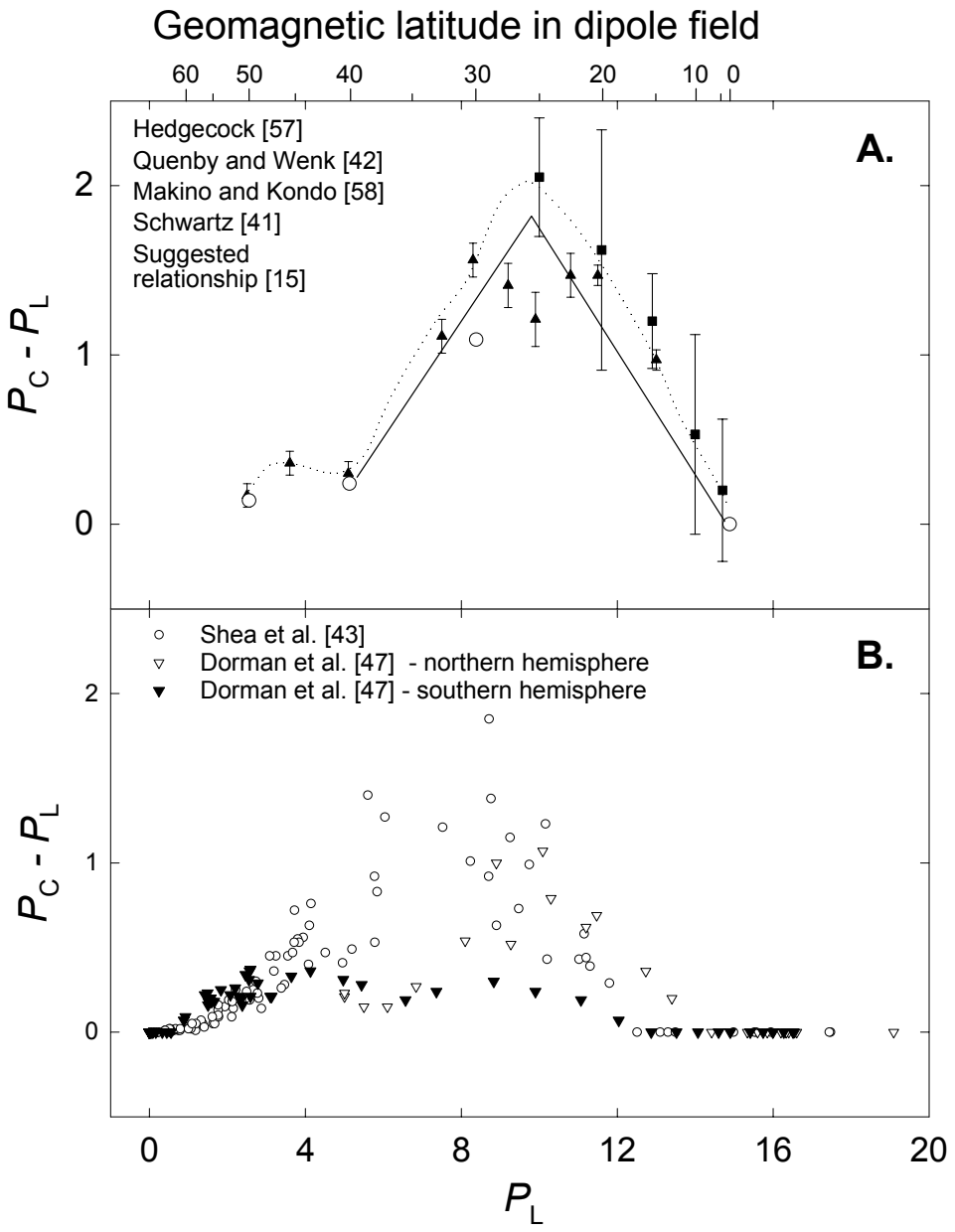

Figure 6. The penumbral correction in (A) a centered dipole field [15, 41, 42, 57, 58] and (B) a high-order model of the real geomagnetic field [43, 47].

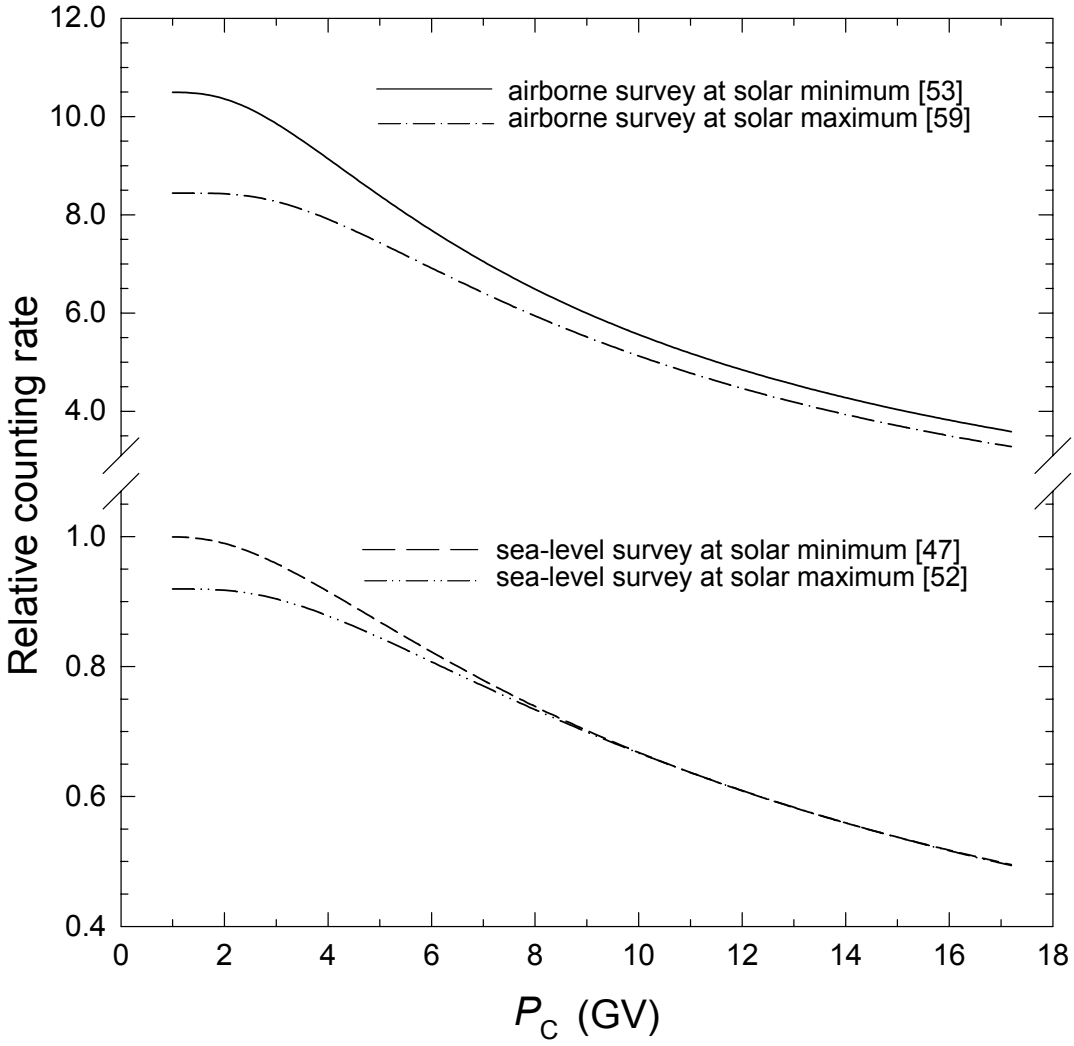

Figure 7. Latitude surveys of nucleon intensity conducted at solar maximum and solar minimum, normalized at 14 GV. Airborne and sea-level curves correspond to atmospheric depths of 680 g cm^{-2} and 1033 g cm^{-2}, respectively [47, 52, 53, 59].

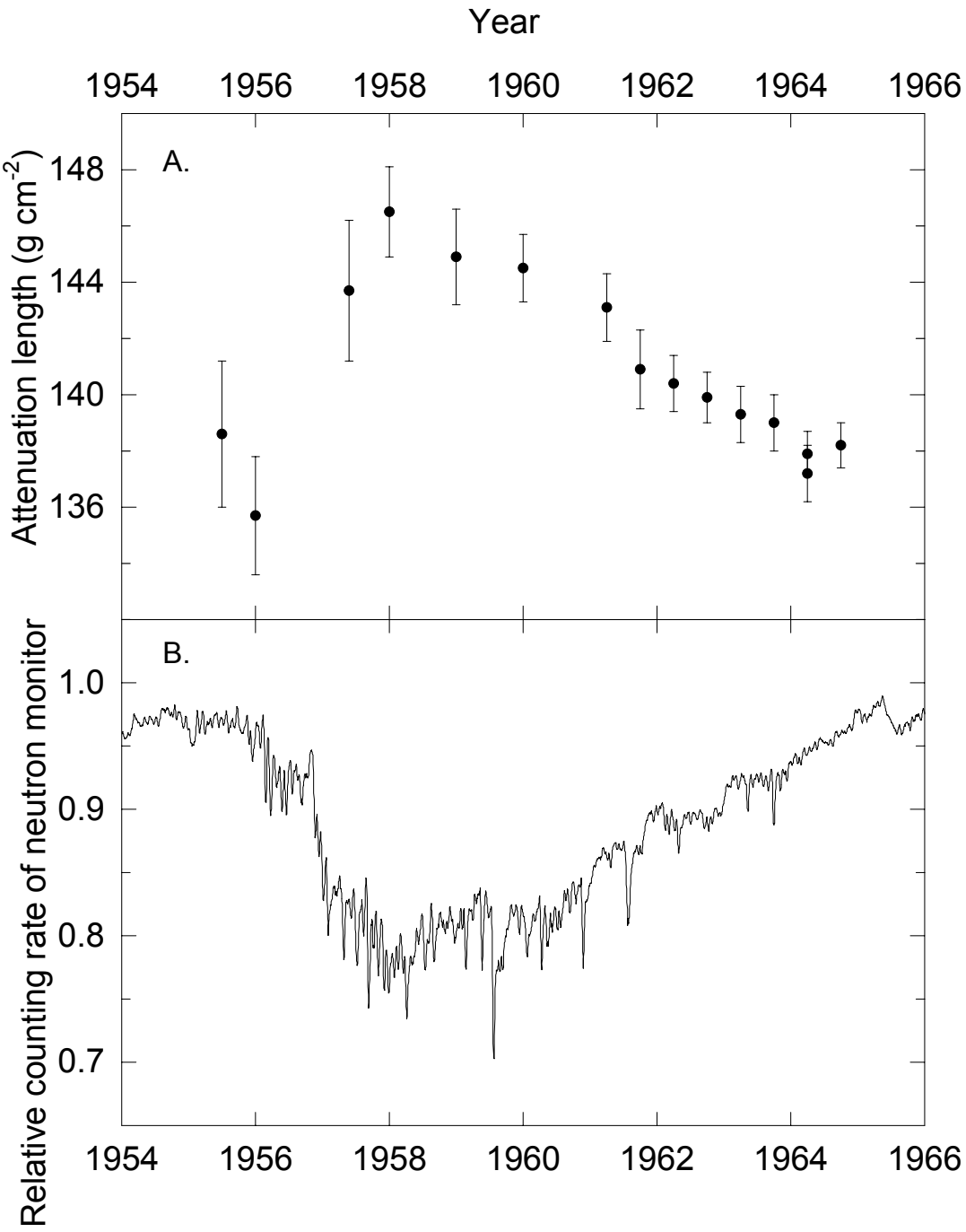

Figure 8. (A) Attenuation lengths measured from an IGY monitor at 2 GV and sea level [60] over one solar cycle. (B) A ten-day moving average of the relative counting rate of the Climax IGY neutron monitor over the same period (http://ulysses.uchicago.edu/NeutronMonitor/).

6. Conclusions

The development of an accurate model for scaling production rates is an essential step towards refining the cosmogenic nuclide dating method. Improvements to existing scaling models [1, 4] could be made by: (1) considering all cosmic-ray data accumulated since the 1950s; (2) using improved corrections for instrumental biases (3) ordering cosmic-ray latitude survey data according to P_C; and (4) using more realistic relationships between atmospheric mass shielding depth and altitude.

There appears to be general agreement that more work is needed to constrain the altitude and latitude dependence of $\Lambda_{Prod,N}$ [1, 5, 54-56]. We are currently working on this issue. By far the largest body of data on nucleon intensity is from neutron monitors, which require corrections. However, without more accurate knowledge of nucleon excitation functions and of the energy dependence of the nucleon attenuation length, any correction to Λ_{NM} could potentially carry a large uncertainty. On the other hand, the direct measurement of $\Lambda_{Prod,N}$ in geological samples, such as lava flows that extend from high altitudes to sea level, requires exceptional field conditions (easily distinguishable flows, evidence of minimal erosion and minimal ash cover) if long lived nuclides are to be applied. It also seems unlikely that a sufficient number of sites can be found to give adequate latitude and altitude coverage for developing an accurate scaling model based entirely on geological samples. Work being done with artificial targets [55, 56] should therefore play an essential role in validating scaling models.

Acknowledgements

We thank Nat Lifton and Devendra Lal for valuable discussions, and Fred Phillips and an anonymous reviewer for their helpful suggestions. This work was supported by National Science Foundation grants EAR-0001191 and ATM-0081403 and Packard Fellowship 95-1832. We also acknowledge National Science Foundation support of the Climax neutron monitor under grant ATM-9912341.

References

1 T.J. Dunai, Scaling factors for production rates of in situ produced cosmogenic nuclides: a critical reevaluation, Earth and Planetary Science Letters 176, 157-169, 2000.

2 D. Lal, Investigation of nuclear interactions produced by cosmic rays, Ph.D, University of Bombay, 1958.

3 D. Lal and B. Peters, Cosmic ray produced radioactivity on earth, in: Encyclopedia of Physics: Cosmic Rays II, K. Sitte, ed., Encyclopedia of Physics 46/2, pp. 551-612, Springer-Verlag, Berlin, 1967.

4 D. Lal, Cosmic ray labeling of erosion surfaces: *in situ* nuclide production rates and erosion models, Earth and Planetary Science Letters 104, 424-439, 1991.

5 D. Desilets, M. Zreda and N.A. Lifton, Comment on "Scaling factors for production rates of in situ produced cosmogenic nuclides: a critical reevaluation", Earth and Planetary Science Letters 188, 283-287, 2001.

6 J. Masarik and R.C. Reedy, Terrestrial cosmogenic-nuclide production systematics calculated from numerical simulations, Earth and Planetary Science Letters 136, 381-396, 1995.

7 L.I. Dorman, Cosmic Rays Variations and Space Explorations, North-Holland Publishing Co., Amsterdam, 1974.

8 J.A. Simpson, Neutrons produced in the atmosphere by the cosmic radiations, Physics Reviews 83, 1175-1188, 1951.

9 K.S. Krane, Introductory Nuclear Physics, 845 pp., John Wiley and Sons, New York, 1988.

10 W.N. Hess, E.H. Canfield and R.E. Lingenfelter, Cosmic-ray neutron demography, Journal of Geophysical Research 66, 665-677, 1961.

11 J.A. Simpson, The cosmic ray nucleonic component: the invention and scientific uses of the neutron monitor, Space Science Reviews 93, 11-32, 2000.

12 H. Messel, The development of a nucleon cascade, in: Progress in Elementary Particle and Cosmic Ray Physics, J.G. Wilson, ed. 2, pp. 134-216, North-Holland Publishing Co., Amsterdam, 1954.

13 U.S. standard atmosphere, 1976, United States committee on extension to the standard atmosphere, NOAA, Washington, D.C., 1976.

14 J.O. Stone, Air pressure and cosmogenic isotope production, Journal of Geophysical Resarch 105(B10), 23753-23759, 2000.

15 D.M. Desilets, The global distribution of secondary cosmic-ray intensity and applications to cosmogenic dating, M.S., University of Arizona, 2001.

16 H. Carmichael, M. Bercovitch, J.F. Steljes and M. Magidin, I. Cosmic-ray latitude survey in North America in summer, 1965, Canadian Journal of Physics 47, 2037-2050, 1969.

17 H. Carmichael, M.A. Shea and R.W. Peterson, III. Cosmic-ray latitude survey in Western USA and Hawaii in summer, 1966, Canadian Journal of Physics 47, 2057-2065, 1969.

18 H. Carmichael and M. Bercovitch, V. Analysis of IQSY cosmic-ray survey measurements, Canadian Journal of Physics 47, 2073-2093, 1969.

19 B.C. Raubenheimer and P.H. Stoker, Various aspects of the attenuation coefficient of a neutron monitor, Journal of Geophysical Research 79, 5069-5076, 1974.

20 F. Bachelet, P. Balata, E. Dyring and N. Iucci, Attenuation coefficients of the cosmic-ray nucleonic component in the lower atmosphere, Il Nuovo Cimento 35, 23-35, 1965.

21 F. Bachelet, N. Iucci, G. Villoresi and N. Zangrilli, The cosmic-ray spectral modulation above 2 GV. IV. The Influence on the attenuation coefficient of the nucleonic component, Il Nuovo Cimento 11 B, 1-12, 1972.

22 F. Bachelet, N. Iucci and G. Villoresi, The cosmic-ray spectral modulation above 2 GV during the descending phase of solar cycle number 19. I. A comprehensive treatment of the neutron monitor data from the worldwide station network and latitude surveys, Il Nuovo Cimento 7 B, 17-32, 1972.

23 J.A. Simpson and W.C. Fagot, Properties of the low energy nucleonic component at large atmospheric depths, Physical Review 90, 1068-1072, 1953.

24 C.J. Hatton, The neutron monitor, in: Progress in Elementary Particle and Cosmic Ray Physics, J.G. Wilson and S.A. Wouthuysen, eds. 10, pp. 1-100, North-Holland Publishing Co., Amsterdam, 1971.

25 H. Bilokon, G.C. Castagnoli, A. Castellina, D. Piazzoli, G. Mannocchi, E. Meroni, P. Picchi and S. Vernetto, Flux of the vertical negative muons stopping at depths .35-1000 hg/cm^2, Journal of Geophysical Research 94, 12,145-12,152, 1989.

26 F. Bachelet, P. Balata, E. Dyring and N. Iucci, On the multiplicity effect in a standard cosmic-ray neutron monitor, Il Nuovo Cimento 31, 1126-1130, 1964.

27 R.A. Nobles, R.A. Alber, E.B. Hughes, L.L. Newkirk and M. Walt, Neutron multiplicity monitor observations during 1965, Journal of Geophysical Research 72, 3817-3827, 1967.

28 D.W. Kent, H. Coxell and M.A. Pomerantz, Latitude survey of the frequency of multiple events in an airborne neutron monitor, Canadian Journal of Physics 46, S1082-S1086, 1968.

29 E.B. Hughes and P.L. Marsden, Response of a standard IGY neutron monitor, Journal of Geophysical Research 71, 1,435-1,444, 1966.

30 B. Rossi, Interpretation of cosmic-ray phenomena, Reviews of Modern Physics 20, 537-583, 1948.

31 J.G. Roederer, Über die Absorption der Nukleonenkomponente der kosmischen Strahlung in -21° geomagnetischer Breite, Zeitschrift für Naturforschung 7a, 765-771, 1952.

32 W.W. Brown, Cosmic-ray nuclear interactions in gases, Physical Review 93, 528-534, 1954.

33 R.K. Soberman, High-altitude cosmic-ray intensity variations, Physical Review 102, 1399-1409, 1956.

34 R.H. Brown, U. Camerini, P.H. Fowler, H. Heitler, D.T. King and C.F. Powell, Nuclear transmutations produced by cosmic-ray particles of great energy. Part I. Observations with photographic plates exposed at an altitude of 11,000 feet, Philosophical Magazine 40, 862-881, 1949.

35 E.P. George and J. Evans, Disintegrations produced by the nuclear capture of slow negative μ-mesons, Proceedings of the Physical Society of London 64A, 193-198, 1951.

36 K.R. Dixit, The statistics of 29000 stars observed in nuclear emulsions in Kenya, Zeitschrift für Naturforschung 10a, 339-341, 1955.

37 C. Störmer, The Polar Aurora, Oxford University Press, London, 1955.

38 A.C. Fraser-Smith, Centered and eccentric geomagnetic dipoles and their poles, 1600-1985, Reviews of Geophysics 25, 1-16, 1987.

39 D.J. Cooke, J.E. Humble, M.A. Shea, D.F. Smart, N. Lund, I.L. Rasmussen, B. Byrnak, P. Goret and N. Petrou, On cosmic-ray cut-off terminology, Il Nuovo Cimento 14, 213-233, 1991.

40 J.J. Quenby and W.R. Webber, Cosmic ray cut-off rigidities and the Earth's magnetic field, Philosophical Magazine 4, 90-113, 1959.

41 M. Schwartz, Penumbra and simple shadow cone of cosmic radiation, Il Nuovo Cimento 11, Serie X, Suppl., 27-59, 1959.

42 J.J. Quenby and G.J. Wenk, Cosmic ray cut-off rigidities and the Earth's magnetic field, Philosophical Magazine 7, 1457-1471, 1962.

43 M.A. Shea, D.F. Smart and K.G. McCracken, A study of vertical cutoff rigidities using sixth degree simulations of the geomagnetic field, Journal of Geophysical Research 70, 4117-4130, 1965.

44 M.A. Shea, D.F. Smart and L.C. Gentile. Estimating cosmic ray vertical cutoff rigidities as a function of the McIlwain *L*-parameter for different epochs of the geomagnetic field, Physics of the Earth and Planetary Interiors 48, 200-205, 1987.

45 M.S. Potgeiter, H. Moraal, B.C. Raubenheimer and P.H. Stoker, Modulation of cosmic rays during solar minimum. Part 3. Comparison of the latitude distributions for the periods of solar minimum during 1954, 1965 and 1976, South African Journal of Physics 3, 90-94, 1980.

46 H. Moraal, M.S. Potgieter and P.H. Stoker, Neutron monitor latitude survey of cosmic ray intensity during the 1986/1987 solar minimum, Journal of Geophysical Research 94, 1459-1464, 1989.

47 L.I. Dorman, G. Villoresi, N. Iucci, M. Parisi, M.I. Tyasto, O.A. Danilova and N.G. Ptitsyna, Cosmic ray survey to Antarctica and coupling functions for neutron component near solar minimum (1996-1997) 3. Geomagnetic effects and coupling functions, Journal of Geophysical Research 105, 21,047-21,056, 2000.

48 J.M. Clem, J.W. Bieber, P. Evenson, D. Hall, J.E. Humble and M. Duldig, Contribution of obliquely incident particles to neutron monitor counting rate, Journal of Geophysical Research 102, 26,919-26,926, 1997.

49 D.C. Rose, K.B. Fenton, J. Katzman and J.A. Simpson, Latitude effects of the cosmic ray nucleon and meson components at sea level from the Arctic to the Antarctic, Canadian Journal of Physics 34, 968-984, 1956.

50 J.M. Licciardi, M.D. Kurz, P.U. Clark and E.J. Brook, Calibration of cosmogenic ^{3}He production rates from Holocene lava flows in Oregon, USA, and effects of the Earth's magnetic field, Earth and Planetary Science Letters 172, 261-271, 1999.

51 M.A. Forman, The relation between latitude and solar-cycle variations in the neutron-monitor mass-absorption coefficient, Canadian Journal of Physics 46, S1087-S1089, 1968.

52 T.M. Aleksanyan, I.V. Dorman, L.I. Dorman, V.K. Babayan, A.V. Belov, Y.L. Blokh, N.S. Kaminer, V.K. Korotkov, I.Y. Libin, A.A. Manshilina, Y.E. Mashkov, I.V. Mymrina, S.I. Rogovaya, A.M. Sitnov, K.F. Yudakhin and V. Yanke, Geomagnetic effects in cosmic rays and spectrum of the increase before magnetic storms, Izvestiya Akademii Nauk SSSR, Seriya Fizicheskaya 46, 1689-1691, 1982.

53 D.W. Kent and M.A. Pomerantz, Cosmic ray intensity variations in the lower atmosphere, Journal of Geophysical Research 76, 1652-1661, 1971.

54 D. Lal, Cosmogenic nuclide production rate systematics in terrestrial materials: Present knowledge, needs and future actions for improvement, Nuclear Instruments and Methods in Physics Research B 172, 772-781, 2000.

55 I.J. Graham, B.J. Barry, R.G. Ditchburn and N.E. Whitehead, Validation of cosmogenic nuclide production rate scaling factors through direct measurement, Nuclear Instruments and Methods in Physics Research B 172, 802-805, 2000.

56 E.T. Brown, T.W. Trull, P. Jean-Baptiste, G. Raisbeck, D. Bourlès, F. Yiou and B. Marty, Determination of cosmogenic production rates of ^{10}Be, ^{3}He and ^{3}H in water, Nuclear Instruments and Methods in Physics Research B 172, 873-883, 2000.

57 J.J. Quenby, The time variations of the cosmic ray intensity, in: Encyclopedia of Physics: Cosmic Rays II, K. Sitte, ed., Encyclopedia of Physics 46/2, pp. 310-371, Springer-Verlag, Berlin, 1967.

58 T. Makino and I. Kondo, Modulation of cosmic ray threshold rigidity due to geomagnetic cavity field, in: Proceedings of the 9th International cosmic-ray conference, pp. 564-567, 1965.

59 H. Coxell, M.A. Pomerantz and S.P. Agarwal, Survey of cosmic-ray intensity in the lower atmosphere, Journal of Geophysical Research 71, 143-154, 1965.

60 W.K. Griffiths, C.V. Harman, C.J. Hatton and P. Ryder, Studies of the barometric coefficients of IGY and NM-64 neutron monitors, in: Proceedings of the 9th International Cosmic Ray Conference, 1965.

APPENDIX C

SPATIAL AND TEMPORAL DISTRIBUTION OF SECONDARY COSMIC-RAY NUCLEON INTENSITIES AND APPLICATIONS TO *IN-SITU* COSMOGENIC DATING

Darin Desilets and Marek Zreda

[*Earth and Planetary Science Letters*, 206: 21-42 (2003)]

Abstract

Cosmogenic nuclide production rates depend critically on the spatio-temporal distribution of cosmic-ray nucleon fluxes. Since the 1950s, measurements of the altitude, latitude and solar modulation dependencies of secondary cosmic ray fluxes have been obtained by numerous investigators. However, until recently there has been no attempt to thoroughly evaluate the large body of modern cosmic-ray literature, to explain systematic discrepancies between measurements or to put these data into a rigorous theoretical framework appropriate for cosmogenic dating.

The most important parameter to be constrained is the dependence of neutron intensity on atmospheric depth. Our analysis shows that effective nucleon attenuation lengths measured with neutron monitors over altitudes 0-5000 m range from 128 g cm^{-2} to 142 g cm^{-2} at effective vertical cutoff rigidities of 0.5 GV and 14.9 GV, respectively. Effective attenuation lengths derived from thermal neutron data are somewhat higher, ranging from 134 g cm^{-2} to 155 g cm^{-2} at the same cutoff rigidities and over the same altitudes. We attribute the difference to a combination of two factors: the neutron monitor is more sensitive to the higher end of the nucleon energy spectrum, and the shape of the nucleon energy spectrum shifts towards lower energies with increasing atmospheric depth.

We have derived separate scaling models for thermal neutron reactions and spallation reactions based on a comprehensive analysis of cosmic-ray survey data. By assuming that cosmic-ray intensity depends only on atmospheric depth and effective vertical cutoff

rigidity, these models can be used to correct production rates for temporal changes in geomagnetic intensity using paleomagnetic records.

1. Introduction

The reliability of cosmogenic methods of surface exposure dating is limited by the accuracy of nuclide production rates. Ideally, production rates are calibrated on landforms that have simple exposure histories and that have been dated accurately and precisely by independent methods. However, because such landforms are rare, the spatial and temporal coverage of calibrated production rates is limited. Production rates corresponding to a few locations and exposure periods are therefore applied to landforms where the time-averaged cosmic-ray intensity may be different by an order of magnitude or more from the intensity at the calibration site. Differences in cosmic-ray intensity at a sample site and a calibration site are accounted for by multiplying the calibrated production rate by a scaling factor.

Cosmic-ray intensity on earth varies spatially due to the interaction of primary cosmic rays with terrestrial and interplanetary magnetic fields and because cosmic rays are attenuated by terrestrial matter. Temporal variations are related mostly to changes in geomagnetic, heliospheric and galactic properties that occur on time scales ranging from minutes (e.g., isolated solar flare events) to millennia (e.g., the earth's magnetic dipole moment). Spatial and temporal variations are linked, since time dependent variations of the cosmic-ray flux affect some locations on earth more than others. The 11-year solar

cycle, for example, affects only the cosmic-ray flux at high and mid latitudes, whereas variations of the geomagnetic dipole intensity affect mainly the mid- and low-latitude flux.

Here, we use measured cosmic-ray fluxes to derive scaling formulas for nucleon-induced spallation reactions and thermal neutron absorption reactions. Our recognition that high-energy neutron reactions and thermal neutron reactions may require different scaling models is an important advance over previous work. Although the models derived by Lal [1], and reported in [2] also imply that scaling models should include the energy dependence of nuclide production (excitation function), Lal [2] gives a parameterization only for the fluxes of nucleons of $E > 40$ MeV. Discrepancies between cosmic-ray surveys conducted with neutron monitors and with unshielded proportional counters (Section 4.0) suggest that the altitude dependence of cosmogenic nuclide production is more sensitive to energy than was appreciated by Lal [1, 2].

The emphasis of this work is on scaling high-energy spallation reactions and thermal neutron absorption reactions. Because the primary data on high-energy nucleons come from neutron monitors, which are also somewhat sensitive to muon fluxes, we derive scaling formulas for fast muon and slow (negative) muon fluxes so that corrections can be applied to neutron monitor counting rates. These functions can also be used to scale cosmogenic nuclide production by fast and slow muons.

Two important differences between our work (as well as that of [3]) and other models are that we express secondary cosmic-ray fluxes as a function of mass shielding depth (x)

in units of g cm^{-2}, in contrast to [2], who used elevation, and as a function of effective vertical cutoff rigidity (R_C) in units of GV, in contrast to [2], who used geomagnetic latitude, and [4] who used geomagnetic inclination. Because x and R_C change over time, the long-term behavior of these parameters must be estimated at both the sample site and the calibration site. The problem of determining R_C from geographic position and magnetic field intensity is discussed later in this paper, whereas the dependence of mass shielding depth on elevation has been discussed by [5] and [6].

2. Review of scaling models derived from cosmic-ray data

Lal's [1, 2] is the most widely cited scaling model. Drawbacks to his pioneering work are that: (1) Cosmic-ray measurements from latitude surveys are ordered according to geomagnetic latitude calculated from an axially-symmetric centered dipole model. Such a model does not accurately describe the geomagnetic field's ability to deflect primary cosmic rays [3, 4, 6]. (2) Atmospheric depth (pressure) data from altitude surveys were converted to elevation using the U.S. standard atmosphere, 1976. The model therefore does not account for spatial variations in the atmospheric pressure structure [4-6]. (3) The model assumes that the shape of the nucleon energy spectrum is independent of altitude at energies below 400 MeV. Measurements performed more recently suggest that the energy spectrum may soften significantly towards sea level, even at energies below 400 MeV [6]. (4) Measurements taken since the 1950s, representing the vast majority of cosmic-ray data, are not included [6, 7]. (5) The effects of solar activity are not explicitly addressed [7].

Dunai [4] has proposed a major revision to Lal's [1, 2] model. Although his work is more recent than [1, 2], Dunai's [4] model is also based on a small subset of the cosmic-ray data from the 1950s [6]. In addition, [4] orders cosmic-ray data according to geomagnetic inclination, which, like geomagnetic latitude, has a non-unique relation with cosmic-ray intensity [8]. He also [4] neglects the effect of solar activity and implicitly assumes that the energy spectrum is independent of altitude (see discussion in [8]). For these reasons, both the accuracy and reported uncertainty (e.g. ~ 2% in the sea-level latitude curve) of Dunai's [4] scaling model are questionable.

An important difference between the scaling models of [2] and [4] is the dependence of nucleon fluxes on altitude. Dunai's [4] scaling model consistently gives effective attenuation lengths that are about 5% lower than those calculated from Lal's [2] model. The different attenuation lengths result in a ~ 10% difference between the two models when production rates are scaled between 1033 g cm^{-2} and 600 g cm^{-2} (0-5000 m). The two authors also give sea-level neutron fluxes that are different by as much as 12%, even though their scaling models utilize the same sea-level neutron monitor survey [9] as a baseline. Given such discrepancies, and considering the inherent problems with these models, there is an obvious need to investigate the scaling problem in more detail.

Only one published scaling model has been derived entirely from neutron monitor data [10]. That model utilized an extensive survey by [11-15] to predict the altitude and latitude dependence of soft fail rates in integrated circuits. Another scaling model for

cosmogenic nuclide production based primarily on neutron monitor data (including the results of [11-15]) has been proposed by Lifton [3].

3. Scaling model for spallation reactions

3.1 Data selection

Since the invention of the neutron monitor in the early 1950s, a wide range of atmospheric depths, cutoff rigidities and solar conditions have been measured [7]. These surveys have yielded consistent results, although there exist minor discrepancies due to differences in instrumental responses and experimental procedures.

A good cosmic-ray data set should have the following characteristics: (1) the data should have been collected using similar methods; (2) the experimental methods should be given in detail; (3) the instruments should be well characterized; (4) the time, date, geographic coordinates and barometric pressure at each measurement location should be recorded; and (5) the data should have extensive coverage in space and time. Corrections for variations in the temperature structure of the atmosphere and high winds (Bernoulli effect) may also improve the quality of a data set [16], but the required meteorological data are often not available for older surveys.

The survey that best meets the criteria above is that conducted by Carmichael and collaborators [11-14] over the International Quiet Sun Year (IQSY), 1965-1966. It comprised 110 measurements of nucleon intensity taken at atmospheric depths of 0-12,000 m (1033-200 g cm^{-2}), and at cutoff rigidities of 0.5-13.3 GV. All measurements at

altitudes less than 5000 m (> 550 g cm^{-2}) were collected with a land-based NM-64 and measurements at higher altitudes were obtained using a cross-calibrated monitor designed for airborne measurements. Neutron monitor counts and counting times are given along with the time, date, barometric pressure, latitude, longitude and effective vertical cutoff rigidity for each location. This survey, described in five back-to-back papers [11-15], is unmatched by any other altitude survey in terms of the detailed experimental description.

Another survey aimed at describing comprehensively the neutron monitor attenuation length (Λ_{NM}) was reported by Raubenheimer and Stoker [17]. To prevent ambient thermal neutrons from reaching the counter, this survey employed an NM-64 monitor with a reflector thickness on all sides double the usual 7.5 cm. There are four important differences between [17]'s survey and that of [11-15]. First, because the reflector thickness was doubled on top, the muon and nucleon energy sensitivities of the monitor in [17] should be slightly different from that of a standard NM-64 monitor. Second, many of the measurements were taken during the 1969 solar maximum. At high and mid latitudes (R_C > 5 GV) attenuation lengths at solar maximum should be higher by ~ 7 g cm^{-2} than those at solar minimum [17]. Additional measurements were obtained by [17] in 1971, when solar activity was lower than in 1969, but still higher than a typical solar minimum. Third, all measurements were performed from an airplane, most at altitudes greater than 1600 m (< 850 g cm^{-2}). [14]'s survey extended to both greater and smaller atmospheric depths. Fourth, and most important for this work, the original counting rates and counting times have not been published by [17]. Nonetheless, despite numerous differences in experimental conditions and approaches, the relation obtained by [17],

after normalizing to solar minimum, is in good agreement with the one found by [15], with attenuation lengths that are on average 2% lower than [15]'s.

Bachelet *et al*. [18] investigated the dependence of Λ_{NM} on R_C and x by evaluating barometric coefficients (the reciprocal of Λ) calculated from 58 stationary IGY and NM-64 monitors. Unfortunately they do not give original data (counting rates, counting time, atmospheric pressure) for the neutron monitors, as do [11-15]. Nonetheless, attenuation lengths derived by [18] for solar minimum (1964-1965) are in good agreement with [15]'s 1965-1966 results (Fig. 1), despite numerous differences in how the attenuation lengths were derived and the slightly different periods covered. Corrected attenuation lengths from [18] are on average only 1.5% higher than those calculated from our regression to data in [15] (Section 3.4).

Although the measurements of [17] and [18] are extensive, their data are not as amenable to analysis as [15]'s because original counting rates and counting durations are not published. Moreover, discrepancies between [18], [17] and [15] are small and are probably related to minor systematic differences rather than random measurement errors. To attempt to account for these small systematic differences would not be worthwhile in view of larger systematic errors (e.g., energy spectrum and solar activity) involved in applying neutron measurements to cosmogenic nuclides [6].

A precise and rigorous measurement of Λ_{NM} in Antarctica ($R_C < 0.5$) was performed during the 1997 solar minimum survey [16, 19, 20]. The attenuation length was measured from a ship by recording changes in counting rates caused by small fluctuations in

barometric pressure. The neutron monitor counting rate was corrected for the Bernoulli effect, sea-state effect (relevant only to shipborne data) and temperature structure of the atmosphere [19]. The attenuation length derived at this location (Fig. 1) gives us further confidence in the reliability of [11-15]'s data.

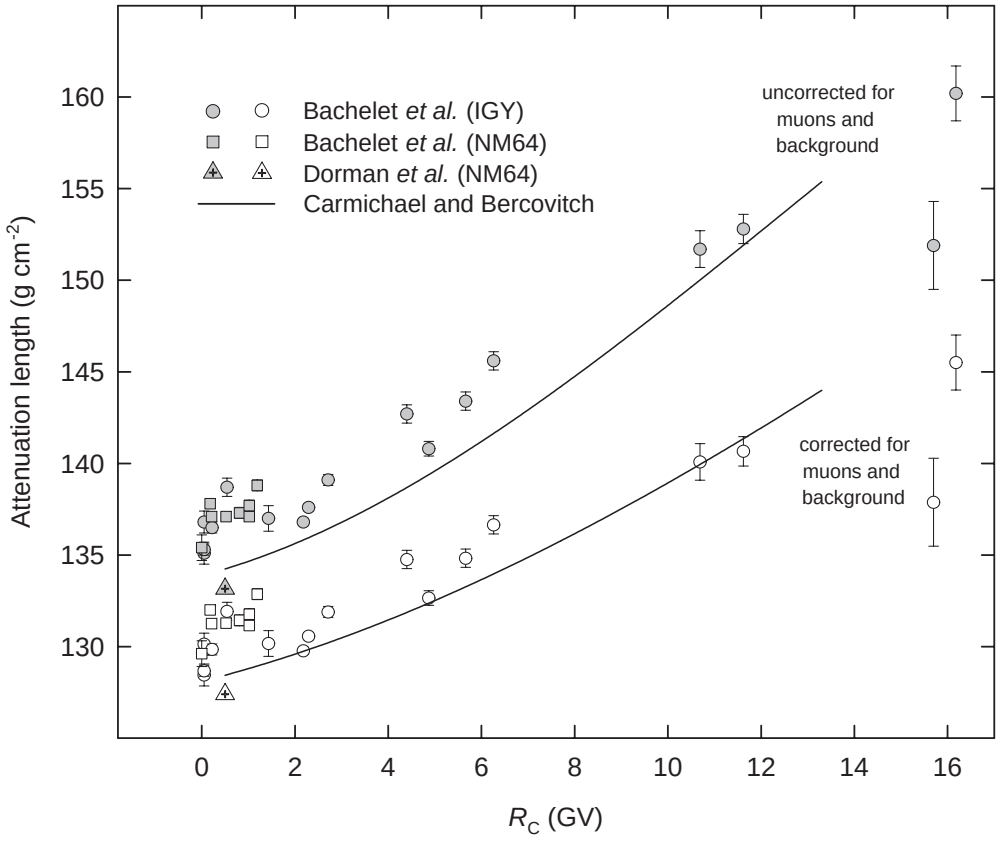

Figure 1. Attenuation lengths at sea level and solar minimum from neutron monitor attenuation coefficients measured by Bachelet *et al*. [18], Dorman *et al*. [20] and Carmichael and Bercovitch [15]. The solid lines are from a surface fitted to [15]'s complete data set, which covers a wide range of R_C and x.

3.2 Parameterization of attenuation lengths from neutron monitors

Throughout most of the atmosphere, the altitude dependencies of secondary cosmic-ray fluxes (J) are described by:

$$\frac{dJ}{dx} = \frac{J}{\Lambda} = \beta J \tag{1}$$

where x is atmospheric depth given in mass-shielding units [g cm^{-2}]. The rate of cosmic-ray absorption is usually expressed by the atmospheric attenuation length, Λ [g cm^{-2}], or its reciprocal, β [cm^2 g^{-1}], the attenuation coefficient. The solution to Eq. 1 is the exponential relation:

$$J_2 = J_1 \, exp\left(\frac{x_1 - x_2}{\Lambda} \right) = J_1 \, exp(\beta(x_1 - x_2)) \tag{2}$$

where J_1 and J_2 are the fluxes at depths x_1 and x_2. It is sometimes more convenient to use β, which represents the slope of dJ/dx versus J. Because β is a slope, the linear average of all β values over a range of depths x_1 to x_2 gives the effective attenuation coefficient between x_1 and x_2. On the other hand, Λ is often used because it carries the physical significance of being equivalent to the value of Δx over which cosmic-ray flux changes by a factor of e.

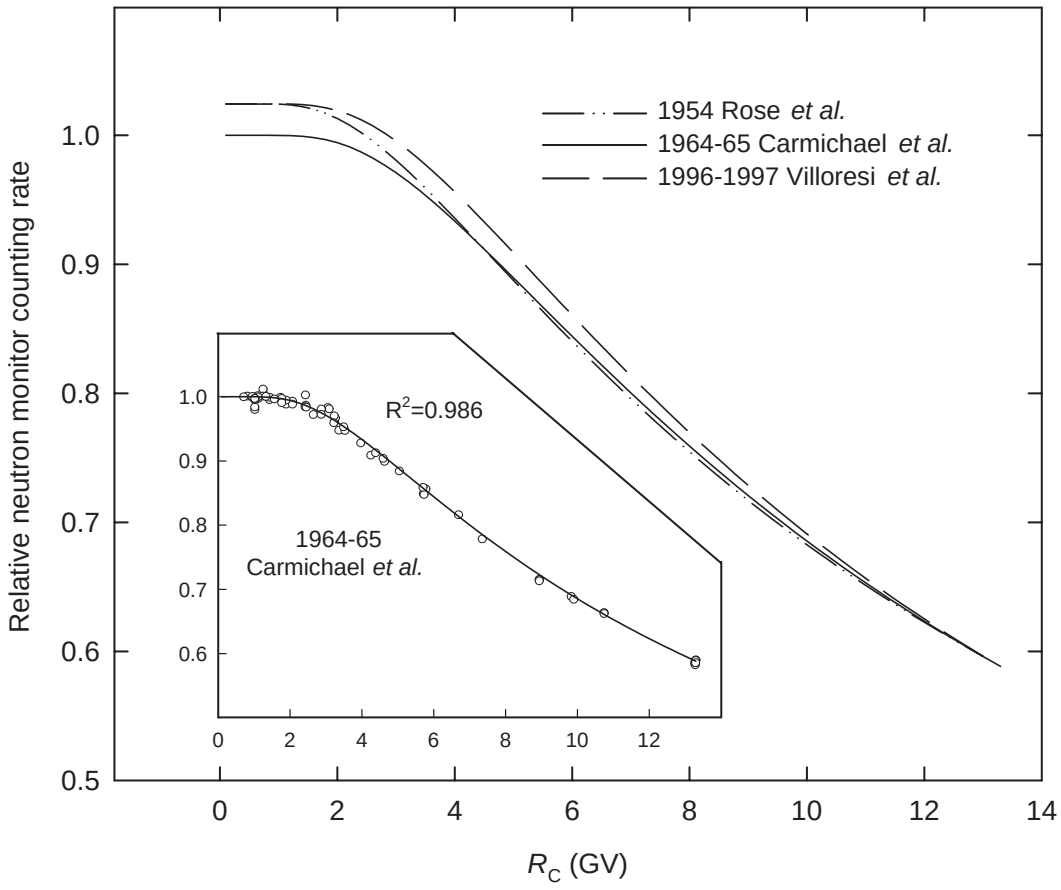

Figure 2. The sea-level latitude effect at solar-minimum, according to Rose *et al*. [9], Carmichael *et al*. [11-14] and Villoresi *et al*. [16], normalized at 13 GV.

Originally, Carmichael and Bercovitch [15] derived the neutron monitor attenuation coefficient, β_{NM}, as a function of R_C and x from the neutron monitor counting rates reported in [11, 13]. These results were given graphically, with the relation $\beta_{NM}(R_C,x)$ drawn by hand. Carmichael and Peterson [21] later parameterized [15]'s results using polynomials, but they did not report the polynomial coefficients. To make [15]'s results useful for scaling spallation reactions, we have parameterized these results in terms of Λ_{NM} using a polynomial.

We derived attenuation lengths by following the iterative procedure described by [15] for deriving $\beta_{NM}(R_C,x)$. A sea-level latitude curve was first established from the counting rates at each survey location. Although several survey locations were nominally at sea level, most were at slightly higher elevations and therefore the counting rates had to be reduced (normalized) to sea level. We accomplished this by making an initial estimate for each location of the effective attenuation length (Λ_e) required to reduce the counting rate at x to the sea level counting rate at the same cutoff rigidity. Then we parameterized the sea-level counting rate, J_{NM}, using the Dorman function [20]:

$$J_{NM}(R_C) = J_0\left[1 - exp\left(-\alpha R_C^{-k}\right)\right] \tag{3}$$

where J_0 is the high-latitude counting rate, and α and k are fitting parameters. The first approximation to the sea-level latitude curve was then used to calculate $\Lambda_{e,NM}$ for each of the survey locations. A polynomial was fitted to $\Lambda_{e,NM}(R_C,x)$ by the inverse-variance method, and a second approximation to the latitude curve was established. Variances of

counting rates were determined by assuming a Poissonian distribution of counting events and using a correction for the multiplicity effect [22]. The procedure was iterated four times, giving a final R^2 of 0.986 (Fig. 2).

The true attenuation length was derived as a continuous function of x from the effective attenuation length by using the relation [15]:

$$\beta(x) = \beta_e(x) + (x - x_0)\frac{\partial \beta}{\partial x} \tag{4}$$

where $\beta=1/\Lambda$, and x_0 is the pressure at sea level.

3.3 Corrections to $\Lambda_{e,NM}$ for muon and background contributions

The contributions of muons and background to the neutron monitor counting rate were removed using the equation:

$$\frac{1}{\Lambda_{\mathrm{NM}}} = \frac{\sum_{i=1}^{n} \frac{C_i}{\Lambda_i}}{\sum_{i=1}^{n} C_i} = \frac{\frac{C_N}{\Lambda_N} + \frac{C_{\mu^-(\mathrm{s})}}{\Lambda_{\mu^-(\mathrm{s})}} + \frac{C_{\mu(\mathrm{f})}}{\Lambda_{\mu(\mathrm{f})}}}{C_N + C_{\mu^-(\mathrm{s})} + C_{\mu(\mathrm{f})} + C_{\mathrm{B}}} \tag{5}$$

where J_i and Λ_i are the counting rate and attenuation length, respectively, for the i^{th} component (note that this equation is incorrect in [6]). At sea level and high latitude,

contributions from nucleons (C_N), slow negative muons ($C_{\mu\text{-(s)}}$), fast muons ($C_{\mu(f)}$) and constant background (C_B), account for more than 98% of the neutron monitor counting rate (Table 1).

Table 1. Relative contributions to the neutron monitor counting rate at high latitude and sea level [57].

	IGY monitor % contribution	NM-64 monitor % contribution
Neutrons	83.6 ± 2.0	85.2 ± 2.0
Protons	7.4 ± 1.0	7.2 ± 1.0
Pions	1.2 ± 0.3	1.0 ± 0.3
Fast muons	4.4 ± 0.8	3.6 ± 0.8
Slow negative muons	2.4 ± 0.4	2.0 ± 0.4
Background	1.0	1.0

Fast muon intensity was scaled for altitude and latitude by using a parameterization of fast muon data [7] collected with a muon telescope (MT-64) during the IQSY survey [11, 13]. This apparatus consisted of two phosphor scintillators placed above and below an NM-64, with the counting circuits arranged in coincidence. The fast muon attenuation length, $\Lambda_{\mu(f)}$, is described well (R^2=0.976) by:

$$\Lambda_{\mu(f)}(R_C, x) = a_0 + a_1 R_C + x(a_2 R_C + a_3) \tag{6}$$

where a_i are fitting coefficients (Table 2). Based on a theoretical range-energy relation [23], muon energies above ~ 10 GeV are needed to penetrate the 5.4 cm of lead and 19 cm of polyethylene of an NM-64. The sea-level latitude dependence of fast muon intensity (Fig. 3) is much less pronounced than that of the neutron component.

Table 2. Coefficients for equation 6.

a_0	2.1658×10^{02}
a_1	8.7830×10^{00}
a_2	-1.3532×10^{-03}
a_3	3.7859×10^{-01}

The effective attenuation length for slow negative muons derived by [7] from measurements between 200 g cm^{-2} and 1033 g cm^{-2} [24-26] is described by:

$$\Lambda_{e,\mu-(s)}(R_C) = 233 + 3.68R_C \tag{7}$$

Slow muons are defined here to be those stopping in 117-83 g cm^{-2} of air equivalent, which corresponds to energies below approximately 0.3 GeV [24-26]. Based on [27] and [7], we assume that the sea-level latitude dependence for slow negative muons is roughly the same as that for fast muons.

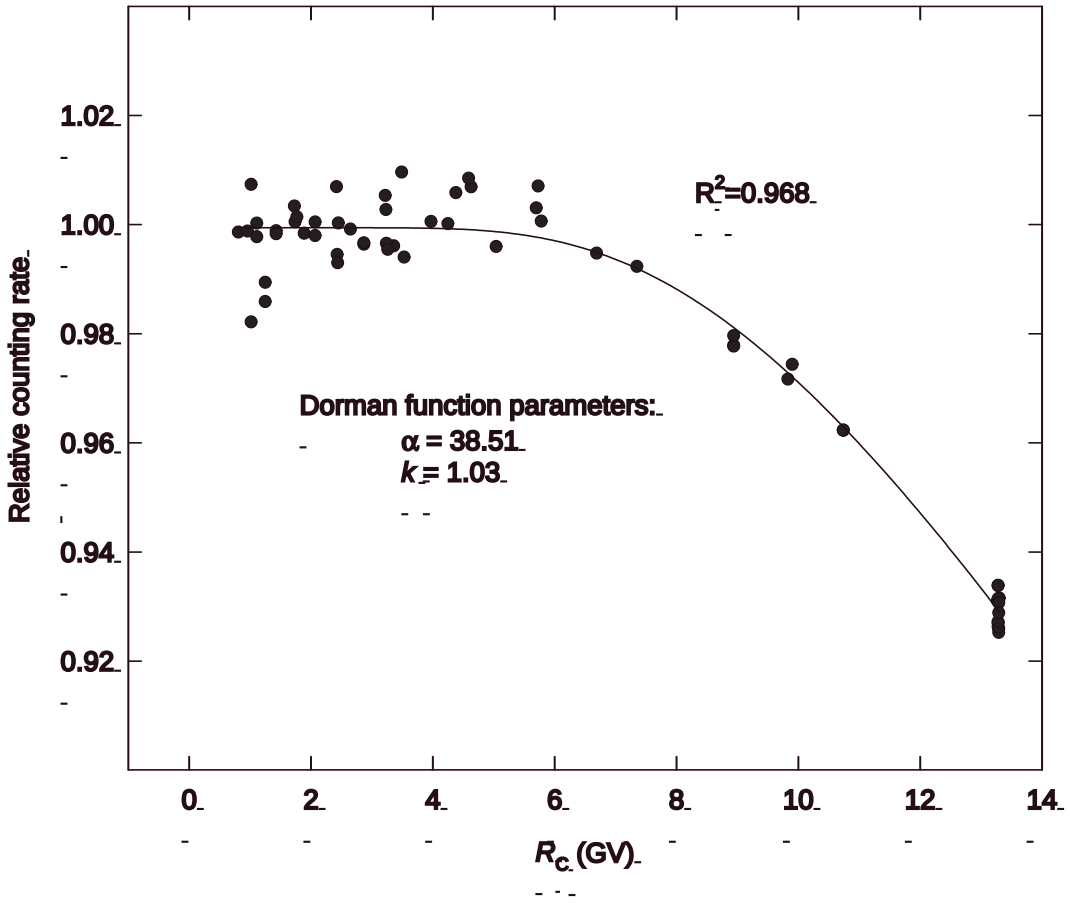

Figure 3. Dorman function (Eq. 3) fit to sea-level muon monitor counting rates of [11-14].

Table 3. Coefficients for equation 8.

N	9.9741 X 10^{-03}
α	4.5318 X 10^{-01}
K	-8.1613 X 10^{-02}
B_0	6.3813 X 10^{-06}
B_1	-6.2639 X 10^{-07}
B_2	-5.1187 X 10^{-09}
B_3	-7.1914 X 10^{-09}
B_4	1.1291 X 10^{-09}
B_5	1.7400 X 10^{-11}
B_6	2.5816 X 10^{-12}
B_7	-5.8588 X 10^{-13}
B_8	-1.2168 X 10^{-14}

3.4 Attenuation lengths for spallation reactions

Based on [15]'s neutron monitor data and the corrections described above, the atmospheric attenuation coefficient for high-energy (E_{med} ~ 120 MeV) spallation reactions (β_{sp}) is well described by the relation:

$$\beta_{sp}(R_C,x) = \beta_{NM,N}(R_C,x) = n\left(1+exp\left(-\alpha R_C^{-k}\right)\right)^{-1} + \left(b_0 + R_C b_1 + b_2 {R_C}^2\right)x + \left(b_3 + R_C b_4 + b_5 {R_C}^2\right)x^2 + \left(b_6 + R_C b_7 + b_8 {R_C}^2\right)x^3 \quad (8)$$

with the coefficients from Table 3. We expressed these results in terms of β rather than Λ for the convenience of calculating effective attenuation lengths. In order to obtain a physically realistic surface (Fig. 4) several parameters in Eq. 8 were constrained during the fitting procedure [7].

The effective attenuation length between two arbitrary atmospheric depths x_1 and x_2 is calculated from the relation:

$$\Lambda_e(R_C, x_1, x_2) = \frac{\int_{x_1}^{x_2} dx}{\int_{x_1}^{x_2} \beta(R_C, x)} \tag{9}$$

and therefore the effective attenuation length for high-energy spallation reactions ($\Lambda_{e,sp}$) between depths x_1 and x_2 is:

$$\Lambda_{e,sp}(R_C, x_1, x_2) = \frac{x_2 - x_1}{\left[n\left(1 + exp\left(-\alpha R_C - k\right)\right)^{-1} x + 1/2\left(b_0 + b_1 R_C + b_2 {R_C}^2\right)x^2 + 1/3\left(b_3 + b_4 R_C + b_5 {R_C}^2\right)x^3 + 1/4\left(b_6 + b_7 R_C + b_8 {R_C}^2\right)x^4 \right]_{x_1}^{x_2}} \tag{10}$$

Strictly speaking, the parameters in Table 3 are valid only for R_C from 0.5 GV to 13.3 GV, the limits of [15]'s coverage, and x from 1033 g cm^{-2} to 500 g cm^{-2}. However, our neutron monitor measurements near Bangalore, India in May, 2002 suggest that Eq. 10 can be accurately extrapolated to R_C of 17.25 GV.

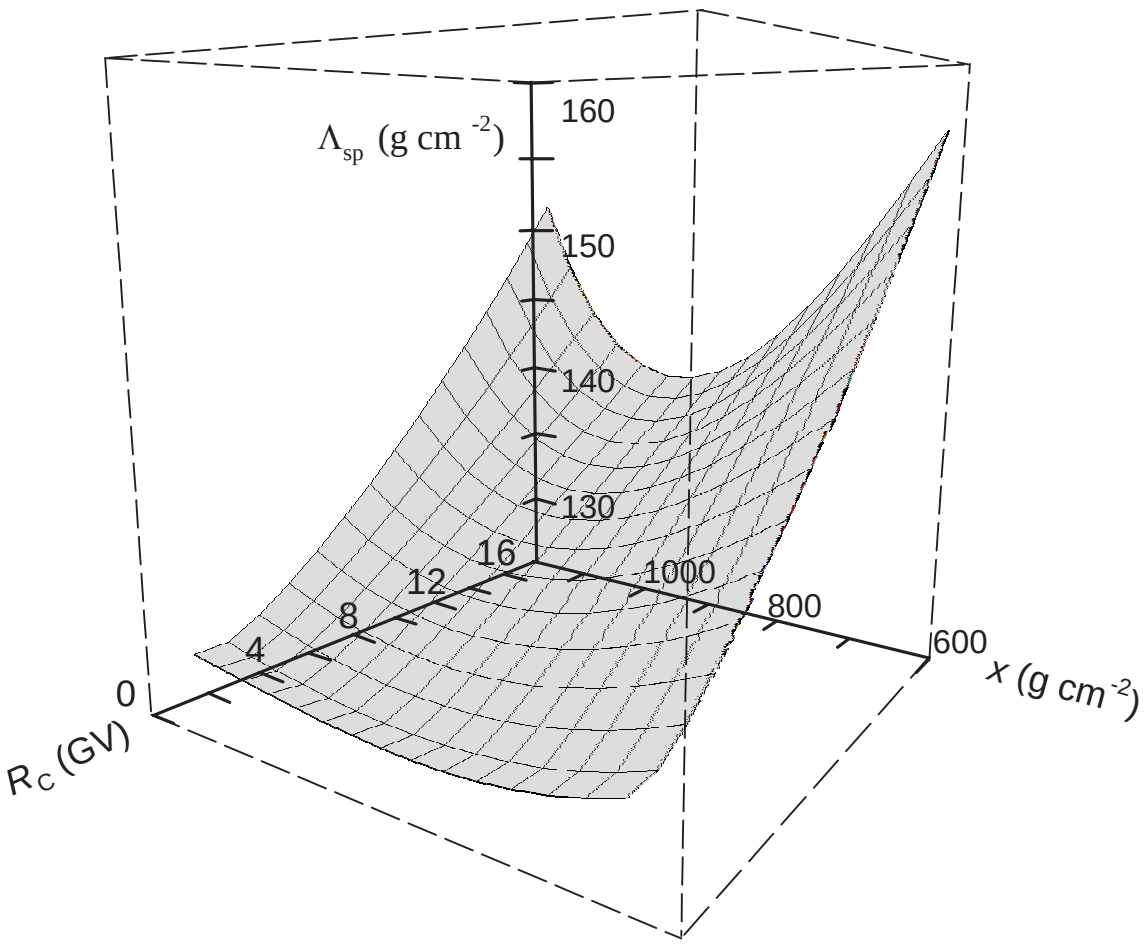

Figure 4. $\Lambda_{sp}(R_C,x)$ according to Eq 8. To avoid over fitting the data, this surface was obtained under the constraints: $\partial\Lambda_{sp}/\partial R_C \neq 0$ and $\partial\Lambda_{sp}/\partial x = 0$ only once at any x [7].

3.5 Latitude distribution of spallation reactions at sea level

In order to calculate nucleon fluxes at any point on earth, the latitude distribution of nucleon fluxes at some reference altitude is needed in addition to Eq. 10. The IQSY sea-level latitude survey (Fig. 2) [11-15] is adequate for this purpose. However, other latitude surveys conducted with neutron monitors (Table 4) provide a check on [11]'s sea level measurements, and extend the available measurements beyond R_C = 13.3 GV.

Because a main motivation for conducting sea-level latitude surveys is the comparison of primary cosmic-ray spectra over different solar minima, most latitude surveys have been conducted during solar quiescence. Their results consistently give a latitude effect (defined here as the ratio of the counting rate at R_C = 14 GV to that at R_C = 0 GV) of ~ 0.56. Differences between the solar minimum survey reported by [9] (used by both Lal [1, 2] and Dunai [4] as a sea-level baseline), the one reported by [11-15], and the most recent one [16] are negligible (Fig. 2) when data are ordered according to R_C, but not when they are ordered according to geomagnetic latitude (λ) [2], geomagnetic inclination (I) [4], or lower cutoff rigidity calculated for a centered dipole field ($R_L^{\text{Störmer}}$) [28] (see Section 6.0).

We suggest using the Dorman function (Eq. 3) parameters obtained from the most recent NM-64 survey [20] (Table 4) to scale spallation reactions because this survey is the most thorough and because it extends to R_C = 16.6 GV.

4. Scaling model for thermal neutron reactions

4.1 Attenuation lengths for thermal neutron reactions

Measurements of neutron multiplicity in neutron monitors and of star-size distributions in cloud chambers and nuclear emulsions suggest that the nucleon attenuation length decreases with increasing energy [6]. However, the importance of this effect at nucleon energies below 400 MeV is uncertain. Data from neutron multiplicity counters suggest that the effect may be important for scaling cosmogenic nuclides [6], contrary to earlier empirical and theoretical evidence [1] and to recent modeling [29]. Although there are currently insufficient data to fully describe the energy dependence of the nucleon attenuation length, it is likely that differences between attenuation lengths for most spallation reactions should be only on the order of 1-2 g cm^{-2}. Because this is smaller than uncertainties of empirical data, a single parameterization can be used to describe attenuation lengths for spallation reactions. However, the difference between attenuation lengths for thermal neutron reactions, Λ_{th}, and those for spallation reactions, Λ_{sp}, may be significant.

Although the altitude dependencies of fast and thermal neutron fluxes have been measured in several studies [30-33], reliable data are limited mostly to high altitudes (< 600 g cm^{-2}, > 4350 m). Because the fluxes of fast neutrons (E ~ 1 MeV) and thermal neutrons (E < 0.5 eV) have been experimentally shown to be in equilibrium [31], in this paper we consider attenuation lengths for fast neutrons (Λ_f) and thermal neutrons (Λ_{th}) to

Table 4. Sea-level latitude surveys of nucleon intensity, 1954-1997.

	Year	Type of monitor	α	k	$\frac{J_{NM}^{Rc=14\ GV}}{J_{NM}^{Rc=0\ GV}}$	Source
Solar minimum	1954	IGY	8.241	0.8756	0.56	[9] †
	1965	IGY	9.236	0.9146	0.56	[58]†
	1965	NM-64	9.819	0.9288	0.57	[11] †
	1974	NM-64	7.28	0.83	0.56	[59]
	1976	NM-64	8.953	0.9159	0.55	[60]†
	1987	NM-64	10.068	0.9519	0.56	[61]
			10.446	0.9644	0.56	
	1997	NM-64	10.275	0.9615	0.56	[20]
		BC‡	9.694	0.9954	0.50	
Solar maximum	1969	NM-64	7.79	0.83	0.58	[59]
	1981	9-NMD§	10.88	0.92	0.62	

†parameters reported by [61]
‡unshielded BF_3 proportional counter (sensitive to thermal neutrons)
§leadless neutron monitor

be equivalent. These energies are substantially below the ~ 40 MeV required to induce spallation reactions [2]. Note that our use of the term 'fast neutron' is different from mostof the cosmogenic literature but is consistent with definitions from nuclear physics (see [6] for definitions of fast neutrons and high-energy neutrons).

One of the most extensive surveys of thermal neutrons was a series of balloon flights carrying unshielded proportional counters [31]. Attenuation lengths reported by [31] agree well with airplane and balloon measurements of fast neutrons performed later [32] and with earlier values of Λ_{th} obtained with a shielded thermal neutron detector [30] over

the range 200-600 g cm^{-2}. Unfortunately, these surveys were restricted to atmospheric depths less than 715 g cm^{-2} (> 3200 m), and the data obtained at depths greater than 400 g cm^{-2} (< 5750 m) have large uncertainties.

A comparison of attenuation lengths measured by shielded and unshielded proportional counters with those measured independently by neutron monitors strongly suggests that the fluxes of neutrons of $E > 100$ MeV and those of $E < 10$ MeV (Table 5) attenuate in the atmosphere at different rates. These results are consistent with an energy spectrum that softens towards sea level. The magnitude of the difference between low- and high-energy nucleon attenuation lengths measured in the upper atmosphere is too large to be attributed to either solar activity or any known instrumental bias other than energy sensitivity [6].

In a more recent airborne survey [33], which extended to lower elevation than previous surveys [30-32], fast neutron fluxes were measured with proportional counters shielded by 7.5 cm and by 12.5 cm of paraffin. The relation between Λ_{th} and atmospheric depth was fitted to a linear regression by [33] (also reported in [34]). Throughout most of the atmosphere, Λ_{th} measured by [33] is greater than $\Lambda_{NM,N}$ (Eq. 10), but at high cutoff rigidities, the relationship is reversed near sea level (Fig. 5). This result is difficult to explain, since it would imply that the energy spectrum of the omnidirectional neutron flux hardens with depth in the lowermost 1000 m of atmosphere. This behavior is probably incorrect and can be explained by a lack of data near sea level ([33]'s measurements extend

Table 5. Comparison of $\Lambda_{e,th}$ and $\Lambda_{e,f}$ from various surveys with $\Lambda_{e,NM,N}$ from equation 10.

	Year	Δx* (g cm^{-2})	R_C† (GV)	$\Lambda_{e,th/f}$ (g cm^{-2})	$\Lambda_{e,NM,N}$ (g cm^{-2})
[30]	1947-49	200-600	<0.5	157	132
			1.7	157	132
			3.0	181	134
			11.5	206	151
			13.5	212	155
[31]	1952-54	200-715	<0.5	164	131
			1.4	164	138
			13.7	212	152
[32]	1964-71	200-715	<0.5	163 ± 10	132
			<0.5	172 ± 13	132
			4.5	181 ± 28	141
			17.0	215 ± 28	163
[33, 34]	1969	200-715	3.1	149	132
			4.9	155	134
			7.3	163	141
			11.7	182	149
			14.2	195	153

*Measurements are not necessarily evenly spaced throughout Δx.
† Cutoff rigidities for [30] and [31] were interpolated from grid values for 1955 [62] or taken directly from [49].

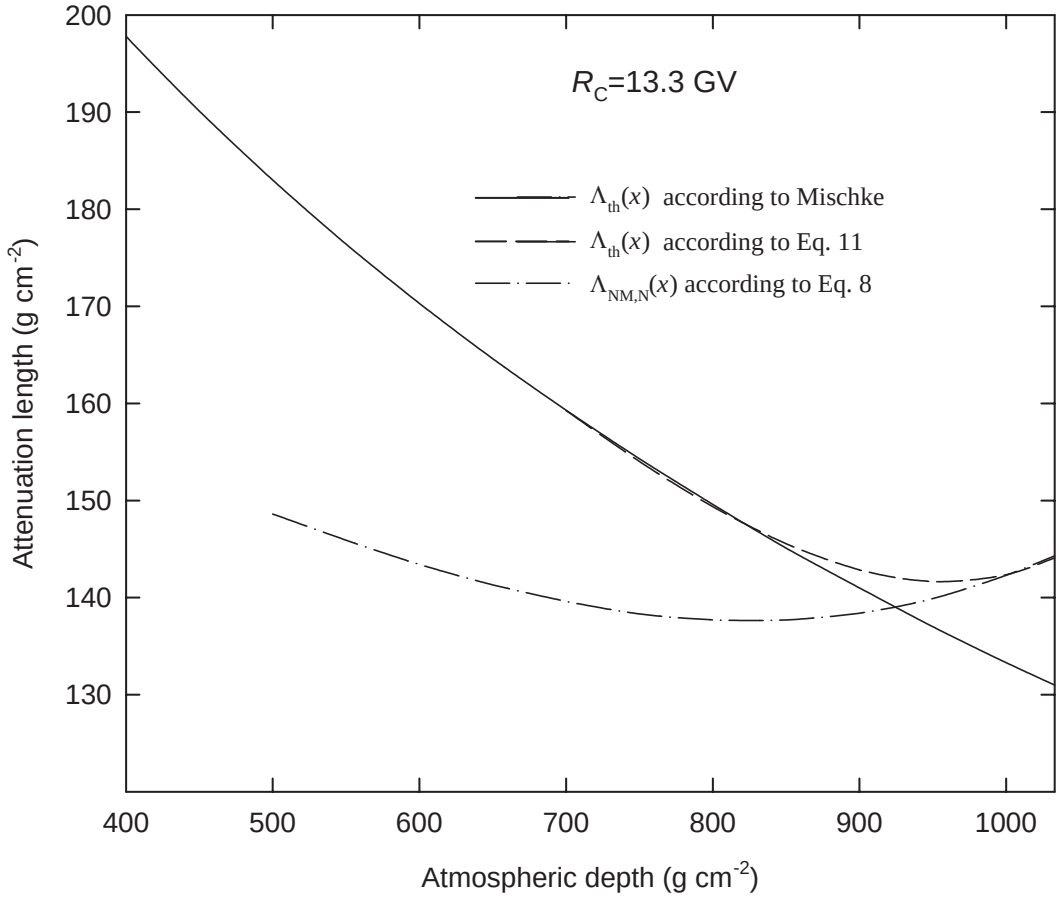

Figure 5. Thermal neutron attenuation lengths at R_C = 13.3 GV [33], with correction at low altitude.

from 307 g cm^{-2} (9500 m) to 960 g cm^{-2} (680 m)). To correct for this probable artifact of [33]'s regression, we modified his relationship so that Λ_{th} is always larger than or equal to $\Lambda_{NM,N}$, even at depths greater than ~ 900 g cm^{-2} (< 985 m) (Fig. 5). The attenuation coefficient for thermal neutron fluxes in the depth range 500-1033 g cm^{-2} is given by:

$$\beta_{th}(R_C, x) = c_0 + c_1 R_C + c_2 R_C^2 + (c_3 + c_4 R_C)x + (c_5 + c_6 R_C)x^2 + (c_7 + c_8 R_C)x^3 \quad (11)$$

and the parameters c_i are in Table 6. The effective attenuation length over the depth interval x_1 to x_2 is given by:

$$\Lambda_{e,th}(R_C, x_1, x_2) = \frac{x_2 - x_1}{\left[\left(c_0 + c_1 R_C + c_2 R_C{}^2\right)x + 1/2\,(c_3 + c_4 R_C)x^2 + 1/3\,(c_5 + c_6 R_C)x^3 + 1/4\,(c_7 + c_8 R_C)x^4\right]_{x_1}^{x_2}} \quad (12)$$

Simultaneous measurements during a 1996-1997 sea-level latitude survey [20] confirm that Λ_{th} approaches Λ_{NM} toward sea level. Aboard a ship in Antarctica, Λ_{th} was found to be 131 ± 2 g cm^{-2}, which is indistinguishable from the value of 129 ± 1 g cm^{-2} for Λ_{NM} (after removing the contribution of muons according to Eq. 5 and Table 1) [20].

Attenuation lengths reported by [33] are about 10% lower than attenuation lengths reported by others [30-32] for the fast and thermal neutron fluxes. The reason for this difference may be that [33]'s instrument was more sensitive to neutrons of higher energy. However, given that Λ_{th} changes rapidly with atmospheric depth, and that [30-32] lack

data in the lower atmosphere, it is probably more accurate to use [33]'s results, than to extrapolate the attenuation lengths of [30-32] to sea level.

Table 6. Coefficients for equation 11.

c_0	5.4196×10^{-01}
c_1	2.2082×10^{-02}
c_2	-5.1952×10^{-05}
c_3	7.2062×10^{-04}
c_4	-1.9702×10^{-04}
c_5	-9.8334×10^{-07}
c_6	3.4201×10^{-07}
c_7	4.9898×10^{-10}
c_8	-1.7192×10^{-10}

4.2 Latitude distribution of thermal neutron reactions at sea level

The only reliable latitude data for thermal neutron fluxes is the 1996-1997 sea-level latitude survey that carried two bare BF_3 thermal neutron counters along with the usual NM-64 [16]. The 10% greater latitude effect measured with the bare counters implies that sea-level latitude distribution of thermal neutron reactions (e.g., $^{35}Cl(n,\gamma)^{36}Cl$ and $^{40}Ca(n,\gamma)^{41}Ca$) should also be scaled separately from spallation reactions (Table 4). We therefore suggest using the Dorman function (Eq. 3) parameters corresponding to the 1997 bare counter (BC) survey as a baseline for scaling thermal neutron fluxes.

5. Solar activity

Nucleon attenuation lengths measured at high latitudes [18, 35] exhibit a strong dependence on solar activity. This dependence is related to changes in the energy spectrum of secondary nucleons and to variations in the relative contributions of muons, background and nucleons to the neutron monitor counting rate. As solar modulation increases, the primary energy spectrum hardens, and secondary cascades tend to penetrate more deeply into the atmosphere. Although the total counting rate of a neutron monitor decreases with increasing solar modulation, the proportion of counts from muons increases because muons have a high-energy progenitor that is less sensitive to solar modulation than is the nucleon flux.

The dependence of $\Lambda_{e,NM,N}$ on solar activity was measured by Raubenheimer and Stoker [35] at R_C = 4.9 GV and 8.3 GV. These results, expressed as the percent increase in the neutron monitor attenuation length ($\%\Delta\Lambda_{e,NM,N}$) over the solar minimum value due to an increase in solar activity, are represented by:

$$\%\Delta\Lambda_{e,NM,N}(C_{DR}, R_C) = d_0 + d_1 C_{DR} + d_2 C_{DR}^2 + (d_3 + d_4 C_{DR}) R_C + (d_5 + d_6 C_{DR}) R_C^2 + (d_7 + d_8 C_{DR}) R_C^3 \quad (13)$$

where C_{DR} is the counting rate of the Deep River, Ontario neutron monitor (R_C = 1.02 GV, x = 1016 g cm^{-2}) relative to that in May 1965; the values of the coefficients are given in Table 7. Raubenheimer and Stoker [35] found that changes in $\Lambda_{e,NM,N}$ over the solar cycle are independent of x, [18] found the dependence to be stronger at greater atmospheric depths, and [21] found the dependence to be greater at smaller atmospheric depths [35].

Raubenheimer and Stoker [35] measured the greatest overall change in attenuation length from solar maximum to solar minimum. Given that experimental results have been contradictory, additional measurements of the time dependence of neutron monitor attenuation lengths are needed.

Table 7. Coefficients for equation 13.

d_0	5.4196×10^{-01}
d_1	2.2082×10^{-02}
d_2	-5.1952×10^{-05}
d_3	7.2062×10^{-04}
d_4	-1.9702×10^{-04}
d_5	-9.8334×10^{-07}
d_6	3.4201×10^{-07}
d_7	4.9898×10^{-10}
d_8	-1.7192×10^{-10}

The usefulness of Eq. 13 for geological applications is limited by the lack of a well-constrained solar modulation record for times older than ~ 400 years BP. There is some promise that records of atmospheric radionuclides deposited in sediments and tree rings can be used to shed light on past solar modulation, however, the solar-activity signal in these records is often obscured by natural processes on earth. Although the behavior of solar modulation in the geologic past is not well known, observations of solar modulation over the past 50 years place reasonable limits on the range of the likely effective (integrated) solar modulation levels for the past several hundreds of thousands of years.

6. Temporal geomagnetic correction

Geomagnetic dipole intensity changes over time [36], and so therefore do cutoff rigidities over much of the earth. The magnitude of the temporal variation in geomagnetic shielding depends on latitude; low latitudes experience stronger fluctuations in primary intensity than do high latitudes. Near the geomagnetic poles, where the magnetic field is mostly in the vertical direction, vertically-incident primaries are admitted to the earth regardless of dipole intensity.

Time-averaged R_C (and also λ and I, which serve analogous functions) can be calculated from geomagnetic field models. For durations longer than 20,000 years, a geocentric axial dipole field is usually assumed (the GAD hypothesis) (e.g., [4, 37, 38]). The basis of the GAD hypothesis is that higher-order components of the geomagnetic field are short-lived, and that over the long term, transitory non-dipole features have canceling effects so that the field averages to a simple dipole. Terrestrial and marine records of the intensity and postion of this assumed dipole are available from several authors (e.g., [36, 39-42]).

In this section we demonstrate how the scaling models derived in Sections 3 and 4 can be used to correct for fluctuations in dipole intensity. We assume that an accurate paleointensity record is available and that for periods greater than 20,000 years the GAD hypothesis is valid. Although additional work is needed to constrain the paleomagnetic record and to determine the minimum averaging period necessary for the GAD hypothesis to apply, these issues will not be discussed here. Also, we disregard the effects

of solar modulation, as did previous investigators working with empirical data [2, 4].

Several investigators have explicitly addressed the problem of correcting cosmogenic nuclide production rates for temporal fluctuations in dipole intensity and position. [43] developed a correction model based on [2]'s scaling formula and published field strength/rigidity relationships. [37] investigated the effects of polar wander on production rates at 44.3° N latitude. [37] and [44] considered the effects of variations in the dipole intensity and concluded that they are negligible for their mid-latitude locations.

Shanahan and Zreda [38] gave the first published description of a dipole intensity correction at the geomagnetic equator. This correction utilized [2]'s scaling model and a relation between global atmospheric production rates of cosmogenic nuclides (Q) and magnetic dipole intensity (M) given by [45]:

$$\frac{Q}{Q_0} = \left(\frac{M}{M_0} \right)^{0.52} \tag{14}$$

This expression was derived from a numerical integration over all latitudes of a first-order analytical relation describing primary particle motion in dipole field.

The geomagnetic correction model described in this section improves on previous approaches ([38, 43]) in two important ways: it is based on a model that better describes the current distribution of cosmic-ray intensity and it does not rely on Eq. 14.

The applicability of Eq. 14 to scaling *in-situ* cosmogenic production rates is limited by several factors. First, in deriving Eq. 14 [45] assumed that the nuclide production per

primary cosmic ray particle in a column of atmosphere is independent of primary energy. This allowed [45] that global production is a function only of the total primary cosmic-ray flux. However, later work [46] showed that nuclide production per primary particle increases by a factor of 2.7 from 60° to 0° geomagnetic latitude, and therefore that the energy spectrum of primaries is an important factor in global cosmogenic nuclide production. Second, [45] assumed a simple power law function for the integral primary energy spectrum that was based on early data from the 1940s and early 1950s. Better estimates (e.g., [47]) are now available. Unfortunately, these assumptions, which were explicitly stated by [45], are often overlooked. Third, the greatest obstacle to using Eq. 14 is that there is no rigorous way to relate the dipole-intensity dependence of global production rates to local production rates using Lal's [2] scaling model, because the parameterization given by [2] is valid only to an altitude of 10 km (~ 260 g cm^{-2}), whereas most atmospheric cosmogenic nuclides are produced at altitudes above 10 km [46].

Recently, [28] proposed a temporal geomagnetic scaling model based on measurements of paleo-inclination and paleo-horizontal field intensity at a sample site. This model uses a relation derived by Rothwell [48] from the Störmer equation for the lower cutoff rigidity of a primary proton in an axial-dipole field:

$$R_{\mathrm{L}}^{\mathrm{Störmer}}\left(\lambda_{\mathrm{dpl}}\right)=\frac{30}{4r_{\mathrm{e}}^{2}}M_{0}\cos^{4}\lambda_{\mathrm{dpl}}\ [\mathrm{GV}] \tag{15}$$

where $R_L^{\text{Störmer}}(\lambda_{dpl})$ is the Störmer lower cutoff rigidity as a function of geomagnetic latitude in a dipole field (λ_{dpl}), r_e [m] is the radius of the earth and M_0 [A m^2] is dipole intensity. Rothwell [48] substituted λ_{dpl} in Eq. 15 with geomagnetic inclination (I_{dpl}) using a relation that applies only to a dipole field:

$$\tan I_{dpl} = 2\tan \lambda_{dpl} \tag{16}$$

He also substituted a relation between dipole intensity and horizontal field intensity (H_{dpl}) that is valid only for a dipole field:

$$H_{dpl} = M_0 r_e^{-3} \cos \lambda_{dpl} \tag{17}$$

The result is a relation between $R_L^{\text{Störmer}}$, horizontal field strength and magnetic inclination:

$$R_L^{\text{Störmer}}\left(I_{dpl}, H_{dpl}\right) = \frac{30}{4} r_e^2 \frac{H_{dpl}}{1 + \frac{1}{4}\tan^2 I_{dpl}} [\text{GV}] \tag{18}$$

Because the geomagnetic field far from the earth influences primary cosmic-ray trajectories, it is always necessary to assume a model of the entire geomagnetic field when calculating cutoff rigidity. In applying Eq. 18 to the real geomagnetic field, one assumes that R_L can be estimated by replacing the earth's complex (short term) magnetic field with a dipole whose magnitude and direction are determined only by the magnitude and direction of the surface field [48]. Rothwell [48] recognized that the path of a

cosmic-ray particle is determined not only by the field at the surface, but also by the main dipole field, and suggested that the value of R_C should lie between $R_L^{Störmer}(\lambda_{dpl})$ and $R_L^{Störmer}(I,H)$, where I and H are calculated from the real magnetic field. Due to the inherent limitations of Eq. 18, Rothwell [48] advocated using this expression *only* in conjunction with an empirical relation that he gives in [48]. He [48] showed that Eq. 18 does not satisfactorily align cosmic-ray data from different latitude transects into a unique relationship (Fig. 6). The inadequacy of $R_L^{Störmer}(I,H)$ is also demonstrated by [4]'s Fig. 1, which shows a non-unique relation between cutoff rigidity and nucleon intensity (cosmic-ray intensity varies by 12% between some locations at constant $R_L^{Störmer}(I,H)$) and [28]'s Fig. 1, which suggests that at 620 g cm^{-2} (4300 m) nucleon intensity is nearly constant with increasing cutoff rigidity beyond 12 GV. The physical reality is that the earth's magnetic field at large distances (many earth radii) influence cosmic rays, and that knowledge of the surface field is useful only insofar as it helps to constrain models of the entire geomagnetic field. Because Eq. 18 poorly accounts for the distribution of cosmic rays in the present geomagnetic field (Fig. 6), it should be used with caution in paleomagnetic fields, and its limitations should be well understood.

6.1 Geomagnetic scaling based on R_C

The problem of scaling production rates for fluctuations in dipole intensity is simplified when cosmic-ray data are ordered according to R_C. R_C is calculated by tracing cosmic-ray trajectories in a model of the geomagnetic field [49]. If we assume that cosmic-ray intensity at a given atmospheric depth is a unique function of R_C, then the

main challenge is calculating R_C for past epochs at the sample site and calibration site. This assumption allows recent cosmic-ray measurements to be directly applied to paleomagnetic fields.

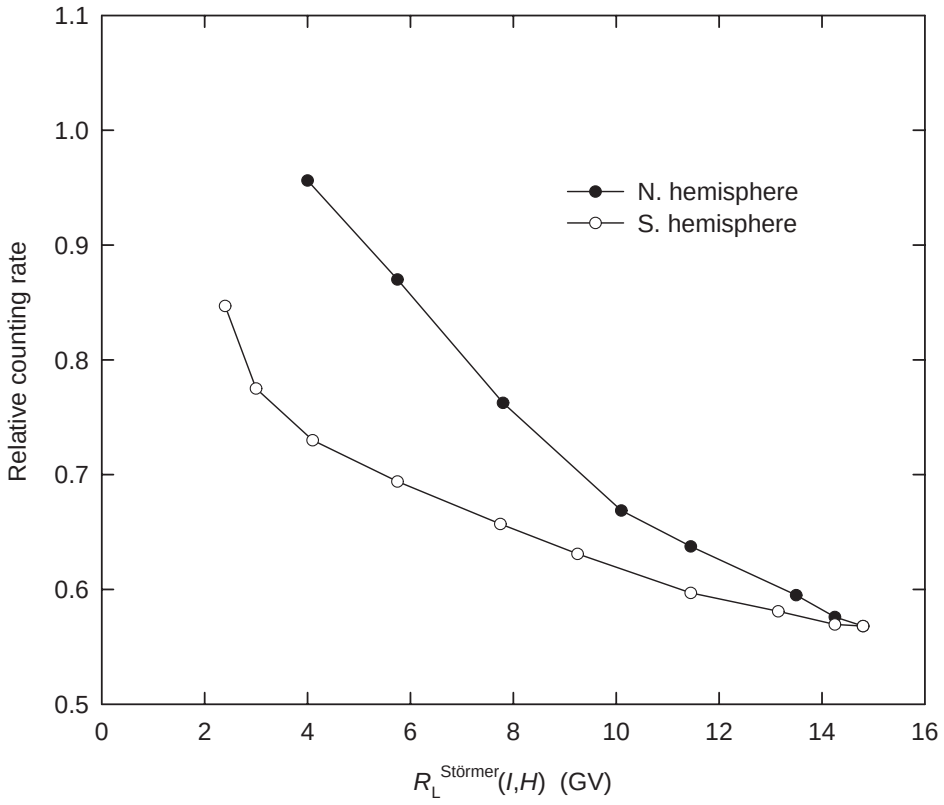

Figure 6. Neutron monitor counting rates at sea level ordered according to $R_L^{Störmer}(I,H)$ where I and H are from the surface field [48].

Usually the approximation is made that over periods greater than ~ 20,000 years, the average behavior of the geomagnetic field converges to an axially-symmetric centered-dipole field [4, 29, 37] with an integrated dipole intensity that depends on the exposure period. We therefore calculated R_C for an axially-symmetric centered-dipole field having an intensity ranging from 1.25 to 0.25 times the 1945 value of 8.084×10^{22} A m^2 [50] (Fig. 7). We used the numerical trajectory tracing code and the methods described by [20, 49] to trace the paths of anti-protons analytically ejected from the earth in the vertical direction. Particles escaping the geomagnetic field to infinity correspond to the trajectories of primary cosmic-ray protons that are admitted to the earth. The lower, upper and effective cutoffs (R_L, R_U and R_C) were calculated by tracing particles at 0.01 GV intervals. R_C was calculated by subtracting the total of the allowed rigidity intervals from the highest forbidden rigidity interval (R_U) (Fig. 8). These results are described ($R^2 > 0.999$) by:

$$R_{C,dpl} = \sum_{i=1}^{i=6} \left(e_i + f_i \left(\frac{M}{M_0} \right) \right) \lambda_{dpl}^{(i)} \tag{19}$$

with the parameters from Table 8. These parameters are valid between $\lambda_{dpl} = 0°$ and 55°. Above $\lambda_{dpl} = 55°$, cosmic-ray fluxes are unaffected by changes in dipole intensity. Note that in Eq. 19, λ_{dpl} is raised to the i^{th} power.

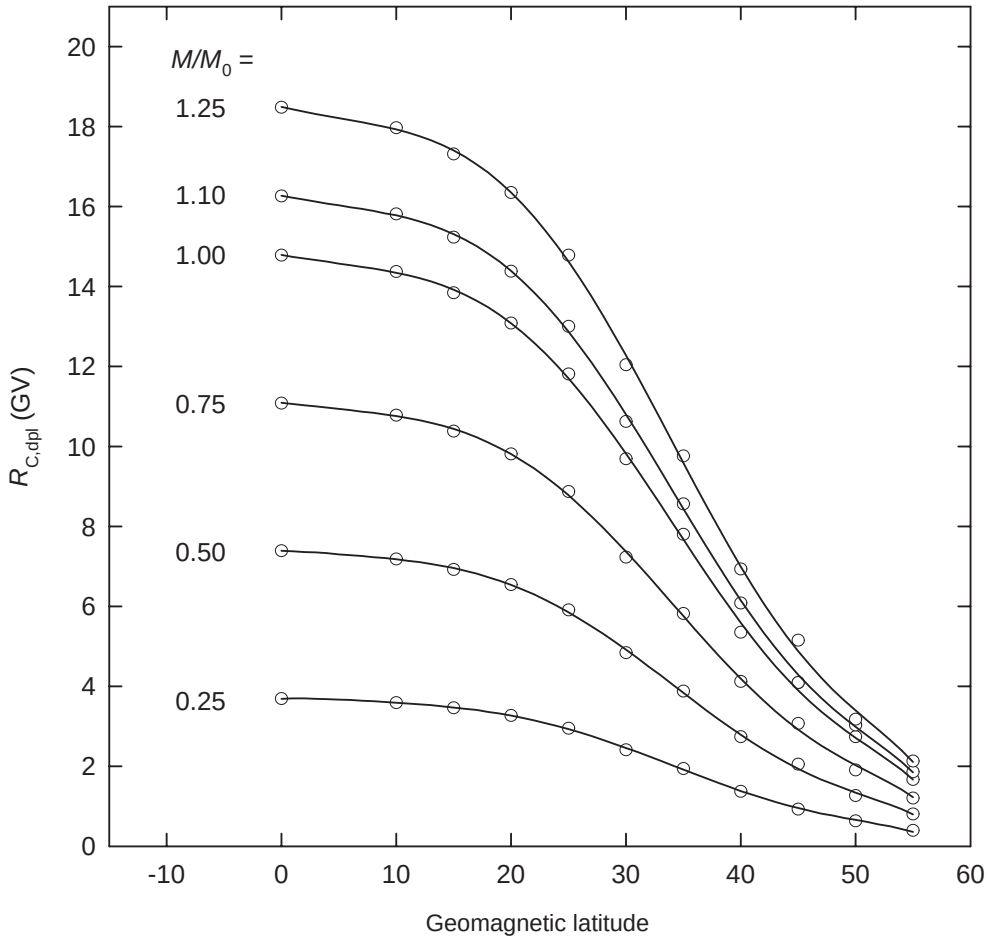

Figure 7. The latitude dependence of R_C in an axially-symmetric centered-dipole field at dipole intensities ranging from 0.25 to 1.25 times the 1945 reference value (M_0 = 8.084 x 10^{22} A m^2 [50]). The lines are according to Eq. 19.

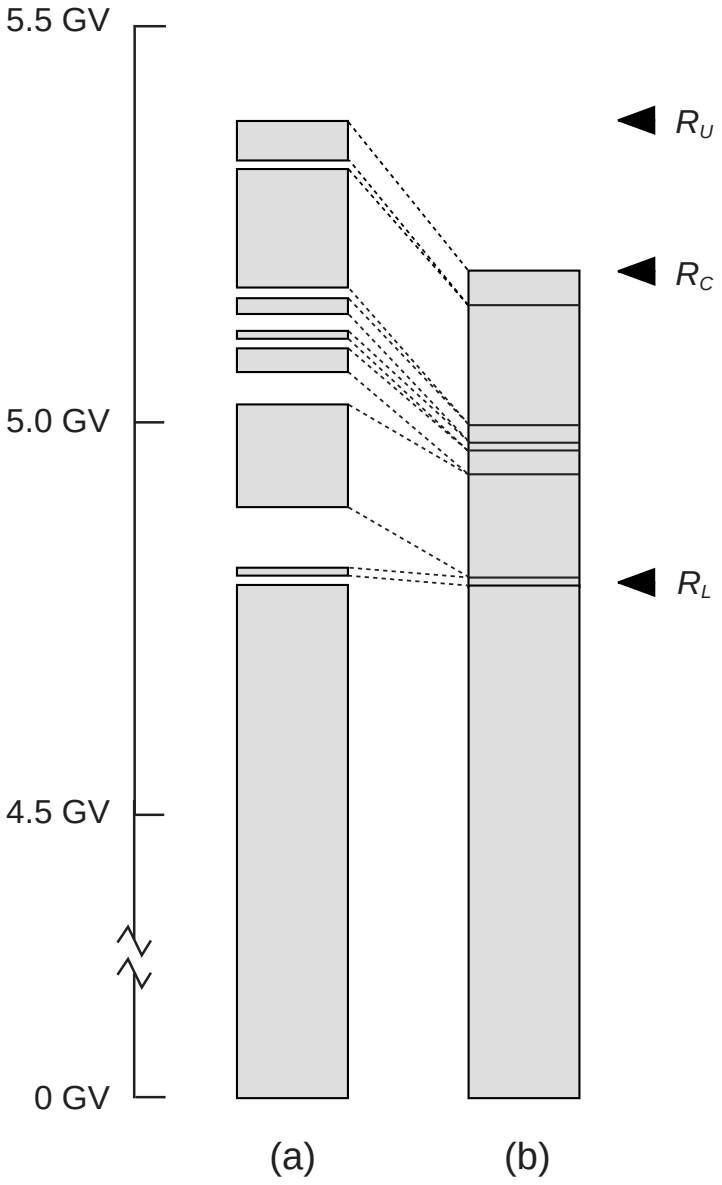

Figure 8. (a) The penumbral structure for vertically incident cosmic-ray protons, 20 km above Tucson, Arizona (32.1° N, 249.1 E) calculated by tracing cosmic-ray trajectories through International Geomagnetic Reference Field 1995. Forbidden rigidity intervals are shaded. (b) R_C is calculated by subtracting the sum of the allowed rigidity intervals from R_U.

Table 8. Coefficients for equation 19.

	e_i	f_i
i=0	-4.3077×10^{-03}	$1.4792 \times 10^{+01}$
1	2.4352×10^{-02}	-6.6799×10^{-02}
2	-4.6757×10^{-03}	3.5714×10^{-03}
3	3.3287×10^{-04}	2.8005×10^{-05}
4	-1.0993×10^{-05}	-2.3902×10^{-05}
5	1.7037×10^{-07}	6.6179×10^{-07}
6	-1.0043×10^{-09}	-5.0283×10^{-09}

For the special case in which the GAD hypothesis is invalid and a time series of *I* and *H* is available at the sample site, but data at other locations are too few to constrain the entire field, there are several methods of calculating either the lower vertical cutoff rigidity or effective vertical cutoff rigidity. Based broadly on the methods proposed by [48] and partially adopted by [28], we calculated cutoff rigidities using three approaches. The first approach assumes an axially-symmetric centered-dipole field with a known pole position. The second approach assumes a centered dipole field with the axial position determined only by a local value of *I* an *H*. The third approach is to take the mean of the values from the first two approaches. For each of these approaches, we separately applied Eqs. 15 and 19.

Cutoff rigidities were calculated on a 5° latitude by 15° longitude grid using a 10^{th} degree spherical harmonics representation of International Geomagnetic Reference Field (IGRF) 1980. We compared these results to effective vertical cutoff rigidities calculated by [51] for IGRF 1980. The purpose of the calculations was to determine which method

gives the closest approximations of cutoff rigidities derived by trajectory tracing, and to quantify the discrepancies (Table 9). Effective vertical cutoffs calculated from an average of the first and second methods proved superior, with the estimated vertical cutoff rigidity being on average within 1 GV and no more than 3.5 GV from the true value [51]. Cutoffs

Table 9. A comparison of methods of estimating R_C from from limited geomagnetic data. The average residual is the average difference between R_C calculated by [51] on a 5° latitude by 15° longitude grid for the IGRF 1980 field and R estimated for the same field the methods listed below. These comparisons cover the range –55° and 55° degrees latitude.

		Field model/method	Average residual (GV)	Average absolute residual (GV)	Maximum absolute residual (GV)
$R_L^{\text{Störmer}}$	a.	axially-symmetric centered dipole	0.6	2.0	6.9
	b.	centered dipole with pole at 78.81° N	0.6	2.5	5.4
	c.	dipole field constructed from surface values of I and H	0.4	1.5	5.7
	d.	average R from b and c	0.5	1.0	4.5
$R_{C,dpl}$	a.	axially-symmetric centered dipole	0.0	1.9	5.3
	b.	centered dipole with pole at 78.81° N	0.0	1.4	4.9
	c.	dipole field constructed from surface values of I and H	-0.2	1.4	5.5
	d.	average of b and c	0.0	0.8	3.5

calculated using Eq. 15 for lower cutoff rigidity also give a reasonable, but slightly less accurate approximation to R_C. The uncertainty in applying each of these methods to real cosmogenic dating scenarios is difficult to assess, since the position of the magnetic poles and local measurements of I and H have associated uncertainties (which may be correlated), and since errors in paleo-cutoff rigidity estimates tend to have canceling effects over large integration periods.

6.2 Calculating time-integrated cosmic-ray fluxes

The equations ordinarily used for interpreting cosmogenic radionuclide data assume that the production rate (P) at a sample location is constant with time [2, 52]. This approximation allows for a straightforward analytical solution to the problem of calculating exposure age (t) from measured sample inventories of spallogenic nuclides (N_{meas}) [2, 52]:

$$N_{meas} = \left(\frac{P_{sp}}{\lambda_{dec} + \varepsilon/\Lambda_{sp,ss}} \right) exp\left(-x_{ss}/\Lambda_{sp,ss}\right)\left[exp\left(\varepsilon t/\Lambda_{sp,ss}\right) - exp\left(-t\left(\lambda_{dec} + \varepsilon/\Lambda_{sp,ss}\right)\right)\right] + N_0\, exp\left(-\lambda_{dec} t\right) \tag{20}$$

where P_{sp} is the production rate of a spallogenic nuclide at the land surface, ε is the erosion rate [g cm^{-2} y^{-1}], λ_{dec} is the decay constant, x_{ss} is the depth of a sample below the earth's surface [g cm^{-2}], $\Lambda_{sp,ss}$ is the effective subsurface attenuation length for spallogenic nuclide production [g cm^{-2}] and N_0 is the inherited inventory.

The time dependence of production rates can be taken into account by discretizing the exposure period into n time intervals of width Δt_i, and calculating an effective production rate ($P_{sp}^{\Delta ti}$) over each Δt_i. The equation relating exposure age to production rates [2] is then given by:

$$N_{calc} = \sum_{i=1}^{i=n} \left(\frac{P_{sp}^{\Delta t_i}}{\lambda_{dec} + \varepsilon/\Lambda_{sp,ss}} \right) exp\left(-x_{ss}/\Lambda_{sp,ss}\right)\left[exp\left(\varepsilon \Delta t_i/\Lambda_{sp,ss}\right) - exp\left(-\Delta t_i\left(\lambda_{dec} + \varepsilon/\Lambda_{sp,ss}\right)\right)\right] + N_{\Delta t_{i-1}}\, exp\left(-\lambda_{dec}\Delta t_i\right) \quad (21)$$

where $N\Delta t_{i\text{-}1}$ is the inventory from the preceding time step. For $i = 1$, $N\Delta t_{i\text{-}1}$ corresponds to the inherited inventory.

Eqs. 20 and 21 require additional terms if thermal and epithermal neutron reactions are important, as in the production of ^{36}Cl [52]. The depth dependencies of thermal and epithermal neutron fluxes follow the form of a triple exponential: $A\ exp(-Bx) + C\ exp(-Dx) + E\ exp(-x/\Lambda_{th,ss})$, where the parameters A,B,C,D and E for a given material are calculated from physical and chemical properties [53], and Λ is the subsurface attenuation length for thermal neutron reactions, which can be assumed to be the same as for spallation reactions. If the profile of combined epithermal and thermal neutron production can be fitted to a single triple exponential function, then the discretized form of the buildup equation for combined thermal, epithermal and spallogenic production is:

$$N_{\text{calc}} = \sum_{i=1}^{i=n} \left(\frac{P_{\text{sp}}^{\Delta t_i}}{\lambda_{\text{dec}} + \varepsilon/\Lambda_{\text{sp,ss}}} \right) exp\left(-x_{\text{ss}} / \Lambda_{\text{sp,ss}}\right)\left[exp\left(\varepsilon \Delta t_i / \Lambda_{\text{sp,ss}}\right) - exp\left(-\Delta t_i \left(\lambda_{\text{dec}} + \varepsilon/\Lambda_{\text{sp,ss}}\right)\right)\right]$$
$$+ \left(\frac{P_{\text{th}}^{\Delta t_i}}{\lambda_{\text{dec}} + B\varepsilon} \right) A\, exp\left(-Bx_{\text{ss}}\right)\left[exp\left(B\varepsilon \Delta t_i\right) - exp\left(-\lambda_{\text{dec}} \Delta t_i\right)\right]$$
$$+ \left(\frac{P_{\text{th}}^{\Delta t_i}}{\lambda_{\text{dec}} + D\varepsilon} \right) C\, exp\left(-Dx_{\text{ss}}\right)\left[exp\left(D\varepsilon \Delta t_i\right) - exp\left(-\lambda_{\text{dec}} \Delta t_i\right)\right]$$
$$+ \left(\frac{P_{\text{th}}^{\Delta t_i}}{\lambda_{\text{dec}} + \varepsilon/\Lambda_{\text{th,ss}}} \right) E\, exp\left(-x_{\text{ss}} / \Lambda_{\text{th,ss}}\right)\left[exp\left(\varepsilon \Delta t_i / \Lambda_{\text{th,ss}}\right) - exp\left(-\lambda_{\text{dec}} \Delta t_i\right)\right]$$
$$+ N_{\Delta t_{i-1}}\, exp\left(-\lambda_{\text{dec}} \Delta t_i\right) \tag{22}$$

For each additional production mechanism having an exponential depth dependence in the subsurface (e.g., slow negative muons and fast muons), an additional term of the same form as the first terms on the right-hand sides of Eqs. 21 and 22 may be added, with the subsurface attenuation length for that component substituted for Λ_{ss}. The production rates for fast muons and slow muons can be scaled from the calibration site to the sample site using the scaling formulas in Section 3.3.

The exposure duration is found by calculating the number of time steps (n) needed to make the calculated nuclide inventory for a sample, N_{calc}, equal to the measured nuclide inventory of a sample (N_{meas}):

$$t = n \cdot \Delta t_i \tag{23}$$

Because the accuracy of Eq. 23 depends on the size of the time steps, it may be necessary

to make Δt_i smaller than would be justified by the resolution of the geomagnetic record alone.

A first approximation to the surface exposure age (t_{app}) can be calculated from Eqs. 20-22 by neglecting geomagnetic effects. A second approximation of n is obtained from $t_{app}/\Delta t_i$. This value of n then is used in Eq. 21 or 22 to calculate a first approximation of N_{calc}. If $N_{calc} > N_{meas}$ then n should be decreased on the next iteration. If $N_{calc} < N_{meas}$ then n should be increased. This iterative procedure yields exposure ages that converge on the true exposure age.

Eqs. 21 and 22 require knowledge of the production rate at a sample site over each time step. A calibrated production rate (P_{clb}) corresponding to a different location and exposure period can be used at any given sample site if differences in atmospheric shielding, cutoff rigidity, topographic shielding, and sample depth are taken into account by applying scaling factors:

$$P^{\Delta t_i} = f_{topo} f_{ss} f_{RC,x}(\Delta t_i) P_{clb} \qquad (24)$$

The factor f_{topo} accounts for differences in topographic shielding and exposure angle at the sample site and calibration site. If both sample site and calibration site are flat and unobstructed, $f_{topo} = 1$. The factor f_{ss} normalizes the subsurface production rate at the calibration site to surface production rate. Since most of the reported production rates are already normalized to the surface value, f_{ss} is usually equal to 1. The factor $f_{Rc,x}(\Delta t_i)$, which accounts for differences in x and R_C between calibration site and sample site, may

have a strong time dependence and therefore should be calculated for each Δt_i. This scaling factor is given by:

$$f_{R_C,x}(\Delta t_i) = \frac{J_{\text{clb}}^{\text{avg}}}{J(\Delta t_i)} \tag{25}$$

where $J_{\text{clb}}{}^{\text{avg}}$ is the average cosmic-ray flux at the calibration site and $J(\Delta t_i)$ is the cosmic-ray flux at the sample site during time interval i. In applying Eq. 24, it is necessary to know only the relative nucleon fluxes, which can be calculated from the effective attenuation lengths and latitude curves in Sections 3-4. The average cosmic-ray flux at the calibration site is given by:

$$J_{\text{clb}}^{\text{avg}} = \frac{\int J_{\text{clb}}^{\text{avg}}(R_C, x)dt}{\int dt} \tag{26}$$

which must be integrated numerically over the exposure duration of the calibration site. A sample calculation demonstrating our geomagnetic procedure is available as an **EPSL online Background Dataset (http://www.elsevier.nl/locate/epsl/)**

Temporal variations in dipole intensity can also be accounted for in a less rigorous way by calculating a single effective production rate at the sample site. This effective production rate can be obtained by calculating an effective R_C for the sample site, which is calculated from the average M/M_0 over the exposure period. Although this approach is less rigorous than the one described above, it can be used to gain an initial estimate of the temporal geomagnetic effect.

Masarik *et al*. [29] have suggested that geomagnetic corrections calculated by [38] for equatorial stromatolite samples with ages of 8-12 ky may be too large. According to [38], the correction was approximately +20%, whereas [29] computed a correction of –1%. Our calculations based on the scaling model given here and the Sint-200 record [36] also give a correction that is smaller and in the opposite direction (~ -5%). Because the production rates used by [38] were based mostly on calibration sites at high and mid latitudes, the production rates at the calibration sites should be mostly independent of dipole intensity. However, near the equator, neutron fluxes were generally greater over the past 8-12 ky, meaning that production rates were higher, and that uncorrected ages would to be too old.

7. Comparison and validation of scaling models

In order to compare scaling models given by [2, 4] with the ones derived here, it is necessary to express these models according to common elevation and geomagnetic parameters. Because the models given here and by [4] are already ordered according to atmospheric depth [g cm^{-2}], we expressed Lal's [2] scaling model in terms of atmospheric depth. The U.S. standard atmosphere, 1976, which [2] used to convert his original scaling model [1] from pressure units to elevation units, was used to reverse that transformation. We converted R_C in our models and geomagnetic inclination in [4]'s model, to geomagnetic latitude in a centered dipole field having the 1945 dipole intensity, M_0 = 8.084×10^{22} A m^2 [50].

Different latitude effects are given by our sea level NM-64 curve, [2]'s sea level curve and [4]'s sea level curve (both derived from [9]) (Fig. 9) because latitude survey data were ordered according to different geomagnetic cutoff parameters by the respective authors. Effective vertical cutoff rigidity, used in this work, is the only one that gives a unique relationship for latitude survey data, regardless of the survey route. The shapes of both [2]'s and [4]'s latitude curves depend on the longitudes as well as the latitudes covered by the surveys they used. Conceivably, the discrepancies in Fig. 9 could have been larger, given the non-unique relations that geomagnetic latitude and geomagnetic inclination have with primary cosmic-ray intensity.

Altitude effects given here also are different from those given by [2, 4]. [4]'s attenuation lengths are closer to attenuation lengths we give for spallation reactions, whereas [2]'s are closer to our thermal neutron attenuation lengths. This later result is expected, since both [2]'s model and our model for thermal neutron reactions incorporate data from shielded and unshielded proportional counters, which consistently give higher attenuation lengths than other instruments.

Recent measurements of cosmogenic nuclide production in artificial targets [54] afford the opportunity to validate our attenuation length model for spallation reactions at a single R_C and over a small range of atmospheric depths. Three water targets were exposed at 960 g cm^{-2} (620 m), 644 g cm^{-2} (3810 m) and 570 g cm^{-2} (4745 m) on Mount Blanc, France from February 1993 to May, 1994 (R_C = 4.82 GV, geomagnetic latitude = 40.5° I = 61.7° for epoch 1995) [54]. The effective attenuation length of 130 ± 4 g cm^{-2} measured for ^{10}Be production in oxygen compares well with both the effective

attenuation length given in this work for spallation reactions and the attenuation length given by [4] for nuclear reactions (both are 131 g cm^{-2}). A value of 148 g cm^{-2} is obtained for this location from [2]'s polynomial for nuclear disintegrations. The neutron monitor data on which our spallation scaling model is based are particularly well suited to scaling ^{10}Be production because neutron monitors are sensitive to the same portion of the nucleon spectrum that produces the ^{16}O(n,x)^{10}Be reaction (Table 10). Future work with artificial or geological targets should focus on low-latitude, high-altitude locations because this is where discrepancies between scaling models are greatest (Fig. 10).

Table 10. Median energies for cosmogenic nuclide production by nucleons [7] and for the neutron monitor response to neutrons [57], both at high latitude and sea level. 1σ uncertainties are approximately 25%.

		E_{med} (MeV)
Reaction	K(n,x) ^{36}Cl	13
	Ca(n,x) ^{36}Cl	55
	Si(n,x) ^{26}Al	70
	O(n,x)^{14}C	105
	O(n,x)^{10}Be	140
Neutron monitor	NM-64	130
	IGY	160

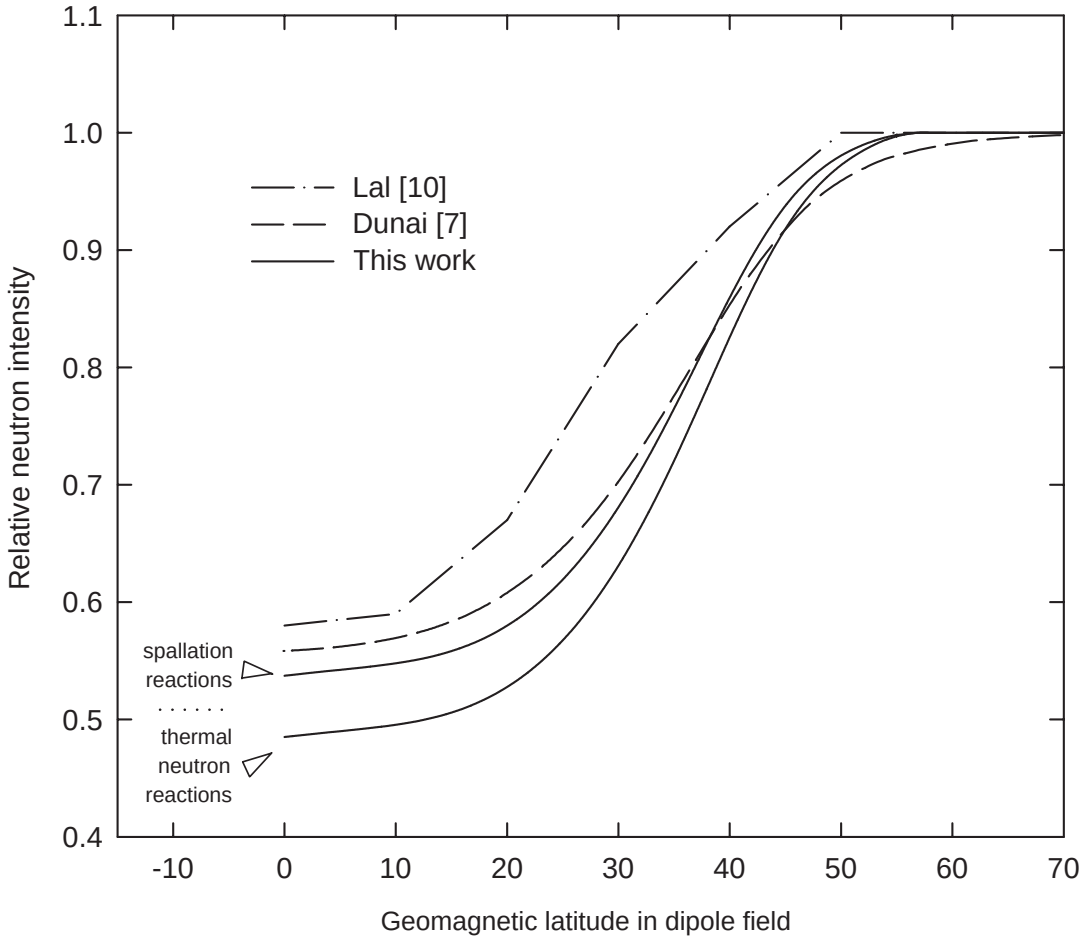

Figure 9. A comparison of sea-level latitude curves given in this work with ones reported by Lal [2] and Dunai [4]. Geomagnetic latitude corresponds to an axially-symmetric centered-dipole representation of the 1945 field ($M_0 = 8.084 \times 10^{22}$ A m^2 [50]).

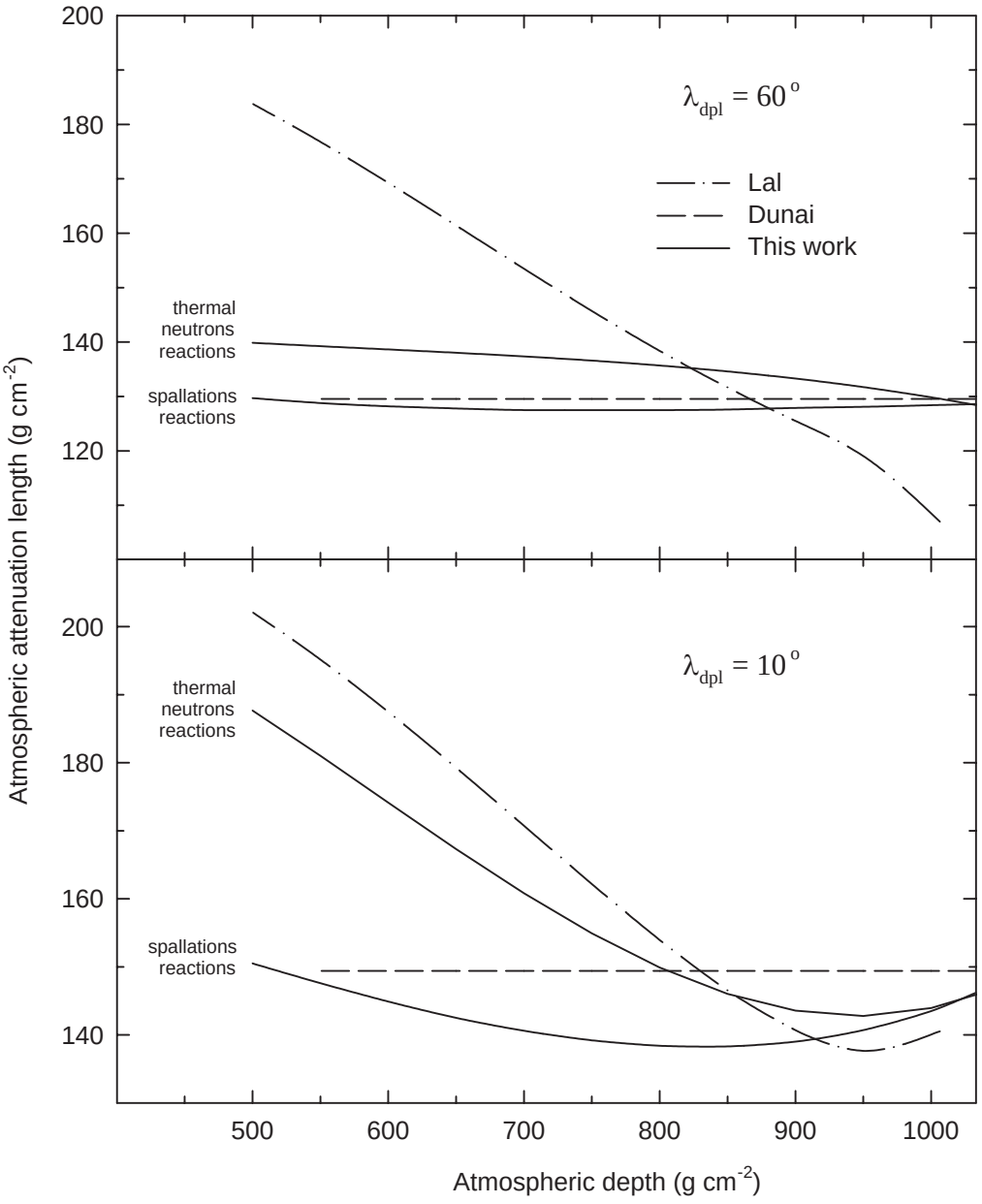

Figure 10. A comparison of attenuation lengths derived in this work with attenuation lengths calculated from Lal's [2] polynomial for neutron fluxes and attenuation lengths given by Dunai [4]. Geomagnetic latitude is calculated from an axially-symmetric centered-dipole field with a dipole moment (M_0) of 8.084×10^{22} A m^2 (1945 value[50]).

8. Uncertainty in scaling models

The uncertainty in applying neutron monitor data to scaling factors is difficult to assess [6, 7]. Others [3, 4] have based their uncertainty estimates on the scatter of data around their regressions. In our model, the 1σ uncertainty is negligible in our weighted fit to the 110 neutron monitor attenuation lengths derived from [11-13]. Before differentiating (Eq. 4) and correcting for muons (Eq. 5) the average 1σ uncertainty in attenuation lengths from our regression is 1% whereas a weighted average gives 0.1%.

Propagating the uncertainties from the weighted regression through Eq. 4 and Eq. 5 yields a final average 1σ uncertainty of 0.5% in the corrected neutron monitor attenuation lengths ($\Lambda_{NM,N}$) from Eq. 8. This uncertainty assumes that the uncertainties on the relative contributions of muons and nucleons (Table 1) are uncorrelated, and that attenuation lengths for muons (Eqs. 6 and 7) are correct to within an assumed 1σ uncertainty of 20%. The low uncertainty in $\Lambda_{NM,N}$ (Eq. 8) shows only that our regression is an excellent fit to Carmichael's [11-13] data, and that the correction for muons does not substantially increase the uncertainty of our model.

For calculating uncertainties on scaled production rates, an uncertainty of 0.5% in Λ_{sp} is unrealistically low, since it does not account for uncertainties related to biases in energy sensitivity and solar activity. At high latitudes, Λ_{sp} varies by about ~4% over the 11-year solar cycle (Eq. 13), and instrumental biases in energy sensitivity are small (Fig. 10), At low latitudes, Λ_{sp} is unaffected by solar activity, but uncertainties in the energy

bias of Λ_{sp} become important. An average 1σ uncertainty of +5/-2% in Λ_{sp} over all latitudes is therefore recommended as a more realistic estimate for scaling prodution rates. Uncertainty is lower on the negative side because the neutron monitor is sensitive to higher energies than are most of the important spallation reactions (Table 10), meaning that $\Lambda_{NM,N}$ should give a lower limit for Λ_{sp}. The attenuation length for thermal neutron reactions (Λ_{th}) is not as well constrained, and a realistic uncertainty is ±6%. Continued efforts are needed to obtain more rigorous and meaningful estimates of uncertainty in scaling models.

9.0 Conclusions

Our analysis of published cosmic-ray data suggests that separate scaling models should be used for thermal neutron absorption reactions and for spallation reactions. We found that neutron monitors give throughout a wide range of atmospheric depths lower attenuation lengths than do proportional counters. A recent latitude survey shows that neutron monitors also yield a less pronounced latitude effect than do proportional counters. Given that proportional counters measure neutrons at a lower range of energies (mostly neutrons of $E < 1$ eV) than neutron monitors (mostly nucleons of $E > 50$ MeV), these findings are consistent with a nucleon energy spectrum that shifts towards lower energies with increasing depth in the atmosphere. If, to the contrary, the shape of the nucleon energy spectrum is invariant in the troposphere, as suggested by recent model calculations [29], then systematic discrepancies between attenuation lengths measured with neutron monitors and those measured in the fast to thermal neutron range must be

explained in some other way. Without the assumption of a softening energy spectrum, there is currently no basis to accept one type of neutron measurement over the other.

A rigorous correction for temporal variations in the geomagnetic field can be applied to production rates directly from the scaling models given here. The accuracy of this correction depends mainly on the accuracy of measured production rates, the robustness of altitude-latitude scaling models and the reliability of the geomagnetic record. The main assumption of our temporal-geomagnetic correction is that at any given atmospheric depth, cosmic-ray intensity varies uniquely as a function of R_C. For paleomagnetic fields having poorly constrained configurations, as is usually the case in cosmogenic dating, it may be necessary to assume a geocentric axially-symmetric dipole field in order to calculate R_C, although this assumption is not intrinsic to our model.

Others working on the scaling aspect of cosmogenic nuclide systematics [4, 54-56] seemed to have reached at least one common conclusion with us: that additional theoretical and experimental cosmic-ray research is needed to improve the accuracy and robustness of surface exposure dating, and to open new applications of cosmogenic nuclides.

Symbol	Name	Units
β	attenuation coefficient (reciprocal of Λ)	$cm^2\ g^{-1}$
$\beta_{e,i}$	effective attenuation coefficient for component *i*	$cm^2\ g^{-1}$
β_{NM}	attenuation coefficient for the neutron monitor counting rate	$cm^2\ g^{-1}$
$\beta_{NM,N}$	attenuation coefficient for the nucleon contribution to the neutron monitor counting rate	$cm^2\ g^{-1}$
β_{sp}	attenuation coefficient for spallation reactions	$cm^2\ g^{-1}$
β_{th}	attenuation coefficient for thermal neutrons	$cm^2\ g^{-1}$
C_B	relative background contribution to neutron monitor counting rate	
C_i	relative contribution of component *i* to neutron monitor counting rate	
C_N	relative contribution of nucleons to neutron monitor counting rate	
$C_{\mu(f)}$	relative contribution of fast muons to neutron monitor counting rate	
$C_{\mu(s)}$	relative contribution of slow muons to neutron monitor counting rate	
C_{DR}	counting rate of the Deep River neutron monitor relative to that of May, 1965	
E	kinetic energy	MeV
E_{med}	median kinetic energy	MeV
ε	erosion rate	$g\ cm^{-2}\ y^{-1}$
$f_{Rc,x}(\Delta t_i)$	altitude and latitude scaling factor for period Δt_i	
f_{topo}	topographic shielding/foreshortening factor	
f_{ss}	factor to account for sample depth in subsurface	
H	horizontal field intensity	nT
H_{dpl}	horizontal field intensity in a dipole field	nT
I	geomagnetic inclination	degrees
I_{dpl}	geomagnetic inclination in a dipole field	degrees
J	relative cosmic-ray flux	
J_{clb}^{avg}	average cosmic-ray flux at calibration site	
J_{clb}	cosmic-ray flux at calibration site at a given time	
J_{NM}	neutron monitor counting rate	
$J(t_i)$	cosmic-ray flux at sample site during interval Δt_i	
λ	geomagnetic latitude	degrees
λ_{dpl}	geomagnetic latitude in a dipole field	degrees
λ_{dec}	radionuclide decay constant	y^{-1}
Λ	attenuation length	$g\ cm^{-2}$
$\Lambda_{e,i}$	effective atteneuation length for component *i*	$g\ cm^{-2}$
$\Lambda_{i,ss}$	effective attenuation length in the subsurface for component *i*	$g\ cm^{-2}$
Λ_f	attenuation length for fast neutrons (assumed to be the same as for thermal neutrons)	$g\ cm^{-2}$
Λ_N	attenuation length for nucleon component	$g\ cm^{-2}$
Λ_{NM}	attenuation length for the neutron monitor counting rate	$g\ cm^{-2}$
$\Lambda_{NM,N}$	attenuation length for the nucleon contribution to the	$g\ cm^{-2}$
Λ_{sp}	attenuation length for spallation reactions	$g\ cm^{-2}$
Λ_{th}	attenuation length for thermal neutrons (assumed to be the same as for fast neutrons)	$g\ cm^{-2}$

Symbol	Name	Units
$\Lambda_{\mu\text{-}(s)}$	attenuation length for slow negative (stopping) muons	g cm^{-2}
$\%\Delta\Lambda_{e,NM,N}$	percent change in the effective attenuation length	
M	magnetic dipole intensity	A m^2
N_{calc}	calculated inventory	atoms g^{-1}
N_{meas}	measured inventory	atoms g^{-1}
$N_{\Delta ti\text{-}1}$	inventory from the previous timestep	atoms g^{-1} y^{-1}
P_{clb}	production rate at calibration site	atoms g^{-1} y^{-1}
$P^{\Delta ti}$	effective production rate at sample site over time interval Δt_i	atoms g^{-1} y^{-1}
P_{sp}	production rate for spallogenic nuclides	atoms g^{-1} y^{-1}
P_{th}	production rate from thermal and epithermal neutron reactions	atoms g^{-1} y^{-1}
Q	global atmospheric production rate	arbitrary
R_C	effective vertical cutoff rigidity calculated by trajectory tracing	GV
$R_{C,dpl}$	effective vertical cutoff rigidity in a dipole field calculated by trajectory tracing	GV
R_L	lower vertical cutoff rigidity calculated by the trajectory tracing	GV
$R_L^{Störmer}(\lambda_{dpl})$	lower vertical cutoff rigidity according to the Störmer equation, calculated in a dipole field	GV
$R_L^{Störmer}(I,H)$	lower vertical cutoff rigidity according to the Störmer equation, calculated from the surface field	GV
R_U	upper vertical cutoff rigidity calculated by the trajectory tracing	GV
r_e	radius of the earth	m
ρ_{ss}	density of subsurface	g cm^{-2}
t	exposure time	y
t_{app}	apparent exposure time (exposure time prior to geomagnetic correction)	y
Δt_i	time interval i	y
x	mass shielding depth in atmosphere	g cm^{-2}
x_0	atmospheric mass shielding depth at sea level	g cm^{-2}
x_{ss}	mass shielding depth in subsurface	g cm^{-2}

Acknowledgements

We thank D. Lal and J. Masarik for their helpful comments on the manuscript. We also acknowledge the invaluable assistance provided by V. Radhakrishnan and his staff at Raman Research Insitute for our neutron measurements in India. This material is based upon work supported by the National Science Foundation under grants EAR-0001191, EAR-0126209 and ATM-0081403 and by Packard Fellowship in Science and Engineering 95-1832.

References

1 D. Lal, Investigation of nuclear interactions produced by cosmic rays, Ph.D, University of Bombay, 1958.

2 D. Lal, Cosmic ray labeling of erosion surfaces: *in situ* nuclide production rates and erosion models, Earth and Planetary Science Letters 104, 424-439, 1991.

3 N. Lifton, A robust scaling model for in situ cosmogenic nuclide production rates, in: Geological Society of America, Annual Meeting, abstracts with programs, pp. A400, Reno, Nevada, 2000.

4 T.J. Dunai, Scaling factors for production rates of in situ produced cosmogenic nuclides: a critical reevaluation, Earth and Planetary Science Letters 176, 157-169, 2000.

5 J.O. Stone, Air pressure and cosmogenic isotope production, Journal of Geophysical Resarch 105(B10), 23753-23759, 2000.

6 D. Desilets and M. Zreda, On scaling cosmogenic nuclide production rates for altitude and latitude using cosmic-ray measurements, Earth and Planetary Science Letters 193, 213-225, 2001.

7 D.M. Desilets, The global distribution of secondary cosmic-ray intensity and applications to cosmogenic dating, M.S., University of Arizona, 2001.

8 D. Desilets, M. Zreda and N.A. Lifton, Comment on "Scaling factors for production rates of in situ produced cosmogenic nuclides: a critical reevaluation", Earth and
Planetary Science Letters 188, 283-287, 2001.

9 D.C. Rose, K.B. Fenton, J. Katzman and J.A. Simpson, Latitude effects of the cosmic ray nucleon and meson components at sea level from the Arctic to the Antarctic, Canadian Journal of Physics 34, 968-984, 1956.

10 J.F. Ziegler, Terrestrial cosmic ray intensities, IBM Journal of Research and Development 40, 19-39, 1996.

11 H. Carmichael, M. Bercovitch, J.F. Steljes and M. Magidin, I. Cosmic-ray latitude survey in North America in summer, 1965, Canadian Journal of Physics 47, 2037-2050, 1969.

12 H. Carmichael and M. Bercovitch, II. Cosmic-ray latitude survey in Canada in December, 1965, Canadian Journal of Physics 47, 2051-2055, 1969.

13 H. Carmichael, M.A. Shea and R.W. Peterson, III. Cosmic-ray latitude survey in Western USA and Hawaii in summer, 1966, Canadian Journal of Physics 47, 2057-2065, 1969.

14 H. Carmichael, M.A. Shea, D.F. Smart and J.R. McCall, IV. Geographically smoothed geomagnetic cutoffs, Canadian Journal of Physics 47, 2067-2072., 1969.

15 H. Carmichael and M. Bercovitch, V. Analysis of IQSY cosmic-ray survey measurements, Canadian Journal of Physics 47, 2073-2093, 1969.

16 G. Villoresi, L.I. Dorman, N. Iucci and N.G. Ptitsyna, Cosmic ray survey to Antarctica and coupling functions for neutron component near solar minimum (1996-1997) 1. Methodolgy and data quality assurance, Journal of Geophysical Research 105, 21,025 - 21,034, 2000.

17 B.C. Raubenheimer and P.H. Stoker, Attenuation coefficients of various cosmic ray components in the lower atmosphere, in: Proceedings of the 12th International Conference on Cosmic Rays, pp. 893-896, 1971.

18 F. Bachelet, N. Iucci, G. Villoresi and N. Zangrilli, The cosmic-ray spectral modulation above 2 GV. IV. The Influence on the attenuation coefficient of the nucleonic component, Il Nuovo Cimento 11 B, 1-12, 1972.

19 N. Iucci, G. Villoresi, L.I. Dorman and M. Parisi, Cosmic ray survey to Antarctica and coupling functions for neutron component near solar minimum (1996-1997) 1. Determination of meteorological effects, Journal of Geophysical Research 105, 21,035-21,045, 2000.

20 L.I. Dorman, G. Villoresi, N. Iucci, M. Parisi, M.I. Tyasto, O.A. Danilova and N.G. Ptitsyna, Cosmic ray survey to Antarctica and coupling functions for neutron component near solar minimum (1996-1997) 3. Geomagnetic effects and coupling functions, Journal of Geophysical Research 105, 21,047-21,056, 2000.

21 H. Carmichael and R.W. Peterson, Dependence of the neutron monitor attenuation coefficient on atmospheric depth and on geomagnetic cutoff in 1966 and in 1970, in: Proceedings of the 12th International Cosmic Ray Conference, pp. 887-892, 1971.

22 C.J. Hatton and H. Carmichael, Experimental investigation of the NM-64 neutron monitor, Canadian Journal of Physics 42, 2443-2472, 1964.

23 F. Ashton, The range-energy relationship for high-energy μ-mesons, Proceedings of the Physical Society 77, 587-592, 1961.

24 B. Rossi, M. Sands and R.F. Sard, Measurements of slow meson intensity at several altitudes, Physical Review 72, 120-125, 1947.

25 M. Sands, Low energy mesons in the atmosphere, Physical Review 77, 180-193, 1950.

26 M. Conversi, Experiments on cosmic-ray mesons and protons at several altitudes and latitudes, Physical Review 79, 749-767, 1950.

27 O.C. Allkofer, R.D. Andresen, K. Clausen and W.D. Dau, Sea-level muon spectrum at two different latitudes, Journal of Geophysical Research 77, 4251-4253, 1972.

28 T.J. Dunai, Inluence of secular variation of the geomagnetic field on production rates of in situ produced cosmogenic nuclides, Earth and Planetary Science Letters 193, 197-212, 2001.

29 J. Masarik, M. Frank, J.M. Schäfer and W. Rainer, Correction of in situ cosmogenic nuclide production rates for geomagnetic field intensity variations during the past 800,000 years, Geochimica et Cosmochimica Acta 65, 2995-3003, 2001.

30 J.A. Simpson, Neutrons produced in the atmosphere by the cosmic radiations, Physics Reviews 83, 1175-1188, 1951.

31 R.K. Soberman, High-altitude cosmic-ray intensity variations, Physical Review 102, 1399-1409, 1956.

32 M. Merker, E.S. Light, H.J. Verschell, R.B. Mendell and S.A. Korff, Time dependent worldwide distribution of atmospheric neutrons and their products, 1. Fast neutron obervations, Journal of Geophysical Research 78, 2,727-2,740, 1973.

33 C.F.W. Mischke, Intensiteisvaiasies van neutrone vanaf kosmiese strale, M.S., University of Potchefstroom, 1972.

34 M.S. Potgeiter, B.C. Raubenheimer, P.H. Stoker and A.J. van der Walt, Modulation of cosmic rays during solar minimum. Part 2. Cosmic ray latitude distribution at sea level during 1976, South African Journal of Physics 3, 77-89, 1980.

35 B.C. Raubenheimer and P.H. Stoker, Various aspects of the attenuation coefficient of a neutron monitor, Journal of Geophysical Research 79, 5069-5076, 1974.

36 Y. Guyodo and J.P. Valet, Relative variations in geomagnetic intensity from sedimentary records: the past 200,000 years, Earth and Planetary Science Letters 143, 23-26, 1996.

37 J.M. Licciardi, M.D. Kurz, P.U. Clark and E.J. Brook, Calibration of cosmogenic ^{3}He production rates from Holocene lava flows in Oregon, USA, and effects of the Earth's magnetic field, Earth and Planetary Science Letters 172, 261-271, 1999.

38 T.M. Shanahan and M. Zreda, Chronology of Quaternary glaciations in East Africa, Earth and Planetary Science Letters 177, 23-42, 2000.

39 M.W. McElhinny and W.E. Senanayake, Variations in the geomagnetic dipole I: the past 50,000 years, Journal of Geomagnetism and Geoelectricity 34, 39-51, 1982.

40 M. Ohno and Y. Hamano, Geomagnetic poles over the past 10,000 years, Geophysical Research Letters 19(16), 1715-1718, 1992.

41 M. Ohno and Y. Hamano, Global analysis of the geomagnetic-field: time variation of the dipole moment and the geomagnetic pole in the Holocene, Journal of Geomagnetism and Geoelectricity 45(11-12), 1455-1466, 1993.

42 Y. Guyodo and J.P. Valet, Global changes in intensity of the Earth’s magnetic field during the past 800 kyr, Nature 399, 249-252, 1999.

43 P.R. Bierman and E.M. Clapp, Estimating geologic age from cosmogenic nuclides: an update, Science 271, 1606, 1996.

44 F.M. Phillips, M.G. Zreda, M.R. Flinsch, D. Elmore and P. Sharma, A reevaluation of cosmogenic ^{36}Cl production rates in terrestrial rocks, Geophysical Research Letters 23(9), 949-952, 1996.

45 W. Elsasser, E.P. Ney and J.R. Winckler, Cosmic-ray intensity and geomagnetism, Nature 178, 1226-1227, 1956.

46 D. Lal and B. Peters, Cosmic ray produced radioactivity on earth, in: Encyclopedia of Physics: Cosmic Rays II, K. Sitte, ed., Encyclopedia of Physics 46/2, pp. 551-612, Springer-Verlag, Berlin, 1967.

47 D. Lal, In situ-produced cosmogenic isotopes in terrestrial rocks, Annual Reviews of Earth and Planetary Sciences 16, 355-388, 1988.

48 P. Rothwell, Cosmic rays in the Earth's magnetic field, Philosophical Magazine 3, 961-970, 1958.

49 M.A. Shea, D.F. Smart and K.G. McCracken, A study of vertical cutoff rigidities using sixth degree simulations of the geomagnetic field, Journal of Geophysical Research 70, 4117-4130, 1965.

50 A.C. Fraser-Smith, Centered and eccentric geomagnetic dipoles and their poles, 1600-1985, Reviews of Geophysics 25, 1-16, 1987.

51 M.A. Shea and D.F. Smart, A world grid of calculated cosmic ray vertical cutoff rigidities for 1980.0, in: Proceedings of the 18th International Cosmic Ray Conference MG 10-3, pp. 415-418, Bangalore, India, 1983.

52 M.G. Zreda and F.M. Phillips, Surface exposure dating by cosmogenic chlorine-36 accumulation, in: Dating in Exposed and Surface Contexts, C. Beck, ed., pp. 161-183, University of New Mexico Press, 1994.

53 F.M. Phillips, W.D. Stone and J.T. Fabryka-Martin, An improved approach to calculating low-energy cosmic-ray neutron fluzes near the land/atmosphere interface, Chemical Geology 175, 689-701, 2001.

54 E.T. Brown, T.W. Trull, P. Jean-Baptiste, G. Raisbeck, D. Bourlès, F. Yiou and B. Marty, Determination of cosmogenic production rates of ^{10}Be, ^{3}He and ^{3}H in water, Nuclear Instruments and Methods in Physics Research B 172, 873-883, 2000.

55 D. Lal, Cosmogenic nuclide production rate systematics in terrestrial materials: Present knowledge, needs and future actions for improvement, Nuclear Instruments and Methods in Physics Research B 172, 772-781, 2000.

56 I.J. Graham, B.J. Barry, R.G. Ditchburn and N.E. Whitehead, Validation of cosmogenic nuclide production rate scaling factors through direct measurement, Nuclear Instruments and Methods in Physics Research B 172, 802-805, 2000.

57 C.J. Hatton, The neutron monitor, in: Progress in Elementary Particle and Cosmic Ray Physics, J.G. Wilson and S.A. Wouthuysen, eds. 10, pp. 1-100, North-Holland Publishing Co., Amsterdam, 1971.

58 O.C. Allkofer, R.D. Andresen, E. Bagge, W.D. Dau and H. Funk, Der Einfluss des Erdmagnetfeldes auf die kosmische Strahlung, 1, Untersuchungen der Nukleonenkomponente der kosmische Strahlung waehrend der atlantischen Expedetion IQSY 1965 auf dem Forschungsschif "Meteor,", in: "Meteor" Forschungsergebnisse, Reihe B, Heft 3, Gebrüder Borntraeger, Berlin, 1969.

59 T.M. Aleksanyan, I.V. Dorman, L.I. Dorman, V.K. Babayan, A.V. Belov, Y.L. Blokh, N.S. Kaminer, V.K. Korotkov, I.Y. Libin, A.A. Manshilina, Y.E. Mashkov, I.V. Mymrina, S.I. Rogovaya, A.M. Sitnov, K.F. Yudakhin and V. Yanke, Geomagnetic effects in cosmic rays and spectrum of the increase before magnetic storms, Izvestiya Akademii Nauk SSSR, Seriya Fizicheskaya 46, 1689-1691, 1982.

60 P.H. Stoker, A.J. van der Walt and M.S. Potgeiter, Modulation of cosmic rays during solar minimum, 1, Cosmic ray intensity survey at sea-level dring 1976: Experimental details, South African Journal of Physics 3, 73-76, 1980.

61 H. Moraal, M.S. Potgieter and P.H. Stoker, Neutron monitor latitude survey of cosmic ray intensity during the 1986/1987 solar minimum, Journal of Geophysical Research 94, 1459-1464, 1989.

62 M.A. Shea, D.F. Smart and J.R. McCall, A five degree by fifteen degree world grid of trajectory-determined vertical cutoff rigidities, Canadian Journal of Physics 46, S1098-S1101, 1968.

APPENDIX D

EXTENDED SCALING FACTORS FOR *IN-SITU* COSMOGENIC NUCLIDES: NEW MEASUREMENTS AT LOW LATITUDE

Darin Desilets[1], Marek Zreda[1], Venkataraman Radhakrishnan[2]

[1]Department of Hydrology and Water Resources, University of Arizona, Tucson, AZ, 85721, USA

[2]Raman Research Institute, Bangalore, India 560 080

[in preparation for *Earth and Planetary Science Letters* (2005)]

Abstract

Production rates of cosmogenic nuclides at the earth's surface are largely determined by the intensity of energetic cosmic-ray nucleon fluxes, which is very sensitive to elevation. An incomplete knowledge of how nucleon fluxes vary with elevation remains a major obstacle to utilizing cosmogenic nuclides as geochronometers in applications requiring small temporal resolution. One problem is that attenuation characteristics depend on nucleon energy. Measurements of high-energy (>50 MeV) nucleon fluxes tend to give shorter attenuation lengths than low-energy (<1 MeV) fluxes, but these differences are not well characterized due to a lack of data at lower energies. Another problem is that the elevation effect varies with cutoff rigidity (a parameter related to geomagnetic latitude), R_C, and that there has been an incomplete mapping of nucleon fluxes at high R_C (low geomagnetic latitude). We report new measurements of nucleon fluxes from altitude transects in Hawaii (R_C=12.8 GV) and Bangalore, India (R_C=17.3 GV). Our measurements in Hawaii of low-energy neutrons (median energy 1 eV) and energetic nucleons (median energy 140 MeV) confirm that nucleon scaling functions are energy dependent in the range of energies at which cosmogenic nuclides are produced. Our measurements in southern India extend our previously reported scaling model for spallation reactions from R_C=13.3 GV to R_C=17.3 GV, nearly the highest modern cutoff rigidity on earth. The anomalously high cutoff rigidity over India provides a geomagnetic shielding condition which is effectively the same as would be observed at the

geomagnetic equator in a dipole field with an intensity 1.2 times the modern value. This makes it possible to scale low-latitude production rates to paleomagnetic fields that are stronger than the present dipole field.

1. Introduction

The application of *in situ* cosmogenic nuclides to surface exposure dating requires accurate knowledge of how production rates vary in space and time. Nucleon interactions are responsible for most cosmogenic nuclide production in surface rocks at sea level, and are by far the dominant production mechanism at mountain altitudes [1]. Because nucleon fluxes are highly variable in the troposphere, increasing by two orders of magnitude from sea level to the tropopause, small inaccuracies in nucleon scaling parameters can lead to large uncertainties in determining production rates when these errors are propagated over a large elevation range.

Cosmic-ray nucleon fluxes at the earth's surface are generated in particle cascades that are initiated at the top of the atmosphere by energetic comic ray protons and heavier nuclei [2]. In the troposphere, cosmic-ray nucleon fluxes diminish with increasing atmospheric depth according to:

$$J_2 = J_1 \exp\left(\frac{x_1 - x_2}{\Lambda}\right) \tag{1}$$

where J_1 and J_2 are the nucleon fluxes at depths x_1 and x_2 [g cm^{-2}] and Λ [g cm^{-2}] is the nucleon attenuation length.

It has long been established that the value of Λ depends on cutoff rigidity and altitude [3]. Recently, Desilets and Zreda [4, 5] pointed out that Λ is also a function of median nucleon energy, and that this dependence explains some inconsistencies between scaling models derived from instruments with different energy sensitivities.

Because cosmogenic nuclides are produced at widely different median energies, scaling factors should be nuclide dependent. However, as an approximation, [5] assumed that median energies for most spallation reactions used in terresrial cosmogenic dating (60-140 MeV) are sufficiently close to the median energy of the neutron monitor (140 MeV) that neutron monitor measurements can be used to scale all spallation reactions. That approximation is necessary because precise experimental data on how the nucleon energy spectrum changes with atmospheric depth are sparse in the 60-140 MeV range. Most of the data on how nucleon fluxes vary in space and time comes from neutron monitor surveys and from airborne measurements of low-energy neutron fluxes. These two types of surveys measure widely separated energy bands which bracket the median energies at which all of the commonly used cosmogenic nuclides are produced.

This investigation has two main purposes. One is to verify that the energy dependence of nucleon scaling functions is important in the troposphere. This question was addressed by measuring nucleon fluxes in two energy bands; one corresponding to low-energy neutron activation reactions, the other corresponding to energetic spallation reactions. We expect based on [5]'s analysis that differences in scaling functions should be greatest at low-latitude. Our measurements were motivated by a lack of low-energy (<1 MeV)

neutron flux surveys below 5000 m and the need to compare such data with more energetic fluxes measured by a neutron monitor. The second purpose of this work is to extend [5]'s scaling model for spallation reactions to lower latitude/higher geomagnetic field strength. That scaling model applies to cutoff rigidities (R_C) from 0 to 13.3 GV, the highest rigidity attained in [6]'s 1965 solar minimum cosmic-ray survey. In a dipole-model of earth's present magnetic field (which in cosmogenic dating is often assumed for paleomagnetic fields for lack of better knowledge [7]), R_C=13.3 is equivalent to a geomagnetic latitude of 19°. Anomalously high cutoff rigidities over Southeast Asia created by non-dipole components of the geomagnetic field make it possible to extend those measurements to both lower geomagnetic (dipole) latitude, and equivalently, higher paleomagnetic field strength. In this work we update our scaling model to incorporate measurements from southern India, which at R_C=17.3 GV is close to the highest cutoff rigidity on earth.

2. Experimental

Altitude profiles of nucleon fluxes were obtained at two low-latitude locations, the Island of Hawaii and near Bangalore, India (Fig. 1). At these locations it was possible to obtain ground-based measurements over a large elevation range at nearly constant R_C. In Hawaii, we measured high-energy nucleon fluxes using a neutron monitor in a car, and low-energy neutron fluxes were measured from an aircraft. In India, an identical neutron monitor was used in a ground-based survey and later was transferred to an airplane for measurements up to 8250 m.

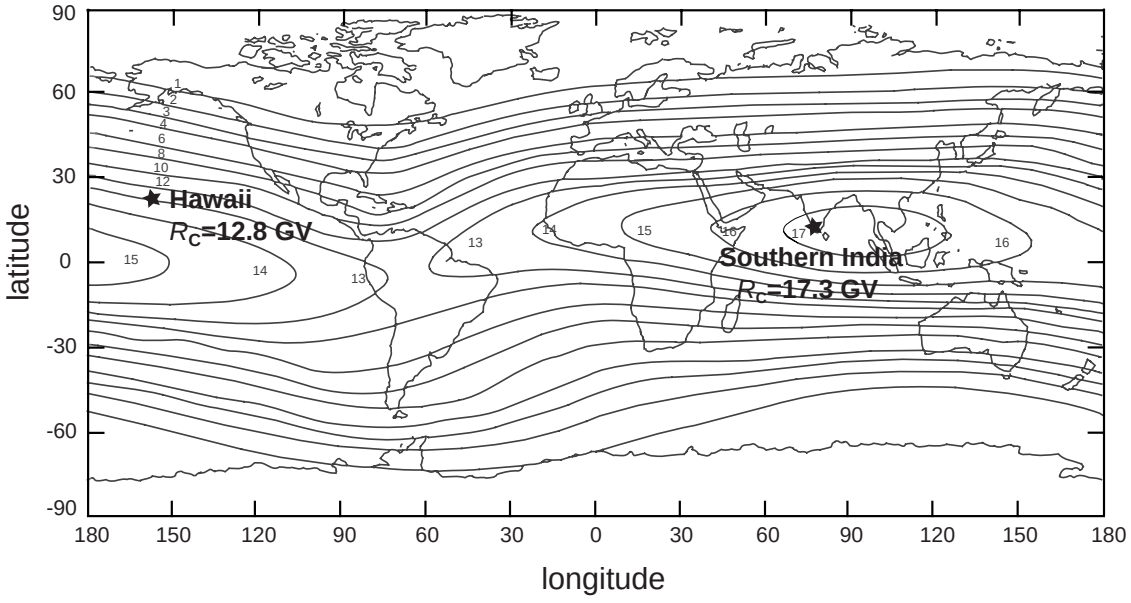

Figure 1. Altitude survey locations. Contours show effective vertical cutoff rigidity (R_C) for 1980 [8].

In this work, 'high-energy' and 'low-energy' are defined by the energy responses of our instruments. Although each instrument records a continuous distribution of energies, the median energy responses are substantially different (Fig. 2). The high-energy nucleon fluxes measured with the mobile neutron monitor correspond to a median nucleon energy of ~140 MeV [9]. Low-energy neutron fluxes were measured using unshielded ^{3}He-filled detectors, which have a median energy response of ~ 1 eV.

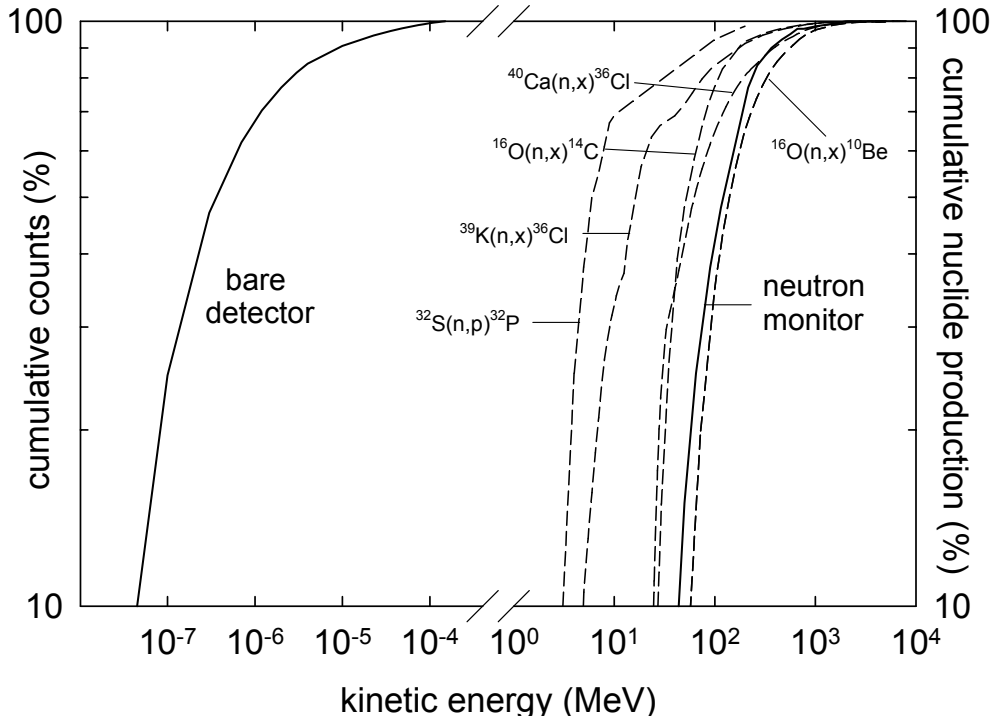

Figure 2. Energy sensitivity of a bare neutron detector and an NM-64 neutron monitor compared with excitation functions for several commonly cosmogenic nuclides [10]. Cumulative production from thermal neutron reactions (e.g. ^{35}Cl(n,γ)^{36}Cl) would closely follow the response for the bare detector.

2.1 High-energy nucleon fluxes in India and Hawaii

Mobile neutron monitor

A neutron monitor records energetic cosmic-ray nucleon fluxes indirectly through a complex series of interactions that occur within the instrument. In the first interaction an energetic nucleon (>50 MeV) excites a lead nucleus, which de-excites by emitting evaporation neutrons with energies in the 1-10 MeV range [9]. These fast neutrons are rapidly thermalized through elastic collisions in a layer of hydrogen-rich material (usually paraffin or polyethylene) that surrounds the lead on all sides. The hydrogenous material on the inside of the lead is referred to as the moderator and the material on the outside is known as the reflector. The reflector serves the dual purpose of moderating the neutrons generated in the lead and shielding the instrument from neutrons generated in outside materials [9]. This shielding is necessary because fluxes of low-energy neutrons from the outside environment depend on local conditions (e.g. soil moisture content, soil chemistry, proximity to high Z objects) that are variable between locations. Along the central axis of the instrument is a proportional counter tubes (filled with ^{10}B or ^{3}He enriched gas) which is sensitive to thermal neutron fluxes. A count is recorded when a thermal neutron is captured in the counter tube by the neutron-sensitive gas.

Advantages of the neutron monitor are that it gives a high counting rate using a simple design that can be constructed from easily obtainable materials and equipment. However, a disadvantage in conventional neutron monitor designs (IGY and NM-64) is that massive amounts of lead are used (1600 kg per counter tube for NM-64 [9]), which presents a formidable logistical challenge in conducting neutron monitor surveys.

To gain greater mobility, we used substantially smaller dimensions (Table 1, Fig.3) than are specified for the IGY and NM-64 type monitors. The use of smaller detectors permitted a proportionate reduction in the amounts of lead and paraffin. To compensate for the smaller sensitive volume of our detectors and the reduced amounts of lead, we used ^{3}He filled tubes that are twice as sensitive per unit volume as the BF_3 filled detectors conventionally used in IGY an NM-64 neutron monitors.

Table 1. Design parameters for standard neutron monitors [9] and for the mobile Arizona neutron monitor.

	IGY	NM-64	Arizona NM
Counters			
active length (cm)	86.4	191	33
diameter (cm)	3.8	14.8	2.5
pressure (atm)	0.6	0.3	10
gas	BF_3	BF_4	^{3}He
Inner moderator thickness (cm)	3.2	2.0	2.5
lead thickness (g cm)	13.5	13.8	10.2
reflector thickness (cm)	28	7.5	18

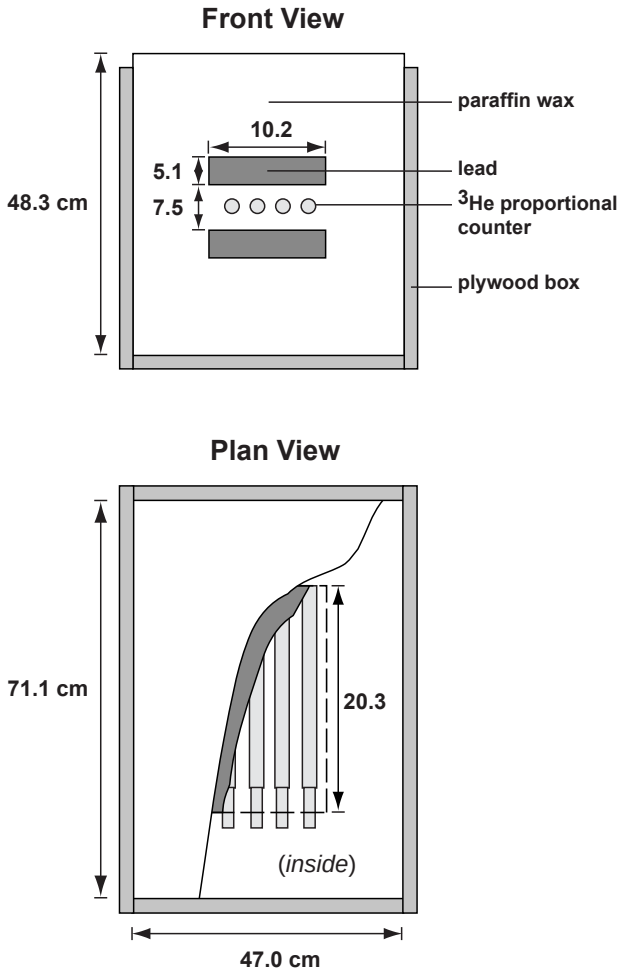

Figure 3. Design of the mobile neutron monitor used in this work to measure high-energy cosmic-ray nucleon fluxes.

Previous experiments have shown that the respective use of smaller horizontal dimensions or ^{3}He instead of BF_3 has a negligible effect on the neutron monitor response [11, 12]. Nonetheless, to check that the response of our instrument is similar to that of neutron monitors employed in the global neutron monitor network and in sea-level latitude surveys, we performed measurements in Hawaii (R_C=12.8 GV), to compare with extensive measurements conducted there previously [11]. Our results from Hawaii are described in Section 3.1.

An upper limit on the constant background counting rate of our detectors was found by shielding a counter tube with a 0.7 mm thick cadmium sleeve surrounded by 30 cm of paraffin. The shielded counter was placed in the basement of a three story building to further reduce the contribution of neutrons generated by cosmic-rays. The resulting counting rate of 0.062±0.010 cpm, (~1% of the sea-level high-lattiude counting rate) is probably caused by trace amounts of alpha-emiting radionuclides in the aluminum counter walls [13, 14]. This level of background is consistent with NM-64 and IGY neutron monitors [13].

Land-based measurements

Altitude transects were obtained by transporting the neutron monitor by car from sea level to mountain sites. In April 2000, we measured neutron monitor counting rates in Hawaii (R_C=12.8 GV) along a transect from Kailua-Kona (sea level) to Mauna Kea (4205 m). In April 2002, we conducted a similar profile in India (R_C=17.3 GV) along a route from Bangalore (949 m) to Calicut (sea level) and then to Doda Beta (2637 m). One

detector malfunctioned in India, and therefore only results from the other two detectors are reported.

Over the duration of the surveys, temporal variations in secondary cosmic-ray intensity recorded by the Haleakala neutron monitor were <2%. Because the correction for these small changes neither significantly changes the value of the attenuation length nor improves their uncertainty, we neglected this correction.

Airborne measurements

On May 8, 2002, we extended the altitude range of our survey at 17.3 GV by measuring neutron fluxes from the cabin of an aircraft provided by the Indian Air Force (data given in Supplemental Table 1). Because a sufficiently high counting rate was recorded at these altitudes with only one detector the other functional detector was removed and used in a separate experiment (not discussed in this paper). The airplane was kept at a uniform pressure-altitude for each of eight different altitudes. Below 3400 m, the airplane flew unpressurized and pressure was logged at five-minute intervals from a pressure sensor located inside of the cabin. The airplane maintained its pressure-altitude to within 1.5 g cm^{-2} (15-20 m) 1σ of the reported pressure at each flight level. Above 3400 m, the cabin was pressurized and we relied on manual recordings of the airplane's altimeter to determine the outside pressure. An airplane altimeter reads pressure from a sensor in the nose or wing and converts this pressure to altitude according to the ICAO standard atmosphere [15]. Pressures were calculated by converting the recorded altitudes back to units of atmospheric pressure according to the ICAO standard atmosphere.

2.2 Low-energy neutron fluxes at Hawaii

Thermal neutron detector

Measurements of low-energy neutron fluxes were made from the tail compartment of a four-seat airplane. To obtain low-energy sensitivity we employed the same ^{3}He counter tubes and electronics modules used in the neutron monitor, but in an unshielded configuration (Fig. 4). The energy sensitivity of this instrument is determined by the thermal neutron absorption cross section of ^{3}He, which has an energy dependence ($1/v$ law) similar to the ^{35}Cl cross section.

The only moderating material surrounding the detectors was 5 cm of light-weight polystyrene foam used to protect the equipment from impacts. Although this material and also the body and fuel tanks of the aircraft perturb the local "equilibrium" neutron flux, there should be very little effect on the attenuation length if these factors are kept constant during the experiment. The fuel level is the only factor that would have changed over the course of the experiment, and this effect was minimized by taking duplicate measurements with nearly full and nearly empty tanks.

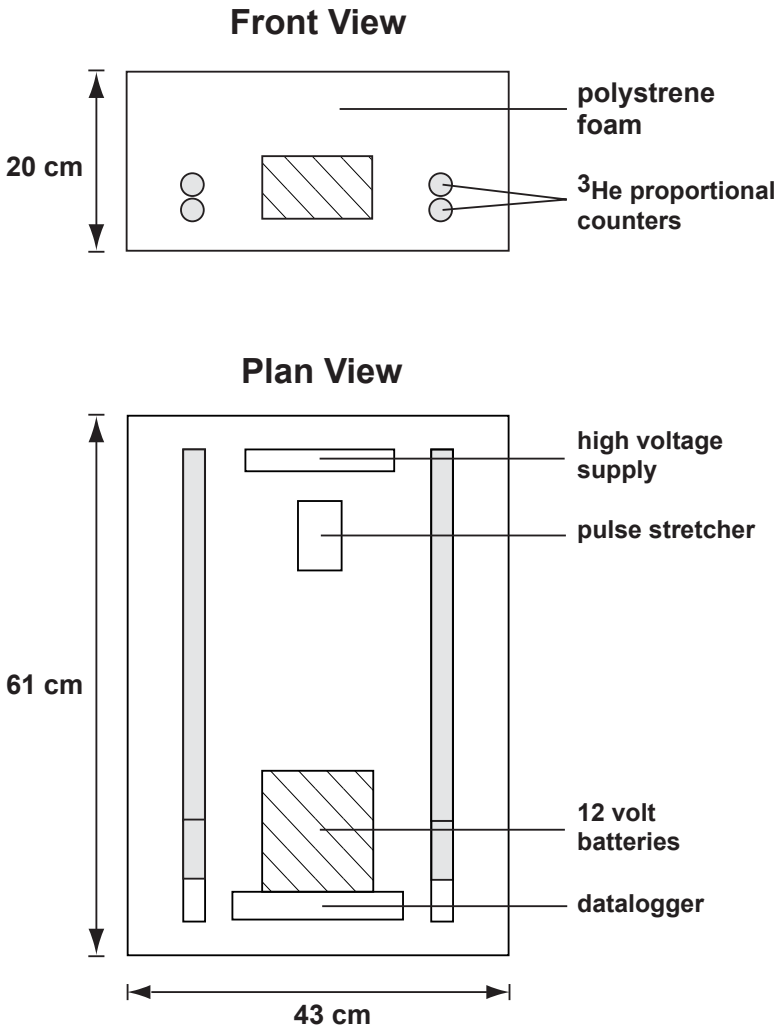

Figure 4. Apparatus used to measure low-energy neutron fluxes.

On June 19, 2003 we conducted two series of flights from Keahole airport at Kailua-Kona, Hawaii (data given in Supplemental table 2). In the first series, measurements were taken at 7 pressure altitudes from 500 m to 3800 m. After landing and refueling, another set of measurements was taken in the reverse order, beginning at 3800 m. To eliminate the possibility of a systematic bias due to decreasing fuel load during each flight, results from the two flights were averaged.

Pressure was logged at one minute intervals from a sensor located in the unpressurized cabin of the airplane. Based on a comparison of GPS readings with open-cabin pressure logged during our flights in India, we estimate that open cabin pressures are correct to within 0.25%.

Neutron transport simulations

A premise of our low-energy neutron flux measurements is that at sufficient distance from the sea or ground surface the rate of production of fast neutrons and the rate of absorption of low-energy neutrons are in equilibrium. Near the interface of two materials having different neutron producing, moderating and absorbing properties, such as the air and water, this equilibrium is known to be perturbed [16]. To ensure that our flight levels were in the equilibrium portion of the atmosphere, we calculated an altitude profile of low-energy neutron fluxes above seawater using the Monte Carlo N-Particle (MCNP) transport code, version 5 [17]. Our calculation assumes that the attenuation length for neutron production in both the atmosphere and sea water is 140 g cm^{-2}, and that neutron production is proportional to $A^{1/2}$ [18, 19]. The neutron source is modeled with an

evaporation energy spectrum with a 1 MeV peak and an isotropic angular distribution. Neutron fluxes were tallied in 20 energy bins from 0.001-150 eV. The detector response was simulated by weighting the fluxes in each energy bin by the average ^{3}He neutron absorption cross section for the energy bin and then summing the weighted fluxes over all bins.

The transport simulation indicates that the low-energy neutron flux is perturbed in the region of atmosphere 1033-950 g cm^{-2} (0-680 m) over the sea (Fig. 5). The direction in which the flux is affected is a function of elevation above water, with fluxes 40 m above the surface being higher than the expected equilibrium flux and those from 5-680 m being lower. This suggests that neutron counting rates recorded at 998 g cm^{-2} (300 m) and 962 g cm^{-2} (600 m) were affected by the air-water boundary and should therefore not be used to determine the attenuation length for the equilibrium portion of the atmosphere.

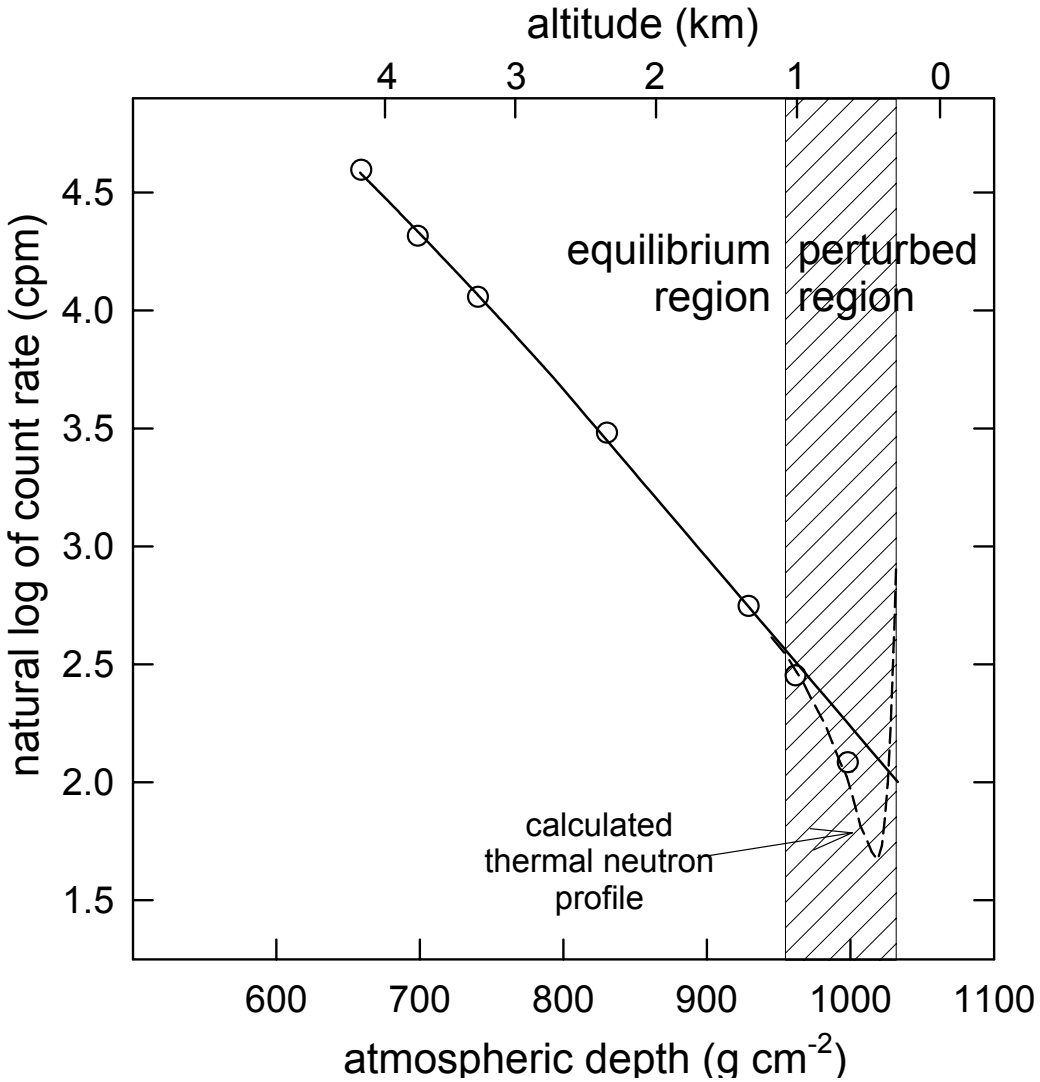

Figure 5. Airborne measurements of low-energy neutron fluxes. The two measurements below 1000 m are perturbed by presence of sea water, as indicated by our neutron transport simulations (dashed line).

2.3 Cutoff rigidities

Cutoff rigidities were calculated by numerically tracing the paths of primary cosmic-ray protons through International Geomagnetic Reference Field model 2000 [8, 20]. The simulated trajectories correspond to vertically-incident particles impinging on the atmosphere 20 km above each survey site. To obtain the effective vertical cutoff rigidity (R_C) we used the relation [21]:

$$R_{\mathrm{C}} = R_{\mathrm{U}} - \sum_{i=R_{\mathrm{L}}}^{R_{\mathrm{U}}} \Delta R_i \qquad (2)$$

where R_{U} is the upper rigidity limit for forbidden trajectories, R_{L} is the lower limit for allowed trajectories, and ΔR_i is the rigidity interval between trajectory calculations. The term $\Sigma\Delta R_i$ represents the sum of allowed rigidity intervals between R_{U} and R_{L}.

The use of R_{C} to account for geomagnetic shielding represents an important advance in cosmogenic dating [4, 5]. Parameters previously used to describe geomagnetic shielding effects were geomagnetic latitude calculated from a dipole model [22], geomagnetic latitude calculated from a high-order field approximation [23], surface values of geomagnetic inclination [24], and cutoff rigidity calculated from surface values of geomagnetic inclination and horizontal field intensity [25]. Each of these previously-used geomagnetic parameters has a non-unique relationship with cosmic-ray intensity, resulting in discrepancies of up to ~15% between fluxes at locations having the same parameter value, whereas discrepancies between fluxes at the same R_{C} are negligible.

3. Results and Discussion

3.1 Energetic nucleons

Hawaii: comparison of neutron monitor responses

In order to verify that the Arizona neutron monitor response is similar to that of the more commonly used NM-64 neutron monitor, we compared our results from Hawaii to the NM-64 altitude survey conducted there during the 1965 solar minimum [6]. A similar altitude response at nearby locations (Mauna Kea and Haleakala) from the two instruments would suggest that data from the instruments could be used interchangeably for scaling cosmogenic nuclide production rates. The altitude dependence, as expressed by the effective attenuation length (Λ), was determined by fitting the equation:

$$\ln C = (1/\Lambda)x + b \tag{3}$$

to the counting rates (C) by minimizing the chi-square merit function. Attenuation lengths obtained from equation 3 are termed "effective" because they assume that Λ is constant with x even though Λ is known to be depth dependent [6]. However, if either the range of x or the dependence of Λ on x are small then the approximation will produce only a small error in calculations of scaling factors.

We obtained a value of 146.8±0.5 g cm^{-2} from our measurements over the depth range 1039.4-630.2 g cm^{-2} (0-4205 m) which is very close to the value of 146.8±0.2 g cm^{-2} obtained from [6]'s measurements over a similar range of altitudes (1033.9-725.0 g cm^{-2}, 0-3030 m) (Fig. 6). The agreement between the two surveys is very good considering that (1) the monitors have different designs; (2) [6]'s measurements are from

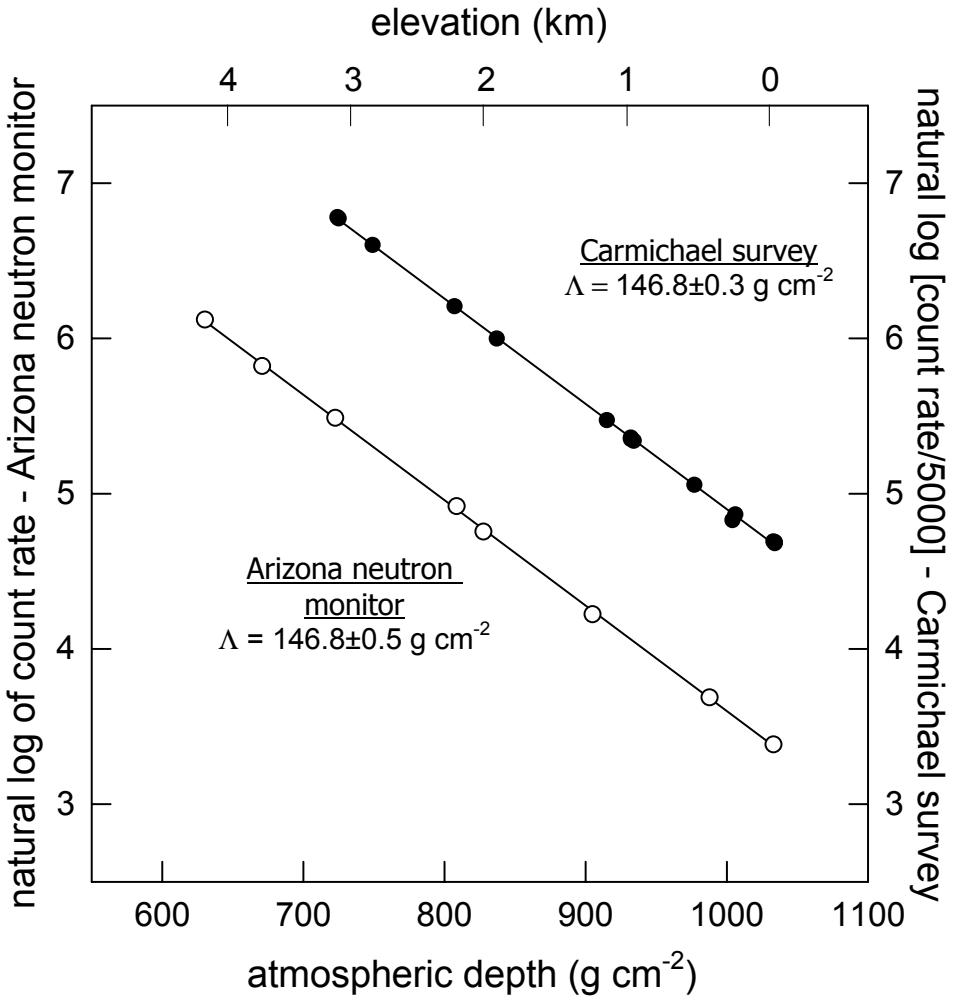

Figure 6. Neutron monitor measurements of high-energy nucleon fluxes at Mauna Kea, HI in 2000 (this work) compared with measurements by Carmichael el al. [11] at Haleakala, HI in 1966.

solar minimum whereas ours are closer to solar maximum; and (3) we covered a slightly larger elevation range. The good agreement with [6]'s data means that the Arizona neutron monitor can be used to extend their measurements, and therefore [5]'s scaling model, to R_C=17.3 GV.

India: improved scaling parameters at low latitude

The attenuation length increases by only a small amount from Hawaii (R_C=12.8-13.3 GV) to India (R_C=17.3 GV), and this increase mostly is restricted to altitudes above 3000 m (Fig. 7). We obtained an apparent attenuation length of 148.4±1.3 g cm^{-2} at R_C=17.3 GV from ground-based measurements (1029.6-763.4 g cm^{-2}, 0-2637 m), which is very close to the values that we and [6] measured in ground-based surveys in Hawaii. At higher altitudes our airborne measurements suggest a more substantial increase from the value of 153.5±0.5 g cm^{-2} obtained from [6]'s transect at 13.3 GV and 724-367 g cm^{-2} (0-3030 m) to 158.8±1.3 g cm^{-2} at 17.3 GV and 773 to 389 g cm^{-2} (2560-8250 m).

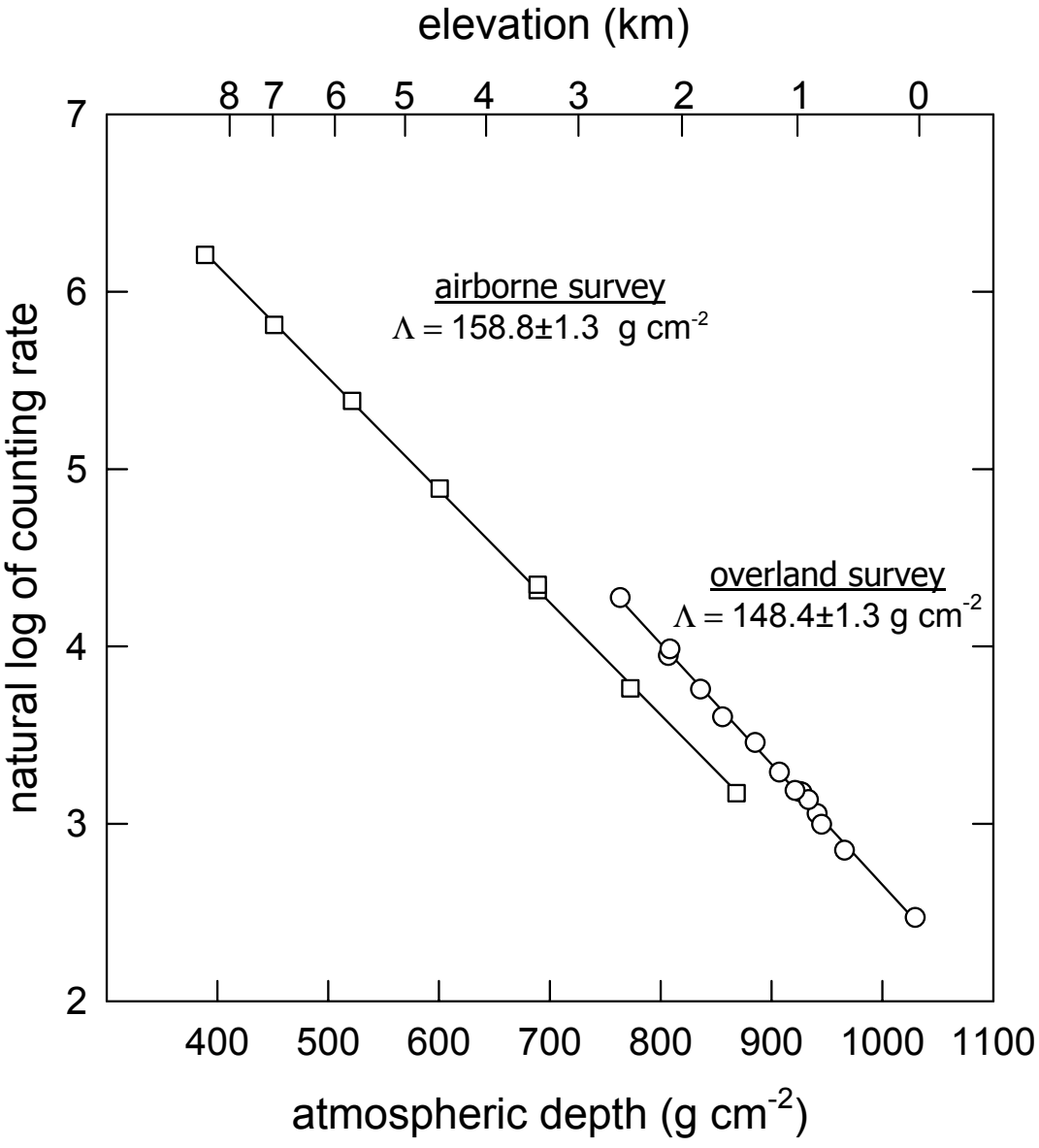

Figure 7. Neutron monitor measurements from southern India, 2002.

Based on the data from India, we give updated polynomial coefficients (Table 2) for scaling spallation reactions. The effective attenuation length for spallation reactions is well-described by the formula:

$$\Lambda_{e,sp}(R_C, x_1, x_2) = \frac{x_2 - x_1}{\left[\begin{array}{c} n\left(1+\exp\left(-\alpha {R_C}^{-k}\right)\right)^{-1} x + 1/2\left(a_3 + a_4 R_C + a_5 {R_C}^2\right)x^2 \\ +1/3\left(a_3 + a_4 R_C + a_5 {R_C}^2\right)x^3 \\ +1/4\left(a_3 + a_4 R_C + a_5 {R_C}^2\right)x^4 \end{array} \right]_{x_1}^{x_2}} \quad (4)$$

where $\Lambda_{e,sp}$ is the effective attenuation length between x_1 and x_2. The new coefficients were determined by iteratively forcing Eq. 5 to agree with the muon-corrected effective attenuation lengths measured in India. This new parameterization is valid from x=1033 g cm^{-2} to x=500 g cm^{-2} (0-5700 m) and from R_C=0 GV to R_C=17.3 GV. Relative nucleon fluxes calculated from the parameters in Table 2 agree with our muon corrected data from India to within 2% on average, which is very good agreement considering that the uncertainty of each measurement is ~2% on average. The previous parameterization matches our India data to within only 6%. We also refitted the high latitude data in order to provide a better agreement with [6]'s results. The new high-latitude attenuation lengths are about 2% higher than before but are still within the +5/-2% uncertainty of the values given by [5]. The uncertainty in Λ propagates to a significant uncertainty in production rates if there is large altitude range between the calibration site and sample site. For example the uncertainty in scaling between 0 m and 5000 m (1033-540 g cm^{-2}) is -15/+16% at high latitude. A reduction of this uncertainty would require better knowledge

of long-term solar activity and accurate nucleon flux data at high latitude over the full range of solar activity conditions.

Table 2. New polynomial coefficients for spallation reaction attenuation lengths

n	1.0177E-02
a	1.0207E-01
k	-3.9527E-01
a0	8.5236E-06
a1	-6.3670E-07
a2	-7.0814E-09
a3	-9.9182E-09
a4	9.9250E-10
a5	2.4925E-11
a6	3.8615E-12
a7	-4.8194E-13
a8	-1.5371E-14

How to applying scaling factors

For scaling cosmogenic nuclide production from a sea-level high-latitude (SLHL) calibration site (x=1033 g cm^{-2}, R_C<2) to a given x and R_C the scaling factor can be expressed as the product of separate latitude and altitude scaling factors:

$$F(R_C, x) = f_{lat} f_{elev} \tag{5}$$

where f_{lat} is the latitude scaling factor at sea level, which is given by the Dorman function:

$$f_{lat} = 1 - exp\left(-\alpha R_C^{-k}\right) \tag{6}$$

where α=10.275 and k=0.9615 for spallation reactions [5, 21]. The elevation scaling

factor, f_{elev}, is then given by:

$$f_{\mathrm{elev}} = \exp \frac{1033 - x}{\left[\begin{array}{l} n\left(1 + exp\left(-\alpha R_{\mathrm{C}}{}^{-k}\right)\right)^{-1} x \\ +1/2\left(a_0 + a_1 R_{\mathrm{C}} + a_2 R_{\mathrm{C}}{}^{2}\right)x^2 \\ +1/3\left(a_3 + a_4 R_{\mathrm{C}} + a_5 R_{\mathrm{C}}{}^{2}\right)x^3 \\ +1/4\left(a_3 + a_4 R_{\mathrm{C}} + a_5 R_{\mathrm{C}}{}^{2}\right)x^4 \end{array}\right]_x^{1033}} \tag{7}$$

The production rate at a sample site $P(R_C,x)$ is then given by:

$$P\left(R_{\mathrm{C}}, x\right) = P_0 \cdot F \tag{8}$$

where P_0 is the production rate at a SLHL calibration site. For scaling production rates between any two arbitrary locations (where neither is at SLHL), the scaling factor is given by the ratio of the scaling factors for each site relative to SLHL. For example, if a sea level low-latitude location has F=0.5, and a mid-latitude high-altitude location has F=4 then the production rate at the second site is eight times the rate at the first site.

3.2 Low-energy neutron fluxes

The apparent attenuation length determined from our airborne measurements of low-energy neutron fluxes is Λ_{th}=149±4 g cm^{-2} over the range 928-658 g cm^{-2} (950-3800 m). For the purpose of comparing with previous work [26], we also calculated Λ_{th} as a continuous function of depth by fitting a second-order polynomial

$$\ln C = b_1 x^2 + b_2 x + b_3 \tag{9}$$

to the natural logarithm of our counting rates. A non-linear fit is justified by the observation that Λ_{th} changes rapidly with altitude [26], and therefore the use of an apparent Λ over the entire altitude range may be inaccurate. The attenuation length is given by:

$$1/\Lambda(x) = \frac{\mathrm{d}\ln C}{\mathrm{d}x} = 2b_1 x + b_2 \tag{10}$$

We performed a Monte Carlo simulation to determine the mean value and confidence limits for $\Lambda_{th}(x)$. For each measurement we generated 1000 synthetic data points, each randomly selected from a Gaussian distribution having the same mean value and standard deviation as the selected measurement. The mean and standard deviation of Λ_{th} was determined as a continuous function of x by fitting equation 9 to the simulated data sets and then differentiating (Fig. 8).

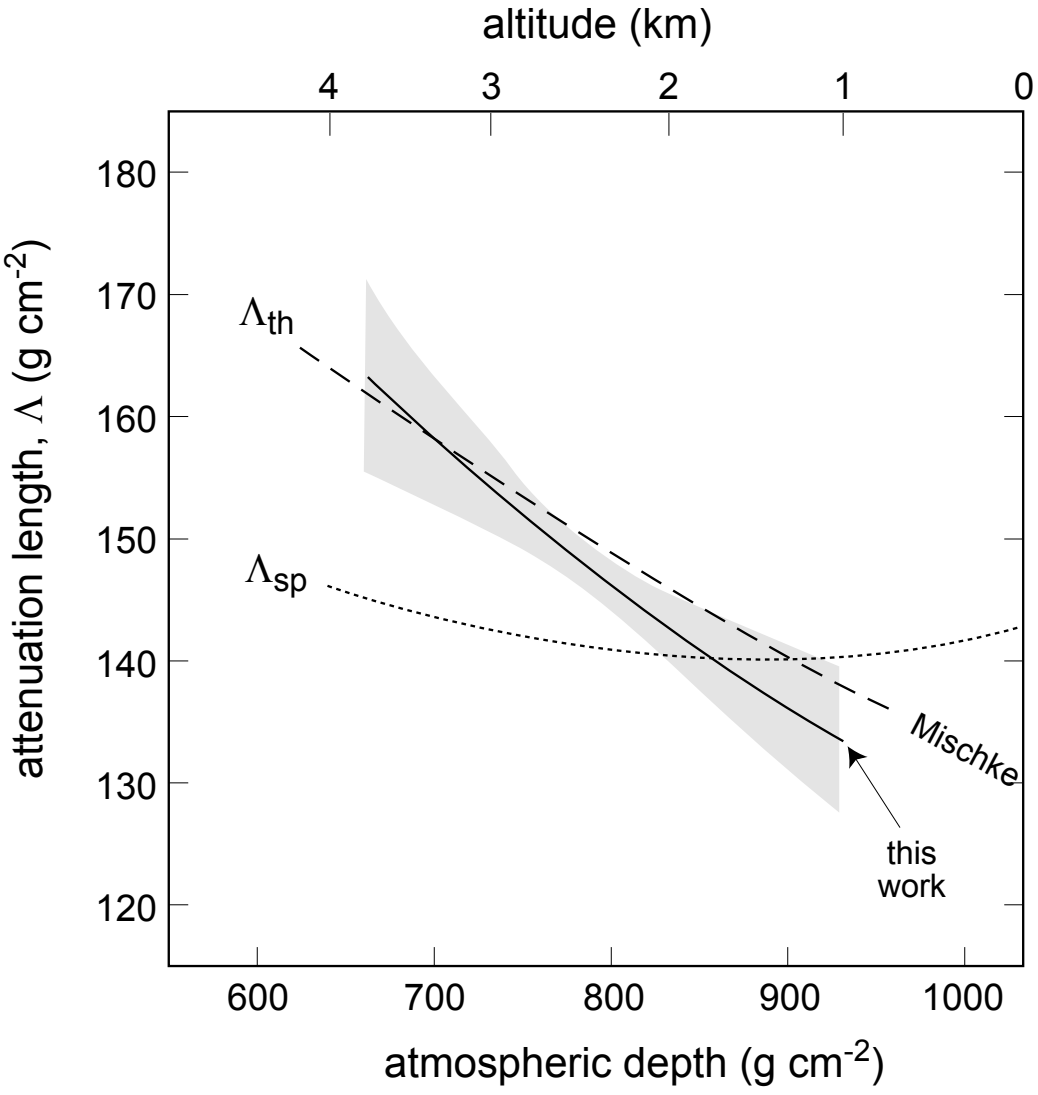

Figure 8. Attenuation length for low-energy neutron fluxes as a continuous function of depth in the atmosphere from this work and from Mischke [26] at R_C=12.8 GV. The attenuation length for spallation reactions, Λ_{sp}, is shown for comparison.

The dependence of Λ_{th} on atmospheric that we determined is in excellent agreement with dependence found by [26]. Both experiments suggest that low-energy neutron fluxes have a different altitude dependence than the more energetic component measured with a neutron monitor. The data on low energy neutrons indicates that Λ_{th} is greater than Λ_{sp} above 1500 m and that the two attenuation lengths diverge with increasing altitude. This behavior is consistent with a nucleon energy spectrum that softens with increasing atmospheric depth. However, in the lowermost 1500 m [26]'s regression suggests that the relation between low- and high-energy neutron attenuation lengths is reversed. Our data do not have the precision to support or reject such a behavier. We point out, however that [26]'s regression includes measurements from closer to sea level than ours (x=960 g cm^{-2} compared to x=929 g cm^{-2}), and that those measurements may have been in the region of perturbed low-energy neutron fluxes near the air/water interface. According to our transport calculation in (Section 2.2) such a contribution to the counting rate would produce a Λ that is smaller than the true "equilibrium" value, and hence could explain why [26] attenuation lengths are lower than expected below 1500 m.

4.0 Implications and considerations for surface exposure dating

4.1 Scaling production rates to higher paleomagnetic field strength

The anomalously high cutoff rigidity over India makes it possible to use modern cosmic-ray measurements to scale production rates to paleo-dipole fields that are greater in strength than the present dipole field (Fig. 9). This works because (1) the relation between cosmic-ray intensity and R_C is unique (to a good approximation [27]); (2) non-dipole components create locally higher (and lower) cutoff rigidities than would occur in a dipole field; (3) cosmogenic nuclide production is integrated over time; and (4) integrated paleomagnetic fields probably average to a dipole over ~10,000 yrs [24, 28, 29]. The new measurements at 17.3 GV are equivalent to measuring nucleon fluxes in a dipole field with a strength (M) ~1.2 times greater than the modern (1945) dipole strength of 8.084×10^{22} A m^2 (M_0). Our earlier parameterization [5] was valid only to M/M_0=0.9 at the equator. At higher latitudes the parameterization is valid for greater field strengths because dipole strength fluctuations have only a small effect on cutoff rigidity toward the poles. For example, M/M_0=1.4 gives R_C=16.3 GV at 25° geomagnetic latitude, which is within the range of our updated scaling parameterization.

The new parameterization covers nearly the full range of R_C values that could be expected over the surface exposure history of most landforms. Over the past 800,000 years, dipole strength has mostly been between 0.3 and 1.4 times the current field strength [30]. Only over the past 10,000 years has the field been stronger than the modern field for prolonged periods [31]. The highest paleomagnetic dipole strengths (averaged

over 500 year intervals) exceeded M/M_0=1.2 for only ~3000 years, which matters only near the geomagnetic equator where the average R_C could have been as high as 20 GV from 1.5-3.5 ka. Extrapolation of our scaling model to higher R_C would be a potential source of additional error only for low latitude samples with exposure ages on the order of a few thousand years.

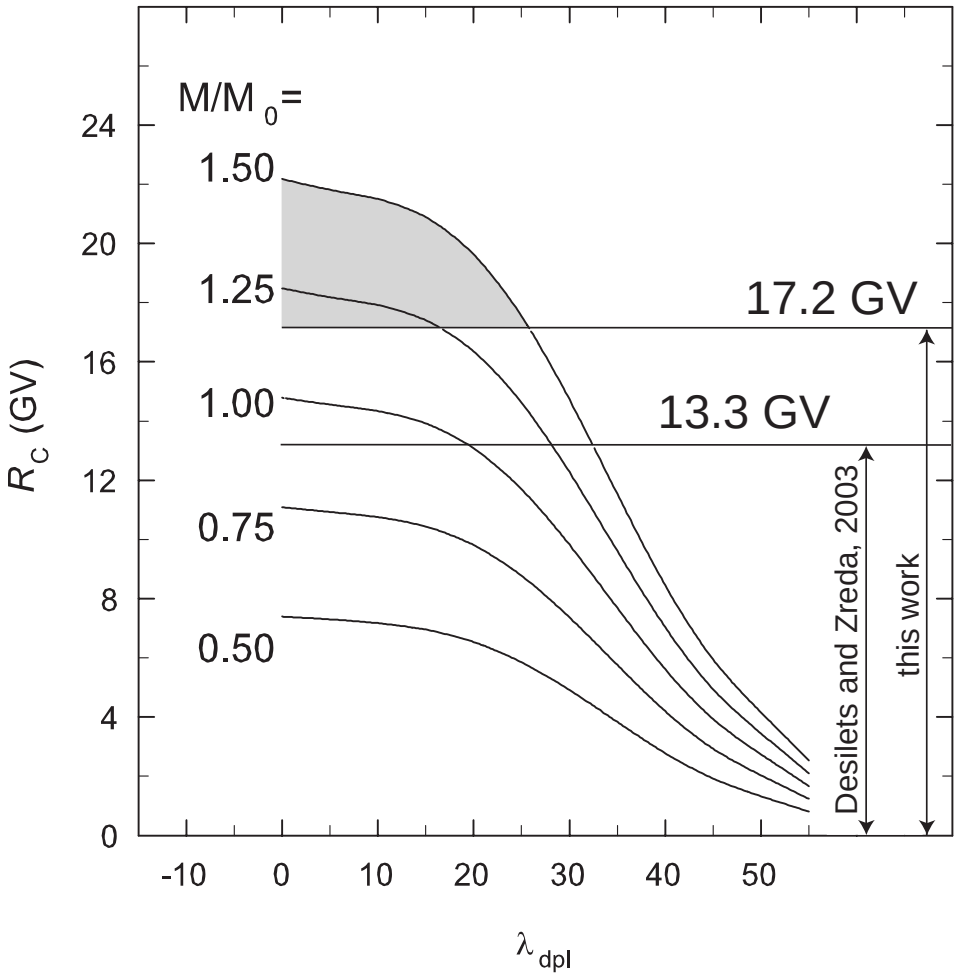

Figure 9. Cutoff rigidity range of spallation scaling model for different dipole strengths.

4.2 Sensitivity of landform ages to energy dependent scaling parameters

Do energy-dependent scaling factors make a difference in calculating landform ages? The answer to this question depends on the dominant nuclide production mechanisms in a sample (e.g. spallation versus thermal neutron activation) and on the location of the sample site relative to the calibration site. An extreme case would be in scaling a calibrated production rate from SLHL to a high-altitude (4,000 m) equatorial (R_C=14.8 GV) sample site. In this case, the scaling factor for low-energy neutron reactions would be 22% lower than for high-energy nucleons, and ages would be ~22% higher using the low-energy scaling.

Another example is in dating Pleistocene moraines on Mauna Kea, Hawaii. In this case, the low-energy scaling factors (scaled from SLHL) are on average 18% lower than for the high-energy component. However, if the energy dependence of scaling factors is neglected and thermal nucleon reactions are assumed to scale the same as spallation reactions, ages will on average be lower by only 3%. Individual samples are lower by 1-12% depending on the ratio of low-energy nucleon activation to high-energy spallogenic production (high Cl samples having proportionately more nucleon-activation production of ^{36}Cl). In most of these samples production is dominated by spallation reactions, and therefore the use of low-energy scaling parameters changes the ages very little and adds only a small uncertainty to the final age.

Samples at high geomagnetic latitude and low elevation are less sensitive to the energy dependence of scaling parameterizations for two reasons. First, calibrated

production rates are usually normalized to high latitude and sea level, and therefore the scaling factor will be closer to unity. Second, the two scaling models converge with increasing latitude and decreasing elevation.

4.3 Uncertainty in scaling factors

There are two categories of uncertainty associated with scaling factors. One category includes the fluctuating paleo-environmental conditions that make determinations of x and R_C difficult for past epochs. Important paleo-environmental parameters include paleo-dipole position and strength (to which R_C is sensitive), and paleo-altitude and paleoclimate (to which x is sensitive). Solar activity can be considered in this category because modulating the galactic cosmic-ray flux is similar to changing the high-latitude R_C. Progress has been made in incorporating some paleo-environmental effects (e.g. from paleomagnetic records) but most (paleo-altitude, paleoclimate and solar activity) are usually neglected.

The second category is related to the measurement and interpretation of historical cosmic-ray data. The precision, spatial and temporal coverage, and parameterization of cosmic-ray data all determine the uncertainty of a scaling model. A larger and more fundamentally significant source of uncertainty is related to systematic differences between attenuation lengths measured at high-energies and low-energies. Another source of uncertainty is in the muon correction to nucleon monitor counting rates. These last two problems will be addressed in the Cronus-Earth project.

It is it impossible to make a blanket assessment of the error in scaled production rates. There are a large number of potential errors and the sizes of these errors have spatial and temporal dependencies. For example, production rates will be most affected by solar activity near the poles and least affected near the equator, whereas the opposite is true for dipole strength variations. Furthermore, temporal fluctuations in production rates at a sample site may be correlated with similar changes at the calibration site and hence the errors at the two sites will cancel to produce a small error in the exposure age. In this case corrections will only be valid if they are applied to both the calibration site and sample site; otherwise landform ages could be overcorrected.

5.0 Conclusions

The measurements reported here extend the cutoff rigidity range of our spallation-reaction scaling model from 13.3 GV to 17.3 GV and provide new experimental evidence confirming that nucleon attenuation lengths depend on energy. The extended scaling model allows our scaling factors to be applied to higher paleomagnetic dipole strengths than were previously possible using other scaling formulations.

The major implication of energy dependent attenuation lengths is that cosmogenic nuclides produced by different portions of the nucleon energy spectrum may require different scaling models. The scaling factor for nucleon activation reactions may be smaller than that for spallation reactions by as much as 22%. The use of low-energy nucleon scaling factors is most relevant to ^{36}Cl dating, where both high- and low-energy

production mechanisms can be important, and is more important for low-latitude samples, where the difference between Λ_{sp} and Λ_{th} is greatest.

This work and previous studies have shown that direct measurements of nucleon intensity can provide high-precision data on the spatial variability of nucleon fluxes. However, knowledge of the nucleon energy spectrum and of excitation functions for cosmogenic nuclide production are still lacking. Currently, extensive nucleon measurements are available only at the high- and low-energy extremes. We may be approaching the limit of what can be accomplished using well-established methods for surveying nucleon intensity due to the difficulty in obtaining precise energy spectra. In order to obtain increased accuracy for cosmogenic nuclide scaling parameters, it would be helpful to combine future experimental work with modeling of atmospheric nucleon fluxes and instrument response functions. Furthermore, it is necessary to test the assumption that measurements of nucleon intensity are an accurate proxy for nuclear spallation rates for commonly used nuclides.

Acknowledgements

We are grateful to Prof. D. Lal for his assistance in arranging experiments in India. The Raman Research Institute in Bangalore provided invaluable technical assistance in India, and the Indian Air Force graciously provided an airplane and pilot. This material is based upon work supported by the National Science Foundation under grants EAR-0001191, EAR-0126209 and ATM-0081403 and by Packard Fellowship in Science and Engineering 95-1832. The Haleakala nucleon monitor is supported by National Science Foundation Grant ATM-9912341.

Supplemental Table 1. Energetic nucleon fluxes measured with neutron monitor near Bangalore, India (R_C=17.3 GV).

Table 1. Measurements in India

location			N. latitude	E. longitude	R_C (GV)	pressure[a] (g cm^{-2})	date UTC	start time UTC	counting time (minutes)	counting rate (cpm)
ground-based measurements										
	1	Begur Cross	11.94	76.67	17.28	941.2	21-Apr-02	8:40	180	21.3
	2	Jungle Lodge	11.56	76.64	17.30	925.3	21-Apr-02	14:20	250	24.1
	3	Jungle Lodge	11.56	76.64	17.30	927.3	22-Apr-02	2:30	60	24.0
	4	Road to Ooty	11.50	76.69	17.30	907.1	22-Apr-02	5:25	150	26.9
	5	Road to Ooty	11.49	76.69	17.30	885.1	22-Apr-02	8:25	120	31.8
	6	Check point	11.48	76.68	17.30	855.8	22-Apr-02	10:59	100	36.7
	7	Hullatti	11.47	76.68	17.30	835.9	22-Apr-02	13:13	90	42.9
	8	Radioastronomy lab	11.38	76.67	17.30	806.8	22-Apr-02	17:39	240	51.8
	9	Radioastronomy lab	11.38	76.67	17.30	808.3	23-Apr-02	4:16	60	53.8
	10	Dodda Betta	11.40	76.74	17.30	763.4	23-Apr-02	6:41	60	71.8
	11	Nedukikarana	11.55	76.18	17.28	933.3	23-Apr-02	13:40	180	23.0
	12	Calicut	11.25	76.77	17.31	1029.6	24-Apr-02	0:43	240	11.8
	13	Road to Ooty	11.51	76.03	17.28	965.8	24-Apr-02	8:07	240	17.3
	14	Western Ghats	11.94	76.67	17.28	945.2	24-Apr-02	-	60	20.0
	15	Bangalore	13.01	77.58	17.24	921.1	25-Apr-02	9:20	130	24.2
airborne measurements										
	1	Bangalore	12.95	77.12	17.23	868.4	8-May-02	5:36	80	23.9
open cabin	2	Bangalore	12.95	77.12	17.23	772.7	8-May-02	7:05	45	43.1
	3	Bangalore	12.95	77.12	17.23	689.1	8-May-02	7:56	30	75.0
	4	Bangalore	12.95	77.12	17.23	689.1	8-May-02	10:01	30	77.3
	5	Bangalore	12.95	77.12	17.23	600.5	8-May-02	10:40	20	133.0
pressurized	6	Bangalore	12.95	77.12	17.23	521.5	8-May-02	11:08	15	218.0
cabin	7	Bangalore	12.95	77.12	17.23	451.2	8-May-02	11:31	15	334.7
	8	Bangalore	12.95	77.10	17.23	388.9	8-May-02	12:01	10	497.0

Supplemental Table 2. Airborne measurements of low-energy nucleons in the vicinity of Kailua-Kona, Hawaii (R_C=12.8 GV).

pressure g cm^{-2}	start date UTC	start time UTC	counting time (minutes)	counting rate (cpm)
flight 1				
998.1	17-Jun-03	9:27	73	8.04 [a]
944.0	17-Jun-03	10:46	73	11.63 [a]
929.3	17-Jun-03	11:33	66	16.59
831.0	18-Jun-03	0:49	42	33.59
741.1	18-Jun-03	1:42	24	59.84
659.0	18-Jun-03	2:24	16	99.28
698.5	18-Jun-03	5:01	16	74.89
flight 2				
659.2	18-Jun-03	4:33	25	98.84
739.8	18-Jun-03	5:23	24	55.85
829.7	18-Jun-03	5:55	39	31.45
928.8	18-Jun-03	7:42	58	14.60

[a] measurement in perturbed region close to sea surface

References

1 J.T. Fabryka-Martin, Production of radionuclides in the earth and their hydrogeologic significance, with emphasis on chlorine-36 and iodine-129, PhD dissertation, University of Arizona, 1988.

2 D. Lal and B. Peters, Cosmic ray produced radioactivity on earth, in: Encyclopedia of Physics: Cosmic Rays II, K. Sitte, ed., Encyclopedia of Physics 46/2, pp. 551-612, Springer-Verlag, Berlin, 1967.

3 J.A. Simpson and W.C. Fagot, Properties of the low energy nucleonic component at large atmospheric depths, Physical Review 90, 1068-1072, 1953.

4 D. Desilets and M. Zreda, On scaling cosmogenic nuclide production rates for altitude and latitude using cosmic-ray measurements, Earth and Planetary Science Letters 193, 213-225, 2001.

5 D. Desilets and M. Zreda, Spatial and temporal distribution of secondary cosmic-ray nucleon intensity and applications to in situ cosmogenic dating, Earth and Planetary Science Letters 206, 21-42, 2003.

6 H. Carmichael and M. Bercovitch, V. Analysis of IQSY cosmic-ray survey measurements, Canadian Journal of Physics 47, 2073-2093, 1969.

7 J.S. Pigati and N.A. Lifton, Geomagnetic effects on time-integrated cosmogenic nuclide production with emphasis on in situ ^{14}C and ^{10}Be, Earth and Planetary Science Letters 226, 193-205, 2004.

8 M.A. Shea and D.F. Smart, A world grid of calculated cosmic ray vertical cutoff rigidities for 1980.0, in: Proceedings of the 18th International Cosmic Ray Conference MG 10-3, pp. 415-418, Bangalore, India, 1983.

9 C.J. Hatton, The neutron monitor, in: Progress in Elementary Particle and Cosmic Ray Physics, J.G. Wilson and S.A. Wouthuysen, eds. 10, pp. 1-100, North-Holland Publishing Co., Amsterdam, 1971.

10 D.M. Desilets, The global distribution of secondary cosmic-ray intensity and applications to cosmogenic dating, M.S., University of Arizona, 2001.

11 H. Carmichael, M.A. Shea and R.W. Peterson, III. Cosmic-ray latitude survey in Western USA and Hawaii in summer, 1966, Canadian Journal of Physics 47, 2057-2065, 1969.

12 R. Pyle, P. Evenson, J.W. Bieber, J.M. Clem, J.E. Humble and M.L. Duldig, The use of ^{3}He tubes in a neutron monitor latitude survey, in: Proceedings of the 26th International Cosmic Ray Conference 7, pp. 386-389., Salt Lake City, 1999.

13 C.J. Hatton and H. Carmichael, Experimental investigation of the NM-64 neutron monitor, Canadian Journal of Physics 42, 2443-2472, 1964.

14 G.F. Knoll, Radiation detection and measurement, 802 pp., Wiley, New York, 2000.

15 Manual of the ICAO Standard Atmosphere extended to 80 kilometres (262 500 feet), International Civil Aviation Organisation, Doc. 7488, 1993.

16 B. Liu, F.M. Phillips, J.T. Fabryka-Martin, M.M. Fowler and R.S. Biddle, Cosmogenic ^{36}Cl accumulation in unstable landforms, 1. Effects of the thermal neutron distribution, Water Resources Research 30(11), 3115-3125, 1994.

17 X-5 Monte Carlo Team, MCNP - A General Monte Carlo N-Transport Code, Version 5, Los Alamos National Laboratory, 2003.

18 L. Dep, D. Elmore, J. Fabryka-Martin, J. Masarik and R.C. Reedy, Production rate systematics of in-situ produced cosmogenic nuclides in terrestrial rocks: Monte Carlo approach of investigating ^{35}Cl(n,γ)^{36}Cl, Nuclear Instruments and Methods in Physics Research B92, 321-325, 1994.

19 S. Croft and L.C.A. Bourva, The specific total and coincidence cosmic-ray-induced neutron production rates in materials, Nuclear Instruments and Methods in Physics Research A 505, 536–539, 2003.

20 M.A. Shea, D.F. Smart and K.G. McCracken, A study of vertical cutoff rigidities using sixth degree simulations of the geomagnetic field, Journal of Geophysical Research 70, 4117-4130, 1965.

21 L.I. Dorman, G. Villoresi, N. Iucci, M. Parisi, M.I. Tyasto, O.A. Danilova and N.G. Ptitsyna, Cosmic ray survey to Antarctica and coupling functions for neutron component near solar minimum (1996-1997) 3. Geomagnetic effects and coupling functions, Journal of Geophysical Research 105, 21,047-21,056, 2000.

22 D. Lal, Cosmic ray labeling of erosion surfaces: *in situ* nuclide production rates and erosion models, Earth and Planetary Science Letters 104, 424-439, 1991.

23 I.J. Graham, B.J. Barry, R.G. Ditchburn and N.E. Whitehead, Validation of cosmogenic nuclide production rate scaling factors through direct measurement, Nuclear Instruments and Methods in Physics Research B 172, 802-805, 2000.

24 T.J. Dunai, Scaling factors for production rates of in situ produced cosmogenic nuclides: a critical reevaluation, Earth and Planetary Science Letters 176, 157-169, 2000.

25 T.J. Dunai, Inluence of secular variation of the geomagnetic field on production rates of in situ produced cosmogenic nuclides, Earth and Planetary Science Letters 193, 197-212, 2001.

26 C.F.W. Mischke, Intensiteisvaiasies van neutrone vanaf kosmiese strale, M.S., University of Potchefstroom, 1972.

27 J.M. Clem, J.W. Bieber, P. Evenson, D. Hall, J.E. Humble and M. Duldig, Contribution of obliquely incident particles to neutron monitor counting rate, Journal of Geophysical Research 102, 26,919-26,926, 1997.

28 J.M. Licciardi, M.D. Kurz, P.U. Clark and E.J. Brook, Calibration of cosmogenic ^{3}He production rates from Holocene lava flows in Oregon, USA, and effects of the Earth's magnetic field, Earth and Planetary Science Letters 172, 261-271, 1999.

29 T.M. Shanahan and M. Zreda, Chronology of Quaternary glaciations in East Africa, Earth and Planetary Science Letters 177, 23-42, 2000.

30 Y. Guyodo and J.P. Valet, Global changes in intensity of the Earth’s magnetic field during the past 800 kyr, Nature 399, 249-252, 1999.

31 M.W. McElhinny and W.E. Senanayake, Variations in the geomagnetic dipole I: the past 50,000 years, Journal of Geomagnetism and Geoelectricity 34, 39-51, 1982.

APPENDIX E

ELEVATION PROFILE OF ^{36}Cl PRODUCTION FROM HAWAIIAN LAVA FLOWS

Darin Desilets and Marek Zreda

[In preparation for *Earth and Planetary Science Letters* (2005)]

Abstract

To directly constrain the elevation dependence of cosmogenic nuclide production rates, we measured an elevation profile of ^{36}Cl in three well-preserved lava flows on Mauna Kea, Hawaii (19.8° N, 155.5° W). Two flows were formed nearly contemporaneously at 40.7±0.5 ka; another, present discontinuously, probably as a series of kipukas, was erupted at 62.6±0.8 ka. The average paleo cutoff rigidity (a measure of geomagnetic shielding of cosmic rays) for these flows is 11 GV and their paleo-elevation range is 2100-3700 m. Production of ^{36}Cl is dominated by neutron reactions, with the high-energy reactions ^{39}K(n,x) and ^{40}Ca(n,x) accounting for nearly half of the ^{36}Cl production and the low-energy reaction ^{35}Cl(n,γ) responsible for the remaining half. Production by negative muons is small at these high elevations, accounting for less than 2% of the total production in the lowest elevation samples. The elevation dependence of ^{36}Cl production measured in these lava flows is described by an attenuation length of 142±5 g cm^{-2}. This result is close to the value of 140 g cm^{-2} determined from neutron monitor surveys of high-energy neutron fluxes, but significantly below the value of 149 g cm^{-2} determined from measurements of low-energy neutrons. The predicted attenuation length for these lava flows, incorporating both high- and low-energy mechanisms, is 144 g cm^{-2}. The observed good agreement between the results from lava flows and from cosmic-ray surveys validates the use of neutron flux measurements to scale ^{36}Cl nuclide production where muon production is unimportant. But potential systematic errors due to

geological complications, such as erosion or burial or inaccuracies in the ratio of production rates, mean that our data lack the precision to confirm or reject the hypothesis [Desilets and Zreda, EPSL, 2003] that separate scaling models are necessary for high- and low-energy reactions.

1. Introduction

The buildup of cosmogenic nuclides in surface materials can provide quantitative information on the surface exposure history of a wide variety of features including neotectonic, erosional, glacial and depositional landforms [1]. Successful application of cosmogenic nuclides requires knowledge of local production rates of cosmogenic isotopes, which at the land surface are controlled mostly by the local secondary cosmic-ray nucleon intensity and to a lesser extent by muon intensity [2]. Because nucleon fluxes attenuate rapidly in the atmosphere, production rates are very sensitive to elevation.

The application of calibrated production rates to sites at different elevations requires direct knowledge of the elevation dependence of production rates or measurements of nucleon fluxes which can be used to infer that dependence. Because copious and precise data from neutron monitors and other instruments have long been available [3], data from cosmic-ray surveys have most often been used to scale production rates [2, 4-6]. However, the scaling models derived by various authors have not been entirely consistent [6], indicating that the use of cosmic-ray measurements can be problematic. One problem is that the spatial distribution of neutron fluxes seems to be energy dependent [6, 7], and that instruments such as neutron monitors have an energy sensitivity that is different from

the excitation functions for production of most cosmogenic nuclides. Furthermore, ^{36}Cl production rates from slow-negative muon capture in potassium and fast muon photodisintegration are not well known, but if significant they would give scaling factors that are less sensitive to elevation than scaling factors based on neutrons alone.

One way of determining the elevation dependence of production rates that avoids the problem of instrumental biases is the direct measurement of nuclide production in artificial targets [8-10]. Most recently, that approach was successfully used to measure ^{10}Be, ^{3}He, ^{3}H production in water targets [10] over an elevation profile spanning 4100 m. A drawback to using artificial targets is that an exposure time on the order of years is required. But for many of the commonly applied nuclides even several years of exposure is insufficient for the accumulation of measurable inventories. New procedures and/or analytical methods must be devised to overcome this problem.

An alternative to conducting neutron flux surveys and exposing artificial targets is the direct measurement of cosmogenic nuclide buildup in natural materials irradiated over a geologic timescale and spanning a significant elevation range. There have been several analogous investigations aimed at measuring the depth-dependence of production rates in rock (e.g. [11, 12]), but there has been only one study where an atmospheric profile was obtained from surface samples [13], and those results are uncertain due to poor constraints on independent ages. The goal of this work is to provide more accurate and precise data than those previously available.

To obtain the elevation dependence of neutron production from a natural exposure requires a landform that (1) is of uniform age or has independent age control; (2) spans a substantial elevation range with little change in latitude; (3) contains the requisite minerals for production and retention of the nuclide of interest; (4) has adequate buildup of cosmogenic nuclides (long enough exposure time); and (5) has a simple exposure history (negligible burial or erosion) if long-lived nuclides are to be applied. The well-preserved, vertically extensive lava flows of the Haleakala and Mauna Kea volcanoes make Hawaii one of few locations where all five of these conditions are satisfied. Extensive measurements of neutron intensity performed there by us and others ([14-16]) also make Hawaii an ideal location for comparing neutron measurements with cosmogenic nuclide production. In this paper we report an altitude profile of ^{36}Cl production determined from sampling lava flows on Mauna Kea, Hawaii and we compare these results to the altitude profile predicted using neutron flux survey results.

2. Site description and methods

2.1 Geology of Mauna Kea

The surficial lavas of Mauna Kea were extruded in two compositionally distinct episodes of post-shield eruption known as the Hamakua and Laupahoehoe substages [17]. The Hamakua Volcanics are characterized by alkali and transitional basalts erupted between 230 ka and 65 ka. These flows typically contain less than 10% of olivine, augite and plagioclase phenocrysts. Eruptions of Hamakua basalts were followed by the typically aphanitic hawaiite, mugearite and benmoreite lavas of the Laupahoehoe

Volcanics substage, deposited between 65 ka and 4 ka. Laupahoehoe lavas erupted from vents scattered along the upper slopes of Mauna Kea, mostly covering the Hamakua Volcanics above 1500 m. These eruptions are characterized by aa flows issuing from vents surrounded by 30-100 m high cinder cones. Air-fall deposits (lapilli and ash) are commonly associated with Laupahoehoe eruptions, locally blanketing flow surfaces and forming sheets and dunes of reworked ash [17].

2.2 Climate of the Island of Hawaii

Steep climate gradients on Hawaii mean that the preservation of primary flow features varies drastically across the island. A major factor controlling rates of surface weathering and erosion is precipitation, which in turn is a function of the intensity and direction of prevailing northeast trade winds. A temperature inversion caps the trade winds at ~1800 m and keeps moisture laden air from reaching the upper slopes of Mauna Kea [18]. Strong local thermal convection over the mountains frequently disrupts the inversion, drawing moisture further up slope, but rarely results in significant rainfall. Precipitation generally increases with elevation to the height of the inversion, and then decreases [18]. Precipitation rates are highly variable across the island, ranging from 600 cm yr^{-1} on the windward eastern slopes of Mauna Kea to <50 cm yr^{-1} on the leeward slopes. Old lava flow surfaces are best preserved at elevations above 1800 m and on the western slopes.

2.3 Sample collection

We collected samples from Laupahoehoe stage hawaiites erupted on the dry southwestern slope of Mauna Kea above the Humuula Saddle (Fig. 1). We selected two adjacent flows mapped by [19], that extend from cinder cones at 3567 m and 3206 m to the Humuula Saddle at 1680 m. These flows were selected because of their large elevation range, good preservation of primary flow features, and assumed age (>16 ka) which provides easily measurable $^{36}Cl/Cl$. Primary flow features (ropes, tumulus, pressure ridges, channels with levees) were present over the entire length of the lava flows, although surfaces are less vegetated and better preserved at higher elevations.

Lava flows of the Laupahoehoe substage are nearly identical in appearance and composition, making the distinction of separate flows difficult either in the field or laboratory. Low rates of erosion and of colonization by vegetation further make it difficult to distinguish individual hawaiite flows from separate eruptions, even when ages are different by thousands of years. We observed that because of the elevation/climate gradient, variations in surface preservation are often greater along a flow then they are between flows of different ages.

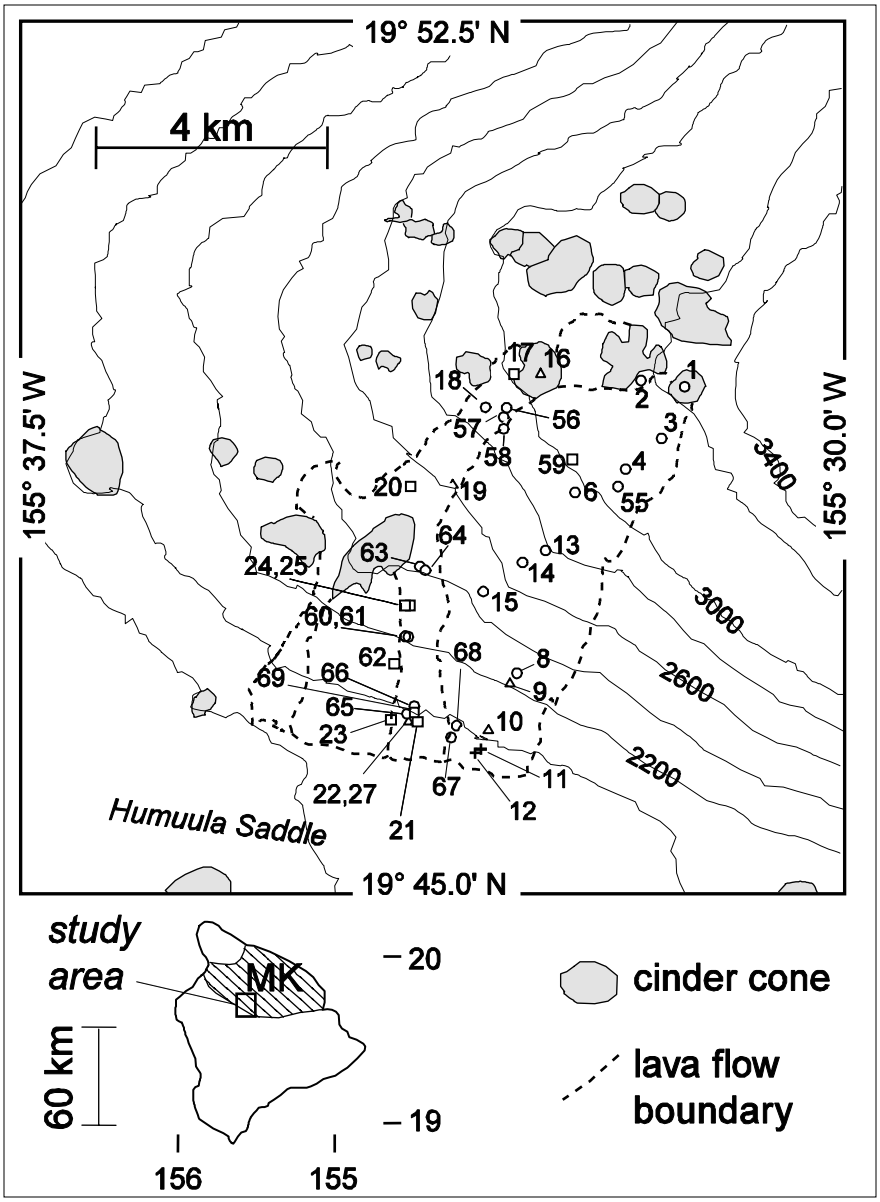

Figure 1. Study area and sample locations. Circles represent samples from flow *C* (39.6 ka), squares represent samples from flow *K* (62.0 ka), triangles represent outliers from the two groups (samples 9,10,16,19) and crosses represent outcrops of Hamakua basalt (samples 11 and 12). Dashed lines are the lava flow boundaries of [17].

The majority of our samples were collected from levees bordering lava flow channels (Fig. 2). For cosmogenic dating, an advantage of sampling levees is that they tend to be topographically prominent, making prolonged burial by ash unlikely. We sampled only from levees and other features that had ropes or rough popcorn-like texture as an indicator of a primary flow surface. Preservation of this intricate popcorn texture suggests that erosion depth is less than 2 cm.

2.4 Laboratory procedures

Whole rock samples were crushed and sieved to the 0.25-1.0 mm size fraction and then leached for 24 hours in 5% HNO_3 to remove meteoric Cl. Samples labeled HAW00-L1 were spiked with ^{35}Cl carrier and digested in a high-pressure acid-digestion vessel according to the procedure in [20]. Samples labeled HAW00-L2 and HAW03-L1 were digested without carrier in open containers according to [20]. For comparison, splits of seven of the L1 samples were also digested without carrier in open vessels [20], with all but one unspiked sample having results consistent with spiked samples. Samples were analyzed for $^{36}Cl/Cl$ by accelerator mass spectrometry (AMS) at PRIME Lab, Purdue University. Analytical errors in measurement of $^{36}Cl/Cl$ and $^{35}Cl/^{37}Cl$ were propagated to landform age uncertainty according to [20].

Figure 2. Typical lava flow levee on upper slopes of Mauna Kea (sample HAW03-17).

3. Age calculations

Three types of landform ages are discussed in this paper: uncorrected, corrected (true) and apparent. Uncorrected ^{36}Cl ages are based on geologically calibrated production rates [21] scaled to Hawaii according to [6] using the current geographic latitude of 19.8° N to calculate the effective vertical cutoff rigidity (R_C) and calculating atmospheric depth from the modern elevation. The corrected age takes into account time-dependent variations in geomagnetic dipole intensity and isostatic sea level and is based on calibrated production

rates that are corrected for changes in geomagnetic dipole intensity and position. These new production rates are based on [21]'s recalibration and have values of P_{Ca}=76.7 atoms g^{-1} yr^{-1}, P_K=161.3 atoms g^{-1} yr^{-1} and $P_f(0)$=764.7 neutrons g^{-1} yr^{-1}.

Apparent ages are a useful measure of the elevation dependence of ^{36}Cl production rates. They are calculated by assuming that all samples have an elevation of 2600 m (x = 760 g cm^{-2}), which is approximately the mean elevation for all samples, and by neglecting corrections that depend on the true exposure age (corrections for radioactive decay, geomagnetic field strength and sea level) since these will have the same percent effect on samples from the same lava flow. Because apparent ages assume a fixed elevation for all samples, high elevation samples will have older apparent ages than low elevation samples. Apparent ages are proportional to the ^{36}Cl production rate in a sample, normalized for chemistry variations in the sample data set.

3.1 Numerical age calculation

Temporal changes in the dipole strength of the geomagnetic field and in relative sea level make production rates in Hawaiian lava flows variable over time. For a non-eroding surface the exposure age, t, can be determined from the stable nuclide inventory according to:

$$t = \frac{N_{\text{total}}}{P f_1 f_2} \qquad (1)$$

where N_{total} is the measured inventory, P is the calibrated production rate (a constant for given sample chemistry) and f_1 and f_2 are the elevation and cutoff rigidity scaling factors. If the scaling factors are time dependent then exposure age is given by:

$$t = \int_0^t \frac{N(t)}{f_1(t) f_2(t) P} \, \mathrm{d}t \tag{2}$$

Because this equation has no closed-form solution and is tedious to solve numerically, we therefore make the following approximation:

$$t = \frac{N_{\text{total}}}{P \, f_{1,\text{avg}} \, f_{2,\text{avg}}} \tag{3}$$

where $f_{1,\text{avg}}$ and $f_{2,\text{avg}}$ are the average scaling factors over the exposure period. For a nuclide with decay constant λ the relation is:

$$t = \frac{-1}{\lambda} \ln\left(1 - \frac{\lambda N_{\text{total}}}{f_{1,\text{avg}} \, f_{2,\text{avg}} P}\right) \tag{4}$$

Corrected lava flow ages were calculated according to the following steps. First, ages were calculated from equation 4 and the scaling model in [6, 16]. These initial age estimates were plotted as a frequency histogram, which (as discussed in Section 4.1), ultimately served as the basis for distinguishing individual flows. Flow ages were calculated from a weighted average of all of the individual ages within a histogram peak. Sample ages were then iteratively recalculated from the latitude scaling in [6] but using the attenuation length determined from the elevation profile of the samples (Section 4.2)

rather than [6, 16]. Final corrected ages reflect a single paleo R_C and paleo elevation determined from the mean age of the flow.

3.2 Paleo R_C

Cutoff rigidity (R_C) was calculated for each time step using paleomagnetic records to determine paleo-geomagnetic latitude (λ_m) at Mauna Kea and by converting λ_m to R_C according to [6]. We used [22]'s marine record of geomagnetic field intensity for the period 11-800 ka combined with the more detailed archeomagnetic record [23] for the period 0.5-11 ka, and we assumed that the geocentric axial dipole (GAD) hypothesis is valid. Time-averaged R_C values were calculated by numerically integrating R_C over 500 yr intervals from 0-4 ka and over 1000 yr intervals from 11-800 ka (Table 1). This calculation is iterative because the determination of exposure age requires knowledge of the temporally-averaged R_C, which is itself a function of exposure age.

3.3 Paleo elevation

Atmospheric pressure over Hawaii has fluctuated over time in response to eustatic and isostatic changes in sea level. First, continental glaciations have caused global average sea level to be as much as 120 m lower over the last 100 ka [24]. Second, Mauna Kea has been slowly subsiding relative to sea level at a rate of ~2.6 mm yr^{-1} [25] from the weight of the Hawaiian volcanoes depressing the sea floor. We corrected only the isostatic sea level changes because these, unlike eustatic sea-level variations, are not correlated with similar changes at the calibration site. Subsidence of the island means that sample sites on Mauna Kea were on average 50 and 80 m higher over the exposure

history compared to their present elevation, meaning that ^{36}Cl production rates were 3-5% higher.

To determine the relation between elevation and air pressure, we fitted a polynomial to the pressure profiles recorded by daily radiosoundings [26] at Hilo International Airport for 1998-2002 (Fig. 3). Although different previous climate (as evidenced by large Pleistocene moraines on Mauna Kea) could mean that the past atmospheric pressure structure at Hawaii different from the present one, the use of local pressure-elevation relationships (e.g. [27]) probably improves the accuracy of age calculations for locations where more generic relations such as the ICAO International standard atmosphere [28] may be inaccurate. The fact that the sea-level atmospheric pressure (1998-2002) in January is greater on average than the July pressure by only 1.5 g cm^{-2} (~1% difference in production rate) implies that the pressure structure could have been similar even during periods of cooler climate, although this would be difficult to prove without precise paleo-barometic data. Using the default sea level pressure of 1033.8 g cm^{-2}, sea level temperature of 15ºC and lapse rate of 6.5ºC km^{-1}, the standard atmosphere gives a pressures at 4000 m that is 9 g cm^{-2} lower than the 5-year average pressures recorded by radiosonde at that altitude, which corresponds to production rate that is higher by 9%. The difference between the standard atmosphere and the true atmosphere would be smaller at mid latitude locations that have a sea level temperature, pressure and lapse rate similar to those assumed by the standard atmosphere.

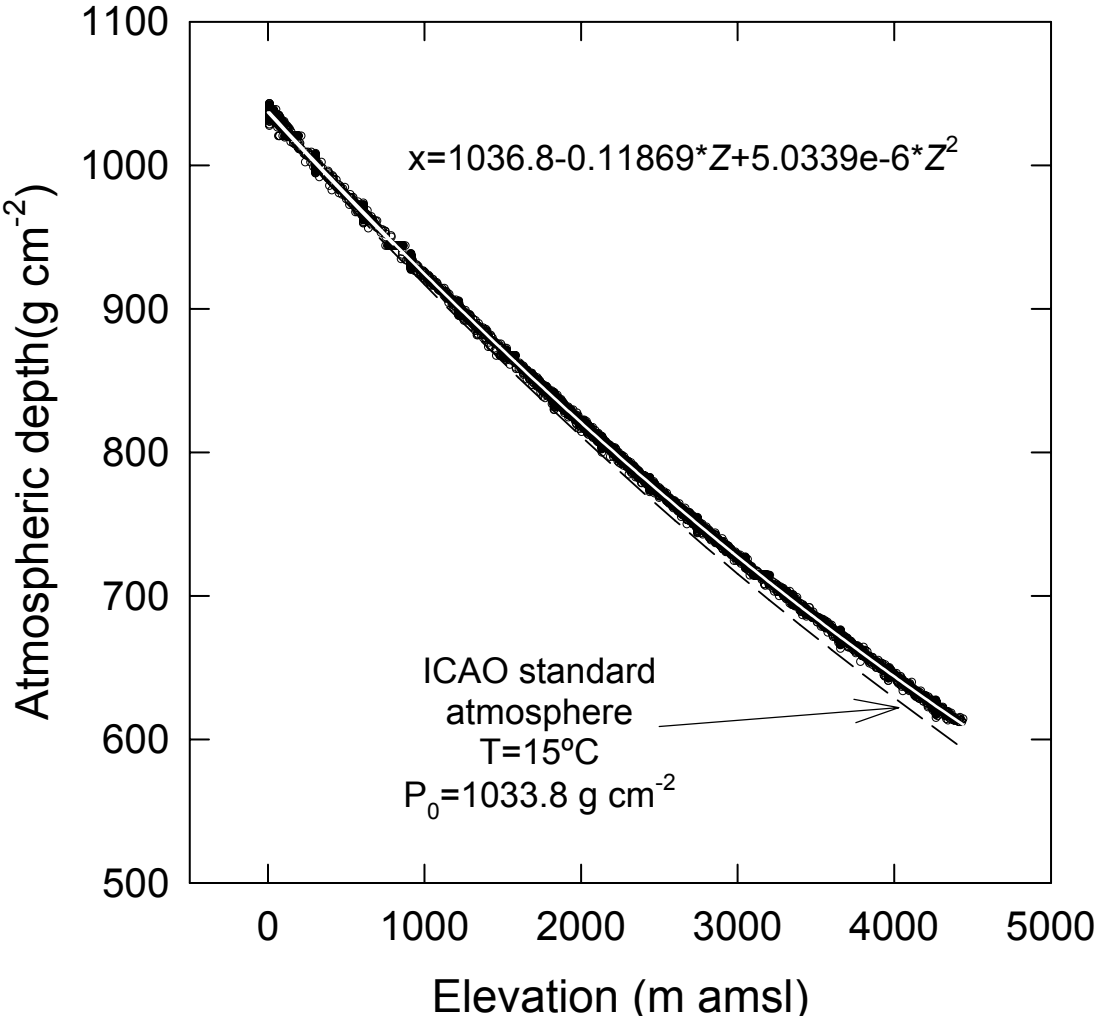

Figure 3. Best fit (white line) to atmospheric pressure data recorded by daily radio soundings at Hilo, Hawaii, 1998-2002 (circles). ICAO International standard atmosphere (black line) shown for comparison.

4. Results and discussion

4.1 Using ^{36}Cl ages to distinguish lava flows

Our results indicate that flow boundaries for L1 and L2 are more complex than is suggested by the most recent geologic map [19]. A first approximation to the age distribution shows two distinct peaks (Fig. 4), indicating two separate flows. However, the field locations of the samples constituting the peaks do not correlate with the mapped boundaries of L1 and L2. The largest peak is centered at 39.6 ka and comprises 12 L1 samples and 9 L2 samples. Our interpretation is that these samples represent either a very large flow that covered most of this area or that two flows erupted from separate vents within ~1 ka of each other, and are thus indistinguishable within the analytical precision of our measurements. We refer to this extensive flow (or combination of flows) as flow *C*. Another grouping of ages centered at 62.0 ka probably represents unmapped kipukas (older outcrops surrounded by younger lava) derived from a single flow that was later mostly covered by flow *C*. Although complementary field or compositional evidence for distinguishing the older lava from the 39.6 ka flow are lacking, we point out that kipukas tend to be topographically high features, and that we preferentially sampled such prominent features because prolonged burial by ash would have been unlikely. Because this histogram peak is clearly distinct from the 39.6 ka peak, the kipuka can be easily distinguished from the L1+L2 complex on the basis of ^{36}Cl ages alone. We refer to the kipuka as flow *K*.

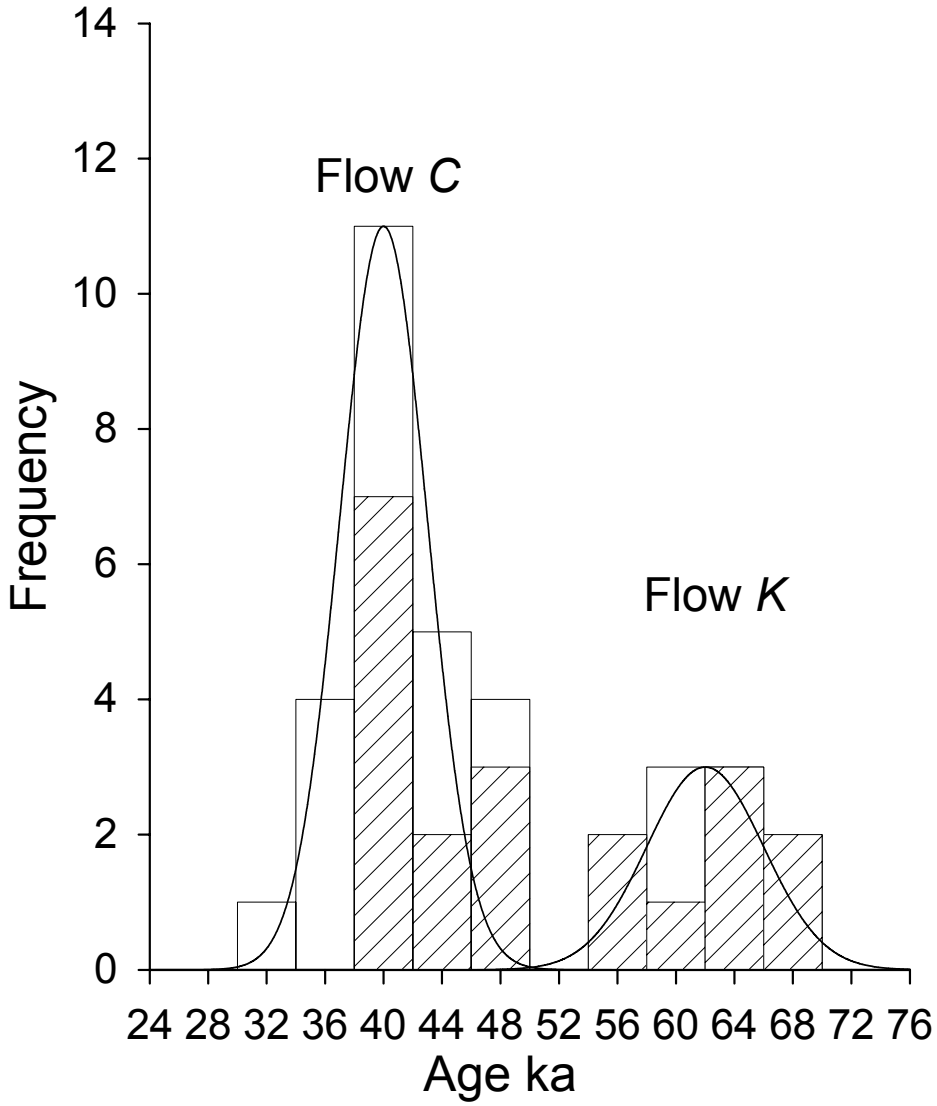

Figure 4. Histogram of lava flow ages of samples from Mauna Kea, HI showing two distinct peaks corresponding to flows *C* and *K*. Striped bars indicate samples labeled L2 and open bars show the total frequency for samples labeled L1 and L2. The solid lines are the Gaussian frequency distributions corresponding to t_C=39.6 ka, σ_C=3 ka and t_K=62.0 ka, σ_K=4 ka, normalized to the peak frequencies of *C* and *K*.

Table 1. ^{36}Cl ages of Mauna Kea lava flow samples. Corrected ages include corrections for paleomagnetic dipole strength variations and for isostatic sinking.

	Average values over exposure period						
	Elevation (m)	Atmospheric depth (g cm^{-2})	R_C (GV)	Uncorrected age (yr)		Corrected age (yr)	
HAW00-1-L1	3684	667.8	10.66	37,782	4,407	32,423	3,747
HAW00-2-L1	3559	678.0	10.97	45,847	2,118	39,269	1,800
HAW00-3-L1	3489	683.9	10.84	48,098	1,504	41,227	1,277
HAW00-4-L1	3344	696.1	11.26	44,033	3,277	37,820	2,794
HAW00-6-L1	3067	720.1	10.53	54,605	5,143	46,684	4,341
HAW00-8-L1	2347	790.2	12.12	40,091	3,444	34,291	2,924
HAW00-9-L1	2324	788.1	11.80	41,307	3,281	35,359	2,789
HAW00-10-L1	2153	804.5	10.36	63,487	21,877	52,458	17,843
HAW00-13-L1	2917	733.3	10.85	48,908	4,878	41,789	4,105
HAW00-14-L1	2816	742.4	11.26	44,433	4,540	37,980	3,828
HAW00-15-L1	2694	753.5	10.53	54,608	3,849	46,764	3,264
HAW00-16-L2	3258	703.5	12.21	26,997	1,931	19,427	1,671
HAW00-17-L2	3266	702.7	10.50	22,656	1,949	68,089	3,888
HAW00-18-L2	3112	716.1	10.40	82,735	4,775	46,519	3,850
HAW00-19-L2	2860	738.5	10.61	54,459	4,536	52,441	3,872
HAW00-20-L2	2698	753.2	10.56	61,424	4,574	57,548	3,906
HAW00-21-L2	2123	807.5	10.64	69,691	4,791	66,772	3,886
HAW00-22-L2	2247	795.5	10.36	81,391	4,817	50,255	2,664
HAW00-23-L2	2270	793.3	10.64	58,971	3,154	65,225	3,831
HAW00-24-L2	2417	779.3	10.61	79,553	4,747	66,276	5,544
HAW00-25-L2	2549	766.9	10.69	80,557	6,864	62,296	3,527
HAW00-27-L2	1992	820.3	10.49	75,811	4,340	56,531	4,154
HAW03-55-L1	3290	700.8	10.48	52,521	2,856	44,927	2,427
HAW03-56-L2	3159	712.1	10.53	53,779	3,593	45,949	3,073
HAW03-57-L2	3116	715.7	10.37	57,410	2,256	49,098	1,916
HAW03-58-L2	3082	718.8	10.98	47,143	2,208	40,365	1,885
HAW03-59-L1	3249	704.2	10.66	72,787	2,863	60,020	2,340
HAW03-60-L2	2394	781.4	11.11	47,101	2,849	40,380	2,403
HAW03-61-L2	2393	781.5	10.98	47,494	8,173	40,552	6,924
HAW03-62-L2	2344	786.2	10.51	84,359	4,597	69,145	3,724
HAW03-63-L2	2497	771.8	10.85	49,783	2,838	42,638	2,409
HAW03-64-L2	2557	766.1	10.98	47,028	2,549	40,302	2,166
HAW03-65-L2	2105	809.2	10.85	47,911	2,757	40,803	2,342
HAW03-66-L2	2155	804.4	10.85	49,230	3,118	42,034	2,649
HAW03-67-L1	2083	811.3	11.43	42,899	2,365	36,761	2,008
HAW03-68-L1	2088	810.8	10.47	56,696	2,728	48,458	2,304
HAW03-69-L1	2145	805.4	10.69	72,693	3,230	59,635	2,610

Samples that plotted midway between the peaks were removed from the data set on the basis that they cannot be clearly assigned to either flow. In practice, this meant removing the only four samples that yielded ages outside of two sample standard deviations (σ_s) from either mean age of either flow. These outliers could by explained as being eroded/exhumed samples from flow *C*, which, because of the double exponential depth-dependence for neutron activation reactions [29], could make these samples appear too old. With these four outliers discarded, the spread of ages within the two peaks can mostly be explained by the analytical uncertainty in the AMS measurements, and therefore geological factors need not be invoked. With the trimmed data set, the standard deviation of sample ages (σ_f) for flow *C* is equal to $\overline{\sigma}_s$ at 3.0 ka, and for flow *K,* σ_f=3.8 ka and $\overline{\sigma}_s$ =3.9 ka.

4.2 Atmospheric attenuation length for ^{36}Cl production

The attenuation length for ^{36}Cl production (Λ) was determined by choosing Λ (the only free parameter) such that the sum of the weighted least-square (χ^2) deviations between sample ages for samples from *K* and *C* is minimized. This yields the value of Λ that most effectively reduces the spread of lava flow ages for samples from both lava flows (Fig. 5). The value of Λ=142±5 g cm^{-2} gives the best fit to the entire data set, and independent fits to flows *K* and *C* yield Λ_C=142±7 g cm^{-2} and Λ_K=143±8 g cm^{-2}. Uncertainties are 1σ (68.3%), which, for one degree of freedom corresponds to $\Delta\chi^2$=1 [30].

For the purpose of comparison we also calculated Λ by fitting a linear regression to the natural logarithm of apparent lava flow age (t_{app}) versus atmospheric depth (x [g cm^2]):

$$\ln\left(t_{app}\right) = -\Lambda^{-1}x + b \tag{5}$$

by minimizing χ^2 (Fig. 6). This yields values of Λ that are close to those found with the first method for both the combined data set (Λ=141±4) and individual flows (Λ_C=139±6 g cm^{-2} and Λ_K=144±9 g cm^{-2}). We adopt the value of 142±5 g cm^{-2} as best representing this data set.

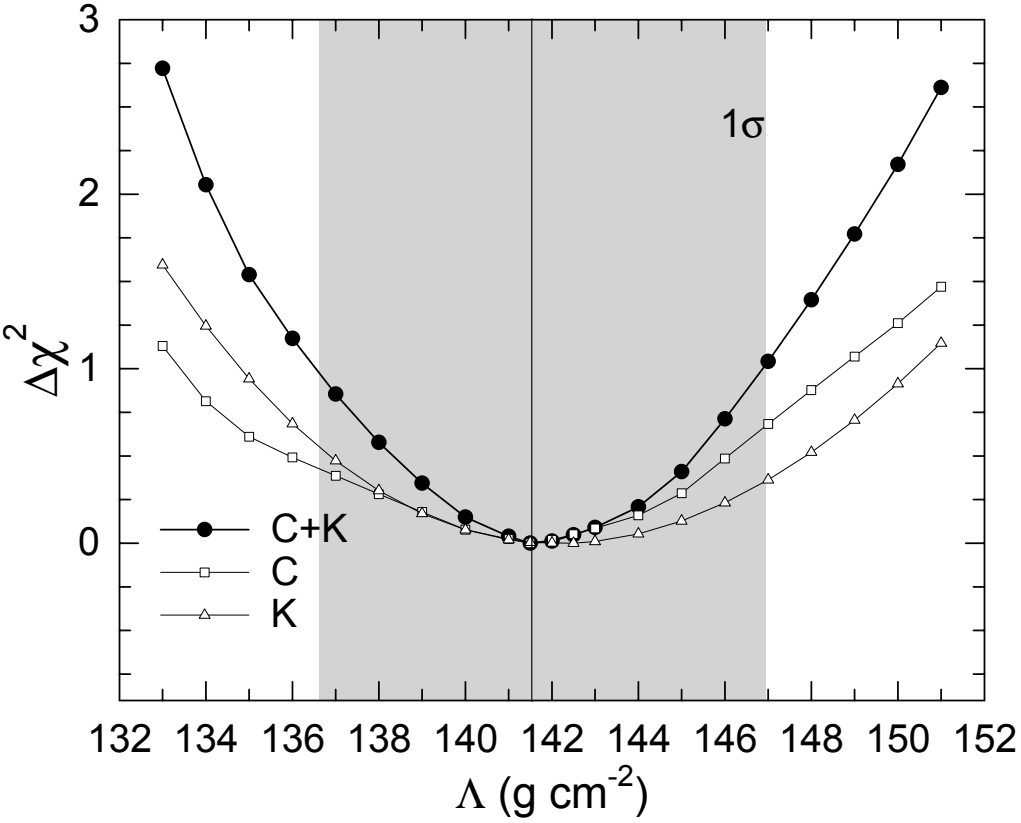

Figure 5. Best fit Λ determined by minimizing the χ^2 deviation of lava flow ages. Shaded area corresponds to 1σ limits of the fit.

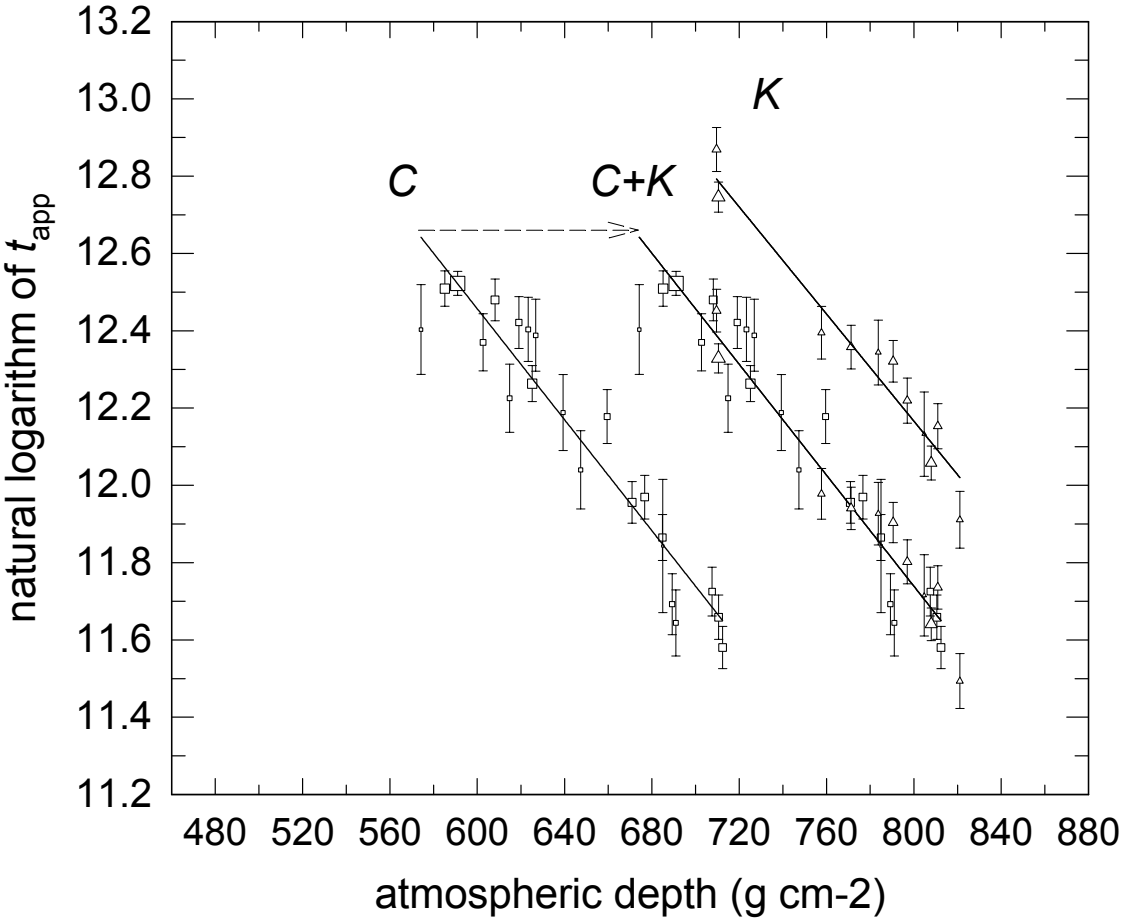

Figure 6. Linear regression to the natural logarithm of apparent lava flow age versus atmospheric depth. Flows *C* and *K* are plotted together (*C*+*K*) by normalizing the age of flow *K* to flow *C*.

4.3 Final corrected lava flow ages

Corrections for changes in geomagnetic dipole intensity and sea level over the exposure period make a large difference in sample ages. Final corrected lava flow ages were calculated using the best-fit attenuation length of 142 g cm^{-2} and the latitude scaling in [6] to scale production rates. The mean exposure ages for flows *C* and *K* are 39.6±0.8 ka and 62.0±1.2 ka. These ages are 15.5 ka and 29.7 ka lower than the uncorrected ages, with 48-53% of the difference between corrected and uncorrected ages being explained by the use of geomagnetic-corrected production rates that are higher than [21], 37-38% of the difference is from the geomagnetic correction to the sample R_C, and 9-15% is due to the isostatic sea level correction. The geomagnetic correction is nearly the same for both lava flows because the integrated field intensity is nearly the same in the range 40-70 ka, whereas the elevation correction is greater for flow *K* because subsidence is assumed to be a linear function of time.

4.4 Comparison of lava flow data with neutron flux scaling model

Elevation profiles in naturally irradiated materials provide an opportunity to validate production rate scaling models derived from measurements of cosmic-ray nucleon fluxes. The attenuation length determined from Hawaiian lava flows (Λ=142±5 g cm^{-2}) corresponds to the paleo-elevation range 3.7-2.1 km and to an average paleo R_C=11 GV. The current R_C (12.8 GV) and elevation range (3.6-2.1 km) of the lava flows is higher than in the past because of the lower average geomagnetic field strength and lower average sea level over the lava flow exposure history. According to [6, 16], Λ for the energetic neutron component is 140 g cm^{-2}, and the low-energy Λ is 149 g cm^{-2} for 3.7-

2.1 km and R_C=11 GV. The current R_C (12.8 GV) and altitude range yields attenuation lengths of 142 g cm^{-2} and 153 g cm^{-2}, which are not much different from the time-averaged values over the exposure period. The lava samples incorporate both high- and low-energy production of ^{36}Cl, with a variable, but on average nearly equal contribution from the three major reactions: spallation of calcium, spallation of potassium and thermal neutron activation of ^{35}Cl. The effective attenuation length for ^{36}Cl production corresponding to the average spallation/neutron activation ratio of our samples and to the average paleo rigidity and paleo elevations of the lava flows is Λ=144 g cm^{-2} (R_C=11 GV), which, within the uncertainties of our data, is consistent with the value we measured in Mauna Kea lava flows.

Although our results support the use of neutron flux measurements to scale production rates, the lava flow data presented here are not precise enough to answer the fundamental question of whether scaling functions depend on energy [6, 16]. The uncertainty on Λ reported here reflects only the scatter of our data, and does not include other factors that could introduce bias. For example, an extensive ash layer at higher altitudes could increase or decrease ^{35}Cl(n,γ)^{36}Cl rates in buried samples at these altitudes but leave lower elevation samples unaffected, thereby lowering the measured Λ. The lava flow Λ is also sensitive to the assumed ratio of production mechanisms, which is subject to uncertainty. For example, increasing the ratio of neutron activation to spallation by 20% brings the lava flow Λ into agreement with the predicted value of 144 g cm^{-2}. If the time-integrated geomagnetic dipole intensity were 20-30% weaker than we calculated,

the predicted Λ would also be in better agreement with Λ measured in lava flows. These factors could introduce small systematic errors in the lava flow Λ that are at present difficult to fully characterize.

The agreement between our geologically derived Λ and nucleon flux measurements confirms that spallation by nucleons is the dominant ^{36}Cl production mechanism at the altitudes of these lava flows. An important mechanism near sea level is slow negative muon capture by calcium [31]. Because slow muons are more highly penetrating (Λ_μ of ~240 g cm^{-2} [32]) than nucleon fluxes, the effective Λ for nuclide production would be significantly greater if muon interactions were an important source of ^{36}Cl in these samples. The production rate in calcium by slow-muons has been determined to be 10% of the SLHL production rate, but is not known for potassium [31]. Assuming that calcium is the only target for muon capture, only 2% of the ^{36}Cl production in the lowest elevation samples should be from slow muon reactions, which would not appreciably affect the atmospheric attenuation length we measured in Hawaii. Our data are consistent with [31]'s estimate in that we found no evidence for a greater muon contribution.

5. Conclusions

We determined the low-latitude elevation dependence of production rates by measuring cosmogenic ^{36}Cl in two Hawaiian lava flows. The elevation profile is best represented by an atmospheric attenuation length of 142±5 g cm^{-2} which corresponds to an average paleo R_C of 11 GV and paleo-elevation range of 2100-3700 m over the exposure period. The effective attenuation lengths determined from cosmic-ray neutron

surveys (R_C=11 GV, 2100-3700 m) are 140 g cm^{-2} for high-energy neutrons (spallation reactions) and 149 g cm^{-2} for thermal neutron reactions, in good agreement with the values measured in lava flows.

The determination of scaling factors directly from cosmogenic nuclide buildup in natural landforms presents several challenges. Except for relatively short-lived isotopes, where in slowly eroding landforms decay outpaces erosion [33], measurement of the altitude effect requires either an extensive, well-delineated, monogenetic landform or several independently calibrated landforms spanning a large elevation range. There are few locations where these restrictive requirements are met. Furthermore, because steep topographic gradients are associated with sharp climate gradients, surface preservation could potentially be a problem along at least some part of any elevation profile. Independently dated surfaces, even if well preserved, add a different level of complexity in that different exposure ages represent different past sea level and geomagnetic conditions. However, a more fundamental problem with empirical scaling is that scaling functions are not necessarily transferable between nuclides because the production mechanisms are different between nuclides (different excitation functions, different muon and radiogenic contributions). Considering the effort required to obtain a reliable elevation profile for a single nuclide at just one latitude, it is clear that geological profiles such as the one described here cannot replace the high-precision data obtained in neutron flux surveys. Instead, geological profiles should be used to check the applicability of neutron flux measurements to production rates. However, naturally irradiated artificial targets, when feasible, afford a better opportunity to answer fundamental questions

because geological uncertainty can be eliminated. Understanding the relation between neutron measurements and cosmogenic nuclide production requires a combination of target experiments, natural calibration work, and neutron flux measurements and modeling. All these components are combined in the new CRONUS-Earth initiative (USA) and its European counterpart, CRONUS-Europe.

Acknowledgements

We thank Frank Trusdell and David Sharrod of the USGS Hawaiian Volcano Observatory for sharing their knowledge and experience with us. This material is based upon work supported by the National Science Foundation under grants EAR-0001191, EAR-0126209 and ATM-0081403 and by Packard Fellowship in Science and Engineering 95-1832.

Supplemental Table 1. Sample location, AMS data, chlorine concentration and production rates

	Sample location			AMS and total Cl data								Production rates			
				Dilution method						Conventional method					
				AMS measurements				Calculated results		Electrode	AMS results	P_{Ca}	P_K	P_{Cl}	
	N Latitude	W Longitude	Elevation (m)	$(^{35}Cl/^{37}Cl)_{meas}$		$(^{36}Cl/Cl)_{meas}$		Cl (ppm)	$(^{36}Cl/Cl)_{rck}$	Cl (ppm)	$(^{36}Cl/Cl)_{rck}$	(atoms ^{36}Cl g_{rck}^{-1} yr^{-1})	(atoms ^{36}Cl g_{rck}^{-1} yr^{-1})	(atoms ^{36}Cl g_{rck}^{-1} yr^{-1})	notes
HAW00-1-L1	19.824	155.523	3567	3.77 ± 0.15		620 ± 60		314 ± 76	719 ± 75	335 ± 13	724 ± 35	13.6	13.5	43.0	
HAW00-2-L1	19.825	155.530	3435	4.11	0.03	690	30	284 8	859 38	296 22	845 38	22.5	20.1	65.1	
HAW00-3-L1	19.816	155.527	3365	4.09	0.04	775	21	210 9	961 28	211 20	923 38	26.8	16.6	44.8	
HAW00-4-L1	19.812	155.532	3228	6.13	0.11	711	50	113 4	1243 94	106 7	-	21.3	21.0	22.5	
HAW00-5-L1	19.810	155.538	3087	3.84	0.09	750	50	146 18	883 62	292 28	842 32	18.8	17.6	25.3	*a*
HAW00-6-L1	19.807	155.542	2951	3.95	0.14	710	50	210 35	855 67	192 16	-	16.9	19.1	36.2	
HAW00-7-L1	19.774	155.555	2082	3.74	0.15	480	40	335 80	553 50	305 20	382 16	10.7	9.8	33.1	*a*
HAW00-8-L1	19.779	155.550	2253	4.37	0.07	349	28	163 9	457 37	224 9	503 13	10.3	9.6	22.1	
HAW00-9-L1	19.778	155.551	2272	5.65	0.04	357	27	120 2	581 44	117 6	-	10.9	10.1	15.0	
HAW00-10-L1	19.773	155.555	2062	14	0.25	500	160	35 1	1885 615	27 16	-	9.7	10.2	3.7	
HAW00-11-L1	19.770	155.556	1976	10.7	0.06	1000	40	40 0	2926 125	46 6	-	21.0	1.3	4.2	*b*
HAW00-12-L1	19.770	155.557	1955	7.6	0.40	810	50	93 8	1717 202	43 20	-	21.2	1.2	9.6	*b*
HAW00-13-L1	19.799	155.546	2811	3.68	0.15	550	30	281 74	626 41	290 30	-	17.5	14.6	44.2	
HAW00-14-L1	19.798	155.550	2722	3.69	0.15	480	30	283 73	547 40	256 30	-	15.7	14.2	40.6	
HAW00-15-L1	19.794	155.554	2589	7.31	0.29	620	40	73 5	1269 123	74 1	-	15.1	12.5	10.3	
HAW00-16-L2	19.826	155.545	3206							650 42	285 16	12.7	10.7	85.3	
HAW00-17-L2	19.826	155.549	3119							295 9	1110 50	20.7	17.4	52.6	
HAW00-18-L2	19.826	155.552	2991							278 11	730 50	19.0	16.0	44.1	
HAW00-19-L2	19.809	155.559	2752							171 5	950 60	17.1	15.0	36.0	
HAW00-20-L2	19.809	155.565	2581							104 3	1240 70	14.9	14.1	13.7	
HAW00-21-L2	19.776	155.564	2019							98 2	970 50	9.7	7.6	10.4	
HAW00-22-L2	19.776	155.565	2155							152 3	640 30	11.2	9.3	15.9	
HAW00-23-L2	19.776	155.568	2162							170 3	760 40	11.0	8.3	18.3	
HAW00-24-L2	19.793	155.565	2302							77 5	1460 70	10.9	11.8	9.2	
HAW00-25-L2	19.793	155.566	2434							182 5	890 40	13.9	10.4	24.7	
HAW00-26-L1	19.819	155.526	3404	4.72	0.17	770	40	73 8	1075 72	200 20	1031 30	17.0	18.5	34.8	*a*
HAW00-27-L2	19.776	155.564	1915							247 12	495 26	9.6	8.5	24.0	
HAW03-55-L1	19.809	155.533	3165							218 5	958 44	20.5	20.2	42.6	
HAW03-56-L2	19.822	155.549	3039							297 18	755 23	21.6	16.6	52.6	

a sample not used because of unresolved discrepancy between Cl concentration and/or 36Cl/Cl measured with and without using spike

b sample not used because chemical analysis indicates that sample is Hamakua basalt

Supplemental Table 1 - *continued*

Sample location				AMS and total Cl data								Production rates			
				Dilution method				Conventional method							
				AMS measurements		Calculated results		Electrode		AMS results		P_{Ca}	P_K	P_{Cl}	
	N Latitude	W Longitude	Elevation (m)	$(^{35}Cl/^{37}Cl)_{meas}$	$(^{36}Cl/Cl)_{meas}$	Cl (ppm)	$(^{36}Cl/Cl)_{rck}$	Cl (ppm)		$(^{36}Cl/Cl)_{rck}$		(atoms ^{36}Cl g_{rck}^{-1} yr^{-1})	(atoms ^{36}Cl g_{rck}^{-1} yr^{-1})	(atoms ^{36}Cl g_{rck}^{-1} yr^{-1})	notes
HAW03-57-L2	19.820	155.550	2994					172	4	1034	32	20.2	18.2	30.5	
HAW03-58-L2	19.818	155.550	2970					190	7	789	24	18.9	16.1	31.1	
HAW03-59-L1	19.813	155.540	3109					262	6	1117	34	20.0	17.8	49.3	
HAW03-60-L2	19.788	155.566	2318					50	2	1238	38	11.0	11.4	5.6	
HAW03-61-L2	19.788	155.566	2317					199	6	500	80	12.1	10.0	22.2	
HAW03-62-L2	19.784	155.567	2230					158	5	870	35	12.4	8.0	17.5	
HAW03-63-L2	19.798	155.563	2405					70	2	1058	49	13.1	11.0	8.5	
HAW03-64-L2	19.798	155.563	2466					76	2	1014	41	13.7	12.0	9.4	
HAW03-65-L2	19.777	155.565	2051					334	13	346	14	10.4	9.1	31.6	
HAW03-66-L2	19.778	155.564	2082					143	6	543	24	10.9	9.3	14.0	
HAW03-67-L1	19.775	155.558	2032					55	1	884	39	9.6	9.3	4.8	
HAW03-68-L1	19.774	155.559	2013					57	1	1067	42	8.9	10.0	5.4	
HAW03-69-L1	19.777	155.564	2049					171	1	665	27	10.7	7.2	17.2	

a sample not used because of unresolved discrepancy between Cl concentration and/or 36Cl/Cl measured with and without using spike

b sample not used because chemical analysis indicates that sample is Hamakua basalt

Supplemental Table 2. Chemical compositions of lava flow samples.

	Major elements - percent abundance										Trace Elements - ppm				
	Na_2O	MgO	Al_2O_3	SiO_2	P_2O_5	K_2O	CaO	TiO_2	MnO	Fe_2O3	B	Sm	Gd	U	Th
HAW00-1-L1	5.0	2.0	18.3	53.7	0.3	2.2	5.4	2.4	0.2	9.1	7.4	8.4	7.3	1.4	4.8
HAW00-2-L1	4.8	1.9	17.6	55.5	0.5	1.9	5.1	2.2	0.1	8.2	4.3	8.4	7.3	1.4	4.8
HAW00-3-L1	4.6	2.8	17.8	52.7	0.5	1.6	6.3	2.7	0.2	8.8	6.9	8.8	7.5	0.9	3.2
HAW00-4-L1	4.9	2.6	17.9	52.8	0.4	2.2	5.5	2.6	0.2	8.8	2.9	6.9	6.1	0.9	3.1
HAW00-5-L1	4.8	2.4	17.6	53.2	0.6	2.1	5.4	2.4	0.2	9.6	3.2	9.8	8.2	1.3	4.3
HAW00-6-L1	5.0	2.5	17.4	53.3	0.3	2.3	4.9	2.3	0.2	9.5	7.9	7.2	6.1	1.1	3.9
HAW00-7-L1	4.7	2.8	17.0	52.9	0.5	2.1	5.5	2.5	0.2	10.2	6.7	8.1	7.0	1.3	4.3
HAW00-8-L1	4.5	2.7	17.5	51.1	0.6	2.0	5.3	2.6	0.2	10.4	8.4	7.4	6.3	1.3	4.3
HAW00-9-L1	4.8	2.4	17.6	53.2	0.6	2.1	5.4	2.4	0.2	9.6	3.2	9.8	8.2	1.3	4.3
HAW00-10-L1	4.8	2.6	17.0	53.9	0.3	2.2	5.0	2.5	0.2	10.2	1.7	5.4	4.8	1.2	3.9
HAW00-11-L1	1.7	8.9	14.1	44.3	0.2	0.3	11.3	3.1	0.2	13.0	3.9	3.9	1.3	1.3	0.3
HAW00-12-L1	1.9	8.6	14.1	45.1	0.1	0.3	11.4	3.0	0.2	12.7	3.8	3.6	3.6	0.3	1.2
HAW00-13-L1	4.6	2.7	17.8	52.2	0.4	2.0	5.7	2.7	0.2	10.1	4.7	6.3	5.5	1.1	3.6
HAW00-14-L1	4.7	2.7	18.2	52.8	0.4	2.1	5.6	2.7	0.2	9.9	4.7	6.3	5.5	1.1	3.6
HAW00-15-L1	4.5	3.3	17.7	51.6	0.4	1.9	5.6	2.7	0.2	10.8	5.1	6.1	5.4	1.2	3.8
HAW00-16-L2	4.8	3.2	17.2	53.1	0.3	1.9	5.5	2.5	0.2	9.4	5.9	7.6	6.7	1.3	4.0
HAW00-17-L2	4.3	3.0	17.2	52.1	0.7	1.9	5.4	2.6	0.2	10.5	10.8	9.9	8.4	1.4	4.5
HAW00-18-L2	4.3	3.0	17.2	52.1	0.7	1.9	5.4	2.6	0.2	10.5	6.1	9.5	8.2	1.2	3.7
HAW00-19-L2	4.9	2.8	17.7	52.0	0.5	2.1	5.7	2.5	0.2	9.4	3.5	7.0	6.0	1.0	3.3
HAW00-20-L2	4.5	3.8	17.0	49.5	0.9	2.1	5.5	2.5	0.2	10.8	8.1	11.8	10.2	1.4	4.7
HAW00-21-L2	4.5	2.5	17.7	52.8	0.4	1.7	5.2	2.5	0.2	10.6	5.9	5.3	4.7	1.2	3.9
HAW00-22-L2	4.6	2.5	18.2	52.5	0.4	1.9	5.4	2.6	0.2	10.0	6.6	7.5	6.5	1.2	4.2
HAW00-23-L2	4.3	2.9	16.9	52.6	0.6	1.7	5.4	2.5	0.2	11.0	3.7	7.5	6.5	4.6	1.4
HAW00-24-L2	4.8	2.3	17.5	53.5	0.4	2.1	4.8	2.2	0.2	9.2	5.1	9.7	8.1	4.9	1.5
HAW00-25-L2	4.5	3.0	17.8	51.4	0.5	1.7	5.7	2.7	0.2	11.2	3.1	7.1	6.2	4.1	1.1
HAW00-26-L1	4.8	2.3	17.5	53.5	0.4	2.1	4.8	2.2	0.2	9.2	5.1	9.2	7.7	1.4	4.7
HAW00-27-L2	4.8	2.6	17.5	52.6	0.4	2.0	5.5	2.5	0.2	10.4	4.4	6.6	5.7	3.9	1.3
HAW03-55-L1	4.8	2.5	17.5	52.1	0.5	2.1	5.2	2.4	0.2	9.7	4.7	10.1	7.9	1.4	4.5
HAW03-56-L2	4.8	3.1	17.5	51.6	0.7	1.9	6.0	2.5	0.2	9.7	9.4	10.0	8.0	1.2	4.0
HAW03-57-L2	5.0	3.1	17.2	51.9	0.6	2.1	5.7	2.5	0.2	9.9	7.2	8.6	7.0	1.2	4.1
HAW03-58-L2	4.6	4.1	16.8	50.9	0.7	2.0	5.6	2.4	0.2	10.6	5.0	10.7	8.6	1.4	4.4
HAW03-59-L1	4.8	2.4	18.0	52.3	0.6	1.9	5.3	2.6	0.2	10.2	5.6	8.5	6.6	1.4	4.7
HAW03-60-L2	4.7	2.9	17.5	51.1	0.6	2.1	5.1	2.6	0.2	10.9	3.9	8.0	6.5	1.4	4.5
HAW03-61-L2	4.7	2.8	17.6	52.0	0.6	1.9	5.5	2.5	0.2	10.6	5.6	8.8	7.1	1.4	4.5

Supplemental Table 2 - *continued*

	Major elements - percent abundance										Trace Elements - ppm				
	Na_2O	MgO	Al_2O_3	SiO_2	P_2O_5	K_2O	CaO	TiO_2	MnO	Fe_2O3	B	Sm	Gd	U	Th
HAW03-62-L2	4.4	3.4	17.7	49.4	0.9	1.5	5.7	2.6	0.2	11.7	4.7	9.5	7.6	1.4	5.1
HAW03-63-L2	4.6	3.8	17.2	50.3	0.5	1.9	5.6	2.6	0.2	11.3	5.8	6.8	5.7	1.3	4.1
HAW03-64-L2	4.7	2.9	17.3	52.4	0.7	2.0	5.7	2.5	0.2	10.2	4.7	9.2	7.4	1.4	4.5
HAW03-65-L2	4.7	2.9	17.3	52.4	0.7	2.0	5.7	2.5	0.2	10.2	4.7	9.2	7.4	1.4	4.5
HAW03-66-L2	4.8	2.7	17.4	52.2	0.5	2.0	5.8	2.5	0.2	9.8	5.9	8.9	7.2	1.3	4.1
HAW03-67-L1	4.8	2.8	16.5	52.0	1.0	2.2	5.5	2.3	0.2	10.0	7.5	11.9	9.8	1.3	4.6
HAW03-68-L1	4.8	2.4	16.8	53.1	0.7	2.2	4.8	2.3	0.2	9.9	9.7	8.3	6.8	1.5	4.6
HAW03-69-L1	4.2	3.1	17.4	50.2	1.0	1.6	5.7	2.4	0.2	11.0	0.0	10.7	8.9	1.4	4.9

References

1 J.C. Gosse and F.M. Phillips, Terrestrial cosmogenic nuclides: theory and application, Quaternary Science Reviews 20, 1475-1560, 2001.

2 D. Lal, Cosmic ray labeling of erosion surfaces: *in situ* nuclide production rates and erosion models, Earth and Planetary Science Letters 104, 424-439, 1991.

3 D. Lal and B. Peters, Cosmic ray produced radioactivity on earth, in: Encyclopedia of Physics: Cosmic Rays II, K. Sitte, ed., Encyclopedia of Physics 46/2, pp. 551-612, Springer-Verlag, Berlin, 1967.

4 T.J. Dunai, Scaling factors for production rates of in situ produced cosmogenic nuclides: a critical reevaluation, Earth and Planetary Science Letters 176, 157-169, 2000.

5 N. Lifton, A robust scaling model for in situ cosmogenic nuclide production rates, in: Geological Society of America, Annual Meeting, abstracts with programs, pp. A400, Reno, Nevada, 2000.

6 D. Desilets and M. Zreda, Spatial and temporal distribution of secondary cosmic-ray nucleon intensity and applications to in situ cosmogenic dating, Earth and Planetary Science Letters 206, 21-42, 2003.

7 D. Desilets and M. Zreda, On scaling cosmogenic nuclide production rates for altitude and latitude using cosmic-ray measurements, Earth and Planetary Science Letters 193, 213-225, 2001.

8 D. Lal, J.R. Arnold and H. Masatake, Cosmic-ray production of ^{7}Be in oxygen and ^{32}P,^{33}P,^{35}S in Argon at mountain altitudes, Physical Review 118, 1626, 1964.

9 H. Mabuchi, G. Reisuke, W. Yukio and H. Hiroshi, Phosphorous-32 induced by atmospheric cosmic rays in laboratory chemicals, Geochemical Journal 4, 105-110, 1971.

10 E.T. Brown, T.W. Trull, P. Jean-Baptiste, G. Raisbeck, D. Bourlès, F. Yiou and B. Marty, Determination of cosmogenic production rates of ^{10}Be, ^{3}He and ^{3}H in water, Nuclear Instruments and Methods in Physics Research B 172, 873-883, 2000.

11 M. Kurz, Cosmogenic helium in a terrestrial igneous rock, Nature 320, 435-439, 1986.

12 E.T. Brown, E.J. Brook, G.M. Raisbeck, F. Yiou and M.D. Kurz, Effective attenuation lengths of cosmic-rays producing 10Be and 26Al in quartz - implications for exposure age dating, Geophysical Research Letters 19(4), 369-372, 1992.

13 M.G. Zreda and F.M. Phillips, Surface exposure dating by cosmogenic chlorine-36 accumulation, in: Dating in Exposed and Surface Contexts, C. Beck, ed., pp. 161-183, University of New Mexico Press, 1994.

14 H. Carmichael, M.A. Shea and R.W. Peterson, III. Cosmic-ray latitude survey in Western USA and Hawaii in summer, 1966, Canadian Journal of Physics 47, 2057-2065, 1969.

15 H. Carmichael and R.W. Peterson, Dependence of the neutron monitor attenuation coefficient on atmospheric depth and on geomagnetic cutoff in 1966 and in 1970, in: Proceedings of the 12th International Cosmic Ray Conference, pp. 887-892, 1971.

16 D. Desilets, M. Zreda and V. Radhakrishnan, Scaling factors for in situ cosmogenic nuclides: new measurements at low latitude, Earth and Planetary Science Letters (in preparation), 2005.

17 E.W. Wolfe, W.S. Wise and G.B. Dalrymple, The Geology and Petrology of Mauna Kea Volcano, Hawaii - A Study of Postshield Volcanism, 129 pp., United States Geological Survey, Washington, 1997.

18 S.P. Juvik, J.O. Juvik and T.R. Paradise, Atlas of Hawaii, University of Hawaii Press, Honolulu, 1998.

19 E.W. Wolfe and J. Morris, Geologic Map of the Island of Hawaii, USGS, 1996.

20 D. Desilets, P.F. Almasi, M. Zreda and D. Elmore, Determination of cosmogenic ^{36}Cl in rocks by isotope dilution, Department of Hydrology and Water Resources Technical Report 05-01, University of Arizona, Tucson, AZ, 2005.

21 F.M. Phillips, W.D. Stone and J.T. Fabryka-Martin, An improved approach to calculating low-energy cosmic-ray neutron fluzes near the land/atmosphere interface, Chemical Geology 175, 689-701, 2001.

22 Y. Guyodo and J.P. Valet, Global changes in intensity of the Earth's magnetic field during the past 800 kyr, Nature 399, 249-252, 1999.

23 S. Yang, H. Odah and J. Shaw, Variations in the geomagnetic dipole moment over the last 12 000 years, Geophysical Journal International 140, 158-162, 2000.

24 K. Lambeck, T.M. Esat and E.K. Potter, Links between climate and sea levels for the past three million years, Nature 419, 199-206, 2002.

25 K.R. Ludwig, B.J. Szabo, J.G. Moore and K.R. Simmons, Crustal subsidence rate off Hawaii determined from $^{234}U/^{238}U$ ages of drowned coral reefs, Geology 19, 171-174, 1991.

26 NOAA, National Climatic Data Center radiosonde database available on-line [http://raob.fsl.noaa.gov/].

27 J.O. Stone, Air pressure and cosmogenic isotope production, Journal of Geophysical Resarch 105(B10), 23753-23759, 2000.

28 Manual of the ICAO Standard Atmosphere extended to 80 kilometres (262 500 feet), International Civil Aviation Organisation, Doc. 7488, 1993.

29 B. Liu, F.M. Phillips, J.T. Fabryka-Martin, M.M. Fowler and R.S. Biddle, Cosmogenic ^{36}Cl accumulation in unstable landforms, 1. Effects of the thermal neutron distribution, Water Resources Research 30(11), 3115-3125, 1994.

30 W.H. Press, B.P. Flannery, S.A. Teukolsky and W.T. Vetterling, Numerical Recipes, 818 pp., University of Cambridge, New York, 1980.

31 J.O.H. Stone, J.M. Evans, L.K. Fifield, G.L. Allan and R.G. Cresswell, Cosmogenic chlorine-36 production in calcite by muons, Geochimica et Cosmochimica Acta 62(3), 433-454, 1998.

32 D.M. Desilets, The global distribution of secondary cosmic-ray intensity and applications to cosmogenic dating, M.S., University of Arizona, 2001.

33 N. Lifton, J.S. Pigati, A.J.T. Jull and J. Quade, Testing cosmogenic nuclide production rate scaling models using in situ cosmogenic ^{14}C from surfaces at secular equilibrium: Preliminary results, in: Eos Transactions AGU, Fall Meeting Supplement, 2002.

APPENDIX F

DETERMINATION OF COSMOGENIC ^{36}Cl IN ROCKS BY ISOTOPE DILUTION

Darin Desilets[1], Peter F. Almasi[1,2], Marek Zreda[1], David Elmore[3]

[1]Department of Hydrology and Water Resources, University of Arizona, Tucson, AZ, 85721, USA

[2]Present address: Lamont-Doherty Earth Observatory, Columbia University, Palisades, NY, 10964, USA

[3]Department of Physics, Purdue University, West Lafayette, IN, 47907, USA

[In preparation for *Nuclear Instruments and Methods in Physics Research B* (2005)]

Abstract

Cosmogenic ^{36}Cl produced *in situ* in terrestrial rocks provides quantitative information about exposure ages of landforms and features at the earth's surface. The isotope dilution method is now widely used for preparing ^{36}Cl samples because it allows ^{36}Cl and Cl to be simultaneously measured on a single accelerator mass spectrometry target, increases the accuracy and precision of Cl determinations and reduces rock sample size and laboratory work. In this paper we describe our implementation of isotope dilution to ^{36}Cl dating and report experimental data verifying the accuracy of our approach.

Successful application of isotope dilution to ^{36}Cl dating, requires that Cl is retained during digestion. To prevent losses we performed extractions in a sealed acid-digestion bomb, which has the added advantage of reducing digestion times by a factor of 30 or more. We found that for silicate rocks isotope dilution in most cases gives $^{36}Cl/Cl$ values and Cl concentrations that agree within 1σ with conventional (unspiked) values. Results for $^{36}Cl/Cl$ from spiked carbonates are also consistent with measurements from unspiked samples, but isotope dilution probably gives more accurate estimates of Cl concentrations. We also prepared two carbonate samples in open vessels in the presence of excess Ag to prevent volatilization of Cl. This method would permit processing of larger samples (the bomb's capacity is 5 g), and would be useful for samples with low concentration of Cl or low $^{36}Cl/Cl$. Results from spiked samples digested in both open

and closed vessels suggest that open-vessel digestion is a reliable way of preparing samples.

1. Introduction

Cosmogenic ^{36}Cl is widely used for surface exposure dating because it is produced at measurable levels from three elements common in most rocks: Ca, K and Cl. Production of ^{36}Cl in terrestrial rocks is dominated by interactions of energetic cosmic-ray neutrons with ^{40}Ca and ^{39}K targets and by thermal neutron activation of ^{35}Cl (Phillips et al., 2001). Because the production rates for these three mechanisms are known from calibrations on independently-dated landforms, exposure ages can be calculated from measurements of the near-surface inventory of ^{36}Cl in mineral grains.

Accelerator mass spectrometry (AMS) is the standard method for measuring ^{36}Cl at the very low levels (part-per-trillion) of terrestrial samples (Elmore and Phillips, 1987). Because AMS measures the atomic ratio of ^{36}Cl to Cl, determination of the ^{36}Cl inventory in a sample requires an independent measurement of Cl concentration. With the conventional method for sample preparation, a sample split is retained for total Cl determinations and elemental analysis while a larger portion is digested in a loosely-capped bottle, from which AgCl is extracted for AMS analysis.

Chlorine concentration in rocks is usually determined by the ion-selective electrode method following digestion of samples in diffusion cells (Aruscavage and Campbell, 1983; Elsheimer, 1987). Precise Cl determinations require at least three ion-selective electrode measurements on separate aliquots. For samples with < 40 ppm Cl, several more measurements may be needed both because the method is less precise and because ^{36}Cl ages are more sensitive to Cl concentration in low Cl rocks. This higher sensitivity is a result of how errors in Cl concentration are propagated to the ^{36}Cl inventory. For example in a high Cl rock (where neutron activation is the dominant production mechanism) an erroneously high Cl determination will lead to an erroneously high ^{36}Cl inventory, and this will be compensated by a proportionately higher estimated abundance of ^{35}Cl targets. In low Cl rocks, where production from Ca and K targets usually dominates, there is much less of a compensating effect and erroneously high (low) Cl contents from the ion-selective electrode will lead to ages that are too young (old). For samples < 10 ppm Cl, the ion-selective electrode method becomes impractical because of poor precision. Moreover, for carbonate samples, we found that the ion-selective electrode overestimates Cl concentration by as much as a factor of two.

An alternative method for measuring Cl concentration is to spike AMS samples with a known amount of isotopically-enriched stable chloride carrier during chemical preparation (Elmore et al., 1997; Sharma et al., 2000). Total Cl concentration is then calculated from the ^{35}Cl/^{37}Cl which is measured on faraday cups in the AMS ion injector before and after acceleration (Elmore et al., 1997). The composite ^{35}Cl/^{37}Cl is the result

of simple binary mixing between carrier Cl, of known $^{35}Cl/^{37}Cl$ and concentration, and sample Cl of unknown concentration and known (natural) $^{35}Cl/^{37}Cl$. Isotope dilution is now widely used in ^{36}Cl dating because it has five advantages:

(1) Both $^{36}Cl/Cl$ and total Cl are determined simultaneously on the same AMS target prepared from the same aliquot of the rock sample.

(2) Total Cl measurements by isotope-dilution mass spectrometry are more precise than by ion-selective electrode, particularly at low Cl concentrations.

(3) Sample size is reduced; in our experience approximately by a factor of ten over samples without Cl carrier.

(4) Total Cl can be measured accurately in carbonates, for which the ion-selective electrode method overestimates values.

(5) Calculated ages are less sensitive to contamination by Cl from reagents and other sources.

Successful application of the isotope dilution technique requires that the ratio of spike-derived Cl to rock-derived Cl must be maintained throughout the chemical extraction and purification processes. Once sample Cl is liberated from mineral grains and has equilibrated with Cl carrier, losses of Cl do not affect $^{36}Cl/Cl$ or $^{35}Cl/^{37}Cl$. But if losses occur prior to isotopic equilibration, ages calculated from AMS results would be inaccurate. The most critical factor is the timing of the carrier addition in relation to the slow release of Cl from the dissolving mineral grains. If added prior to digestion carrier could be preferentially lost before rock Cl is released, resulting in erroneously old ages;

if carrier is added after digestion rock Cl might be preferentially lost, leading to erroneously young ages.

Our work was partially motivated by the possibility that Cl losses could occur during open-vessel digestions before attainment of isotopic equilibrium between sample Cl and carrier Cl. This concern was prompted by our observation that yields of AgCl are typically 25-50% of the expected yield. One suspected reason for low yields was volatilization and escape of Cl from the low-pH and (for silicates) high-temperature (90°C) digestion environment.

Another potential complication in isotope dilution mass spectrometry is that there is a small memory in the ion source and injector magnet from contamination by previous samples. After several days of running samples, cross-contamination can reach 1% of the ion current. For samples that are isotopically enriched, a substantial fraction of the low beam current for the less abundant isotope may consist partly of cross contamination from samples that contain a natural ratio of $^{35}Cl/^{37}Cl$ (e.g. ^{36}Cl standard). Although in principle the background can be measured in blanks and subtracted from samples, recent measurements at PRIME Lab show that the cross-contamination is variable (different by as much as a factor of two between spike blanks loaded on an 8-sample wheel) and therefore adds additional uncertainty to the final $^{35}Cl/^{37}Cl$ (the new ion source at PRIME Lab produces beam currents that are 5–10 times more intense than most AMS ion sources and should greatly reduce the problem at that facility (Jackson et al., 2004)). We show in

Section 4 that although large errors in $^{35}Cl/^{37}Cl$ propagate to proportionally large errors in both Cl concentration and $^{36}Cl/Cl$, because of canceling effects exposure ages of low Cl samples are insensitive to stable isotope errors.

Isotope dilution is now widely used in ^{36}Cl dating (Barrows et al., 2002; Benedetti et al., 2003; Phillips, 2003), but there are no published experimental data confirming its accuracy. To test the accuracy of this method, we compared measurements on samples digested in a high-pressure acid digestion bomb with those from unspiked samples digested in loosely-capped PTFE (poly-tetra-fluoro-ethylene) bottles. Advantages of the pressure bomb are that Cl loss is minimized or eliminated and that samples can be digested at high temperature (up to 150°C) and pressure (up to 13 MPa), reducing the digestion time for silicates tenfold. A disadvantage is that a maximum of 5 g of rock can be digested at a time, thus requiring multiple digestions (usually no more than 3) for larger samples.

In this paper we discuss experimental results from paired samples that were digested in open vessels without adding spike and in the bomb with ^{35}Cl spike added after digestion. We also discuss paired open-vessel and closed vessel digestions of two spiked carbonates, and we give equations for propagating analytical uncertainties in measurements of $^{35}Cl/^{37}Cl$ to uncertainties in Cl concentration, $^{36}Cl/Cl$ and landform age.

2. Theory

Two conditions must be met when diluting samples with stable Cl. First, $^{36}Cl/Cl$ in the sample must remain above the detection limit for AMS analysis. Currently, $^{36}Cl/Cl$ can be measured by AMS with 5% accuracy at ratios as low as 30 (units of 10^{-15}), with better accuracy being obtained at higher ratios. Second, $^{35}Cl/^{37}Cl$ must be high enough that Cl concentration can be accurately determined. Our experiments show that accurate Cl determinations can be made from samples with $^{35}Cl/^{37}Cl$ as low as 4, however because Cl concentration is not well-known in most samples before analysis, we recommend aiming for $^{35}Cl/^{37}Cl>10$ in order to give a safe margin for samples with unexpectedly high Cl. Furthermore, as discussed in Section 4, ages are less sensitive to errors in the stable isotope ratio at greater ratios, but the sensitivity depends on the relative abundances of K, Ca and Cl in the sample.

The measured stable Cl ratio, $(^{35}Cl/^{37}Cl)_{meas}$ is the ratio of the sum of Cl from rock, Cl_{rck}, carrier, Cl_c and background, Cl_b:

$$\left(\frac{^{35}Cl}{^{37}Cl}\right)^{*}_{meas} = \frac{\left[^{35}Cl^{*}\right]}{\left[^{37}Cl^{*}\right]} = \frac{\left[^{35}Cl_{rck}\right]+\left[^{35}Cl_{c}\right]+\left[^{35}Cl_{b}\right]}{\left[^{37}Cl_{rck}\right]+\left[^{37}Cl_{c}\right]+\left[^{37}Cl_{b}\right]} \quad (1)$$

where the star indicates that the measured quantity includes cross contamination.

The contaminated isotope ratio can be corrected by subtracting the background component according to:

$$\left(\frac{^{35}\mathrm{Cl}}{^{37}\mathrm{Cl}}\right)_{\mathrm{meas}} = \frac{\left[^{35}\mathrm{Cl}^{*}\right]-\left[^{35}\mathrm{Cl}_{\mathrm{b}}\right]}{\left[^{37}\mathrm{Cl}^{*}\right]-\left[^{37}\mathrm{Cl}_{\mathrm{b}}\right]} \tag{2}$$

The total moles of rock Cl, $[\mathrm{Cl}_{\mathrm{rck}}]$, in a spiked sample can be obtained from measurements of $^{35}\mathrm{Cl}/^{37}\mathrm{Cl}$ using the relation:

$$\left[\mathrm{Cl}_{\mathrm{rck}}\right]=\left[\frac{\left(\frac{^{35}\mathrm{Cl}}{^{37}\mathrm{Cl}}\right)_{\mathrm{meas}}\left[^{37}\mathrm{Cl}_{\mathrm{c}}\right]-\left[^{35}\mathrm{Cl}_{\mathrm{c}}\right]}{\left(\frac{^{35}\mathrm{Cl}}{^{37}\mathrm{Cl}}\right)_{\mathrm{rck}}-\left(\frac{^{35}\mathrm{Cl}}{^{37}\mathrm{Cl}}\right)_{\mathrm{meas}}}\right]\left[1+\left(\frac{^{35}\mathrm{Cl}}{^{37}\mathrm{Cl}}\right)_{\mathrm{rck}}\right] \tag{3}$$

where $[^{37}\mathrm{Cl}_{\mathrm{c}}]$ and $[^{35}\mathrm{Cl}_{\mathrm{c}}]$ are the moles of $^{35}\mathrm{Cl}$ and $^{37}\mathrm{Cl}$ in the carrier, $(^{35}\mathrm{Cl}/^{37}\mathrm{Cl})_{\mathrm{meas}}$ is the measured sample ratio, and $(^{35}\mathrm{Cl}/^{37}\mathrm{Cl})_{\mathrm{rck}}$ is the natural ratio of 3.127.

The $^{36}\mathrm{Cl}/\mathrm{Cl}$ in the rock, $(^{36}\mathrm{Cl}/\mathrm{Cl})_{\mathrm{rck}}$, can be calculated from the measured ratio $(^{36}\mathrm{Cl}/\mathrm{Cl})_{\mathrm{meas}}$ using:

$$\left(\frac{^{36}\mathrm{Cl}}{\mathrm{Cl}}\right)_{\mathrm{rck}} = \left(\frac{^{36}\mathrm{Cl}}{\mathrm{Cl}}\right)_{\mathrm{meas}} \cdot \left[1+\frac{\left[\mathrm{Cl}_{\mathrm{c}}\right]}{\left[\mathrm{Cl}_{\mathrm{rck}}\right]}\right] \tag{4}$$

where $[\mathrm{Cl}_{\mathrm{rck}}]$ is from Equation 1 or 2 and $[\mathrm{Cl}_{\mathrm{c}}]$ is the spike amount.

The optimal carrier amount is determined from initial estimates of $(^{36}Cl/Cl)_{rck}$ and $[Cl_{rck}]$. A single ion-selective electrode measurement should give an adequate initial estimate of Cl concentration, even for carbonates. The $^{36}Cl/Cl$ of a sample can be obtained from an estimate of the minimum exposure age and the ^{36}Cl production rates for the sample.

Three examples illustrating spike optimization are shown in Fig. 1. Sample *A* has high $^{36}Cl/Cl$ (6000), but low Cl concentration and therefore requires a large addition of carrier to achieve adequate AgCl yield. This is typical of samples that have a combination of the following: old age (hence high ^{36}Cl content), low Cl concentrations (hence high $^{36}Cl/Cl$), and high production rates (high concentration of Ca and/or K, and/or located at high altitudes). Sample *B* has a lower $^{36}Cl/Cl$ (750) and a higher Cl concentration (120 ppm). The main challenge is to achieve adequate yield by adding spike while keeping $(^{36}Cl/Cl)_{meas} > 100$. The optimization results in a small area (*B*) that can be expanded only by digesting a larger sample. Sample *C* has the lowest $^{36}Cl/Cl$ and highest Cl concentration (350 ppm). It is typical of samples that are young, have high Cl concentration and/or have low production rates (low altitude and/or low concentration of target elements Ca and K). This problem is similar to *B* except that the lower constraint on $(^{35}Cl/^{37}Cl)_{meas}$ must also be considered. In this type of sample, high yields are possible but the optimal spike amount is narrowly confined. If too little spike is used, $(^{35}Cl/^{37}Cl)_{meas}$ will drop below 10, if too much is used, $(^{36}Cl/Cl)_{meas}$ will drop below 100.

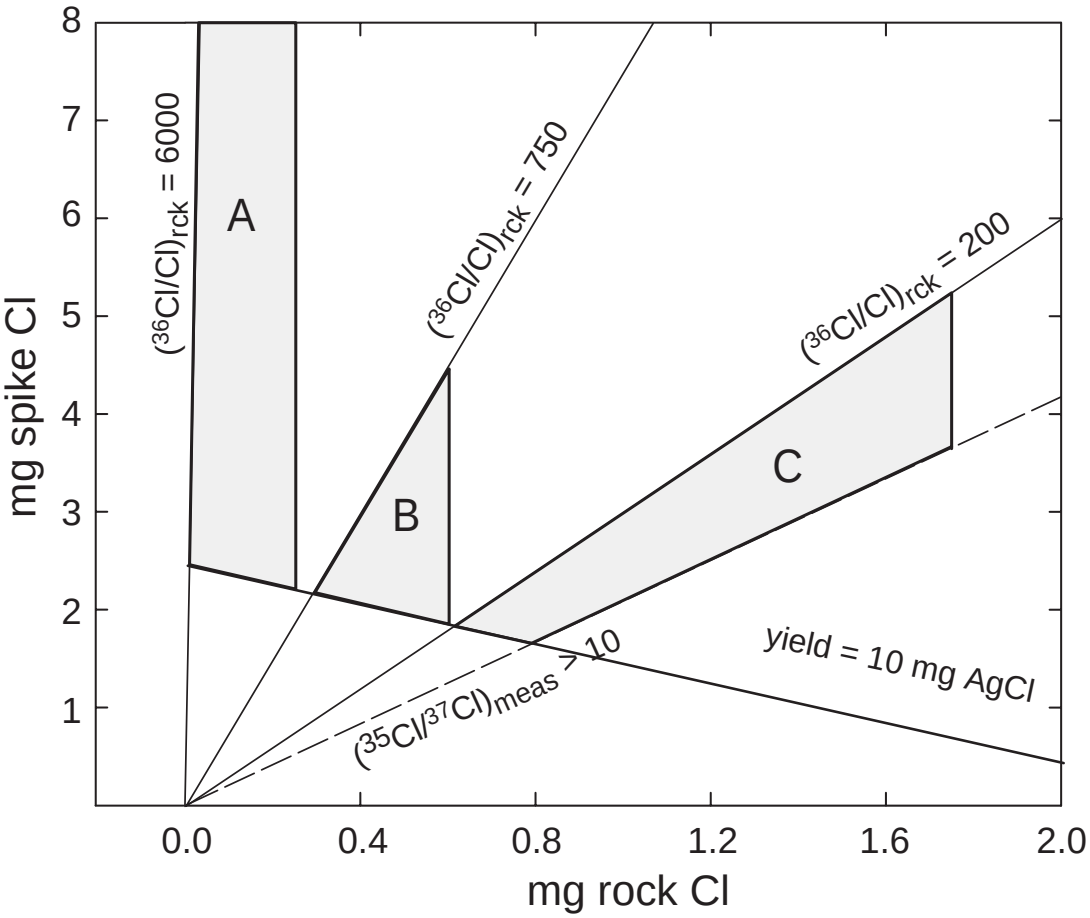

Figure 1. Graphical illustration of the spike optimization problem. The solid lines labeled $(^{36}Cl/Cl)_{rck}$ define the maximum amount of spike that can be added to a sample while satisfying the constraint $(^{36}Cl/Cl)_{meas}$ >100 for the given value of $(^{36}Cl/Cl)_{rck}$. The dashed line defines the minimum spike needed to obtain $(^{35}Cl/^{37}Cl)_{meas}$ >10 for carriers having $^{35}Cl/^{37}Cl$ from 50-300. Spike-sample combinations plotting above the negatively sloping line will yield at least 10 mg of AgCl. The constraints above define a domain (shaded) of optimal AMS results for a given $(^{36}Cl/Cl)_{rck}$, rock amount and spike isotopic composition. Optimal domain *A* corresponds to a 5 gram sample with $(^{36}Cl/Cl)_{rck}$ = 6000 and 50 ppm Cl. Because of low Cl content and high $(^{36}Cl/Cl)_{rck}$, a large amount of spike can be added. Optimal domain (B) corresponds to a 5 gram sample with $(^{36}Cl/Cl)_{rck}$ = 750 and 120 ppm Cl. The constraint $(^{36}Cl/Cl)_{meas}$ > 100 controls the amount of spike that can be safely added. Optimal domain (C) corresponds to 5 grams of 350 ppm Cl rock with $(^{36}Cl/Cl)_{rck}$ = 200. Here, both the constraints $(^{35}Cl/^{37}Cl)_{meas}$ > 10 and $(^{36}Cl/Cl)_{rck>100}$ tightly define the minimum and maximum amounts of spike that should be added.

3. Isotope dilution experiments

3.1. Procedure for closed vessel digestions

A closed-system was maintained during extraction of Cl by digesting samples in a large-capacity acid-digestion bomb. We used Parr Instrument Co. Model 4748 with removable 125 ml PTFE cup designed to digest up to 5 grams of crushed rock. The stainless-steel case and threaded bronze cap withstand pressures up to 13.1 MPa, allowing digestion temperatures up to 150° C. The high temperature and pressure achieved in the bomb results in a substantially shorter digestion time than for conventional open-vessel digestion. For example, complete digestion of 2 g of silicate rock can be achieved in 2 hours at 130°C, compared with 72 hours at 90° C in an open vessel.

All silicate samples were first crushed, sieved (0.25-1 mm fraction) and then leached for 24 hours in dilute HNO_3. Dried samples were then loaded into the PTFE cup and weighed. A known mass of 250 ppm NaCl spike (99.66% ^{35}Cl, from Isotec, Inc) was added to the cup, followed by the addition of ~40 g of 45% HF and ~5 g of 70% HNO_3. At room temperature the digestion of silicates was sufficiently slow that the bomb could be assembled and sealed before significant vapor losses occurred. The sealed bomb was placed in an oven at 130°C for 2-8 hours. Before opening, the bomb was air cooled for 30 minutes. Approximately 5 ml of 0.1 M $AgNO_3$ were then added to the sample to precipitate the mixed spike and sample Cl as AgCl. The resulting AgCl was purified of

the interfering ^{36}S isobar by performing several sequences of barium sulfate extractions followed by rinses in deionized water (Zreda et al., 1991; Almasi, 2001).

Carbonate samples were prepared similarly to silicates, but were digested in HNO_3 at room temperature for 30 minutes. Because acids react violently with carbonates, it was necessary to isolate samples from digestion acid until the bomb could be closed. This was accomplished by encasing the sample in ice before placing it in the bomb.

3.2. Results for closed vessel digestions

Silicate rocks

Closed-vessel isotope dilution results mostly agree with results from the conventional (without carrier) open-vessel method (Tables 1, Fig. 2). Data from granites and hawaiitic lavas show that for most samples, total Cl concentrations calculated from isotope dilution agree with ion-selective electrode determinations.

There are three exceptions in the HAW00 samples: Samples HAW00-5, HAW00-8 and HAW00-26 give lower Cl concentration by isotope dilution. Chlorine loss during digestion can be ruled out as a possible explanation because losses could only have occurred either preferentially from the carrier during digestion before the sample had completely dissolved or while spike Cl and sample Cl were in equilibrium. The first scenario would give erroneously high Cl concentrations, in contrast to the observed lower Cl concentrations, and the second scenario would produce no effect at all. Moreover,

Table 1. Comparison of Cl and $^{36}Cl/Cl$ (10^{-15}) determined by dilution method with values from conventional method for silicate rocks. Spike $^{35}Cl/^{37}Cl = 293.1$.

	dilution method							*conventional method*	
	dilution data			*AMS measurements*		*calculated results*		*electrode*	*AMS results*
sample ID	sample mass (g)	NaCl spike (ml)	^{35}Cl spike (ppm)	$(^{35}Cl/^{37}Cl)_{meas}$	$(^{36}Cl/Cl)_{meas}$	Cl (ppm)	$(^{36}Cl/Cl)_{rck}$	Cl (ppm)	$(^{36}Cl/Cl)_{rck}$
granite									
CH96-6-A2F	2.00	10.10	150.18	11.40 ± 0.60	1230 ± 60	367 ± 28	3811 ± 268	374 ± 7	4030 ± 90
CH96-6-A2F	2.01	20.54	150.18	19.05 ± 0.30	781 ± 31	376 ± 6	4021 ± 122		
CH96-6-A2F	1.00	20.45	147.91	29.60 ± 0.80	436 ± 21	428 ± 13	3563 ± 196		
					mean:	384 ± 33	3882 ± 118	374 ± 7	4030 ± 90
hawaiites and basalts									
HAW00-1-L1	11.99	4.01	156.79	3.77 ± 0.15	620 ± 60	314 ± 76	719 ± 75	335 ± 13	724 ± 35
HAW00-2-L1	6.51	3.00	147.91	4.11 ± 0.03	690 ± 30	284 ± 8	859 ± 38	296 ± 22	845 ± 38
HAW00-3-L1	12.01	4.01	147.91	4.09 ± 0.04	775 ± 21	210 ± 9	961 ± 28	211 ± 20	923 ± 38
HAW00-4-L1	8.00	4.51	147.91	6.13 ± 0.11	711 ± 50	113 ± 4	1243 ± 94	106 ± 7	-
HAW00-5-L1	6.00	1.03	147.91	3.84 ± 0.09	750 ± 50	146 ± 18	883 ± 62	292 ± 28	842 ± 32
HAW00-6-L1	14.05	4.01	147.91	3.95 ± 0.14	710 ± 50	210 ± 35	855 ± 67	192 ± 16	-
HAW00-7-L1	16.53	5.53	150.18	3.74 ± 0.15	480 ± 40	335 ± 80	553 ± 50	305 ± 20	382 ± 16
HAW00-8-L1	9.00	3.01	147.91	4.37 ± 0.07	349 ± 28	163 ± 9	457 ± 37	224 ± 9	503 ± 13
HAW00-9-L1	12.02	6.01	147.91	5.65 ± 0.04	357 ± 27	120 ± 2	581 ± 44	117 ± 6	-
HAW00-10-L1	9.00	5.72	147.91	13.95 ± 0.25	500 ± 160	35 ± 0.8	1885 ± 615	27 ± 16	-
HAW00-11-L1	18.06	9.01	150.18	10.74 ± 0.06	1000 ± 40	40 ± 0.3	2926 ± 125	46 ± 6	-
HAW00-12-L1	12.02	8.16	150.18	7.6 ± 0.40	810 ± 50	93 ± 8	1717 ± 202	43 ± 20	-
HAW00-13-L1	9.01	2.29	150.18	3.68 ± 0.15	550 ± 30	281 ± 74	626 ± 41	290 ± 30	-
HAW00-14-L1	6.00	1.56	150.18	3.69 ± 0.15	480 ± 30	283 ± 73	547 ± 40	256 ± 30	-
HAW00-15-L1	17.99	9.00	150.18	7.31 ± 0.29	620 ± 40	73 ± 5	1269 ± 123	74 ± 1	-
HAW00-26-L1	13.33	2.52	150.18	4.72 ± 0.17	770 ± 40	73 ± 8	1075 ± 72	200 ± 20	1031 ± 30

Most of the HAW00 samples have $(^{35}Cl/^{37}Cl)_{meas}$ well below our target ratio of 10. These samples tend to be high in Cl (150-300 ppm) and therefore require large additions of spike in order to reach high stable isotope ratios. However, because high levels of preferential Cl loss from carrier or sample would produce large errors in calculations of $(^{36}Cl/Cl)_{rck}$ from spiked samples, which are not observed (Table 1). Laboratory mix-ups or recording errors resulting in erroneous total Cl would likewise produce erroneous $(^{36}Cl/Cl)_{rck}$. Because ages for these three samples calculated from dilution-method Cl values agree much better with other samples from the same landform, we conclude that the Cl concentrations determined by isotope dilution are the more accurate values.natural Cl in samples tends to dilute ^{36}Cl produced from Ca and K, thereby lowering $(^{36}Cl/Cl)_{rck}$,

the amount of spike that can be safely added to a sample is limited, especially when, as was the case with these lava flows, the approximate landform age is not well constrained beforehand.

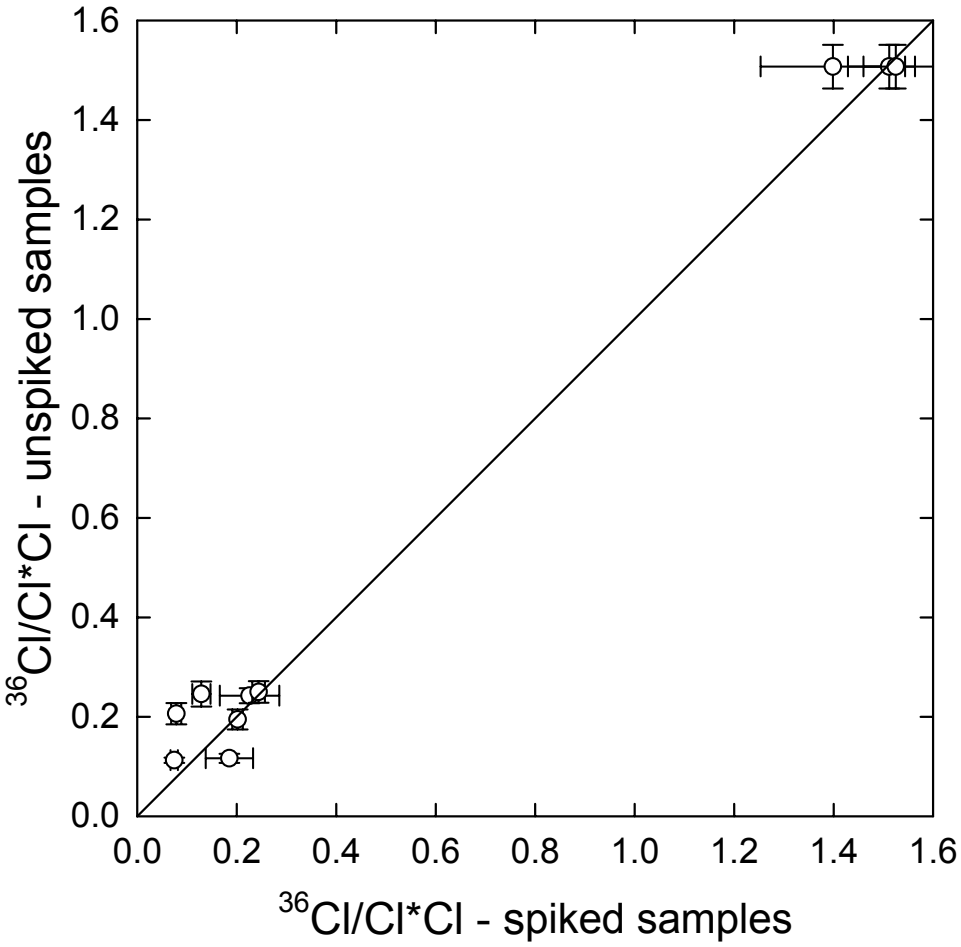

Figure 2. Comparison of relative ^{36}Cl inventories for spiked samples and unspiked samples.

Carbonate rocks

Our results show that for carbonates the ion selective electrode method consistently gives higher Cl concentrations than the isotope dilution method (Table 2). At the relatively low concentrations measured here (< 20 ppm), ion selective electrode values are on average higher by 45%. Given that $^{36}Cl/Cl$ results from spiked digestions in the bomb agree with open-vessel, unspiked results, we believe that the isotope dilution Cl concentrations are correct, and that there is a systematic problem in applying the ion-selective electrode method to carbonate rocks.

Our results show that within analytical uncertainties spiked samples give $^{36}Cl/Cl$ values identical to unspiked samples, confirming the accuracy and precision of the bomb technique of isotope dilution.

Table 2. Comparison of Cl and $^{36}Cl/Cl$ (10^{-15}) determined by dilution method with values from conventional method for carbonate rocks.

	dilution method							*conventional method*	
	dilution data			*AMS measurements*		*calculated results*		*electrode*	*AMS results*
sample ID	sample mass (g)	NaCl spike (ml)	^{35}Cl spike (ppm)	$(^{35}Cl/^{37}Cl)_{meas}$	$(^{36}Cl/Cl)_{meas}$	Cl (ppm)	$(^{36}Cl/Cl)_{rck}$	Cl (ppm)	$(^{36}Cl/Cl)_{rck}$
HL96-34	15.00	6.04	150.76	20.03 ± 0.30	1433 ± 52	14.1 ± 0.2	7700 ± 352	20.0 ± 0.4	7550 ± 150
HL96-34	10.00	8.00	150.76	33.94 ± 0.50	831 ± 38	14.6 ± 0.3	7814 ± 378		
HL96-34	5.00	7.99	150.76	62.00 ± 0.80	376 ± 18	13.4 ± 0.2	7214 ± 297		
					mean:	14.0 ± 0.6	7522 ± 199	20.0 ± 0.4	7550 ± 150

3.3. Open-vessel digestions

Two disadvantages of closed-vessel digestions are the expense of digestion bombs compared to PTFE bottles and the need to use smaller samples in the bomb (5 g) than in PTFE bottles (100 g). We therefore investigated the viability of performing isotope dilution in samples extracted in open-vessel PTFE bottles. A major concern with open-vessel digestions is the possibility of Cl volatilization in the acidic conditions of typical digestions. Stone et al. (1996) reported that volatilization of Cl can occur in the presence of concentrated HNO_3 but indicated that losses could be avoided if samples are exposed to strengths less than 2 M for silicates and 0.5 M for carbonates. If Cl losses are significant, it would be difficult to ensure that preferential losses of carrier or rock Cl do not occur before isotopic equilibrium is attained, and calculated ages could be inaccurate. In our open-vessel procedure we ensure retention of Cl loss by $AgNO_3$ before dissolving the sample so that Cl is immediately precipitated and remains in the vessel. We show in the appendix that the addition of sufficient $AgNO_3$ ensures full precipitation of Cl even from low Cl rocks and ensures minimal losses of volatile HCl molecules.

Validation of open vessel procedure for spiked carbonates

To verify the accuracy of our isotope open-vessel isotope dilution procedure, we performed paired open-vessel (O) and closed-vessel (C) digestions of two spiked carbonate samples. In the closed-vessel digestions we followed essentially the same procedure as in Section 3.1. Open-vessel digestions were performed in 500 ml PTFE

beakers by adding 1 g of $AgNO_3$ to the spiked samples followed by 10 ml of deionized water and 20 ml of 30% HNO_3. After allowing samples to dissolve for 10 minutes, the resulting AgCl precipitate was purified according to standard methods (Zreda et al., 1991; Almasi, 2001).

The results shown in Table 3 verify that the dilution method gives the same age for open- and closed-vessel digestion of carbonates. For sample PV03-80, the calculated [Cl] and $^{36}Cl/Cl$ agree to well within 1σ between the two digestion methods. Because of the analytical error in $(^{35}Cl/^{37}Cl)_{meas}$, $^{36}Cl/Cl$ and $[Cl_{rck}]$ calculated for PV03-60-O differ by a factor of four from the closed vessel results. However, spallation of ^{40}Ca dominates ^{36}Cl production in these samples, and therefore the error in $(^{36}Cl/Cl)_{meas}$ from $(^{35}Cl/^{37}Cl)_{meas}$ is compensated by an error of equal magnitude but opposite direction in $[Cl_{rck}]$, and consequently the ages from the PV03-60-O and PV03-60-C are in excellent agreement. These results demonstrate that ages of samples low in Cl and high in Ca+K are insensitive to errors in spike amount or $(^{35}Cl/^{37}Cl)_{meas}$. The reason for this insensitivity is explored further in the following section which deals with propagating analytical errors to landform ages.

Table 3. Open-vessel versus closed-vessel dilution experiments for carbonate rock. $^{36}Cl/Cl$ in units of 10^{-15}.

	AMS measurements		*calculated results*		
sample ID	$(^{36}Cl/Cl)_{meas}$	$(^{35}Cl/^{37}Cl)_{meas}$	$(^{36}Cl/Cl)_{rck}$	Cl (ppm)	age (yrs)
PV03-80-C	1020 ± 32	8.2 ± 0.90	7,670 ± 3,975	21.5 ± 12.8	36,715 ± 3,687
PV03-80-O	950 ± 35	8.3 ± 0.80	7,438 ± 3,486	20.5 ± 11.0	34,333 ± 3,100
PV03-60-C	728 ± 24	7.9 ± 0.07	17,978 ± 3,459	4.5 ± 0.8	22,240 ± 800
PV03-60-O	782 ± 35	6.6 ± 1.10	4,941 ± 4,516	20.7 ± 22.4	24,203 ± 4,593

4. Error analysis

We asssume that the general relation:

$$\sigma_z^2 = \left[\sigma_x \frac{\partial z}{\partial x}\right]^2 + \left[\sigma_y \frac{\partial z}{\partial y}\right]^2 + 2r\sigma_x\sigma_y \frac{\partial z}{\partial x}\frac{\partial z}{\partial y} \tag{5}$$

for a function $z(x,y)$ with Gaussian errors and correlation coefficient r is valid for propagating analytical errors in AMS measurements to calculations of $[Cl_{rck}]$, $(^{36}Cl/Cl)_{rck}$ and exposure age. Equation 10 is valid only when σ_z^2 is not large compared with $z(x,y)$; a condition which is met in most error propagation problems related to isotope dilution calculations.

AMS measurements of $^{35}Cl/^{37}Cl$ can sometimes include a systematic error related to cross contamination between samples. The contaminated isotope ratio can be corrected by subtracting the background. The uncertainty in the corrected ratio, $\sigma(^{35}Cl/^{37}Cl)_{meas}$, is then given by:

$$\left[\sigma\left(\frac{^{35}Cl}{^{37}Cl}\right)_{meas}\right]^2 = \frac{\left(\sigma\left[^{35}Cl_b\right]\right)^2}{\left(\left[^{37}Cl_t\right]-\left[^{37}Cl_b\right]\right)^2} + \left(\sigma\left[^{37}Cl_b\right]\right)^2\left[\frac{\left(\left[^{35}Cl_t\right]-\left[^{35}Cl_b\right]\right)}{\left(\left[^{37}Cl_t\right]-\left[^{37}Cl_b\right]\right)^2}\right]^2 + \left[\sigma\left(\frac{^{35}Cl}{^{37}Cl}\right)^*_{meas}\right]^2 \quad (6)$$

where the first two terms account for the effect of uncertainty in the background contamination $\sigma[Cl_b]$ on $\sigma(^{35}Cl/^{37}Cl)_{meas}$, and the last term accounts for the uncertainty on the original AMS measurement.

The uncertainty in $[Cl_{rck}]$ due only to $\sigma(^{35}Cl/^{37}Cl)_{meas}$ is given by:

$$\left(\sigma[Cl_{rck}]\right)^2 = \left[\sigma\left(\frac{^{35}Cl}{^{37}Cl}\right)_{meas}\right]^2\left[\left[\frac{\left(\frac{^{35}Cl}{^{37}Cl}\right)_{meas}\left[^{37}Cl_c\right]-\left[^{35}Cl_c\right]}{\left[\left(\frac{^{35}Cl}{^{37}Cl}\right)_{rck}-\left(\frac{^{35}Cl}{^{37}Cl}\right)_{meas}\right]^2}\right]\left[1+\left(\frac{^{35}Cl}{^{37}Cl}\right)_{rck}\right]+\left[\frac{\left[^{37}Cl_c\right]\left[1+\left(\frac{^{35}Cl}{^{37}Cl}\right)_{rck}\right]}{\left[\left(\frac{^{35}Cl}{^{37}Cl}\right)_{rck}-\left(\frac{^{35}Cl}{^{37}Cl}\right)_{meas}\right]}\right]\right]^2 \quad (7)$$

The uncertainties in $[Cl_{rck}]$ and $(^{36}Cl/Cl)_{meas}$ propagate to $(^{36}Cl/Cl)_{rck}$ through the relation:

$$\left[\sigma\left(\frac{^{36}\mathrm{Cl}}{\mathrm{Cl}}\right)_{\mathrm{rck}}\right]^2 = \left[\left[\sigma\left(\frac{^{36}\mathrm{Cl}}{\mathrm{Cl}}\right)_{\mathrm{meas}}\right]\left[1+\frac{[\mathrm{Cl}_{\mathrm{spk}}]}{[\mathrm{Cl}_{\mathrm{rck}}]}\right]\right]^2 + \left[\sigma[\mathrm{Cl}_{\mathrm{rck}}]\left[1-\frac{[\mathrm{Cl}_{\mathrm{spk}}]\cdot\left(\frac{^{36}\mathrm{Cl}}{\mathrm{Cl}}\right)_{\mathrm{meas}}}{[\mathrm{Cl}_{\mathrm{rck}}]^2}\right]\right]^2 \quad (8)$$

which assumes that there is no correlation between analytical errors in $(^{35}\mathrm{Cl}/^{37}\mathrm{Cl})_{\mathrm{meas}}$ and $(^{36}\mathrm{Cl}/\mathrm{Cl})_{\mathrm{meas}}$. The first term accounts for uncertainty in $(^{36}\mathrm{Cl}/\mathrm{Cl})_{\mathrm{meas}}$ and the second term accounts for uncertainty in $[\mathrm{Cl}_{\mathrm{rck}}]$.

Propagation of uncertainty in $(^{35}\mathrm{Cl}/^{37}\mathrm{Cl})_{\mathrm{meas}}$ to exposure age requires consideration of the relative importance of $^{36}\mathrm{Cl}$ production mechanisms, the relation between $(^{36}\mathrm{Cl}/\mathrm{Cl})_{\mathrm{calc}}$ and $[\mathrm{Cl}_{\mathrm{rck}}]$ and the exposure age. The inventory (N) of $^{36}\mathrm{Cl}$ increases over time according to (Zreda and Phillips, 1994):

$$\frac{\mathrm{d}N}{\mathrm{d}t} = -\lambda N + [n_{\mathrm{sp}}]P_{\mathrm{sp}} + \frac{[\mathrm{Cl}_{\mathrm{rck}}]}{M_{\mathrm{rck}}}P_{\mathrm{th}} \quad (9)$$

where P_{sp} and P_{th} are the respective production rates per quantity of target element for spallation reactions and thermal neutron activation, $[n_{\mathrm{sp}}]$ is the concentration of target elements (K+Ca) for spallation reactions, M_{rck} is the mass of rock digested, and λ is the $^{36}\mathrm{Cl}$ decay constant. The solution to Equation 13 is (Zreda and Phillips, 1994):

$$t = -\frac{1}{\lambda}\ln\left[1 - \frac{\lambda \cdot \frac{[\mathrm{Cl}_{\mathrm{rck}}]}{M_{\mathrm{rck}}} \cdot \left(\frac{^{36}\mathrm{Cl}}{\mathrm{Cl}}\right)_{\mathrm{rck}}}{[n_{\mathrm{sp}}]P_{\mathrm{sp}} + \frac{[\mathrm{Cl}_{\mathrm{rck}}]}{M_{\mathrm{rck}}}P_{\mathrm{th}}}\right] \tag{10}$$

where t is the exposure age. The uncertainty t is given by:

$$\sigma_t^2 = \left[\sigma\left(\frac{^{36}\mathrm{Cl}}{\mathrm{Cl}}\right)_{\mathrm{meas}} \frac{\partial t}{\partial\left(\frac{^{36}\mathrm{Cl}}{\mathrm{Cl}}\right)_{\mathrm{meas}}}\right]^2 + \left[\sigma[\mathrm{Cl}_{\mathrm{rck}}]\frac{\partial t}{[\mathrm{Cl}_{\mathrm{rck}}]}\right]^2 \tag{11}$$

where the first term accounts for the uncertainty from AMS measurement of ^{36}Cl/Cl, the second term accounts for the uncertainty in the measurement of ^{35}Cl/^{37}Cl, and the there is assumed to be no correlation between the two measurements. The partial derivatives in Eq. 18 are given by:

$$\frac{\partial t}{\partial\left(\frac{^{36}\mathrm{Cl}}{\mathrm{Cl}}\right)_{\mathrm{meas}}} = \frac{[\mathrm{Cl}_{\mathrm{rck}}]}{M_{\mathrm{rck}}}\left[\left[\frac{[\mathrm{Cl}_{\mathrm{rck}}]}{M_{\mathrm{rck}}}P_{\mathrm{th}} + [n_{\mathrm{sp}}]P_{\mathrm{sp}}\right]\left[1 - \frac{\lambda\frac{[\mathrm{Cl}_{\mathrm{rck}}]}{M_{\mathrm{rck}}}\left(\frac{^{36}\mathrm{Cl}}{\mathrm{Cl}}\right)_{\mathrm{meas}}}{\frac{[\mathrm{Cl}_{\mathrm{rck}}]}{M_{\mathrm{rck}}}P_{\mathrm{th}} + [n_{\mathrm{sp}}]P_{\mathrm{sp}}}\right]\right]^{-1} \tag{12}$$

$$\frac{\partial t}{\partial [\mathrm{Cl}_{\mathrm{rck}}]} = \left[-\frac{\left(\frac{^{36}\mathrm{Cl}}{\mathrm{Cl}}\right)_{\mathrm{meas}}}{M_{\mathrm{rck}}\left(\frac{[\mathrm{Cl}_{\mathrm{rck}}]}{M_{\mathrm{rck}}}P_{\mathrm{th}} + [n_{\mathrm{sp}}]P_{\mathrm{sp}}\right)} \left[-\left(\frac{[\mathrm{Cl}_{\mathrm{c}}]}{[\mathrm{Cl}_{\mathrm{rck}}]} + 1\right) + \frac{[\mathrm{Cl}_{\mathrm{c}}]}{[\mathrm{Cl}_{\mathrm{rck}}]} + \frac{[\mathrm{Cl}_{\mathrm{rck}}]P_{\mathrm{th}}\left(\frac{[\mathrm{Cl}_{\mathrm{c}}]}{[\mathrm{Cl}_{\mathrm{rck}}]} + 1\right)}{M_{\mathrm{rck}}\left(\frac{[\mathrm{Cl}_{\mathrm{rck}}]}{M_{\mathrm{rck}}}P_{\mathrm{th}} + [n_{\mathrm{sp}}]P_{\mathrm{sp}}\right)} \right] \right] \left[1 - \frac{\Lambda[\mathrm{Cl}_{\mathrm{rck}}]\left(\frac{^{36}\mathrm{Cl}}{\mathrm{Cl}}\right)_{\mathrm{meas}}\left(\frac{[\mathrm{Cl}_{\mathrm{c}}]}{[\mathrm{Cl}_{\mathrm{rck}}]} + 1\right)}{M_{\mathrm{rck}}\left(\frac{[\mathrm{Cl}_{\mathrm{rck}}]}{M_{\mathrm{rck}}}P_{\mathrm{th}} + [n_{\mathrm{sp}}]P_{\mathrm{sp}}\right)} \right]^{-1} \quad (13)$$

The effect of analytical uncertainty in $(^{35}Cl/^{37}Cl)_{meas}$ on exposure age depends on the abundance of Ca and K target elements, Cl concentration, spike amount and exposure age. The largest uncertainties in age from $\sigma(^{35}Cl/^{37}Cl)_{meas}$ are for samples with low abundances of Ca and K and high Cl concentrations. For samples with high Ca and/or K and low Cl concentration, exposure ages are generally unaffected by errors in $(^{35}Cl/^{37}Cl)_{meas}$. Exposure age is insensitive to $(^{35}Cl/^{37}Cl)_{meas}$ because $(^{36}Cl/Cl)_{rck}$ and $[Cl_{rck}]$ are affected in opposite directions by errors in $(^{35}Cl/^{37}Cl)_{meas}$, and these effects cancel if ^{36}Cl production through $^{35}Cl(n,\gamma)^{36}Cl$ is small. Similarly, trace Cl contamination in reagents should have little effect on ages calculated from contaminated samples when isotope dilution is used, although contamination would erroneously increase calculated Cl concentrations and decreases $^{36}Cl/Cl$

Figure 3 shows the sensitivity of calculated ages to errors in $(^{35}Cl/^{37}Cl)_{meas}$ for three samples in Tables 1 and 3. Sample PV03-60 has the lowest thermal neutron activation component and the least sensitivity to errors in $(^{35}Cl/^{37}Cl)_{meas}$. However, all samples become insensitive at large $(^{35}Cl/^{37}Cl)_{meas}$, which compensates for the tendency for uncertainty in $\sigma(^{35}Cl/^{37}Cl)_{meas}$ due to background contamination to increase with increasing $(^{35}Cl/^{37}Cl)_{meas}$. Most of our measurements in Table 1 are at low $(^{35}Cl/^{37}Cl)_{meas}$ and therefore are in the region of high sensitivity. Calculated ages are nonetheless generally precise because stable Cl uncertainties are small.

Figure 4 shows that calculated ages are insensitive to the assumed carrier isotopic composition over a wide range of $(^{35}Cl/^{37}Cl)_c$. If the assumed $(^{35}Cl/^{37}Cl)_c$ is lower than the true $(^{35}Cl/^{37}Cl)_c$, the calculated $(^{36}Cl/Cl)_{rck}$ will be too high and the calculated $[Cl_{rck}]$ will be too low. Because the errors in $(^{36}Cl/Cl)_{rck}$ and $[Cl_{rck}]$ are inversely correlated, they largely cancel out when calculating exposure ages.

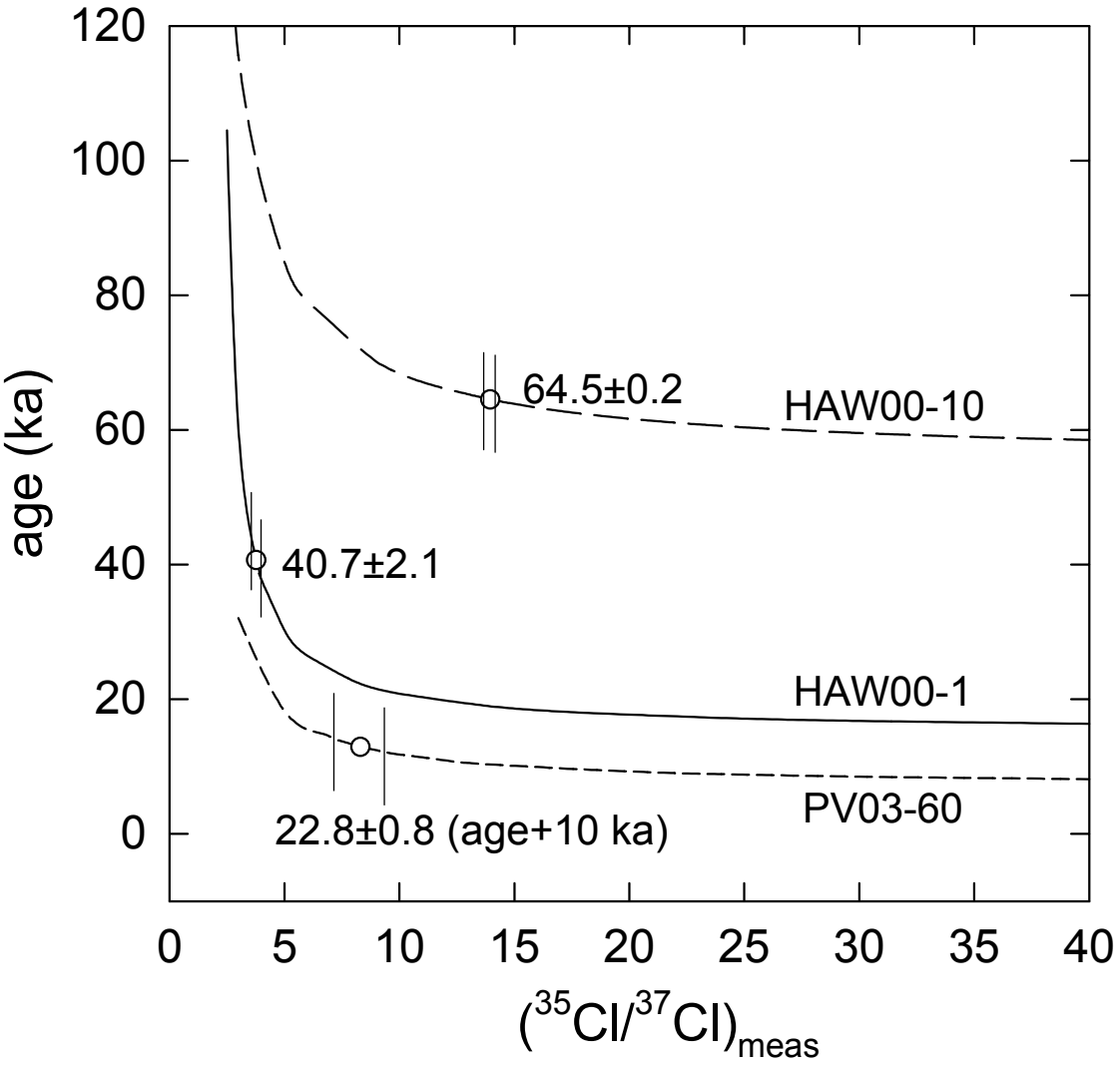

Figure 3. Sensitivity of calculated ages to uncertainty in $(^{35}Cl/^{37}Cl)_{meas}$ for three rock compositions. For clarity, the line labeled PV03-60 is offset by -10 ka from the true age.. The circles represent the measured $(^{35}Cl/^{37}Cl)_{meas}$, and the bars give the corresponding 1σ uncertainty. Sample HAW00-1 is a hawaiite with 40% spallation and 60% neutron activation, HAW00-10 is a hawaiite with 84% spallation and 16% neutron activation, and PV03-60 is a limestone with 90% spallation and 10% neutron activation.

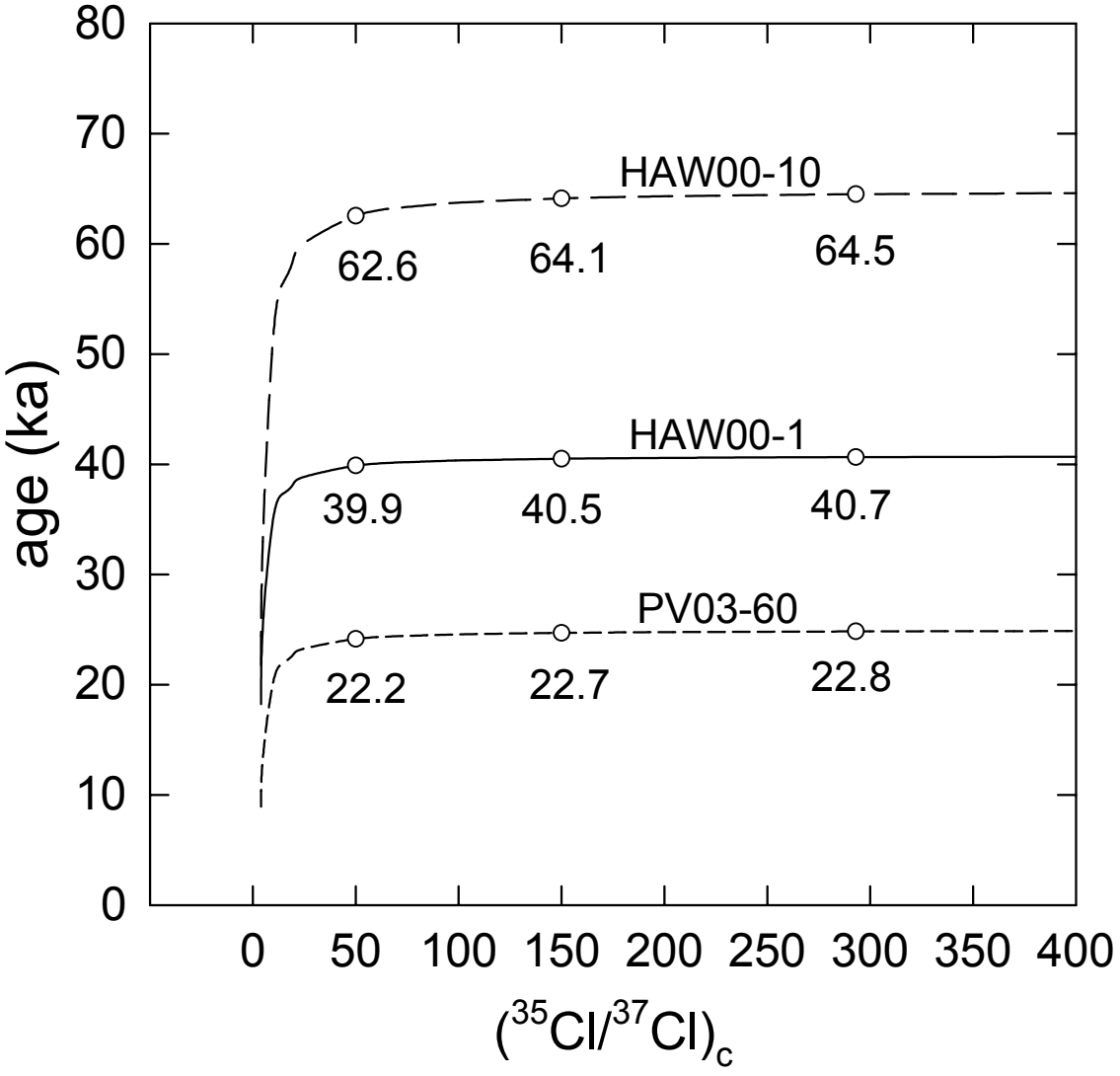

Figure 4. Sensitivity of calculated age to carrier composition for samples HAW00-1, HAW00-10 and PV03-60. The assumed spike composition is $(^{35}Cl/^{37}Cl)_c = 293$.

5. Summary

(1) $^{36}Cl/Cl$ values calculated from closed-vessel isotope dilutions agree with values from the conventional (no carrier) method.

(2) Our experiments confirm that closed-vessel and open-vessel methods of isotope dilution give similar results. However, to prevent inaccurate ages due to Cl loss, $AgNO_3$ should be added to the sample prior to digestion.

(3) Our calculations show that volatilization of Cl in the presence of $AgNO_3$ is negligible during an open-vessel digestion in a loosely capped bottle. This suggests that the isotope dilution method is valid for this type of open system.

(4) For silicate rocks, Cl concentrations calculated from isotope dilution experiments agree with results from the ion-selective electrode in most cases. The cause for disagreements could be inaccuracies in the ion-selective electrode measurements.

(5) The ion-selective electrode method overestimates Cl concentrations of carbonate rocks.

(6) Ages for samples with low Cl and high K+Ca concentrations are insensitive to analytical uncertainty in $(^{35}Cl/^{37}Cl)_{meas}$, although calculations of $[Cl_{rck}]$ and $(^{36}Cl/Cl)_{rck}$ are sensitive. The reason is that errors in $(^{35}Cl/^{37}Cl)_{meas}$ have canceling effects when propagated to age. Conversely, errors in sample mass produce larger percent errors in exposure age.

(7) Stable isotope measurements of spiked samples may include a background contamination from previously measured samples having a natural $^{35}Cl/^{37}Cl$ ratio. Although percent error in $(^{35}Cl/^{37}Cl)_{meas}$ due to this contamination increases with increasing $^{35}Cl/^{37}Cl$, ages are less sensitive to $\sigma(^{35}Cl/^{37}Cl)_{meas}$ at high $(^{35}Cl/^{37}Cl)_{meas}$.

(8) Ages from the dilution method are inherently less sensitive to natural Cl contamination from reagents because the calculated values of $(^{36}Cl/Cl)_{rck}$ and $[Cl_{rck}]$ are affected in opposite directions.

Appendix – Calculation of open vessel Cl loss

We calculated the molar fraction of Cl lost to the vapor phase over the course of a typical open-vessel silicate digestion. Because some chemical parameters are not well defined at the pH, temperature and ionic strength of digestion solutions, the model described here is accurate to within no better than an order of magnitude. The following assumptions are implicit in our calculation of Cl loss:

(1) The only mechanism for Cl loss at high temperature and low pH is volatilization of neutral HCl molecules.

(2) Vapor in the headspace of the PTFE bottle contains an equilibrium partial pressure of HCl(v).

(3) The total vapor loss from the headspace is proportional to the total vapor production during the digestion process.

In the presence of $AgNO_3$(aq), Cl is precipitated through the reaction:

$$Ag^+ + Cl^- = AgCl(s) \quad \text{(A1)}$$

The equilibrium molality of aqueous chloride is given by:

$$m_{Cl} = K_{sp}/(\gamma_{Cl}\gamma_{Ag}m_{Ag}) = K_{sp}/(\gamma^2 m_{Ag}) \quad \text{(A2)}$$

where γ is the activity coefficient. We assumed $\gamma = 0.5$ based on Solmineq.88 (Kharaka et al., 1988) calculations of the Pitzer model at pH = 2 (the lower pH limit for Solmineq.88), T = 90°C and ionic strength = 2.6 mols/kg. The equilibrium constant K_{sp} for AgCl association from 0-350°C as given by Kharaka et al. (1988) was parameterized as a function of temperature (T) in degrees C:

$$\log K_{sp} = -7.808 \times 10^{-05} T^2 + 3.770 \times 10^{-02} T - 1.066 \times 10 \quad \text{(A3)}$$

The vapor-phase molality of HCl, m_v, is then given by (Simonson and Palmer, 1993):

$$\log m_v = \log K + \log m_{Cl} + 2 \log \gamma_{HCl} - \text{pH} \quad \text{(A4)}$$

where γ_{HCl} is the activity coefficient for HCl(aq), assumed to be unity, and K is the equilibrium constant for HCl liquid-vapor partitioning for 323-623°K (Simonson and Palmer, 1993):

$$\log K = -13.4944 - 934.466/T - 11.0029 \log \rho + 5.4847 \log T \quad \text{(A5)}$$

where T is in Kelvin and ρ is the density of water in g cm^{-3}.

We calculated Cl losses for 100 g SiO_2 with 50 ppm of Cl, digested in 250 ml of HF, 100 ml of HNO_3, and 20 ml of 0.1 M $AgNO_3$ at 90°C and 1 atm. The digestion vessel was modeled as a 1000 cm^3 PTFE bottle with a loosely fitting cap to allow advective

vapor loss when the headspace is under pressure. We assume that 10% of the HF evaporates during digestion, and that the only other significant vapor production is from the dissolution of SiO_2 through the reaction:

$$SiO_2 + 4HF \rightarrow 2H_2O + SiF_4(v) \quad \text{(A6)}$$

Our calculations show that Cl losses for typical digestions in one liter PTFE bottles are $< 10^{-5}$ %. The concentration of HCl(v) in headspace is controlled mostly by the solubility of AgCl(s) and by the formation of HCl(aq) vapor from aqueous chloride ions. Although AgCl(s) solubility and HCl(aq) formation are respectively enhanced at the high temperature and low pH of digestion solutions, Cl losses are too low by four orders of magnitude to affect the accuracy of isotope dilution calculations. For extractions from carbonate rocks Cl losses should be even lower due to lower digestion temperatures.

These calculations apply only to loosely-capped PTFE bottles. In this system vapor loss from headspace occurs only in response to the buildup of pressure from the liberation of CO_2(v) and SiF_4(v) and from the vapor pressures of digestion acids. In an uncapped vessel, HCl(v) losses would be more difficult to constrain due to high diffusion rates.

There are two potential concerns related to the addition of $AgNO_3$ to the sample bottle prior to rock digestion. Because silicates are digested in concentrated HF, calcium fluoride is co-precipitated with AgCl when calcium is present. To ensure that all Cl is recovered from the vessel, the insoluble CaF_2 cake should be broken up by vigorous

shaking, leached in ammonium hydroxide to dissolve Cl, and then centrifuged and decanted. This procedure should be performed at least twice.

Another concern is that rock Cl could be left in solution if $AgNO_3$ concentrations are too low. If $AgNO_3$ and spike are added prior to digestion it is particularly important for low Cl rocks that there is sufficient Ag^+ to force the low levels of Cl^- out of solution by the common ion effect. In our open-vessel carbonate experiments $AgNO_3$ concentration is 0.1 M, and therefore the Cl in solution is $>10^{-8}$ M, which is less than 0.02 % of the Cl released from the lowest Cl rocks that we prepared. This potential problem could be further mitigated by adding spike at the end of the digestion, which would ensure that the very small fraction lost to solution is from the spike rather than from the sample. However, our results from low Cl carbonates (Tables 3) suggest that recovery of rock Cl is not a problem even if spike Cl is precipitated at the beginning of the digestion.

Acknowledgements

We thank two anonymous referees for reviewing this manuscript. The data reported in this work were obtained under National Science Foundation Grants EAR-0001191, EAR-0126209, EAR-9903227, EAR-9530857 and EAR-9632277 and Packard Fellowship in Science and Engineering 95-1832. The PRIME Lab facility is supported by National Science Foundation Grants EAR-9809983, EAR-0112480 and 9510040.

References

Almasi P. F. (2001) Dating the paleobeaches of Pampa Mejillones, Northern Chile by cosmogenic chlorine-36. M.S., University of Arizona.

Aruscavage P. J. and Campbell E. Y. (1983) An ion-selective electrode method for determination of chlorine in geological materials. *Talanta* **30**, 745-749.

Barrows T. T., Stone J. O., Fifield K., and Cresswell R. G. (2002) The timing of the Last Glacial Maximum in Australia. *Quaternary Science Reviews* **21**, 159-173.

Benedetti L., R. Finkel, G. King, R. Armijo, Papanastassiou D., Ryerson F. J., Flerit F., Farber D., and Stavrakakis G. (2003) Motion on the Kaparelli fault (Greece) prior to the 1981 earthquake sequence determined from ^{36}Cl cosmogenic dating. *Terra Nova* **15**(2), 118.

Elmore D. and Phillips F. M. (1987) Accelerator mass spectrometry for measurement of long-lived radioisotopes. *Science* **236**, 543-550.

Elmore, D., Ma, X., Miller, T., Mueller, K. et al. (1997) Status and plans for the PRIME Lab AMS facility. *Nuclear Instruments and Methods in Physics Research B*, **123**, 69-72.

Elsheimer, H.N., 1987, Application of an ion-selective electrode method to the determination of chloride in 41 international geochemical reference materials. *Geostandards Newsletter* **11**, 115-122.

Jackson, G.S. et al., 2004. Ion source modeling and design at PRIME Lab. Nuclear Instruments and Methods in Physics Research, B 223-224: 155-160.

Kharaka Y. K., Gunter W. D., Aggarwal P. K., Perkins E. H., and DeBraal J. D. (1988) Solmineq.88: A computer program for geochemical modeling of water-rock interactions. U.S. Geological Survey Report 88-4227.

Phillips, F.M., Stone, W.D. and Fabryka-Martin, J.T. (2001). An improved approach to calculating low-energy cosmic-ray neutron fluzes near the land/atmosphere interface. *Chemical Geology* **175**, 689-701.

Phillips F.M. (2003) Cosmogenic ^{36}Cl ages of Quaternary basalt flows in the Mojave Desert, California, USA. *Geomorphology* **53**, 199-208.

Sharma P., Bourgeois M., Elmore D., Vogt S., Phillips F., and Zreda M. (2000) Simultaneous Determination of Cl and ^{36}Cl Geological Samples Using AMS. *Eos Transactions AGU 81, Fall Meeting Supplement*, Abstract U21A-22.

Simonson J. M. and Palmer D. A. (1993) Liquid-vapor partitioning of HCl(aq) to 350°C. *Geochimica et Cosmochimica Acta* **57**, 1-7.

Stone, J.O., Allan, G.L., Fifield, L.K. and Cresswell, R.G., 1996. Cosmogenic chlorine-36 from calcium spallation. *Geochimica et Cosmochimica Acta* **60**: 679-692.

Zreda M. G. and Phillips F. M. (1994) Surface exposure dating by cosmogenic chlorine-36 accumulation. In *Dating in Exposed and Surface Contexts* (ed. C. Beck), pp. 161-183. University of New Mexico Press.

Zreda M. G., Phillips F. M., Elmore D., Kubik P. W., Sharma P., and Dorn R. I. (1991) Cosmogenic chlorine-36 production rates in terrestrial rocks. *Earth and Planetary Science Letters* **105**, 94-109.